Modeling and simulation of the nucleation and propagation of damage in quasi-brittle materials: Contribution of the variational approach

Paul Sicsic

Thèse de doctorat

pour obtenir le titre de

Docteur de l'École Polytechnique

Spécialité : Mécanique

Présentée par
Paul Sicsic

Modélisation et simulation de l'initiation et de la propagation de l'endommagement dans les matériaux quasi-fragiles : Apports de l'approche variationnelle

Thèse soutenue à l'École Polytechnique le 11 Octobre 2013 devant le Jury composé de :

Pierre Suquet	Directeur de recherche, LMA	Président du Jury
Luc Dormieux	Chercheur IGPEF, Laboratoire NAVIER	Rapporteur
Matteo Negri	Researcher, University of Pavia	Rapporteur
Alain Combescure	Prof. INSA Lyon	Examinateur
Christian Miehe	Prof. University of Stuttgart	Examinateur
Jean-Jacques Marigo	Prof. École Polytechnique	Directeur de thèse
Arnaud Delaplace	Dr., Lafarge	Encadrant Industriel

Laboratoire de Mécanique des Solides
École Polytechnique
91120 Palaiseau, France

Remerciements

Avant tout, je souhaite remercier Jean-Jacques Marigo de m'avoir fait découvrir un monde dont je ne soupçonnais pas l'existence. Les sujets passionnants proposés par Jean-Jacques ont été parfaitement éclairés par ses connaissances de la mécanique et sa remarquable pédagogie. Au cours de ces trois années, ses conseils ont toujours été particulièrement enrichissants. Tout en me laissant la plus grande liberté, Jean-Jacques a fait preuve de patience, d'une extrême disponibilité et de beaucoup d'attention à mon égard. Scientifiquement et humainenemt, j'ai tant appris de son exemple

Messieurs Luc Dormieux et Matteo Negri ont bien voulu relire l'ensemble de ce travail, je les remercie d'avoir écrit des rapports riches et détaillés qui m'ont conduit à améliorer la rédaction. Je remercie Pierre Suquet d'avoir accepté de présider mon jury de thèse, ainsi que Alain Combescure et Christian Miehe d'avoir bien voulu examiner ce travail. Leurs multiples points de vus ont été très enrichissants.

Au sein du LMS, j'ai bénéficié d'un environnement de grande qualité. Lev Truskinovsky et Quo-Sonc Nguyen ont toujours gardé un regard bienvaillant sur mes travaux. Je remercie Habibou Maitournam de m'avoir guidé dès mon stage de recherche de l'X, pour la définition de la thèse et jusqu'à me faire confiance pour des TD à l'ENSTA. Je remercie également Patrick Le Tallec, directeur du laboratoire, qui a toujours soutenu ce travail.

Le numérique n'aurait pas pu voir le jour sans les conseils avisés, en provenance de Bâton Rouge et de l'institut d'Alembert, de la part de Blaise Bourdin et Corrado Maurini. Les discussions que nous avons eues, et qui ont dépassé le cadre de cette thèse, ont été très constructives. Leurs visions des approches variatonnelles ont aussi favorisé la construction de ma démarche.

Je remecie la direction du centre de recherche de Lafarge, et en particulier Gilles Chanvillard et Bruno Zuber, d'avoir lancé cette thèse. L'appui indéfectible d'Arnaud Delaplace ainsi que ses conseils avisés ont été d'un grand soutien tout au long de la thèse.

Je remercie également mes co-thésards, Andrès, Céline, Clément, Hiep, Jessica, Pierre, Qing, Raman, Roberto et Tuyet pour les bons moments. Je souhaite bon courage à ceux qui sont encore en route. Enfin, je tiens à dédier cette thèse à mes parents, qui m'ont montré la voie de l'*ambition intellectuelle* et mes soeurs, Aude et Hélène, qui m'ont toujours poussé à l'entretenir.

Contents

Notations, units and nomenclature

Throughout this thesis the following conventions are used:

- The summation convention on repeated indices is implicitly adopted.
- The vectors and second order tensors are indicated by boldface letters, like $\mathbf{u}$ and $\boldsymbol{\sigma}$ for the displacement field and the stress field. Their components are denoted by italic letters, like u_i and σ_{ij}.
- The fourth order tensors as well as their components are indicated by a calligraphic letter, like A or A_{ijkl} for the stiffness tensor. Such tensors are considered as linear maps applying on vectors or second order tensors and the application is denoted without dots, like $\mathsf{A}\boldsymbol{\varepsilon}$ whose ij-component is $\mathsf{A}_{ijkl}\varepsilon_{kl}$.
- The material constants are in sans serif letter *e.g.* $\mathsf{a}, \mathsf{E}, \mathsf{G_c}, \mathsf{w}_1$
- The inner product between two vectors or two tensors of the same order is indicated by a dot, like $\mathbf{a} \cdot \mathbf{b}$ which stands for $a_i b_i$ or $\boldsymbol{\sigma} \cdot \boldsymbol{\varepsilon}$ for $\sigma_{ij}\varepsilon_{ij}$.
- The symbol $\otimes$ denotes the tensor product and $\otimes_s$ its symmetrized, *i.e.* $2\mathbf{e}_1 \otimes_s \mathbf{e}_2 = \mathbf{e}_1 \otimes \mathbf{e}_2 + \mathbf{e}_2 \otimes \mathbf{e}_1$.
- $\mathbb{M}_s$ denotes the space of 2×2 or 3×3 symmetric tensor and $\mathbf{I}$ is its identity tensor.
- The classical convention is adopted for the orders of magnitude: $o(\epsilon)$ denotes functions of ϵ such that $\lim_{\epsilon \to 0} o(\epsilon)/\epsilon = 0$.
- If $\mathcal{A}(\cdot)$ represents a quadratic form defined on a Hilbert space, the associated symmetric bilinear form is denoted by $\mathcal{A}\langle \cdot, \cdot \rangle$, *i.e.*

$$4\mathcal{A}\langle \boldsymbol{\chi}, \boldsymbol{\xi} \rangle := \mathcal{A}(\boldsymbol{\chi} + \boldsymbol{\xi}) - \mathcal{A}(\boldsymbol{\chi} - \boldsymbol{\xi}).$$

- The dot stands for the time derivative, *e.g.* $\dot{\alpha} = \partial\alpha/\partial t$
- The physical quantities are expressed in the international system of units.
- The Equations and Figures are numbered by chapter, whereas the Proposition, Hypothesis and Remarks only use a single counter in the entire thesis.

A list of the main symbols and notations adopted in this thesis are reported in the following tables. The notations of Table 1 are used in the entire thesis and concern the geometry, the loading and the gradient damage model. Those introduced in Table 2 are used in Chapter 2 during the nucleation process. The propagation of a damage band in Chapter 2 uses Table 3. Table 4 introduces the notations for the thermal shock setting, they are primarily used in Chapter 3 but also partially in Chapter 4.

Material constants	
E, ν	Young modulus and Poisson ratio (sound material)
a, $\mathsf{k_c}$	Thermal expansion and thermal diffusivity
σ_c	Critical stress (1.29) and internal length of the damage model
η, η_n	Internal length of the damage model
$\mathsf{w}_1 = \mathsf{w}(1)$	Total energy dissipation per unit volume
$\mathsf{G_c}$	Toughness
$\mathsf{A}(\alpha)$, $\mathsf{C}(\alpha)$	Rigidity and compliance tensor
Internal variables	
$\mathbf{u}$	Displacement
T	Temperature
α	Damage scalar variable
$\mathbf{g} = \nabla\alpha$	Gradient of the damage
Dual quantities	
$\boldsymbol{\sigma}$	Stress tensor (1.1)
s	Entropy (1.1)
Y	Energy release rate density (1.1)
$\mathbf{q}$	Damage flux vector (1.1)
Space and time variables	
$\mathbf{x}$	Space variables in the physical space
t	Physical time variable
Loading	
$\mathbf{U}_t$	Displacement
$\mathbf{F}_t$	Surface forces
$\mathbf{f}_t$	Volumetric Forces
$\boldsymbol{\varepsilon}_t^0(\mathbf{x})$	Imposed strain field
$\boldsymbol{\varepsilon}_t(\mathbf{x})$	Total strain field
$\boldsymbol{\varepsilon}_t^e(\mathbf{x}) = \boldsymbol{\varepsilon}_t(\mathbf{x}) - \boldsymbol{\varepsilon}_t^0(\mathbf{x})$	Elastic strain field
The 1D bar in traction	
S	Localization
L_c	Width of localized damage band
$\boldsymbol{\varepsilon}^d$	Jump of the displacement (1.25) over a localization
Energies	
$\mathcal{W}$	Strain and temperature work (1.2)
W	Bulk energy density of the gradient damage model
W_0	Bulk energy density of the underlying local damage model
ψ	Elastic energy density
$\mathsf{w}(\alpha)$	Energy dissipation per unit volume
$\mathcal{W}_t^e$	Potential of the given external forces
$\mathcal{P}_t$	Total Energy of the structure composed of the non local damage model
$\mathcal{P}_t^G$	Total Energy of the structure for a Griffith surface energy (1.33)
$\mathcal{P}_t^{reg}$	Total Energy of the structure for a regularized Griffith surface energy(1.34)

Table 1: Main nomenclature for the material parameter and the non local gradient damage model

Space, time variables and geometry	
$\mathbf{x} = (x_1, x_2)$	Space variables in the physical space
(r, θ)	Polar coordinates from the tip of the notch
$\bar{\mathbf{x}} = \mathbf{x}/\mathsf{L}$	Rescaled coordinates
ω	Notch angle
$\Gamma^{\pm}$	Lips of the notch
Ω_{L}	The domain of characteristic size L
$\mathbf{e}_1, \mathbf{e}_2$	Unit vectors at the tip of the notch
Nucleation near a notch	
ϱ	Notch singularity
K_m, K_g, K_c	Stress intensity factors
$\epsilon = \eta_n/\mathsf{L}$	Small parameter (2.1)
$\mathbf{u}^\epsilon, \boldsymbol{\sigma}^\epsilon$	Real displacement and stress
$\mathbf{U}^\epsilon, \mathbf{f}^\epsilon, \mathbf{F}^\epsilon, \boldsymbol{\varepsilon}^{0\epsilon}$	Real loading
Dimensionless setting	
$\tilde{\mathbf{u}}^\epsilon, \tilde{\boldsymbol{\sigma}}^\epsilon$	Dimensionless displacement and stress
$\tilde{\mathbf{U}}^\epsilon, \tilde{\mathbf{f}}^\epsilon, \tilde{\mathbf{F}}^\epsilon, \tilde{\boldsymbol{\varepsilon}}^{0\epsilon}$	Dimensionless loading (2.4)
$\mathbf{H}^\omega(\theta)$	Angular function of the singularity
$\tilde{\mathbf{x}} = \mathbf{x}/\mathsf{L}$	Rescaled Cartesian coordinated
$\tilde{r} = r/\mathsf{L}$	Rescaled radius for the polar coordinates
The outer problem	
$\bar{\Omega}_1$	Rescaled domain of characteristic domain size 1
$\mathbf{u}^i, \boldsymbol{\sigma}^i$	*i outer* expansion term of the dimensionless displacement and stress field $\bar{\mathbf{u}}^\epsilon, \bar{\boldsymbol{\sigma}}^\epsilon$
$f_i(\epsilon)$	*outer* expansion
The inner problem (Fig. 2.4)	
$\bar{\Omega}_\infty$	The inner domain
$\mathbf{v}^i, \boldsymbol{\tau}^i$	*i inner* expansion term of the dimensionless displacement and stress field $\bar{\mathbf{u}}^\epsilon, \bar{\boldsymbol{\sigma}}^\epsilon$ (2.9)
$g_i(\epsilon)$	*inner* expansion coefficient
$\mathbf{y} = \tilde{\mathbf{x}}/\epsilon = \mathbf{x}/\eta_n$	Cartesian coordinated in the *inner* problem
$\rho = \tilde{r}/\epsilon = r/\eta_n$	Radius for the polar coordinates in the *inner* problem

Table 2: Main nomenclature the nucleation and the rescaling due to the matched asymptotic expansion

The crack and its tip	
ℓ_t	Length of the cracks at time t
$\mathbf{P}_t$	Tip of the crack
$\mathbb{B}_r(t)$	Ball of radius r of center $\mathbf{P}_t$
$\mathbb{C}_r(t)$	Boundary of $\mathbb{B}_r(t)$
$\mathsf{I}_r(t)$	Weakly singular part in the energy balance transport
$\boldsymbol{\tau}_t$	Unit normal to the crack at its tip
$\Omega_r(t)$	Uncracked part of the body outside the ball $\mathbb{B}_r(t)$
$\mathsf{J}_r(t)$	Flux of energy (2.19)
Separation of scales	
$\mathbf{U}^\eta, \mathbf{f}^\eta, \mathbf{F}^\eta, \boldsymbol{\varepsilon}^0$	Loading
$\mathbf{u}^\eta, \boldsymbol{\sigma}^\eta$	Displacement and stress field
$\mathbf{U}, \mathbf{f}, \mathbf{F}, \boldsymbol{\varepsilon}^0$	Dimensionless loading
$\mathbf{u}, \sigma$	First order displacement and stress field
Moving variables	
$\hat{\cdot}$	Moving variables
Rescaled by η	
$\bar{\cdot}$	Rescaled quantities by η
$\bar{G}$	Energy release rate
$\mathsf{G}_\mathsf{c}^\eta$	Toughness
α_*	Damage field in the crack band
(s, ζ)	Curvilinear coordinates of the crack
$\boldsymbol{\chi}(s)$	Parametrization of Γ
The tip problem	
$\mathbf{y} = (\mathbf{x} - \mathbf{P})/\eta$	Rescaled coordinated with origin the tip of the crack
$\rho = \|\mathbf{y}\| = r/\eta$	Normalized radius from the tip of the crack

Table 3: Main nomenclature for the convergence of non local damage models towards Griffith

Material and geometric constants	
L	Width of the slab (Fig. 3.2)
Space and time variables	
$\mathbf{x} = (x_1, x_2)$	Space variables in the physical space
t	Physical time variable
$y = x_2/2\sqrt{\mathsf{k_c} t}$	Rescaled depth variable adapted to the diffusion process
$\tau = 2\sqrt{\mathsf{k_c} t}/\theta\ell$	Rescaled time adapted to the fundamental solution (3.19)
Thermal Loading	
ϑ	Temperature drop at the surface
$\mathsf{f_c}$	Complementary error function (Fig. 3.2)
$\theta = \sigma_c/\mathsf{a}\vartheta\mathsf{E}$	Thermal shock mildness parameter (3.18)
$\boldsymbol{\varepsilon}_t^{\text{th}}(\mathbf{x})$	Thermal strain field (3.5)
$\boldsymbol{\varepsilon}_t(\mathbf{x})$	Total strain field
$\boldsymbol{\varepsilon}_t^e(\mathbf{x}) = \boldsymbol{\varepsilon}_t(\mathbf{x}) - \boldsymbol{\varepsilon}_t^{\text{th}}(\mathbf{x})$	Elastic strain field (3.5)
Fundamental Branch	
$\alpha_t^*(\mathbf{x}),\ \mathbf{u}_t^*(\mathbf{x}),\ \boldsymbol{\sigma}_t^*(\mathbf{x})$	Damage, displacement and stress fields in the physical variables $t, \mathbf{x}$
$\boldsymbol{\chi}_t^* = (\mathbf{u}_t^*, \alpha_t^*)$	state fields vector
$\bar{\alpha}_\tau(y), \bar{\boldsymbol{\sigma}}_\tau(y)$	Damage and stress field in the scaled variables τ, y
D_t^*	Damage penetration in the physical variables $t, \mathbf{x}$
$\delta_\tau = D_t^*/2\sqrt{\mathsf{k_c} t}$	Damage penetration in the scaled variables τ, y (3.19)
Bifurcation and Stability	
$\zeta = x_2/\mathsf{D}_t^*$	Rescaled depth variable adapted to the damage penetration (3.41)
$\mathcal{R}_t^*(\mathbf{v}, \beta)$	Rayleigh Ratio (3.37) studying the positivity of $\mathcal{P}_t''(\boldsymbol{\chi}_t^*)$
R_t^b	Minimum value of the Rayleigh ratio $\mathcal{R}_t^*(\mathbf{v}, \beta)$ over $\mathcal{C} \times \dot{\mathcal{D}}_t$ (3.38) and of $\bar{\mathcal{R}}_\tau^\kappa(\mathbf{V}, \beta)$ over $\mathbb{R}^+ \times \mathbf{H} \times \mathcal{H}_0$ (3.44)
R_t^s	Minimum value of the Rayleigh ratio $\mathcal{R}_t^*(\mathbf{v}, \beta)$ over $\mathcal{C} \times \dot{\mathcal{D}}_t^+$ (3.39)
t_b, t_s	First time of bifurcation and loss of stability (3.49)
$\mathbf{v}^b, \beta^b$	Mode of bifurcation (3.50)–(3.51)
k, κ	Wave number corresponding to the periodic solution (3.41)–(3.42)
$(\kappa_b, \hat{\mathbf{V}}^b, \hat{\beta}^b)$	Normalized minimizers of $\bar{\mathcal{R}}_{\tau_b}^\kappa(\mathbf{V}, \beta)$
$\tau_b,\ \delta_{\tau_b}$	Rescaled time and damage penetration associated to the first bifurcation time
$\lambda_b = 2\pi\theta\delta_{\tau_b}\tau_b\ell/\kappa_b$	Wavelength of the first bifurcation solution (3.52)
$\mathsf{D}_b = 2\delta_{\tau_b}\sqrt{\mathsf{k_c} t_b} = \theta\delta_{\tau_b}\tau_b\ell$	Damage penetration at the first bifurcation point (3.53)
Crack Spacing	
a	Penetration
d	Spacing between cracks

Table 4: Main nomenclature for the thermal shock semi analytical analysis of Chapter 3

Introduction

The presence of cracks in structures and soils may or may not be desirable. They usually are not as they impair the functionality of the structure. The later can be of different nature, for example in the case of cement based materials: structural, durable or aesthetic. Thereby, not only is the presence of cracks important but their distribution, length and opening as well. This means that the topology is a concern to develop structures. Unfortunately, topology is very specific information on cracks. The source of cracks can come from structural loading *i.e.* an external load is applied to the structure or non structural as cooling, drying or relaxation of the constitutive materials. The aim of the mechanical or civil engineer is thus to limit the crack setting to prevent the deterioration of the functionality of the structure. Conversely, in the case of petroleum engineers, for extracting resources, a connected network can be sought for.

The difficulty in giving a proper crack model is the multitude of behaviors. Indeed, one has to predict the nucleation of cracks as well as their evolution. The former is concerned by the position, the orientation and the size of the initial cracks. The latter tackles the issue of the direction and rate of the propagation. Both can encounter discontinuous evolutions. Complex morphogenesis are observed in nature: mud drying, bark of trees, or in structures: crazing of concrete or paintings. Furthermore complex crack patterns can arise from the onset and they develop on several order of magnitude. Finally, for a given loading, material aspects overlap with structure considerations. For all these tasks a coherent framework to predict their evolution is sought for.

In the thesis, the focus is reduced to brittle fracture, that is behaviors such that the cracks appear with little deformations in the material, as opposed to ductile fracture. These behaviors are dangerous as they occur for small changes in the geometry of the structure and often exhibit a softening behavior, source of instabilities leading to catastrophic failures. Monotonic loading will be considered and thus any cyclic behavior (nucleation by fatigue) is put aside. Although the materials considered such as concrete and geo-materials have variable properties depending on the point considered, only sound materials of uniform material properties will be considered. Indeed even in this simplified framework complex phenomena will be accounted for.

In the last decade, the use of continuous models to predict the evolution of cracks have arisen. In these models a genuine unknown on the entire domain which describes the crack is added to the description of the bulk of the material. On the one hand this allows to numerically track the crack set in a continuous matter. On the other hand cracks are discontinuous objects by nature and the regularization might be *to* strong, this is a defect of the phenomenological approach. These approaches can be viewed as damage models which have arisen in the 70's where a variable [Lemaitre & Chaboche 1978] captures the loss of a material property and especially the rigidity in the wake of the pioneer work by Lazar M. Kachanov. In the 90's, these damage models have been regularized to avoid spurious localization [Benallal *et al.* 1993].

At the same time a multitude of ad hoc criteria have been proposed to evolve from damage to cracks, but with no definite answer. The approach used here is in the continuity of the variational approach to fracture [Francfort & Marigo 1998] where the evolution problem is constructed from an energy and a stability principle. These approaches allow to capture complex phenomena as the periodic nucleation and then crack selection mechanisms in the case of a thermal shock setting (Fig. 1). The regularized approach [Bourdin *et al.* 2000] introduces a gradient of the genuine unknown and thus resembles the gradient damage models [Comi 1999]. Further from this historical perspective, the gradient damage model is considered as such and the evolution is based on a local stability principle [Benallal & Marigo 2007].

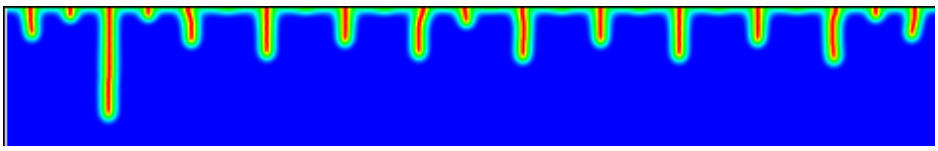

Figure 1: Damage distribution obtained at a "large" time with an alternate minimization algorithm in the case of a thermal shock *i.e.* the body at an initial homogeneous temperature is exposed to a cooler temperature on its top surface. The blue zones correspond to an undamaged point, the midline of the red zones to a totally damaged point.

Let us raise a warning, many results in this thesis are based on asymptotic behaviors [Lagerstrom 1988]. This way of thinking, which is not new in any sens, allows to extract the main physical mechanisms when passing to the limit. Yet the small parameter always takes a finite value and never vanishes whatever the material or the structure. This is the base of linearized theories. Some physical behaviors are better explained in these simplified theories then with the entire one, a famous example is that of boundary layers in fluid mechanics [Cousteix & Mauss 2006]. This also allows to underline some properties that are local, typically a set of cracks tips that are far apart can be studied independently one from an other. But at the same time, taking the limit gives raise to a loss on information which can reveal itself essential. This will be observed in the case of crack nucleation.

The dissertation is organized as follows. The second to forth chapters are independent from one an other. In the first chapter the construction of gradient damage model in a variational framework is introduced. These models are based on a scalar variable, representing the loss of rigidity of the material. The evolution problem is based on three principles in the framework of rate independent problems [Mielke 2006]: irreversibility, stability and energy balance. The gradient of the scalar variable controls the localization process and thus the dissipated energy is always finite. The main results of the construction [Pham & Marigo 2010a, Pham & Marigo 2010b, Pham & Marigo 2013] are recalled and the properties which will be used in the following chapters are underlined. Especially the evolution of damage in a one dimensional bar in traction is given in details.

In the second chapter the nucleation near a notch of cracks and their propagation are studied using separation of scales methods. In a first part the nucleation process of damage around a notch where the

elastic solution is singular is examined. A careful study of the evolution problem allows to decompose the critical loading that leads to crack nucleation in three terms. Only one of them is due to the damage model, the two other being linked with the geometry and a scale effect. A simple method is proposed for the mechanical engineer. In a second part, assuming that a damage band exists its evolution law is established. Especially, using only the stability principle and under the condition of a separation of scales it is proven that the gradient damage model converges towards Griffith's propagation law. This extends previous results in the sens that it uses a local minimal principle and not a global one. The damage and stress evolution in the tip of the damage zone are particular as the stress in not singular but the damage is until the crack propagates. Let us emphasize that the variational character of the damage evolution law is fundamental to make the link with Griffith's law. Therefore one can suspect that such a result is no longer true if one adopts constitutive laws which are not connected with these energy principles. The last point of this second chapter is the numerical investigation of the propagation of damage bands. Especially, does the propagation happen for the expected loading and does one observe the expected vanishing of the singularity in damage ? The stress, displacement and damage field near the tip of the damage band is investigated. Here, the link with Griffith's law is made with the sole help of the *first* order stability conditions and not with the complete stability condition. It is interesting to explore all the consequences of the stability. In particular, one notes in the numerical simulations of the thermal shock that the cracks are periodically distributed (Figs. 1-2). The following chapter tackles the use of *second* order stability conditions to achieve the proof of *global* property of periodicity.

In the third chapter, the thermal shock problem with the gradient damage model, at very short times, is extensively described. The originality is here a non-trivial two dimensional case of bifurcation which allows to shed some light on the nucleation of complex morphogenis crack patterns in quasi-static evolutions. This explains the beginning of the localization process and the global property of periodicity of initial cracks from a sound homogeneous material. The periodic nucleation (Fig. 2) is established, where after a damage evolution depending only on one direction, the beginning of the localization process arises. This allows to better understand the morphogenesis of complex crack patterns. The solution is parameterized by the mildness of the thermal shock *i.e.* the ratio between the materials critical stress and the maximal stress induced by the thermal loading. A remarkable property is that the spacing is proportional to the materials internal length. This setting should be seen as more than a specific example. Indeed, this idealized context allows to have an almost entire analytical solution, but the behavior is inherent of the gradient damage model used.

In the last chapter, cooling and drying problems from the nucleation phase towards the propagation, crack selection and arrest are investigated numerically. This part of the work is closer to the applications possible in an engineering context. Thus the physical values of the material parameters, that a reader non accustomed to dimensionless quantities would have found missing in the previous chapters, are introduced. In the evolution process, this is the continuation of the previous chapter, but its presentation is independent. The numerical algorithm captures the nucleation phase, although there is a competition between different time and space regimes. As time increases and thus the temperature field penetrates

(a) the onset of damage occurs at $t = 0$ at the upper side where the thermal shock happens

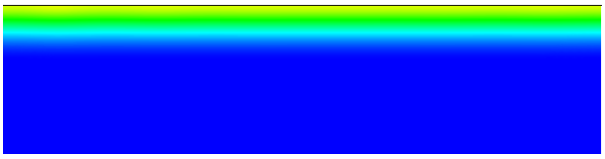

(b) for small times t, the damage penetrates progressively inside the body and remains homogeneous in the horizontal direction

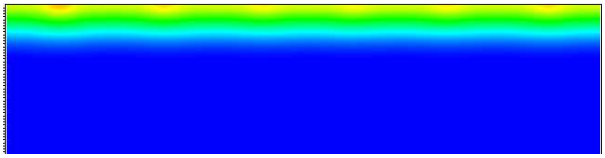

(c) damage localizes in a set of periodically distributed zones

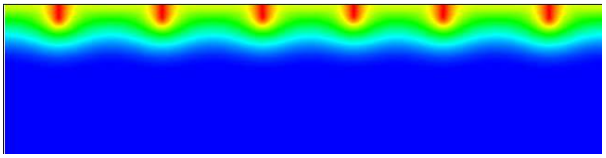

(d) the damage parameter grows until 1 in the midline of these zones whose width remains of the order of η_n

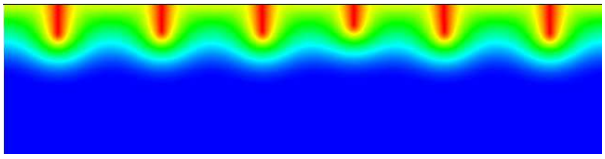

(e) the length of all the damage bands grows

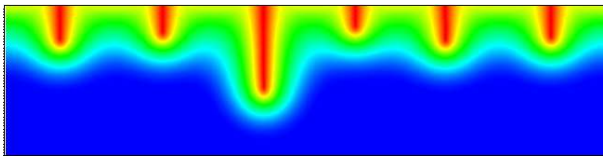

(f) some damage bands stop to propagate whereas the other ones continue

Figure 2: Main stages captured by the alternate minimization algorithm for "short" times in the thermal shock problem. A homogeneous material at uniform temperature is exposed at a smaller temperature at $t = 0$

the body a crack selection mechanism appears. The nucleation phase is indeed controlled by the critical stress, whereas the propagation phase depends on the material's toughness. The results are confronted to experimental data from ceramics. In three-dimensional simulations cracks form an hexagonal pattern which also follows a coarsening phenomenon. Even more impressive, for thin slabs the limit between two and three-dimensional behavior is captured. Extensions to gas storage caverns and composite materials exhibit the robustness of the method and the results.

Chapter 1

The variational approach to gradient damage models and fracture

Contents

In this chapter the construction of the variational approach to damage and the necessary hypothesis to capture brittle fracture is presented. Using arguments based on a work property, the fact that the constitutive relation is standard is justified. Then the evolution law based on the three ground principle of irreversibility, stability and energy balance is introduced. The bulk energy density is supposed to depend on the gradient of the damage variable, which allows to *control* the localization process inherent to softening behaviors. The main characteristics of a localized damage band are mentioned. These models are used in the framework of the variational approach to fracture which is called to mind as well as its numerical implementation. Most results of this chapter have already been published and the only claim of novelty is taking into account the thermal effects. The link between the work property and the standard formulation go back to the 80's [Marigo 1981, Marigo 1989]. The variational formulation to brittle fracture has been introduced in the 90's by [Francfort & Marigo 1998] and has been regularized following the initial work

by [Ambrosio 1990] primely in [Bourdin *et al.* 2000]. The reinterpretation as a gradient damage model [Marigo 2000] and thorough investigate more recently [Benallal & Marigo 2007, Pham & Marigo 2010a, Pham & Marigo 2010b, Pham & Marigo 2013].

1.1 General hypothesis and construction

In this thesis, the evolution of damage is assumed to be the only dissipative mechanisms. Thus other dissipative processes such as plasticity are neglected. The state $\mathfrak{s}$ of the material is given by the four internal variables, the strain $\boldsymbol{\varepsilon}$ defined as the symmetric gradient of the displacement $\mathbf{u}$, the temperature T, the damage variable α, and the gradient of the damage variable $\mathbf{g} = \nabla\alpha$. Thus $\mathfrak{s} = (\boldsymbol{\varepsilon}(\mathbf{u}), \mathrm{T}, \alpha, \nabla\alpha)$. Therefore, the material behavior is *non local* in the sense that it depends on the gradient of damage [Pijaudier-Cabot & Bazant 1987, Comi 1999]. The damage variable represents the degradation of the material such as micro-defects or micro-cracks. Furthermore it is assumed that a scalar is sufficient to represent this state and that the variable evolves between 0 and an ultimate state α_m (strictly positive) after which it does not evolve any more. These two extremal values 0 and α_m correspond to the sound and the totally damaged material. The choice of the damage variable α is arbitrary, yet a change of variable is always possible. The goal of this section is to justify that the bulk energy density of the material is the function of state $W : \mathfrak{s} = (\boldsymbol{\varepsilon}, \mathrm{T}, \alpha, \mathbf{g}) \mapsto W(\boldsymbol{\varepsilon}, \mathrm{T}, \alpha, \mathbf{g})$. The dual quantities associated with the state variables are respectively the stress tensor $\boldsymbol{\sigma}$, the entropy s, the energy release rate density Y and the damage flux vector $\mathbf{q}$:

$$\boldsymbol{\sigma} = \frac{\partial W}{\partial \boldsymbol{\varepsilon}}(\boldsymbol{\varepsilon}, \mathrm{T}, \alpha, \mathbf{g}), \quad s = -\frac{\partial W}{\partial \mathrm{T}}(\boldsymbol{\varepsilon}, \mathrm{T}, \alpha, \mathbf{g}) \quad \mathsf{Y} = -\frac{\partial W}{\partial \alpha}(\boldsymbol{\varepsilon}, \mathrm{T}, \alpha, \mathbf{g}), \quad \mathbf{q} = \frac{\partial W}{\partial \mathbf{g}}(\boldsymbol{\varepsilon}, \mathrm{T}, \alpha, \mathbf{g}). \tag{1.1}$$

1.1.1 State functions, energies and dual quantities

Considering an elementary volume, the variable which can be controlled are the strain and the temperature $\mathfrak{q} = (\boldsymbol{\varepsilon}, \mathrm{T})$ and one notes $\mathfrak{Q}(\mathfrak{q}, \alpha)$ the force function associated.

Hypothesis 1 (Admissible deformation and temperature field)**.** *The admissible strain and temperature lie in an open connected subset of* $\mathbb{M}_s \times \mathbb{R}$ *defined by the yield function* $\phi(\boldsymbol{\varepsilon}, \mathrm{T}, \alpha)$

$$\mathcal{R}(\alpha) := \{\boldsymbol{\varepsilon} \in \mathbb{M}_s, \mathrm{T} \in \mathbb{R} \quad | \quad \phi(\boldsymbol{\varepsilon}, \mathrm{T}, \alpha) \leq 0\}$$

Furthermore a reference temperature T_0 *such that the vanishing strain belongs to this subset is assumed to exist.*

This hypothesis can be justified hereafter the construction of the damage model. It is based on an homogenization argument and will be sketched out in Appendix A. Drucker-Ilyushin postulate is extended to cases where the evolution is not isothermal:

Hypothesis 2 (Work property). *For any strain and temperature evolution $t \mapsto \boldsymbol{\varepsilon}(t), \quad t \mapsto \mathrm{T}(t)$ compatible strain and temperature path imposed at the material point M. The strain and temperature work on this cycle is defined by:*

$$\mathcal{W} := \int_0^1 \mathfrak{Q}(\mathfrak{q}(t), \alpha(t)) \cdot \dot{\mathfrak{q}}(t)\, \mathrm{d}t \tag{1.2}$$

and is positive in any admissible strain-temperature cycle starting from equilibrium state.

A state is said to be at equilibrium if it evolves only if the configuration evolves. From Drucker-Ilyushin postulate one can prove that a material is necessarily hyperelastic at a given damage state α, derives from a potential ψ dual of the controllable variables:

$$\mathfrak{Q} = (\boldsymbol{\sigma}, s) \qquad \mathfrak{Q} = \frac{\partial \psi}{\partial \mathfrak{q}}(\mathfrak{s})$$

this leads us to make the following assumption:

Hypothesis 3 (Hyperelastic behavior at fix damage). *The elastic energy density is assumed to be strictly convex for a given damage $\alpha < \alpha_m$.*

$$\psi(k\boldsymbol{\varepsilon}, \mathrm{T}, \alpha) = k^2 \psi(\boldsymbol{\varepsilon}, \mathrm{T}, \alpha) \quad \forall k \geq 0 \qquad \forall \boldsymbol{\varepsilon} \in \mathbb{M}_s, \quad \forall \alpha \in [0, \alpha_m) \quad \forall \mathrm{T} \in \mathbb{R}.$$

Moreover the material's energy release rate as the damage increases reads:

$$\frac{\partial \psi}{\partial \alpha}(\boldsymbol{\varepsilon}, \mathrm{T}, \alpha) \leq 0 \quad \forall \boldsymbol{\varepsilon} \in \mathbb{M}_s, \quad \forall \alpha \in [0, \alpha_m), \quad \forall \mathrm{T} \in \mathbb{R}.$$

The homogeneity property can be justified by the theory of homogenization [Marigo 1985] in the case where there is no contact between the lips of the microcracks.

1.1.2 Restriction from the work property

The results from [Marigo 1989] are extended to the thermo-elasto-damage material. A generic path (Fig. 1.1) is considered having the following properties: (o) the initial state $\mathfrak{q}_0$ belongs to the elastic-domain, (i) the material is loaded till a point $\mathfrak{q}_1$ situated on the surface $\partial\mathcal{R}$; (ii) an infinitively small increase $\delta\mathfrak{q}$ of the controllable variables $\mathfrak{q} = (\boldsymbol{\varepsilon}, \mathrm{T})$ such that $\mathfrak{q}_0 + \delta\mathfrak{q}$ remains in the elastic domain; (iii) elastic unloading from $\mathfrak{q}_1 + \delta\mathfrak{q}$ to $\mathfrak{q}_0$, where the damage remains constant. (A small increase in the hardening is considered sufficiently small such that $\boldsymbol{\varepsilon}_0$ remains in the elastic domain.) No assumption is made on $\delta\mathfrak{q}$ which may take any of the form between $(\delta\boldsymbol{\varepsilon}, 0)$, $(0, \delta\mathrm{T})$ and $(\delta\boldsymbol{\varepsilon}, \delta\mathrm{T})$.

Then the strain work can be decomposed as the sum on each part of the cycle $\mathcal{W} = \mathcal{W}_1 + \mathcal{W}_2 + \mathcal{W}_3$. To pass from $\mathfrak{q}_0$ to $\mathfrak{q}_1$, the work $\mathcal{W}_1$ is purely elastic and thus $\mathcal{W}_1 = \int_0^1 \mathfrak{Q} \cdot \dot{\mathfrak{q}}\, \mathrm{d}t = \psi(\mathfrak{q}_1, \alpha_0) - \psi(\mathfrak{q}_0, \alpha_0)$. In the same manner the work on the last phase, which is an elastic unloading, reads $\mathcal{W}_3 = \int_1^0 \mathfrak{Q} \cdot \dot{\mathfrak{q}}\, \mathrm{d}s =$

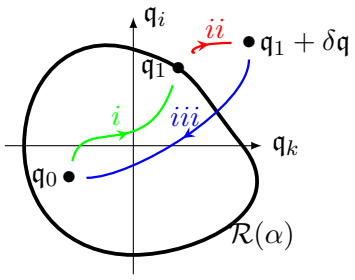

Figure 1.1: Specific path in the controllable variable space

$\psi(\mathfrak{q}_0, \alpha_0 + \delta\alpha) - \psi(\mathfrak{q}_1 + \delta\mathfrak{q}, \alpha_0 + \delta\alpha)$. The second step is irreversible $\mathcal{W}_2 = \psi_{,\mathfrak{q}}(\boldsymbol{\varepsilon}_1, \alpha_0) \cdot \delta\mathfrak{q} + o(\delta\mathfrak{q})$. At the first order in $\delta\mathfrak{q}$, the positivity of the work in this cycle leads to:

$$\left(\frac{\partial\psi}{\partial\alpha}(\mathfrak{q}_0, \alpha_0) - \frac{\partial\psi}{\partial\alpha}(\mathfrak{q}_1, \alpha_0)\right) \delta\alpha \geq 0. \tag{1.3}$$

Let us stress that (1.3) is valid for any $\mathfrak{q}_0 \in \mathcal{R}(\alpha)$ and $\mathfrak{q}_1 \in \partial\mathcal{R}(\alpha)$. From this inequality, one deduces the evolution of the damage parameter:

1. *Irreversibility.* Taking $\mathfrak{q}_0 = (0, \mathrm{T}_0)$ in (1.3) and as $-\partial_{,\alpha}\psi(\mathfrak{q}_1, \alpha_0)$ is positive according to Hypothesis 3, (1.3) leads to $\dot{\alpha} \geq 0$, under the assumption of a regular evolution in time.

2. *Evolution from the thermodynamical force.* The yield function is now established, $w(\alpha) = -\partial_{,\alpha}\psi(\mathfrak{q}_1, \alpha_0)$ and thus (1.3) becomes

$$\forall \mathfrak{q}_0 \in \mathcal{R}(\alpha) \quad -\partial_{,\alpha}\psi(\mathfrak{q}_0, \alpha) \leq w(\alpha)$$

Thus the following has been established

Proposition 1 (Evolution of the damage parameter)**.** *In any cycle verifying the work property the damage is not decreasing and the evolution of damage α is governed by the* Kuhn-Tucker *conditions:*

$$\dot{\alpha} \geq 0, \qquad -\frac{\partial\psi}{\partial\alpha}(\boldsymbol{\varepsilon}, \mathrm{T}, \alpha) - w(\alpha) \leq 0 \qquad \left(-\frac{\partial\psi}{\partial\alpha}(\boldsymbol{\varepsilon}, \mathrm{T}, \alpha) - w(\alpha)\right) \dot{\alpha} = 0 \tag{1.4}$$

Thus the evolution of damage is formulated in terms of an elastic energy release rate and the equation of the surface is given by

$$\phi(\boldsymbol{\varepsilon}, \mathrm{T}, \alpha) := -\frac{\partial\psi}{\partial\alpha}(\boldsymbol{\varepsilon}, \mathrm{T}, \alpha) - w(\alpha)$$

A major consequence of this variational transcription is that the internal (*i.e.* strain and temperature) work $\mathcal{W}$ is a state function, *i.e.* the work to evolve from the reference temperature T_0 and vanishing strain and damage to a state $\boldsymbol{\varepsilon}, \mathrm{T}, \alpha$ does not depend on the path. Indeed, considering a path

$$[0, 1] \mapsto \mathbb{M}_s \times \mathbb{R}, \qquad t \to \boldsymbol{\varepsilon}(t), \mathrm{T}(t)$$

such that $(\boldsymbol{\varepsilon}(0), \mathrm{T}(0)) = (0, \mathrm{T}_0)$ and $(\boldsymbol{\varepsilon}(1), \mathrm{T}(1)) = (\boldsymbol{\varepsilon}, \mathrm{T})$, at each time t the damage is denoted $\bar{\alpha}(t)$ and is assumed to be sound in the initial state and take the value $\bar{\alpha}(1)$in the final state. During this transformation the work of the temperature and strain reads

$$\mathcal{W} = \int_0^1 \mathfrak{Q}(\mathfrak{q}(t), \alpha(t)) \cdot \dot{\mathfrak{q}}(t)\, \mathrm{d}t$$

Denoting $\mathsf{w}(\alpha)$ the antiderivative of w vanishing in 0 and according to (1.4):

$$\frac{d}{dt}\left(\psi(\boldsymbol{\varepsilon}(t), \mathrm{T}(t), \bar{\alpha}(t)) + \mathsf{w}(\bar{\alpha}(t))\right) = \psi_{,\boldsymbol{\varepsilon}}(\boldsymbol{\varepsilon}(t), \mathrm{T}(t), \bar{\alpha}(t)) \cdot \dot{\boldsymbol{\varepsilon}}(t) + \psi_{,\mathrm{T}}(\boldsymbol{\varepsilon}(t), \mathrm{T}(t), \bar{\alpha}(t)) \cdot \dot{\mathrm{T}}(t)$$

The strain and temperature work is thus the integral of an exact derivative

$$\mathcal{W} = \int_0^1 \frac{d}{dt}\left(\psi(\boldsymbol{\varepsilon}(t), \mathrm{T}(t), \bar{\alpha}(t)) + \mathsf{w}(\bar{\alpha}(t))\right)\, \mathrm{d}t.$$

Given the values at the extremity of the path:

$$\mathcal{W}(\boldsymbol{\varepsilon}, \mathrm{T}, \alpha) = \psi(\boldsymbol{\varepsilon}, \mathrm{T}, \alpha) + \mathsf{w}(\alpha).$$

Accordingly, the local bulk energy density is defined by

$$W_0(\boldsymbol{\varepsilon}, \mathrm{T}, \alpha) := \mathcal{W}(\boldsymbol{\varepsilon}, \mathrm{T}, \alpha).$$

The bulk energy density W is assumed to also depend on the gradient of the damage $\mathbf{g} = \nabla\alpha$ and to remain a state function that verifies

$$W(\boldsymbol{\varepsilon}, \mathrm{T}, \alpha, 0) = W_0(\boldsymbol{\varepsilon}, \mathrm{T}, \alpha)$$

and thus one can define (1.1) which reads:

$$\boldsymbol{\sigma} = \frac{\partial W}{\partial \boldsymbol{\varepsilon}}(\boldsymbol{\varepsilon}, \mathrm{T}, \alpha, \mathbf{g}), \quad s = -\frac{\partial W}{\partial \mathrm{T}}(\boldsymbol{\varepsilon}, \mathrm{T}, \alpha, \mathbf{g}) \quad \mathsf{Y} = -\frac{\partial W}{\partial \alpha}(\boldsymbol{\varepsilon}, \mathrm{T}, \alpha, \mathbf{g}), \quad \mathbf{q} = \frac{\partial W}{\partial \mathbf{g}}(\boldsymbol{\varepsilon}, \mathrm{T}, \alpha, \mathbf{g}).$$

1.1.3 Dissipation and thermal effects

The second thermodynamic principle under the form of Clausius-Duhem inequality reduces to the condition $0 \leq \dfrac{1}{\mathrm{T}}\mathbf{q}_\mathrm{T} \cdot \nabla\mathrm{T} \quad \forall(\boldsymbol{\varepsilon}, \mathrm{T}, \alpha, \nabla\mathrm{T})$, where $\mathbf{q}_\mathrm{T}$ stands for the local heat flux density. Indeed the dissipation is given by

$$\begin{aligned}
\mathsf{D} &= \sigma \cdot \dot{\boldsymbol{\varepsilon}} - \dot{\psi} - s\dot{\mathrm{T}} + \frac{1}{\mathrm{T}}\mathbf{q}_\mathrm{T} \cdot \nabla\mathrm{T} \\
&= \sigma \cdot \dot{\boldsymbol{\varepsilon}} - \left(\frac{\partial\psi}{\partial\boldsymbol{\varepsilon}}\dot{\boldsymbol{\varepsilon}} + \frac{\partial\psi}{\partial\alpha}\dot{\alpha} + \frac{\partial\psi}{\partial\mathrm{T}}\dot{\mathrm{T}}\right) - s\dot{\mathrm{T}} + \frac{1}{\mathrm{T}}\mathbf{q}_\mathrm{T} \cdot \nabla\mathrm{T} \\
&= \mathsf{w}(\alpha)\dot{\alpha} + \frac{1}{\mathrm{T}}\mathbf{q}_\mathrm{T} \cdot \nabla\mathrm{T}
\end{aligned}$$

Remark 1. *The gradient of the temperature* $\nabla \mathrm{T}$ *could have been introduced as an internal variable. But the Clausius-Duhem inequality, which should be true for any process would lead us to prove that* W *is independent of* $\nabla \mathrm{T}$*. Furthermore,* W *is independent of the displacement and the skew-symmetric part of the gradient of the displacement.*

The damage process is assumed to be dissipative and thus the increase of α is source of a dissipation process which should lead to a volumetric temperature source in the bulk. In the case of concrete [Huon *et al.* 2009] measure that the elevation in temperature is of $0.5°C$ thus this temperature source can be neglected in front of the loading which will be considered in Chapters 3-4. Thus, the temperature T is now considered to impose a loading $\boldsymbol{\varepsilon}^{\mathrm{th}}$ which can be taken into account in more generic term of pre-strain $\boldsymbol{\varepsilon}^0$. Furthermore, this prestrain is assumed to be considered in the configuration work through the elastic strain $\boldsymbol{\varepsilon}^e = \boldsymbol{\varepsilon} - \boldsymbol{\varepsilon}^0$. Thus the four internal variables are now $\boldsymbol{\varepsilon}, \boldsymbol{\varepsilon}^0, \alpha, \nabla\alpha$ and W can be referred to as the strain work and one has:

$$\begin{cases} \mathfrak{s} = (\boldsymbol{\varepsilon}, \mathrm{T}, \alpha, \mathbf{g}) \mapsto W(\boldsymbol{\varepsilon}, \mathrm{T}, \alpha, \mathbf{g}) \\ \mathfrak{s} = (\boldsymbol{\varepsilon}^e, \alpha, \mathbf{g}) \mapsto W(\boldsymbol{\varepsilon}^e, \alpha, \mathbf{g}) \end{cases}$$

will be indiscriminately used. The local bulk energy density is the the sum of two terms

$$W_0(\boldsymbol{\varepsilon}, \mathrm{T}, \alpha) = \psi(\boldsymbol{\varepsilon}, \mathrm{T}, \alpha) + \mathsf{w}(\alpha)$$

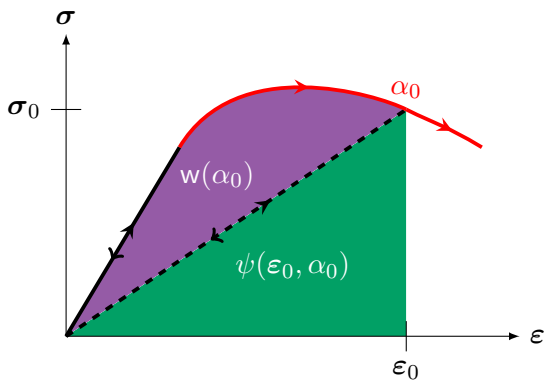

Figure 1.2: Dissipation an elastic energy for linear elasticity in the case of a hardening then softening damage law. Green the elastic stores energy $\psi(\boldsymbol{\varepsilon}, \alpha)$. Purple the dissipated energy $\mathsf{w}(\alpha)$. Red line damaging path. Full black line: initial loading. Dashed black line: Unloading - Loading path for the damage state α_0

1.1.4 Hardening and softening properties

The underlying local behavior is characterized by the function W_0 defined by $W_0(\boldsymbol{\varepsilon}^e, \alpha) = W(\boldsymbol{\varepsilon}^e, \alpha, 0)$. The elastic domain in the strain space and in the stress space are respectively defined by

$$\mathcal{R}(\alpha) = \left\{ \boldsymbol{\varepsilon}^e \in \mathbb{M}_s \ : \ \frac{\partial W_0}{\partial \alpha}(\boldsymbol{\varepsilon}^e, \alpha) \geq 0 \right\}, \qquad \mathcal{R}^*(\alpha) = \left\{ \boldsymbol{\sigma} \in \mathbb{M}_s \ : \ \frac{\partial W_0^*}{\partial \alpha}(\boldsymbol{\sigma}, \alpha) \leq 0 \right\} \tag{1.5}$$

where $W_0^*(\boldsymbol{\sigma},\alpha) = \sup_{\boldsymbol{\varepsilon}^e\in\mathbb{M}_s}\left\{\boldsymbol{\sigma}\cdot\boldsymbol{\varepsilon}^e - W_0(\boldsymbol{\varepsilon}^e,\alpha)\right\}$ and $\mathbb{M}_s$ denotes the space of symmetric tensors.

Definition 1. *For a given damage state α, a material is said to be* strain hardening *if $\alpha\mapsto\mathcal{R}(\alpha)$ is increasing,* stress hardening *(or* hardening*) if $\alpha\mapsto\mathcal{R}^*(\alpha)$ is increasing and* softening *if $\alpha\mapsto\mathcal{R}^*(\alpha)$ is decreasing.*

The belonging of a state to the elastic domain as well as the the hardening and softening are now expressed in term of stability principle:

Property 1 (Hardening and Softening)**.** *A state $(\boldsymbol{\varepsilon}^e,\alpha)$ belongs to the elastic domain and is hardening in strain if and only if*

$$W_0(\boldsymbol{\varepsilon}^e,\alpha)\leq W_0(\boldsymbol{\varepsilon}^e,\beta),\qquad \forall\beta\in[0,\alpha_m)$$

A state $(\boldsymbol{\sigma},\alpha)$ belongs to the elastic domain and is hardening in stress if and only if

$$W_0^*(\boldsymbol{\sigma},\alpha)\leq W_0^*(\boldsymbol{\sigma},\beta),\qquad \forall\beta\in[0,\alpha_m)$$

Proof. In the strain space the stability condition reads as

$$\frac{\partial W_0}{\partial\alpha}(\boldsymbol{\varepsilon}^e,\beta)\beta+\frac{\partial^2 W_0}{\partial\alpha^2}(\boldsymbol{\varepsilon}^e,\beta)\beta\beta\geq 0\qquad\forall\beta\in[0,\alpha_m)$$

First order stability criterion gives the damage criterion (1.5). When the equality holds in the first order condition, *i.e.* the state is on the surface, the second order stability condition gives that $\alpha\mapsto\mathcal{R}(\alpha)$ is increasing and thus is hardening in stress. The same argumentation can be done in the case of the stress space $\mathcal{R}^*(\alpha)$. □

Thus, the hardening and softening properties are a second order stability condition on the bulk energy density. They can also be reformulated in terms of convexity properties [Pham & Marigo 2010a].

Definition 2. *A material is said to be strongly brittle material, see [Pham & Marigo 2013, Hypothesis 1] if the material has a softening behavior as well as a finite dissipated energy during any process where the damage evolves from 0 to α_m.*

Accordingly in the case of a strongly brittle material the elastic domain in the strain space $\mathcal{R}(\alpha)$ is an increasing function of α while the elastic domain in the stress space $\mathcal{R}^*(\alpha)$ is a decreasing function of α. A linearized theory in $\boldsymbol{\varepsilon}^e$ and $\mathbf{g}$ is considered for *the bulk energy density.* The neighborhood of the state $(0,\alpha,0)$ is studied:

$$W(\boldsymbol{\varepsilon}^e,\alpha,\mathbf{g}) = \mathsf{w}(\alpha)+\boldsymbol{\sigma}_0(\alpha)\cdot\boldsymbol{\varepsilon}+\Lambda_1(\alpha)\cdot\mathbf{g}+\psi(\boldsymbol{\varepsilon}^e,\alpha)+\Lambda_2(\alpha)\boldsymbol{\varepsilon}^e\cdot\mathbf{g}+\boldsymbol{\Lambda}_3(\alpha)\mathbf{g}\cdot\mathbf{g},\tag{1.6}$$

considering linearized elasticity

$$\psi(\boldsymbol{\varepsilon}^e,\alpha)=\frac{1}{2}\mathsf{A}(\alpha)\boldsymbol{\varepsilon}^e\cdot\boldsymbol{\varepsilon}^e$$

and the terms of the expansions are all functions of the damage state α around which the elasticity is linearized. The term $\mathsf{w}(\alpha)$ is identified with the dissipated energy in a homogeneous process. The prestress term $\boldsymbol{\sigma}_0(\alpha)$ can be chosen to be fixed to zero.

Let us now considers the terms $\Lambda_{i\in\{1,2,3\}}$ corresponding to the gradient terms $\mathbf{g} = \nabla\alpha$. They are tensors of different orders. Under the assumption that damage is isotropic (and thus α is scalar) Λ_1, Λ_2 vanish and Λ_3 is proportional to the identity. The goal of the regularization being to penalize strong gradients the tensor $\boldsymbol{\Lambda}_3$ should be positively defined, thus $\boldsymbol{\Lambda}_3(\alpha) = \Lambda(\alpha)\mathbf{I}$. Finally the strain work only can be determined by three functions of the damage $\mathsf{A}, \mathsf{w}, \Lambda$

$$W(\boldsymbol{\varepsilon}^e, \alpha, \mathbf{g}) = \frac{1}{2}\mathsf{A}(\alpha)\boldsymbol{\varepsilon}^e \cdot \boldsymbol{\varepsilon}^e + \mathsf{w}(\alpha) + \Lambda(\alpha)\nabla\alpha\nabla\alpha \tag{1.7}$$

Thus, the identification of the damage model requires to define the three functions of the damage variable.

Remark 2 (Choice of the damage variable)**.** *In the case of a strongly brittle material it is always possible to chose α such that it evolves between 0 and 1. Another interesting choice from a practical viewpoint consists in changing the damage variable so that the mutiplicative factor $\Lambda(\alpha)$ becomes a constant. From now on this change of variable will have been assumed to be done.*

Furthermore between the two functions A, w and Λ the dimension difference is the square of a length, thus the length η is introduced

$$W(\boldsymbol{\varepsilon}^e, \alpha, \mathbf{g}) = \frac{1}{2}\mathsf{A}(\alpha)\boldsymbol{\varepsilon}^e \cdot \boldsymbol{\varepsilon}^e + \mathsf{w}(\alpha) + \Lambda\eta^2\nabla\alpha\nabla\alpha \tag{1.8}$$

where Λ is independent of α and has the dimension of a pressure such that η has the dimension of a length. By doing this a characteristic dimension has been introduced to our problem which obviously depends on the choice of Λ. In the case of the family of damage models given by the bulk energy density (1.8), in order for the softening properties to be satisfied, $\alpha \mapsto \mathsf{A}'(\alpha)/\mathsf{w}'(\alpha)$ and $\alpha \mapsto \mathsf{C}'(\alpha)/\mathsf{w}'(\alpha)$ must be increasing, where $\mathsf{C} = \mathsf{A}^{-1}$ is the compliance tensor.

1.2 Evolution of gradient damage models in a structure

The evolution of the damage parameter given in Proposition 1 yet it says nothing of the evolution in the structure. One should keep in mind that the stability is inherently depending on the geometry and the loading applied to a structure and exceed the material properties.

1.2.1 Setting of the gradient damage model

Let us consider a homogeneous body whose natural reference configuration is the open connected bounded set $\Omega \subset \mathbb{R}^3$ of characteristic size L. The body is submitted to a time dependent loading which

consists of a density of volume forces $\mathbf{f}_t$, a density of surface forces $\mathbf{F}_t$ prescribed on the part $\partial_N\Omega$ of the boundary and prescribed displacements $\mathbf{U}_t$ on the complementary part $\partial_D\Omega$ of the boundary, t denoting the time parameter. The potential of the given external forces at time t can read as the following linear form $\mathcal{W}_t^e$ defined on the set $\mathcal{C}_t$ of kinematically displacement fields

$$\mathcal{W}_t^e(\mathbf{v}) := \int_\Omega \mathbf{f}_t \cdot \mathbf{v}\,\mathrm{d}\mathbf{x} + \int_{\partial_N\Omega} \mathbf{F}_t \cdot \mathbf{v}\,\mathrm{d}s$$

The kinematically admissible displacement fields is formerly introduced

$$\mathcal{C}_t = \big\{\mathbf{v} \,:\, \mathbf{v} = \mathbf{U}_t \text{ on } \partial_D\Omega\big\},$$

and also introduce the set of admissible damage fields

$$\mathcal{D} := \{\beta \,:\, 0 \le \beta \le \alpha_m \text{ a.e. in } \Omega\}.$$

thus $\mathcal{C}_t = \mathcal{C}_t + \mathbf{U}_t$ is a linear space and is time dependent.

Remark 3 (Regularity of the admissible displacement and damage field)**.** *The choice of the functional space raises in issue. When $\alpha = \alpha_m$ the presentation of functional spaces will remain informal as above. The fields are assumed sufficiently smooth so that all calculations make sense. A natural requirement is that the total energy is finite at each time, the damage field should belong to $L^\infty(\Omega) \cap H^1(\Omega)$. Because of the lost of stiffness when $\alpha = 1$, the question is more difficult for the displacement field. A precise statement of the of the functional space remains out of the scope of this dissertation. If $\alpha(\mathbf{x}) < \alpha_m$ then the bulk density is defined as soon as the fields belong to $H^1(\Omega)$ and the admissible fields read*

$$\mathcal{C}_t = \big\{\mathbf{v} \in H^1(\Omega)\times H^1(\Omega) \,:\, \mathbf{v} = \mathbf{U}_t \text{ on } \partial_D\Omega\big\} \qquad \mathcal{D} = \{\beta \in H^1(\Omega) \,:\, 0 \le \beta < \alpha_m \text{ a.e. in } \Omega\}.$$

The law of evolution of the damage in the body is written in a variational form and based on the definition of the total energy of the body associated with admissible states. Specifically, if $(\mathbf{v}, \beta)$ denotes a pair of admissible displacement and damage fields at time t, *i.e.* if $\mathbf{v} \in \mathcal{C}_t$ and $\beta \in \mathcal{D}$ then the total energy of the body at time t in this state is given by

$$\mathcal{P}_t(\mathbf{v}, \beta) := \int_\Omega W(\boldsymbol{\varepsilon}(\mathbf{v}) - \boldsymbol{\varepsilon}_t^0, \beta, \nabla\beta)\,\mathrm{d}\mathbf{x} - \mathcal{W}_t^e(\mathbf{v}) \tag{1.9}$$

where $\boldsymbol{\varepsilon}(\mathbf{v})$ denotes the symmetrized gradient of $\mathbf{v}$. Following the variational approach presented in [Pham & Marigo 2010a] and [Pham & Marigo 2010b], the evolution of the damage in the body is governed by the three principles of irreversibility, stability and energy balance. Precisely the evolution follows:

Hypothesis 4 (**The damage evolution law**)**.** *Specifically these conditions read as follows:*

(IR) **Irreversibility:** *$t \mapsto \alpha_t$ must be non decreasing and, at each time $t \ge 0$, $\alpha_t \in \mathcal{D}$.*

(ST) **Stability:** *At each time $t > 0$, the real state $(\mathbf{u}_t, \alpha_t)$ must be stable in the sense that for all $\mathbf{v} \in \mathcal{C}_t$ and all $\beta \in \mathcal{D}$ such that $\beta \geq \alpha_t$, there exists $\bar{h} > 0$ such that for all $h \in [0, \bar{h}]$*

$$\mathcal{P}_t(\mathbf{u}_t + h(\mathbf{v} - \mathbf{u}_t), \alpha_t + h(\beta - \alpha_t)) \geq \mathcal{P}_t(\mathbf{u}_t, \alpha_t). \tag{1.10}$$

(EB) **Energy balance:** *At each time $t > 0$ the following energy balance must hold:*

$$\mathcal{P}_t(\mathbf{u}_t, \alpha_t) = \mathcal{P}_0(\mathbf{u}_0, \alpha_0) + \int_0^t \left(\int_\Omega \boldsymbol{\sigma}_s \cdot \boldsymbol{\varepsilon}(\dot{\mathbf{U}}_s) - \boldsymbol{\sigma}_s \cdot \dot{\boldsymbol{\varepsilon}}_t^0 \, \mathrm{d}\mathbf{x} - \mathcal{W}_s^e(\dot{\mathbf{U}}_s) - \dot{\mathcal{W}}_s^e(\mathbf{u}_s) \right) \mathrm{d}s. \tag{1.11}$$

where:

- α_0 denotes the given damage state at the beginning of the loading process
- $\mathbf{u}_0$ is the associated displacement field obtained by solving the elastostatic problem at time 0: $\mathbf{u}_0 = \operatorname{argmin}_{\mathbf{v} \in \mathcal{C}_0} \mathcal{P}_0(\mathbf{v}, \alpha_0)$
- $\boldsymbol{\sigma}_s$ denotes the real stress field at time s and is given by (1.1)
- $\dot{\mathbf{U}}_s$ is the rate of a given, but yet arbitrarily chosen, admissible displacement field at time s
- $\dot{\boldsymbol{\varepsilon}}_s^0$ is the rate of the imposed strain at time s
- $\dot{\mathcal{W}}_s^e$ denotes the linear form associated with the rate of the prescribed volume or surface forces at time s and reads

$$\dot{\mathcal{W}}_s^e(\mathbf{v}) = \int_\Omega \dot{\mathbf{f}}_s \cdot \mathbf{v} \, \mathrm{d}\mathbf{x} + \int_{\partial_N \Omega} \dot{\mathbf{F}}_s \cdot \mathbf{v} \, \mathrm{d}s$$

In essence this formulation falls in the modern mathematical treatment of rate independent processes [Mielke 2006]. Note that the concept of stability adopted here is that of *directional* stability. In this sense it is a weaker condition than global stability, and this will play a major role in this thesis. For a given admissible direction $(\mathbf{v}, \beta)$, the inequality (1.10) must hold for sufficiently small h, this neighborhood depending on the direction. Accordingly, for a given direction considering small h and expanding the energy of the perturbed state with respect to h up to the second order, the inequality (1.10) becomes

$$0 \leq \mathcal{P}_t'(\mathbf{u}_t, \alpha_t)(\mathbf{v} - \mathbf{u}_t, \beta - \alpha_t) + \frac{h}{2} \mathcal{P}_t''(\mathbf{u}_t, \alpha_t)(\mathbf{v} - \mathbf{u}_t, \beta - \alpha_t) + o(h), \tag{1.12}$$

where $\mathcal{P}_t'$ and $\mathcal{P}_t''$ denote the first and second directional derivatives of $\mathcal{P}_t$ and $o(h)$ higher order terms in h. Precisely the first derivative of the total energy reads

$$\mathcal{P}_t'(\mathbf{u}_t, \alpha_t)(\mathbf{v}, \beta) = \int_\Omega \Big(\boldsymbol{\sigma}_t \cdot \boldsymbol{\varepsilon}(\mathbf{v}) - \mathsf{Y}_t \cdot \beta + \mathbf{q}_t \cdot \nabla \beta \Big) \, \mathrm{d}\mathbf{x} - \mathcal{W}_t^e(\mathbf{v}), \tag{1.13}$$

where $\boldsymbol{\sigma}_t$, Y_t and $\mathbf{q}_t$ denote respectively the stress tensor, the energy release rate density and the damage flux vector at time t which are given in terms of the current state by the constitutive relations (1.1).

Passing to the limit when h goes to 0 in (1.12) and using the fact that $\mathcal{C}_t$ is a linear space, one immediately deduces that the stability condition (1.10) is satisfied *only if*, at each time, the body is at equilibrium and the damage criterion is satisfied. Specifically, these necessary conditions are the weak form of the equilibrium

$$\int_\Omega \boldsymbol{\sigma}_t \cdot \boldsymbol{\varepsilon}(\mathbf{v})\,\mathrm{d}\mathbf{x} = \mathcal{W}_t^e(\mathbf{v}), \quad \forall \mathbf{v} \in \mathcal{C}_t, \tag{1.14}$$

and the weak form of the damage criterion

$$\int_\Omega \left(-\mathsf{Y}_t \cdot (\beta - \alpha_t) + \mathbf{q}_t \cdot \nabla(\beta - \alpha_t)\right)\,\mathrm{d}\mathbf{x} \geq 0, \quad \forall \beta \in \mathcal{D} \ : \ \beta \geq \alpha_t. \tag{1.15}$$

The two conditions (1.14)-(1.15) can be seen as the *first order stability conditions*. They are necessary but not always sufficient in order for (1.10) to hold. More precisely, if the direction β is such that the inequality is strict in (1.15), then (1.12) is satisfied for h small enough and hence the stability is ensured in this direction. However, if the direction β is such that the inequality is an equality in (1.15), then (1.12) requires that the second derivative be non negative in order that the state be stable with respect to this direction of perturbation (and the stability in this direction is ensured if the second derivative is positive). The following has been obtained

Proposition 2 (Second order stability conditions)**.**

1. *When* $\mathcal{P}_t'(\mathbf{u}_t, \alpha_t)(\mathbf{v} - \mathbf{u}_t, \beta - \alpha_t) > 0$*, then* $(\mathbf{u}_t, \alpha_t)$ *is stable with respect to the direction of perturbation* $(\mathbf{v}, \beta)$*;*
2. *When* $\mathcal{P}_t'(\mathbf{u}_t, \alpha_t)(\mathbf{v} - \mathbf{u}_t, \beta - \alpha_t) = 0$*, then* $(\mathbf{u}_t, \alpha_t)$ *is stable with respect to the direction of perturbation* $(\mathbf{v}, \beta)$
   - *(a)* only if $\mathcal{P}_t''(\mathbf{u}_t, \alpha_t)(\mathbf{v} - \mathbf{u}_t, \beta - \alpha_t) \geq 0$ *(necessary condition)*
   - *(b)* if $\mathcal{P}_t''(\mathbf{u}_t, \alpha_t)(\mathbf{v} - \mathbf{u}_t, \beta - \alpha_t) > 0$ *(sufficient condition).*

Remark 4. *In the Hypothesis 4, the energy balance has been written under an integral form which allows for discontinuous time evolutions.*

By standard arguments of the calculus of variations [Dacorogna 2008] and by virtue of the hypothesis of regularity of the fields, one easily deduces from the first order stability conditions (1.14)–(1.15) the following

Proposition 3. *The first order stability conditions are satisfied if and only if the following local conditions hold:*

$$\operatorname{div} \boldsymbol{\sigma}_t + \mathbf{f}_t = \mathbf{0} \text{ in } \Omega \setminus \Omega_t^c, \qquad \boldsymbol{\sigma}_t \mathbf{n} = \mathbf{F}_t \text{ on } \partial_N \Omega, \qquad \boldsymbol{\sigma}_t \mathbf{n} = \mathbf{0} \text{ on } \partial \Omega_t^c, \tag{1.16}$$

$$\mathsf{Y}_t + \operatorname{div} \mathbf{q}_t \leq 0 \text{ in } \Omega \setminus \Omega_t^c, \qquad \mathbf{q}_t \cdot \mathbf{n} \geq 0 \text{ on } \partial\Omega. \tag{1.17}$$

where Ω_t^c *denotes the part of the domain, assumed not to evolve, such that* $\alpha = \alpha_m$*.*

In (1.16) the natural boundary arise not only on the surface of the domain but also on the interface between the damage part of the domain and the sound part.

In chapter 2 the case where Ω_t^c is a crack that evolves will be treated. Note that the two bulk conditions hold only in the uncracked part of the body. It remains to use energy balance (1.11). Owing to the smoothness assumption on the time evolution, taking the derivative of (1.11) with respect to t leads to

$$\begin{aligned}
0 &= \frac{d}{dt}\mathcal{P}_t(\mathbf{u}_t,\alpha_t) - \int_\Omega \boldsymbol{\sigma}_t\cdot\boldsymbol{\varepsilon}(\dot{\mathbf{U}}_t) - \boldsymbol{\sigma}_t\cdot\dot{\boldsymbol{\varepsilon}}_t^0\,\mathrm{d}\mathbf{x} - \mathcal{W}_t^e(\dot{\mathbf{U}}_t) - \dot{\mathcal{W}}_t^e(\mathbf{u}_t)\\
0 &= \frac{d}{dt}\int_{\Omega\setminus\Omega_t^c} W(\boldsymbol{\varepsilon}(\mathbf{u}_t)-\boldsymbol{\varepsilon}_t^0,\alpha_t,\nabla\alpha_t)\,\mathrm{d}\mathbf{x} - \int_{\Omega\setminus\Omega_t^c}\boldsymbol{\sigma}_t\cdot\left(\boldsymbol{\varepsilon}(\dot{\mathbf{U}}_t)-\dot{\boldsymbol{\varepsilon}}_t^0\right)\,\mathrm{d}\mathbf{x} - \mathcal{W}_t^e(\dot{\mathbf{u}}_t-\dot{\mathbf{U}}_t)\\
&= \int_{\Omega\setminus\Omega_t^c}\left(\boldsymbol{\sigma}_t\cdot\boldsymbol{\varepsilon}(\dot{\mathbf{u}}_t-\dot{\mathbf{U}}_t) - \mathsf{Y}_t\dot{\alpha}_t + \mathbf{q}_t\cdot\nabla\dot{\alpha}_t\right)\mathrm{d}\mathbf{x}\\
&= -\int_{\Omega\setminus\Omega_t^c}\left(\operatorname{div}\boldsymbol{\sigma}_t\cdot(\dot{\mathbf{u}}_t-\dot{\mathbf{U}}_t) + (\mathsf{Y}_t+\operatorname{div}\mathbf{q}_t)\dot{\alpha}_t\right)\mathrm{d}\mathbf{x} + \int_{\partial\Omega}\left(\boldsymbol{\sigma}_t\mathbf{n}\cdot\dot{\mathbf{u}}_t + \mathbf{q}_t\cdot\mathbf{n}\dot{\alpha}_t\right)\mathrm{d}s. \qquad (1.18)
\end{aligned}$$

Taking into account the equilibrium and the boundary conditions (1.16), the terms containing $\boldsymbol{\sigma}_t$ vanish in (1.18). Therefore, one gets

$$0 = -\int_\Omega (\mathsf{Y}_t+\operatorname{div}\mathbf{q}_t)\,\dot{\alpha}_t\,\mathrm{d}\mathbf{x} + \int_{\partial\Omega}\Lambda\eta^2\frac{\partial\alpha_t}{\partial n}\dot{\alpha}_t\,\mathrm{d}s. \qquad (1.19)$$

By virtue of the irreversibility conditions and the inequalities (1.15), the equality (1.19) holds if an only if the following pointwise equalities hold

$$(\mathsf{Y}_t+\operatorname{div}\mathbf{q}_t)\,\dot{\alpha} = 0 \text{ in } \Omega\setminus\Omega_t^c, \qquad \frac{\partial\alpha_t}{\partial n}\dot{\alpha}_t = 0 \text{ on } \partial\Omega. \qquad (1.20)$$

Hypothesis 4 gives the variational evolution of the damage on which this thesis is built. The strong first order stability equations (1.16) give the equilibrium and the damage criteria. When the first derivatives cancels out the second order stability conditions should be studied (Proposition 2). Let us know briefly evoke the evolution in a one dimensional framework.

1.2.2 Results from the one dimensional evolution of a bar in traction

Our goal is to use the non local gradient based damage models to account for fracture. As will be seen in the following chapters, the damage evolutions tends to structure itself in *bands*. To understand the cross-section of these bands, the main results from a one dimensional analysis of a bar in traction which has been studied at length in [Pham & Marigo 2013] are summarized. The reader should keep an open eye for the critical loading at which the initiation of damage occurs, the width of the damage localization zone and the total energy dissipated in a single localization. In a one-dimensional context the bulk energy (1.7) is given by

$$W(u',\boldsymbol{\varepsilon}^0,\alpha,\alpha') = \frac{1}{2}\mathsf{E}(\alpha)(u_t'-\boldsymbol{\varepsilon}_t^0)^2 + \mathsf{w}(\alpha) + \frac{1}{2}\Lambda\eta^2(\alpha')^2 \qquad (1.21)$$

where $()' = \frac{\partial}{\partial x}$ is the first derivative with respect to the space coordinate x and $\mathsf{E}(\alpha)$ denotes the one dimensional stiffness. The domain is a bar of length L: $\Omega = (0, L)$. The end $x = 0$ is blocked while the end $x = L$ has a displacement $U_t = tL$ imposed by a hard device (Fig. 1.3). No volumic loading is imposed:

$$\forall x \in (0, L) \qquad \boldsymbol{\varepsilon}^0(x) = 0, \quad \mathbf{f}_t(x) = 0.$$

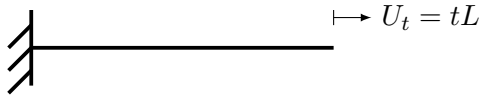

Figure 1.3: One dimensional bar in traction

The total energy of the body becomes

$$\mathcal{P}_t(u, \alpha) = \int_0^L \left(\frac{1}{2}\mathsf{E}(\alpha)(u_t')^2 + \mathsf{w}(\alpha) + \frac{1}{2}\Lambda\eta^2(\alpha')^2 \right) \mathrm{d}x,$$

the first order derivative of which reads as

$$\mathcal{P}_t'(u, \alpha)(v\beta) = \int_0^L \left(\mathsf{E}(\alpha)(u_t')v + \frac{1}{2}\mathsf{E}'(\alpha)(u_t')^2 + \mathsf{w}'(\alpha)\beta + \Lambda\eta^2\alpha'\beta' \right) \mathrm{d}x,$$

and the strong formulation (1.16) is written as

Equilibrium $\sigma_t'(x) = 0$

Irreversibility $\dot{\alpha}_t \geq 0$

Damage criterion $\frac{1}{2}\mathsf{E}'(\alpha_t)(u_t')^2 + \mathsf{w}'(\alpha_t) - \Lambda\eta^2\alpha_t'' \geq 0$

Energy Balance $\left(\frac{1}{2}\mathsf{E}'(\alpha_t)(u_t')^2 + \mathsf{w}'(\alpha_t) - \Lambda\eta^2\alpha_t''\right)\dot{\alpha}_t = 0$

Boundary Conditions $\alpha_t'(0) \leq 0, \qquad \alpha_t'(L) \geq 0$

One immediately deduces that the stress is constant in the entire bar $\sigma(x) = \mathsf{E}(\alpha_t(x))u_t'(x)$. At time $t = 0$, the structure is assumed sound $\alpha_0 = 0$ and unloaded $u_0 = 0$.

The homogeneous solution and its stability: First, a homogeneous solution (tx, α_t) of the evolution problem is studied. The solution of the elastic problem is given by the displacement $u_t(x) = tx$ and the stress $\sigma_t(x) = t\mathsf{E}(\alpha_t)$ thus the damage criterion is also homogeneous and reads

$$\mathsf{E}'(\alpha_t)\frac{t^2}{2} + \mathsf{w}'(\alpha_t) \geq 0$$

and thus an elastic phase exists, as soon as $\mathsf{w}'(0) > 0$, its limit is given by the loading

$$t^c = \sqrt{\frac{-2\mathsf{w}'(0)}{\mathsf{E}'(0)}} \qquad \sigma_c = \sqrt{-2\mathsf{w}'(0)\mathsf{E}'(0)}$$

and the square roots are defined as $\mathsf{E}'(\alpha) < 0$. For $t > t^c$ the equality in the damage criterion is reached in each point and damage can evolve. The associated stress-strain response,introducing the compliance $\mathsf{C} = \mathsf{E}^{-1}$

$$\sigma_t = \mathsf{E}(\alpha_t)t = \sqrt{\frac{2\mathsf{w}'(\alpha_t)}{\mathsf{C}'(\alpha_t)}}$$

The second order derivative at the state (tx, α_t) reads

$$\mathcal{P}_t''(tx,\alpha_t)(v,\beta) = \int_0^L \left(\frac{1}{2}\mathsf{E}(\alpha_t)(v')^2 + 2\mathsf{E}'(\alpha_t)(u_t')\beta + \left(\frac{1}{2}\mathsf{E}''(\alpha_t)(u_t')^2 + \mathsf{w}''(\alpha_t)\right)\beta^2 + \Lambda\eta^2(\beta')^2\right) \mathrm{d}x,$$

Proposition 2 reduces to the comparison of the Rayleigh ratio:

$$\mathcal{R}_t(v,\beta) = \frac{\int_0^L \mathsf{E}(\alpha_t)\left(v' + t\beta\mathsf{E}'(\alpha_t)/\mathsf{E}(\alpha_t)\right)^2 + \Lambda\eta^2(\beta')^2\,\mathrm{d}x}{\int_0^L \left(\frac{1}{2}\mathsf{C}''(\alpha_t)\sigma_t^2 - \mathsf{w}''(\alpha_t)\right)\,\mathrm{d}x}$$

with 1, *i.e.* a sufficient (respectively necessary) condition for stability is

$$\min_{v,\beta\in\mathcal{C}_t\times\mathcal{D}} \mathcal{R}_t(v,\beta) > \text{ (respectively } \geq) \, 1.$$

Property 2 (Stability of homogeneous state)**.** *In the elastic phase the homogeneous strain-damage state is stable.*

$$\frac{L^2}{\eta^2} \leq \frac{\pi^2\Lambda\mathsf{E}(\alpha_t)^2\mathsf{C}'(\alpha_t)^2\sigma_t^4}{\left(\frac{1}{2}\mathsf{C}''(\alpha_t)\sigma_t^2 - \mathsf{w}''(\alpha_t)\right)^2}$$

Proof. The proof is not reproduced here, see [Pham 2010] and [Pham *et al.* 2011] for a thorough investigation on the stability □

Thus η actually introduces a size effect, thus for large bars the homogeneous solution will be unstable and another solution will appear. Actually, even during a stable solution an infinite number of solution can appear [Benallal & Marigo 2007] through bifurcation. The localized solution is now reestablished.

Optimal damage profile: Construction of damage localized states. From a homogeneous damage α_0 consider a single localization S of center x_0. The equilibrium stress $\sigma \in (0, \sigma_c)$ is considered and thus

$$-\sigma_t^2\mathsf{C}'(\alpha_t) + 2\mathsf{w}'(\alpha_t) - 2\Lambda\eta^2\alpha_t'' = 0 \text{ on } S, \quad \alpha_t = \alpha_0 \text{ on } (0,L)\backslash S \tag{1.22}$$

since α and α' must be continuous at $x_0 \pm L_c$ then $\alpha(x_0 \pm L_c) = \alpha_0$ and $\alpha'(x_0 \pm L_c) = 0$ multiplying (1.22) by α' and integrating with respect to x, the first integral gives

$$-\sigma_t^2\mathsf{C}(\alpha) + 2\mathsf{w}(\alpha_t) - \Lambda\eta^2\alpha_t'^2 = C \text{ on } S$$

is obtained, where C is a constant. Evaluating $C = -\sigma_t/\mathsf{E}$. Hence the first integral may be written in the form

$$\eta^2 \alpha_t'(x)^2 = \mathbf{H}(\sigma_t, \alpha_t(x)) \text{ in } S \tag{1.23}$$

where

$$\mathbf{H}(\sigma, \beta) := \frac{2}{\Lambda}\left(\mathsf{w}(\beta) - \mathsf{w}(\alpha_0)\right) - \frac{\sigma^2}{\Lambda \mathsf{E}}\left(\mathsf{E}\mathsf{C}'(\beta) - 1\right) \text{ with } \beta \in [0, 1)$$

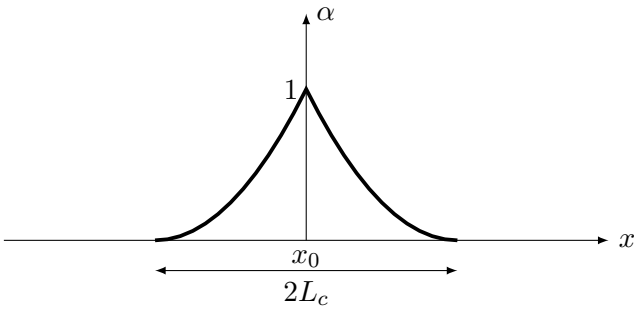

Figure 1.4: The localized damage profile with no residual stress: Evolution of the damage field in the localization for the specific damage law of Example 1. Localization from an elastic state $\alpha_0 = 0$ if the bar is long enough.

Characteristic size of the localization: The half-size $L_c(\sigma)$ of the localization is deduced from (1.23) and is a function of the stress. Let us define $\bar{\alpha}(\sigma)$ the maximal value along the localization of the damage reached at x_0

$$L_c(\sigma_t) := \eta \int_{\alpha_0}^{\bar{\alpha}(\sigma_t)} \frac{\mathrm{d}\beta}{\sqrt{\mathbf{H}(\sigma_t, \beta)}}$$

A damage localization corresponding to a stress $\sigma = 0$ can be viewed as a crack. Considering the localization from a sound material $\alpha = 0$, the energy dissipated in the creation of a single crack is identified with the fracture toughness of the material. Thus the half damage band and the toughness read

$$L_c = L_c(0) = \eta \int_0^1 \sqrt{\frac{\Lambda}{2\mathsf{w}(\beta)}}\,\mathrm{d}\beta \qquad \mathsf{G_c} = 2\eta \int_0^1 \sqrt{2\Lambda \mathsf{w}(\beta)}\,\mathrm{d}\beta \tag{1.24}$$

The damage profile localization is given implicitly from the first integral by integration over (x, x_0) (or (x_0, x)):

$$|x - x_0| = \eta \int_{\alpha(x)}^{\bar{\alpha}(\sigma_t)} \frac{\mathrm{d}\beta}{\sqrt{\mathbf{H}(\sigma_t, \beta)}}$$

Global force displacement response and critical crack opening The overall stress-strain relation

$$\boldsymbol{\varepsilon}_t = \boldsymbol{\varepsilon}^e(\sigma_t) + n\frac{\eta}{L}\boldsymbol{\varepsilon}^d(\sigma_t) \qquad \boldsymbol{\varepsilon}^d(\sigma_t) := \int_{\alpha_0}^{\bar{\alpha}(\sigma_t)} \left(\mathsf{C}(\beta) - \mathsf{C}(\alpha_0)\right) \frac{\mathrm{d}\beta}{\sqrt{\mathbf{H}(\sigma_t, \beta)}}$$

The critical jump $\boldsymbol{\varepsilon}^d$ is very sensitive to the constitutive relation. In the case where the elastic energy density $\psi(\boldsymbol{\varepsilon}^e_t, \alpha_t) = \frac{1}{2}(1-\alpha_t)^q \boldsymbol{\varepsilon}^e_t \cdot \boldsymbol{\varepsilon}^e_t$, if $q < 2$ then $\boldsymbol{\varepsilon}^d$ vanishes. Conversely, if $q > 2$ $\boldsymbol{\varepsilon}^d$, goes to infinity. As this critical jump will be linked to the crack opening in the case of a crack, this justifies the choice of $q = 2$, in the case (1.21) this

$$\boldsymbol{\varepsilon}^d = \frac{\pi}{2}\frac{\Lambda}{\mathsf{E}} \tag{1.25}$$

where a thorough study can be found in [Pham & Marigo 2013].

Choice of the normalization Λ. The choice to break down the constant of the gradient term into a length η and a pressure Λ has been made. A first option is to set its value Λ to $\mathsf{w}_1 = \mathsf{w}(1)$ then (1.24) reads:

$$L_c = \eta \int_0^1 \sqrt{\frac{\mathsf{w}_1}{2\mathsf{w}(\beta)}}\,\mathrm{d}\beta \qquad \mathsf{G_c} = 2\eta \int_0^1 \sqrt{2\mathsf{w}_1 \mathsf{w}(\beta)}\,\mathrm{d}\beta \qquad \boldsymbol{\varepsilon}^d = \frac{\pi}{2}\frac{\mathsf{w}_1}{\mathsf{E}}$$

An other choice of normalization could be made in (1.21) normalizing the gradient term by the sound young modulus $\mathsf{E} = \mathsf{E}(0)$. This would have changed the interpretation of η as the damage band and the dissipated energy would read (1.24):

$$L_c = \eta \int_0^1 \sqrt{\frac{\mathsf{E}}{2\mathsf{w}(\beta)}}\,\mathrm{d}\beta \qquad \mathsf{G_c} = 2\eta \int_0^1 \sqrt{2\mathsf{E}\mathsf{w}(\beta)}\,\mathrm{d}\beta \qquad \boldsymbol{\varepsilon}^d = \frac{\pi}{2}$$

1.2.3 A specific damage model

The fact that the damage parameter is a scalar which can only grow from 0 to 1 has already been discussed, $\alpha = 0$ denoting the undamaged state and $\alpha = 1$ the completely damaged state. It depends on the normalizations associated with the choices of the critical value 1 for α and $\mathsf{w}(1)$ for the multiplicative factor. Here W is specified, and most results will be established in the specific case of the damage model of:

Example 1. *A typical example of such a behavior is when the bulk energy density*

$$W(\boldsymbol{\varepsilon}, \boldsymbol{\varepsilon}^0, \alpha, \nabla\alpha) = \frac{1}{2}(1-\alpha)^2 \mathsf{A}(\boldsymbol{\varepsilon} - \boldsymbol{\varepsilon}^0) \cdot (\boldsymbol{\varepsilon} - \boldsymbol{\varepsilon}^0) + \mathsf{w}_1 \alpha + \frac{1}{2}\mathsf{w}_1 \eta^2 \nabla\alpha \cdot \nabla\alpha, \tag{1.26}$$

is the sum of three terms: the stored elastic energy $\psi(\boldsymbol{\varepsilon}, \alpha) = \frac{1}{2}(1-\alpha)^2 \mathsf{A}(\boldsymbol{\varepsilon} - \boldsymbol{\varepsilon}^0) \cdot (\boldsymbol{\varepsilon} - \boldsymbol{\varepsilon}^0)$*, the local part of the dissipated energy by damage* $\mathsf{w}(\alpha) = \mathsf{w}_1 \alpha$ *and its non local part* $\frac{1}{2}\mathsf{w}_1 \eta^2 \nabla\alpha \cdot \nabla\alpha$*, Therefore* w_1 *represents the energy dissipated during a complete, homogeneous damage process of a volume element:* $\mathsf{w}_1 = \mathsf{w}(1)$.

Accordingly, the dual quantities at time t (1.1) are given by the state functions:

$$\boldsymbol{\sigma}_t = (1-\alpha_t)^2 \mathsf{A}\boldsymbol{\varepsilon}^e_t, \qquad \mathsf{Y}_t = (1-\alpha_t)\mathsf{A}\boldsymbol{\varepsilon}^e_t \cdot \boldsymbol{\varepsilon}^e_t - \mathsf{w}_1, \qquad \mathbf{q}_t = \mathsf{w}_1 \eta^2 \mathbf{g}_t$$

Then the damage criterion (1.16) reads:

$$(1-\alpha_t)\mathsf{A}\boldsymbol{\varepsilon}^e_t \cdot \boldsymbol{\varepsilon}^e_t - \mathsf{w}_1 + \mathsf{w}_1 \eta^2 \Delta\alpha_t \leq 0 \tag{1.27}$$

and the consistency condition

$$\big((1-\alpha_t)\mathsf{A}\boldsymbol{\varepsilon}^e_t\cdot\boldsymbol{\varepsilon}^e_t-\mathsf{w}_1+\mathsf{w}_1\eta^2\Delta\alpha_t\big)\,\dot\alpha_t=0 \tag{1.28}$$

The elastic domains $\mathcal{R}(\alpha_t)$ and $\mathcal{R}^*(\alpha_t)$ at the damage state α_t now read

$$\mathcal{R}(\alpha_t)=\{\boldsymbol{\varepsilon}\in\mathbb{M}_s\,:\,(1-\alpha_t)\mathsf{A}(\boldsymbol{\varepsilon}-\boldsymbol{\varepsilon}^0_t)\cdot(\boldsymbol{\varepsilon}-\boldsymbol{\varepsilon}^0_t)\le\mathsf{w}_1\},\quad \mathcal{R}^*(\alpha_t)=\{\boldsymbol{\sigma}\in\mathbb{M}_s\,:\,\frac{\mathsf{C}}{(1-\alpha_t)^3}\boldsymbol{\sigma}_t\cdot\boldsymbol{\sigma}_t\le\mathsf{w}_1\}$$

The critical stress σ_c in a uniaxial tensile test such that $\boldsymbol{\sigma}=\sigma_c\mathbf{e}_1\otimes\mathbf{e}_1$ is then given by

$$\sigma_c=\sqrt{\frac{2\mathsf{w}'(0)}{\mathsf{C}'_{1111}(0)}}=\sqrt{\mathsf{w}_1\mathsf{E}}. \tag{1.29}$$

The non local dissipated energy density is assumed to be a quadratic function of the gradient of damage. Since the damage parameter is dimensionless and by virtue of the above definition of w_1, η has the dimension of a length. Accordingly, η can be considered as an internal length characteristic of the material while having always in mind that the definition of η depends on the normalizations associated with the choices of the critical value 1 for α and $\mathsf{w}(1)$ for the multiplicative factor.

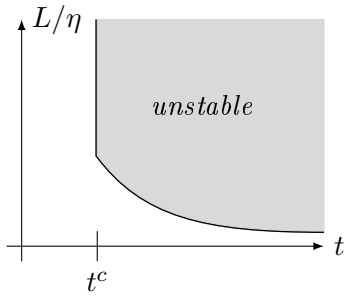

Figure 1.5: Stability of the Example 1. For long bars at the end of the elastic phase the homogeneous state is unstable. For short bars a homogeneous solution can exist with a positive damage field

The choice of the Example 1 is made for a variety of reasons. First for its simplicity and the fact that it is convex in each variable: the displacement $\mathbf{u}$ and the damage α. Then the choice of $\mathsf{w}(\alpha)$ leads to the existence of an elastic domain, *non empty* and thus a stress threshold which has been called *critical stress* (1.29). Furthermore, the jump of the displacement at the boundary of the damage band is finite but not vanishing. This will allow a jump of the displacement on the lips of the crack. Less importantly, the choice of normalization in front of the gradient term, allows to introduce another length for the crack opening then that of the damage band.

The damage model is defined from the w_1 and the internal length η. Thus the critical stress, the half width of the damage band and the toughness read:

$$\sigma_c=\sqrt{\mathsf{w}_1\mathsf{E}}\qquad L_c=2\sqrt{2}\eta\qquad \mathsf{G_c}=\frac{4\sqrt{2}}{3}\mathsf{w}_1\eta \tag{1.30}$$

In this dissertation the damage model of Example 1 will be used. This damage model is based on only three material parameters $\mathsf{E}, \sigma_c, \eta$ and accounts for complex phenomena. Nevertheless the distinction between the behavior in traction or in compression is not satisfactory but has been partially addressed in [Amor *et al.* 2009].

Example 2. *A damage model similar to the one presented in Example 1 is*

$$W^n(\boldsymbol{\varepsilon}, \boldsymbol{\varepsilon}^0, \alpha, \nabla\alpha) = \frac{1}{2}(1-\alpha)^2 \mathsf{A}(\boldsymbol{\varepsilon}-\boldsymbol{\varepsilon}^0)\cdot(\boldsymbol{\varepsilon}-\boldsymbol{\varepsilon}^0) + \frac{\mathsf{w}_1^{\mathsf{n}}}{\eta_n}\alpha + \mathsf{w}_1^{\mathsf{n}}\eta_n \nabla\alpha\cdot\nabla\alpha. \tag{1.31}$$

One can establish that $\eta = \sqrt{2}\eta_n$, and thus the critical stress and the width of the damage localization zone and the dissipated energy read:

$$\eta = \sqrt{2}\eta_n, \qquad \sigma_c = \sqrt{\frac{\mathsf{w}_1^{\mathsf{n}}\mathsf{E}}{\eta_n}} \qquad L_c = 4\eta_n \qquad \mathsf{G_c} = \frac{8}{3}\mathsf{w}_1^{\mathsf{n}} \tag{1.32}$$

This formulation is introduced as it is the one used in the numerical implementation (see Section 1.3.3), except for a rescaling it is identical to that of Example 1 and thus presents the same properties. In this thesis, as soon as numerical implementations are considered the damage model of Example 2 will be used. In the case of analytical work we will stick with that of Example 1).

1.3 The variational approach to Griffith's theory of fracture and its numerical implementation

Setting aside for a moment the damage model introduced we turn back to the genesis of the variational approach to fracture.

1.3.1 Variational approach to Griffith's theory of fracture

The variational approach to fracture introduced in [Francfort & Marigo 1998] is based on two ingredients which are a surface energy in the sens first introduced by Griffith and a global minimization problem. The total energy of the structure with a Griffith surface energy reads as

$$\mathcal{P}_t^G(\mathbf{u}, \ell) := \int_{\Omega\setminus\Gamma} \psi_0(\boldsymbol{\varepsilon}(\mathbf{u})(\mathbf{x}), \boldsymbol{\varepsilon}^0(\mathbf{x}))\,\mathrm{d}\mathbf{x} + \mathsf{G_c}\mathcal{S}_\ell(\mathbf{u}) - \mathcal{W}_t^e(\mathbf{u}) \tag{1.33}$$

where $\psi_0(\boldsymbol{\varepsilon}(\mathbf{u}), \boldsymbol{\varepsilon}^0) = \psi(\boldsymbol{\varepsilon}(\mathbf{u}), \boldsymbol{\varepsilon}^0, 0)$ is the elastic strain energy density, $\mathcal{S}_\ell(\mathbf{u})$ is the length of the crack and $\mathsf{G_c}$ the material's toughness. This "drawback" of Griffith's theory was one of the motivations which led [Francfort & Marigo 1998] to replace the Griffith criterion by a principle of least energy, in the spirit of the original idea of Griffith. It turns out that the principle of least energy is really able to predict the nucleation of cracks in a sound body initiation [Marigo 2010] and contains the evolution of the crack

direction [Chambolle *et al.* 2009]. However, the nucleation is necessarily brutal in the sense that a crack of finite length suddenly appears at a critical loading.

The numerical approach is based on a variational approximation, originally proposed in [Ambrosio 1990], of the total energy (1.33) by elliptic functionals. The regularized functional originally used in [Bourdin *et al.* 2000] is modified to account for the inelastic strain:

$$\boldsymbol{\varepsilon}_t^e(\mathbf{x}) = \boldsymbol{\varepsilon}(\mathbf{u}_t)(\mathbf{x}) - \boldsymbol{\varepsilon}_t^0(\mathbf{x}).$$

Proceeding by induction, in the setting of [Bourdin *et al.* 2000, Bourdin *et al.* 2008], one can introduce a function α taking its values in $[0,1]$ and representing in some sense the crack set, a regularization parameter η_n homogeneous to a length one gets the regularized energy depending on the parameter η_n (1.34). It is then possible to show that (1.34) converges in the sense of Γ-convergence to the fracture total energy (1.33), from which one derives convergence of global minimizers [see Braides 1998, for instance for more details on the construction of the regularized energy]. This analysis can then be carried out for the time evolution as shown in [Giacomini 2005]. The interested reader should refer to [Ortner & Negri 2008, Marigo 2010, Negri 2010] for comparison between Griffith's initial formulation and the one revisited in the variational approach.

For any $\mathbf{u}, \alpha$ the regularized energy is of the form

$$\mathcal{P}_t^{reg}(\mathbf{u},\alpha) := \int_\Omega \frac{1}{2}\left((1-\alpha)^2 + k_{\eta_n}\right) \mathsf{A}(\boldsymbol{\varepsilon}(\mathbf{u}) - \boldsymbol{\varepsilon}_t^0) \cdot (\boldsymbol{\varepsilon}(\mathbf{u}) - \boldsymbol{\varepsilon}_t^0) + \frac{3}{8}\mathsf{G_c}\left(\frac{\alpha}{\eta_n} + \eta_n \nabla\alpha \cdot \nabla\alpha\right) \mathrm{d}\mathbf{x} \qquad (1.34)$$

where surface energy term $\int \frac{3}{8}\mathsf{G_c}\left(\frac{\alpha}{\eta_n} + \eta_n \nabla\alpha.\nabla\alpha\right) \mathrm{d}\mathbf{x}$ differs from the one used in [Bourdin *et al.* 2000] while still falling with the more general scope of [Braides 2002]. The regularized energy (1.34) can be viewed as a damage model as the one proposed in Example 2 where $\mathsf{w}_1^{\mathsf{n}} = 3/8\mathsf{G_c}$. The parameter k_{η_n} is a small residual rigidity introduced for numerical purposes. The convergence results remains valid provided that $k_{\eta_n} = o(\eta_n)$.

In the literature the field representing the crack is often denoted $v = 1 - \alpha$. Here $\mathsf{G_c}$ denotes the toughness of the material. As η_n tends towards zero this model approximate Griffith's brittle fracture. The proof uses a global minimum argument though Γ-convergence. By doing this the material's toughness is overestimated

$$\mathsf{G_c}^{num} = \mathsf{G_c}\left(1 + \frac{3h}{8\eta_n}\right),$$

where h is the characteristic size of discretization of the mesh. The error on the surface energy is independent of the type of elements (linear versus quadratic) used. Furthermore, an unstructured mesh is used such that no favored direction be introduced and to avoid overestimating the energy [Negri 1999]. Yet, two flaws can be addressed. First, it does not contain a critical stress, commonly accepted as a physical parameter for brittle materials. Secondly the minimization problem is global. In [Bourdin *et al.* 2008], the variational approach to fracture is viewed in a broader sens with the definition of an energy and a minimization principle, especially they investigate cohesive surface energies as well.

1.3.2 Local and global minimization

The variational approach to fracture (in the broadest sense of the term), [Bourdin *et al.* 2008] is based on the two main ingredients being the choice of an energy and the variational principle. These choices lead to different behaviors. In their pioneer work [Francfort & Marigo 1998] state:

> "[...] the driving principle is global minimization. Such a principle is not dictated by any known thermodynamical argument ; it is rather a convenient postulate which provides for useful insight into a variety of behaviors [...] A more realistic approach that would investigate local minimizers is doomed for the want of the necessary mathematical apparatus."

The variational approach to fracture in the Griffith model [Francfort & Marigo 1998] is based on Global minimization. Yet this principle is physically unacceptable as it requires to pass energy barriers (Fig. 1.6) and may not admit any solution? Thus, the uncracked state is always a local minimum (Proposition 4 in [Charlotte *et al.* 2006] for the one dimensional case and [Marigo 2010]) and thus the nucleation of a crack is necessarily brutal (path p_0 which jumps from the state $\mathfrak{s}_0$ to the state $\mathfrak{s}_1$ whatever the height of the energy barriers). Furthermore, when forces (body or surfacic) are applied to the body, the global minimum is minus infinity and the solution is totally broken state (path p_1 to go to a state $\mathfrak{s}_3$ where $\mathcal{P}(\mathfrak{s}_3) = -\infty$). Here the local stability principle is used. An other argument in favor of study of the local stability is the numerical implementation (see Section 1.3.3) The use of local stability principle has also been used in the

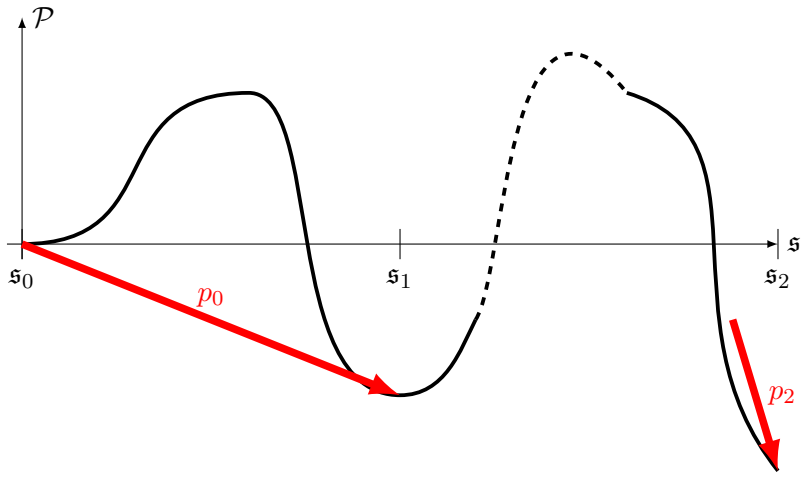

Figure 1.6: Diagram of the total energy as a function of the state. Energy barriers in the case of a Griffith surface energy as the state with no crack $\mathfrak{s}_0$ is always a local minimum. If surfacic or volumic forces ares imposed the global minimum is minus infinity $\mathfrak{s}_2$.

case cohesive cracks. Where leaving the pure Griffith setting, cohesive forces are added between the lips of the cracks [Charlotte *et al.* 2006].

Referring to the regularized energy (1.34), [Bourdin *et al.* 2008] write

> "Mechanicians may be tempted to lend significante to the resulting model as a damage gradient model [...] we view it merely as an approximation and will resist any further discussion of its intrinsic physical meaning"

In this dissertation, the opposite is done, and this damage model is considered as the physical relevant model. The stability principle is that of local minimums, even if the cost is less mathematical rigor. The Griffith behavior will only be a limit behavior as shown in the following chapter.

1.3.3 Alternate Minimization in a F.E.A

We wish to use the non local damage model introduced above in a finite element analysis (F.E.A.). The time-continuous quasi-static evolution is approached by a time discretized regularized evolution law by considering a discrete set of loads t_i, and iteratively seeking minimizers $(\mathbf{u}_i, \alpha_i\ )$ of $\mathcal{P}$ (1.9) under the irreversibility condition $\alpha_i \geq \alpha_{i-1}$. The alternate minimization algorithm is briefly mentioned and refer to the literature to [Bourdin 2007] and [Bourdin *et al.* 2008] for the interested reader. From the numerical point of view one uses an algorithm of alternate minimization in order to find the state of the body at each time step. That consists in constructing at time step t_i a sequence $(\mathbf{u}_{t_i}^n \alpha_{t_i}^n)$, $n \in \mathbb{N}$, such that

$$\mathbf{u}_{t_i}^n = \operatorname*{argmin}_{\mathbf{v}\in\mathcal{C}_{t_i}} \mathcal{P}_{t_i}(\mathbf{v}, \alpha_{t_i}^n),$$

$$\alpha_{t_i}^{n+1} = \operatorname*{argmin}_{\beta\in\mathcal{D}\,:\,\beta\geq\alpha_{t_{i-1}}} \mathcal{P}_{t_i}(\mathbf{u}_{t_i}, \beta) \tag{1.35}$$

(with an initial condition, for example $\alpha_{t_i}^0 = \alpha_{t_{i-1}}$). This algorithm is an algorithm of descent of the total energy, indeed

$$\mathcal{P}_{t_i}(\mathbf{u}_{t_i}^n, \alpha_{t_i}^n) \leq \mathcal{P}_{t_i}(\mathbf{u}_{t_i}^{n-1}, \alpha_{t_i}^n) \leq \mathcal{P}_{t_i}(\mathbf{u}_{t_i}^{n-1}, \alpha_{t_i}^{n-1}),$$

which in general converges. In such a case it converges to a state $(\mathbf{u}_{t_i},\ \alpha_{t_i})$ which satisfies the first order stability conditions (1.14)–(1.15) at time step t_i. This time discrete minimization problem is in turn discretized in space by means of linear finite elements, following the lines of the work cited above. No attempt at proving the convergence of the regularized model or its discretization to the continuous evolution law is made. The numerical implementation is that of [Bourdin 2007] and is based on the following libairies: PETSc [Balay *et al.* 2012b, Balay *et al.* 2012a, Balay *et al.* 1997] is used for data distribution, parallel linear algebra, and TAO [Munson *et al.* 2012] for the constrained optimization.

Remark 5 (**The implementation of irreversibility**). *In the case of a crack set cracks are not allowed to heal. That is should a crack exist at time t it should also exist at any later time. Actually, the condition enforced here, is stricter. Indeed the condition* (IR) *is enforced by a projection at each minimization set in* (1.35) *of* $\alpha_{t_i}^{n+1}$ *on* $\alpha_{t_i}^n$ *with an irreverisibility threshold set at* $\alpha = 10^{-2}$.

1.3.4 Other regularization techniques

The variational approach to fracture and its interpretation as a gradient damage model presented above is very close to two other regularization techniques the so called phase field approach and the thick level set approach. Both introduce a genuine unknown, as a scalar field, to approximate the crack set. In the physics community, regularized representation of cracks are commonly regarded as *phase field methods* [Karma *et al.* 2001, Henry & Levine 2004, Karma & Lobkovsky 2004, Henry 2010] originating from the Ginzburg-Landau theory of phase transition. These models also approximate the cracks as the localization of an internal scalar variable, denoted as damage or order parameter, and is based on a variational formulation including a gradient term in the internal variable. One main difference in the theoretical formulation is that the phase-field models are viscous in nature, whilst the evolution of damage models obtained within the variational approach to fracture is formulated in a rate-independent setting. More importantly, all available works using phase field methods consider the propagation of a pre-existing cracks and does not include any initiation criterion. More recently a coherent thermodynamical framework has been proposed for the phase field models [Miehe *et al.* 2010a] where the regularized numerical implementation is based on rate-independent and rate-dependent models. A robust algorithmic implementation of these models for updating the displacement and damage field in a given time step by operators splits [Miehe *et al.* 2010b]. In the mechanical numerical community, the *thick level set approach* is used [Moës *et al.* 2011, Bernard *et al.* 2012, Stolz & Moës 2012]. The evolution of the damage is governed by a driving force, which is the weighed average of Y on the width of the level set. The damage increases progressively as the level set value rises. At some distance from the front the material is completely degraded unveiling a crack. The nucleation criteria converges towards a local criteria as presented here.

Conclusion of Chapter 1

A model to capture defect evolution in brittle materials has been introduced. This work is concerned with the modeling of softening material (Definition 1.1.4) by regularized damage models. The main elements of the justification of the variational approach for damage models of a scalar variable are given. As the thermal loading is of interest in this dissertation the results have been extended to take it into account. This implies an extension of the work property which justifies the local variational approach. The strain work becomes a state function. Thus the local evolution can written under the form of Kuhn-Tucker conditions (Proposition 1). Unfortunately these conditions are not sufficient for the evolutions in structure due to the softening behavior.

Thus a stability principle and an energy balance are introduced (Hypothesis 4). The evolution of the displacement and damage field are governed by a rate independent process based on the three item of irreversibility, stability and energy balance. The local model is then enhanced by inserting gradient of damage into the energy expression. This allows to control localization. From the stability principle the first order conditions give the strong formulation (Proposition 3) which are completed with a consistency

condition (1.20). For the stability to be verifies the so called second order stability conditions must hold (Proposition 2) The case of the evolution of a one dimensional bar under traction is studied. This allows to exhibit some properties of the damage model and its evolution. Very quickly the main steps of the construction of localized states have been given. From these parameters the toughness $\mathsf{G_c}$ is identified as the energy dissipated in a single localization (1.24). Especially, the damage model is self-consistent and depends on two elastic parameters (E, ν) and two *non-linear* parameters the critical stress σ_c and the internal length η. Among the varieties of models [Pham & Marigo 2013] the simplest exhibiting the required properties is chosen: strong brittleness and a stress threshold.

This damage model can also be viewed as a regularization of the variational approach to fracture introduced in [Francfort & Marigo 1998]. Indeed, one can prove that the gradient based damage models converges towards Griffith's evolution law. These results are based on global minimization which presents the of brutal nucleation and not being able to predict the evolution of a structure with imposed forces. Finally, the numerical implementation based on an alternate minimization algorithm, which is a descent algorithm, is introduced.

Chapter 2

Strength and toughness from crack nucleation to propagation

Contents

This chapter is devoted to the nucleation and propagation of damage bands. Damage theory aims at modeling progressive degradation and failure of structures. Materials exhibiting stress softening lead to localization of the damage in bands. The nucleation and propagation phase are separated. Variational principles enable to capture the entire evolution in a single framework and have been studied in the case of stress concentration in a one dimensional context [Pham & Marigo 2013]. This chapter extends

these results in the case of a singular stress and to a multidimensional context. In Section 2.1, the crack nucleation in singular stress due to a notch is investigated. A critical stress intensity factor is revealed. It depends only on the notch angle and the damage model but is independent of the material parameters and the geometry of the structure. Taking into the scale effect and the geometry of the structure gives a simple framework to determine the critical loading at nucleation. Once the regularized crack is established its propagation is studied. The first challenge is to make sens of the energy balance in the case of a moving band (Section 2.2.1). Two properties are extension of the one dimensional case: the entire construction of the damage profile in a crack band happens at the crack tip and the stress field is modified by the damage at the tip of the band, and no singularity in stress ever exist. More importantly, the evolution law of these damage band is constructed with the sole help of local stability (Section 2.2.6). Finally in Section-2.3, the propagation of a damage band is investigated numerically. The evolution is confronted to the analytical results and at the same time to the nucleation for a flat notch.

2.1 Nucleation of a damage band near a notch

Let us consider a homogeneous body whose reference configuration is the open connected bounded set $\Omega_L \subset \mathbb{R}^2$ of characteristic size L. This body includes a notch characterized by its angle ω (Fig. 2.1). The tip of the notch is taken as the origin of space. This body is made of a brittle material modeled by a gradient damage model. Let us consider the specific damage model of Example 2. For a given material and thus considering different size of structures a family of problems are cast by the parameter

$$\epsilon = \frac{\eta_n}{L} \tag{2.1}$$

the dependence on any quantity is indicated by the superscript ϵ. Here the n index corresponds to numerics as the damage model of Example 2 is used. Typically for the material considered ϵ is small in front of the unit. The internal length can be characterized either directly or from the critical stress and toughness (1.30). For example, in the case of concrete [Comi & Perego 2001] the typical size is of the order of the centimeter thus for structures of characteristic size varying from 10 centimeters to the meter ϵ varies from one tenth to one hundredth. In the case of polymethylmethacrylate (PMMA) [Dunn *et al.* 1997] the internal length is of the order the millimeter and thus for L between 1 and 10 centimeters, ϵ also varies from one tenth and one hundredth.

The body is submitted to a time dependent loading which consists of a density of volume forces $\mathbf{f}_t^\epsilon$, a density of surface forces $\mathbf{F}_t^\epsilon$ prescribed on the part $\partial_N\Omega_L$ of the boundary and prescribed displacements $\mathbf{U}_t^\epsilon$ on the complementary part $\partial_D\Omega_L$ of the boundary, t denoting the time parameter. The edges of the notch are free in stress and damage, accordingly the boundary condition on $\Gamma^\pm$ of outer normal $\mathbf{n}$ are

$$\frac{\partial u}{\partial \mathbf{n}} = 0 \quad \frac{\partial \alpha}{\partial \mathbf{n}} = 0 \text{ on } \Gamma^\pm.$$

The potential of the given external forces at time t can read as the following linear form $\mathcal{W}_t^e$ defined formally on the set $\mathcal{C}_t^\epsilon = \left\{\mathbf{v} \,:\, \mathbf{v} = \mathbf{U}_t^\epsilon \text{ on } \partial_D\Omega\right\}$ of kinematically displacement fields total energy of the

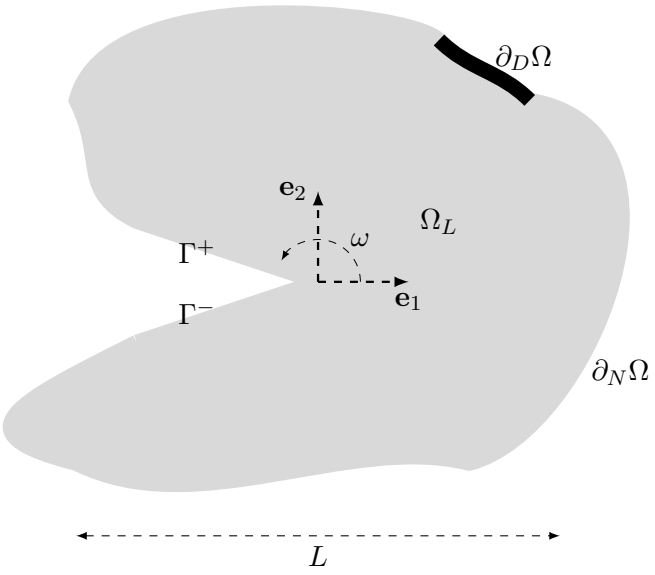

Figure 2.1: The real problem of characteristic size L

structure

$$\mathcal{W}_t^e(\mathbf{v}) := \int_\Omega \mathbf{f}_t^\epsilon \cdot \mathbf{v}\,\mathrm{d}\mathbf{x} + \int_{\partial_N\Omega} \mathbf{F}_t^\epsilon \cdot \mathbf{v}\,\mathrm{d}s,$$

and the total energy $\mathcal{P}_t$ (1.9) reads

$$\mathcal{P}_t(\mathbf{v},\beta) := \int_\Omega W(\boldsymbol{\varepsilon}(\mathbf{v}) - \boldsymbol{\varepsilon}_t^0, \beta, \nabla\beta)\,\mathrm{d}\mathbf{x} - \mathcal{W}_t^e(\mathbf{v}).$$

The strong formulation composed of the equilibrium, the damage criteria and the consistency condition is deduced from this variational formulation, Proposition 3 reads:

$$\forall \mathbf{x} \in \Omega_L \setminus \Omega_t^c \qquad \begin{cases} \operatorname{div}\boldsymbol{\sigma}_t + \mathbf{f}_t = 0 \\ (1-\alpha_t)\mathsf{A}\left(\boldsymbol{\varepsilon}(\mathbf{u}_t) - \boldsymbol{\varepsilon}_t^0\right)\cdot\left(\boldsymbol{\varepsilon}(\mathbf{u}_t) - \boldsymbol{\varepsilon}_t^0\right) - \frac{\mathsf{w}_1}{\eta_n} + 2\mathsf{w}_1\eta_n\Delta\alpha_t \le 0 \\ \left((1-\alpha_t)\mathsf{A}\left(\boldsymbol{\varepsilon}(\mathbf{u}_t) - \boldsymbol{\varepsilon}_t^0\right)\cdot\left(\boldsymbol{\varepsilon}(\mathbf{u}_t) - \boldsymbol{\varepsilon}_t^0\right) - \frac{\mathsf{w}_1}{\eta_n} + 2\eta_n\mathsf{w}_1\Delta\alpha_t\right)\dot{\alpha}_t = 0 \end{cases} \tag{2.2}$$

which holds in any point of the bulk material where the damage does not reach it's ultimate value $\alpha = 1$. The boundary conditions become:

$$\begin{cases} \mathbf{u}^\epsilon = \mathbf{U}^\epsilon & \text{on } \partial_D\Omega_L \\ \boldsymbol{\sigma}^\epsilon\mathbf{n} = \mathbf{F}^\epsilon & \text{on } \partial_N\Omega_L \\ \boldsymbol{\sigma}^\epsilon\mathbf{n} = \mathbf{0} & \text{on } \Gamma^\pm \\ \frac{\partial\alpha^\epsilon}{\partial\mathbf{n}} = \mathbf{0} & \text{on } \Gamma^\pm \cup \partial_D\Omega_L \cup \partial_N\Omega_L \end{cases} \tag{2.3}$$

The nucleation of cracks around a notch is the primely interest. As the analysis will show, the notch induces a stress concentration and the evolution is essentially local. Hence the loading can be characterized by a stress intensity factor K. The choice is made to decompose K into three terms to underline the different impacts. The nucleation process of cracks can be decomposed in the product of three stress intensity factors (this choice of vocabulary is done as each term is independent). The first is a scale effect, linking the dimension of the structure to that of the material. The second is a global coefficient linking the loading to the geometry of the structure. The third is a dimensionless parameter which only depends on the angle, the type of damage law and the Poisson ratio ν. The physical domain Ω_L is rescaled to the dimensionless domain Ω_1 Section 2.1.1. Using matched asymptotic expansion, from the outer domain Ω_1 one can build the stress intensity factor K_g (Section 2.1.2), with a purely elastic analysis eventually using finite elements. In the inner domain $\tilde{\Omega}_\infty$, for a generic problem, the loading comes through the matching conditions which allows to compute the stress intensity factor K_c (Section 2.1.3) using the non local damage model.

2.1.1 Dimensionless setting: scale effect

Our damage model will introduce size effects. To be sure to make them explicit, the physical domain Ω_L is rescaled into a normalized domain denoted Ω_1 in new (dimensionless) coordinates $\tilde{\mathbf{x}} = \mathbf{x}/L$. The normalized displacement and stress ($\tilde{\mathbf{u}}^\epsilon$, $\tilde{\boldsymbol{\sigma}}^\epsilon$) are given by:

$$\mathbf{u}^\epsilon(\mathbf{x}) = \eta_n \tilde{\mathbf{u}}^\epsilon(\tilde{\mathbf{x}}) \qquad \boldsymbol{\sigma}^\epsilon(\mathbf{x}) = \sigma_c \epsilon \tilde{\boldsymbol{\sigma}}^\epsilon(\tilde{\mathbf{x}}), \quad \alpha^\epsilon(\mathbf{x}) = \tilde{\alpha}^\epsilon(\tilde{\mathbf{x}})$$

and thus the normalized strain becomes $\tilde{\boldsymbol{\varepsilon}}(\tilde{\mathbf{u}}^\epsilon)$

$$\boldsymbol{\varepsilon}(\mathbf{u}^\epsilon) = \frac{\eta_n}{L} \tilde{\boldsymbol{\varepsilon}}(\tilde{\mathbf{u}}^\epsilon) = \epsilon \tilde{\boldsymbol{\varepsilon}}(\tilde{\mathbf{u}}^\epsilon).$$

All these normalized quantities continue to depend on the small parameter ϵ. The rescaling of the loading reads:

$$\mathbf{U}_t^\epsilon = \eta_n \tilde{\mathbf{U}}^\epsilon, \quad \mathbf{f}_t^\epsilon = \frac{\sigma_c}{L} \epsilon \tilde{\mathbf{f}}^\epsilon, \quad \mathbf{F}_t^\epsilon = \sigma_c \epsilon \tilde{\mathbf{F}}^\epsilon, \quad \boldsymbol{\varepsilon}_t^{0\epsilon} = \epsilon \tilde{\boldsymbol{\varepsilon}}^{0\epsilon} \tag{2.4}$$

where the time index is dropped for the sake of conciseness.

Reminding the reader that the energy density w_1^n can be written as $\mathsf{w}_1^\mathsf{n} = \sigma_c^2 \eta_n / \mathsf{E}$, the dimensionless problem on the rescaled domain Ω_1 (Fig. 2.2) is composed of the bulk conditions which read as

$$\forall \tilde{\mathbf{x}} \in \Omega_1 \setminus \tilde{\Omega}_t^c \qquad \begin{cases} \operatorname{div} \tilde{\boldsymbol{\sigma}}^\epsilon + \tilde{\mathbf{f}}^\epsilon = 0 \\ (1-\alpha^\epsilon)\epsilon^2 \bar{\mathsf{A}} \left(\tilde{\boldsymbol{\varepsilon}}(\tilde{\mathbf{u}}^\epsilon) - \tilde{\boldsymbol{\varepsilon}}^{0\epsilon}\right) \cdot \left(\tilde{\boldsymbol{\varepsilon}}(\tilde{\mathbf{u}}^\epsilon) - \tilde{\boldsymbol{\varepsilon}}^{0\epsilon}\right) - 1 + 2\epsilon^2 \tilde{\Delta}\alpha^\epsilon \leq 0, \\ \left((1-\alpha^\epsilon)\epsilon^2 \bar{\mathsf{A}} \left(\tilde{\boldsymbol{\varepsilon}}(\tilde{\mathbf{u}}^\epsilon) - \tilde{\boldsymbol{\varepsilon}}^{0\epsilon}\right) \cdot \left(\tilde{\boldsymbol{\varepsilon}}(\tilde{\mathbf{u}}^\epsilon) - \tilde{\boldsymbol{\varepsilon}}^{0\epsilon}\right) - 1 + 2\epsilon^2 \tilde{\Delta}\alpha^\epsilon\right) \dot{\alpha}^\epsilon = 0 \end{cases} \tag{2.5}$$

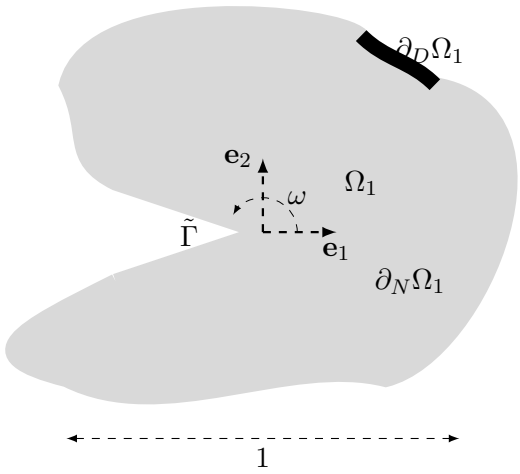

Figure 2.2: The rescaled problem of characteristic size 1.

and the boundary conditions

$$\begin{cases} \tilde{\mathbf{u}}^\epsilon = \tilde{\mathbf{U}}^\epsilon & \text{on } \partial_D\Omega_1 \\ \tilde{\boldsymbol{\sigma}}^\epsilon \mathbf{n} = \tilde{\mathbf{F}}^\epsilon & \text{on } \partial_N\Omega_1 \\ \tilde{\boldsymbol{\sigma}}^\epsilon \mathbf{n} = 0 & \text{on } \tilde{\Gamma}^\pm \\ \frac{\partial \alpha}{\partial \mathbf{n}} = 0 & \text{on } \tilde{\Gamma}^\pm \cup \partial_D\Omega_1 \cup \partial_N\Omega_1. \end{cases} \tag{2.6}$$

In the following subsection the solution to (2.5)-(2.6) will be searched under two forms: the first in the outer domain valid far away from the notch *i.e.* when $||\tilde{\mathbf{x}}|| >> 1$, the second close to the notch $||\tilde{\mathbf{x}}|| << 1$. Thus using matched asymptotic expansions [Lagerstrom 1988], the displacement field and stress fields are searched as series of powers of ϵ. Both approximations are simultaneously valid which allows to write the so called matching conditions.

2.1.2 The outer problem: an elastic computation

Due to the stress concentration near the tip of the notch, and assuming that the loading is regular enough, damage initiates near the notch. In the outer domain, the displacement $\tilde{\mathbf{u}}^\epsilon$ is searched under the form

$$\tilde{\mathbf{u}}^\epsilon(\tilde{\mathbf{x}}) = f_0(\epsilon)\mathbf{u}^0(\tilde{\mathbf{x}}) + f_1(\epsilon)\mathbf{u}^1(\tilde{\mathbf{x}}) + \cdots,$$

where $\cdots$ represents terms of higher order as $\epsilon \to 0$ and $f_i(\epsilon)$ are powers of ϵ.

$$\alpha^\epsilon(\mathbf{x}) = \alpha^0(\mathbf{x}) + \cdots$$

Then the stress reads $\tilde{\boldsymbol{\sigma}}^\epsilon$ as

$$\tilde{\boldsymbol{\sigma}}^\epsilon(\tilde{\mathbf{x}}) = f_0(\epsilon)\boldsymbol{\sigma}^0(\tilde{\mathbf{x}}) + f_1(\epsilon)\boldsymbol{\sigma}^1(\tilde{\mathbf{x}}) + \cdots$$

The solution depends linearly on the loading which thus can be expended according to the same power series:

$$\tilde{\mathbf{U}}^\epsilon = f_0(\epsilon)\mathbf{U}, \quad \tilde{\mathbf{f}}^\epsilon = f_0(\epsilon)\mathbf{f}, \quad \tilde{\mathbf{F}}^\epsilon = f_0(\epsilon)\mathbf{F}, \quad \tilde{\boldsymbol{\varepsilon}}^{0\epsilon} = f_0(\epsilon)\boldsymbol{\varepsilon}^0$$

Under the condition that $f_0(\epsilon)$ is small in front of ϵ^{-2} (This condition will be verified when the loading is characterized in the following subsection), the equilibrium and damage criterion (2.5) becomes at the first order:

$$\forall \tilde{\mathbf{x}} \in \Omega_1 \setminus \tilde{\Omega}_t^c \qquad \begin{cases} \operatorname{div} \tilde{\boldsymbol{\sigma}}^0 + \mathbf{f} = 0 \\ \tilde{\boldsymbol{\sigma}}^0 = (1-\alpha)\mathsf{A}\tilde{\boldsymbol{\varepsilon}}(\tilde{\mathbf{u}}^0) \\ -1 \leq 0 \\ \frac{d\tilde{\alpha}^0}{dt} = 0 \end{cases}, \tag{2.7}$$

and thus $\tilde{\alpha}^0 = 0$ and the problem becomes purely elastic. Therefore, for loading small enough, the damage zone remains confined in the vicinity of the singularity.

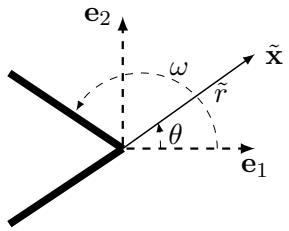

Figure 2.3: Polar coordinates at the tip of the notch in the outer domain Ω_1.

In a structure composed of an elastic material a notch generates a singularity in the stress field. In the vicinity of the notch (Fig. 2.3) polar coordinates are used and the first term of the displacement field can be written under the form:

$$\tilde{\mathbf{u}}^0 = K_g \tilde{r}^\varrho \mathbf{H}^\omega(\theta) \tag{2.8}$$

where $\mathbf{H}^\omega(\theta)$ is a function of the notch angle ω, the notch singularity ϱ and of the angle θ of the polar coordinates. The method to compute $\mathbf{H}^\omega$ is classical result from plane elasticity [Dauge 1988, Grisvard 1992]. In appendix B.1 these functions are recalled for a vanishing Poisson ratio. A description of the method to compute K_g with the use of dual singular function is given in appendix B.2. It is solution of an elastic computation which can be performed with any finite element code. Thus from (2.8) the real displacement field reads

$$\mathbf{u}^\epsilon(\mathbf{x}) = K_g f_0(\epsilon)\eta_n L^{-\varrho} r^\varrho \mathbf{H}^\omega(\theta) + \text{higher order terms}$$

where $f_0(\epsilon)\eta_n L^{-\varrho}$ captures the scale effect and is a function of the materials characteristic and of the notch angle ω. The power function $f_0(\epsilon)$ such that the damage criteria be initiated has yet to be determined.

2.1.3 The inner problem at the vicinity of the notch: the constitutive law intensity factor

A solution is now searched for near the tip of the notch in a zone of dimension ϵ. In the vicinity of the notch the problem is rescaled using the microscopic coordinates $\mathbf{y} = \tilde{\mathbf{x}}/\epsilon$. Accordingly, the inner problem

is the infinite domain

$$\bar{\Omega}_\infty = \{(\rho, \theta) \in [0, +\infty) \times (-\omega, +\omega)\}.$$

The dimensionless displacement $\tilde{\mathbf{u}}^\epsilon$ is sought for as functions of the shape

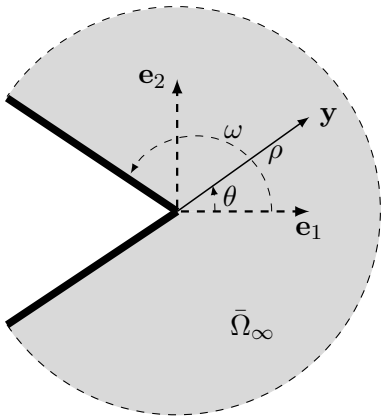

Figure 2.4: The inner domain $\bar{\Omega}_\infty$.

$$\tilde{\mathbf{u}}^\epsilon(\mathbf{x}) = g_0(\epsilon)\mathbf{v}^0(\frac{\tilde{\mathbf{x}}}{\epsilon}) + g_1(\epsilon)\mathbf{v}^1(\frac{\tilde{\mathbf{x}}}{\epsilon}) + \cdots \tag{2.9}$$

where $\cdots$ represent terms of higher order as $\epsilon \to 0$ and $g_i(\epsilon)$ are power series of ϵ. Thus the stress $\tilde{\boldsymbol{\sigma}}^\epsilon$ field will be of the form

$$\tilde{\boldsymbol{\sigma}}^\epsilon(\mathbf{x}) = \frac{g_0(\epsilon)}{\epsilon}\boldsymbol{\tau}^0(\frac{\tilde{\mathbf{x}}}{\epsilon}) + \frac{g_1(\epsilon)}{\epsilon}\boldsymbol{\tau}^1(\frac{\tilde{\mathbf{x}}}{\epsilon}) + \cdots. \tag{2.10}$$

Injecting the inner expansion (2.9)-(2.10) into the equilibrium $\operatorname{div}\boldsymbol{\tau}^0 = 0$ and damage criterion (2.5) becomes over the domain $\bar{\Omega}_\infty$: $\forall \bar{\mathbf{x}} \in \bar{\Omega}_\infty \setminus \bar{\Omega}_t^c$ the damage criteria expands as

$$(1-\alpha^0)g_0(\epsilon)^2\bar{\mathsf{A}}\tilde{\boldsymbol{\varepsilon}}(\mathbf{v}^0)\cdot\tilde{\boldsymbol{\varepsilon}}(\mathbf{v}^0) - 1 + 2\tilde{\Delta}\alpha^0 \leq 0, \tag{2.11}$$

and the boundary conditions read $\boldsymbol{\tau}^0\mathbf{n} = 0$ and $\frac{\partial\alpha^0}{\partial\mathbf{n}} = 0$ on $\tilde{\Gamma_n}^{\pm}$. The inner and outer expansions are both valid in a domain such that the radius $\epsilon \ll r \ll L$ giving the so called matching conditions in displacement

$$\lim_{\rho\to\infty} \left(g_0(\epsilon)\mathbf{v}^0(\rho,\theta) - \epsilon^\varrho f_0(\epsilon)K_g\rho^\varrho\mathbf{H}^\omega(\theta)\right) = 0, \tag{2.12}$$

$$\lim_{\rho\to\infty} \alpha^0(\rho,\theta) = 0.$$

Specifically, (2.12) induces that the first order coefficient from the inner and outer expansion are such that

$$g_0(\epsilon) = f_0(\epsilon)\epsilon^\varrho K_g.$$

Let us point out that in (2.11) the bulk loadings $\tilde{\mathbf{f}}^\epsilon$ and $\tilde{\boldsymbol{\varepsilon}}^{0\epsilon}$ do not appear as they are of higher order. However, they appear through the matching conditions (2.12) as they influence on K_g in the outer domain. This allows to characterize the dimensionless loading parameters introduces (2.4) and to state the first fundamental result:

Property 3. *For the damage criteria to be activated the loading must be of the order $\epsilon^{-\varrho}$ and thus $f_0(\epsilon) = t\epsilon^{-\varrho}$. This gives the order of the loading for the initiation of damage.*

Proof. In (2.11) if $g_0(\epsilon) \ll 1$ then the damage criteria is never activated. Indeed, for $g_0(\epsilon) \ll 1$, the damage field α^0 is solution of

$$-1 + 2\tilde{\Delta}\alpha_t^0 \leq 0, \quad \left(-1 + 2\tilde{\Delta}\alpha_t^0\right)\dot{\alpha}_t^0 = 0$$

with the boundary and initial conditions

$$\frac{\partial \alpha_t^0}{\partial n} = 0 \text{ on } \tilde{\Gamma_n}^{\pm}, \ \lim_{\rho\to\infty} \alpha_t^0(\rho,\theta) = 0, \ \alpha_{t=0}^0 = 0.$$

The only solution is $\alpha_t^0 = 0$. If $g_0(\epsilon) \gg 1$ is too large, the first term dominates and the criteria is violated. □

ω	$\bar{t}_c$	α_{max}	R_α
.99 π	$.191 \pm .001$	.53	$2.5\eta_n$
.95 π	$.194 \pm .001$	.54	$2.6\eta_n$
.9 π	$.205 \pm .001$	.62	$2.5\eta_n$
.8 π	$.248 \pm .001$	.55	$2.3\eta_n$
.75 π	$.283 \pm .002$	.46	$2.1\eta_n$
.7 π	$.337 \pm .002$	.38	$2.0\eta_n$
.6 π	$.530 \pm .003$	.27	$2.0\eta_n$
.55 π	$.705 \pm .004$	.14	$1.9\eta_n$
.51 π	$.934 \pm .005$	.02	$1.63\eta_n$

Table 2.1: Value of the critical stress intensity factor $K_c = \bar{k}\bar{t}_c$ in the case of plane elasticity for $\nu = 0$ for the damage law (1.26).

The order of magnitude of the loading for the damage evolution has just been given. By design, the loss of stability leading to a real crack (*i.e.* such that $\alpha = 1$ at some given point) happens at the same scale of the loading.

Computation of the value K_c. Instead of the computation on an infinite domain, a large domain with respect to the internal length is considered.

$$\bar{\Omega}_R = \{(\rho,\theta) \in [0,R] \times (-\omega,+\omega)\}.$$

The internal length is such that in the dimensionless problem both $\mathsf{G_c} = 1$ and $\sigma_c = 1$, *i.e.* $\eta_n = .375$. Thus the radius of the domain is fixed at $R = 10$. The monotonically increasing loading is divided into 200 time steps. For the notch angles $\omega = .51\pi$ and $.55\pi$ a homogeneous mesh of size $h = .05$ is used. For

the other notches a coin near the notch with a finer notch $h = .02$ is used. The loading is imposed as $t\mathbf{H}^\omega(\theta)$ on the boundary $\rho = R$:

$$\mathbf{v}^0(R,\theta) = \bar{t}\bar{k}R^\varrho \mathbf{H}^\omega(\theta)$$

where $\mathbf{H}^\omega(\theta)$ is the same as in (2.8) and $\bar{k}$ is a rescaling of the loading. The value taken by $\bar{t}$ where the nucleation of a crack appears is denoted $\bar{t}_c$. Thus τ^0, α^0 are solution of

$$\forall \bar{\mathbf{x}} \in \bar{\Omega}_R \setminus \bar{\Omega}_t^c \qquad \begin{cases} \operatorname{div} \boldsymbol{\tau}^0 = 0 \\ (1-\alpha^0)\bar{\mathsf{A}}\tilde{\boldsymbol{\varepsilon}}(\mathbf{v}^0) \cdot \tilde{\boldsymbol{\varepsilon}}(\mathbf{v}^0) - 1 + 2\tilde{\Delta}\alpha^0 \leq 0 \\ \left((1-\alpha^0)\bar{\mathsf{A}}\tilde{\boldsymbol{\varepsilon}}(\mathbf{v}^0) \cdot \tilde{\boldsymbol{\varepsilon}}(\mathbf{v}^0) - 1 + 2\tilde{\Delta}\alpha^0\right)\dot{\alpha}^0 = 0 \\ \mathbf{v}^0(R,\theta) = \bar{t}\bar{k}R^\varrho \mathbf{H}^\omega(\theta) \\ \alpha^0(R,\theta) = 0 \end{cases}$$

The rescaling chosen

$$\bar{k} := \frac{1}{(2\pi)^\varrho(1-\varrho)^2},$$

and thus the critical time $K_c = \bar{k}\bar{t}_c$

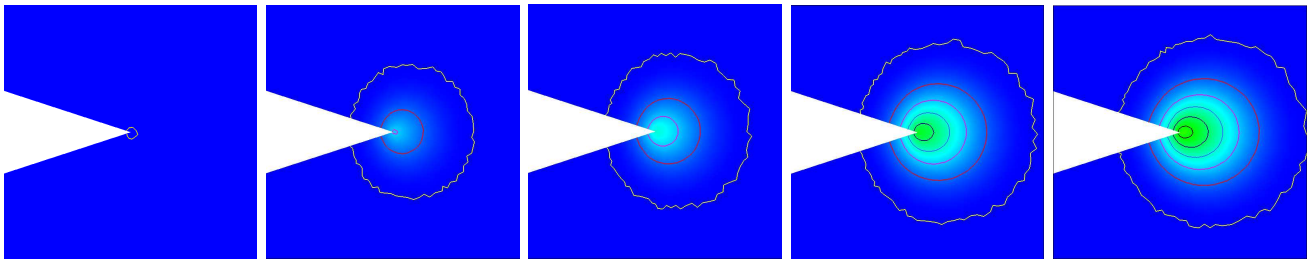

Figure 2.5: Damage evolution leading to the loss of stability for a notch of angle $\omega = .9\pi$. Zoom on a domain of size domain $2.5\eta_n \times 2.5\eta_n$ centered on the tip of the notch for the time steps $\{50, 161, 170, 180, 182\}$ corresponding to the loading $t = \{.06, .18, .19, .203, .205\}$. Isovalues of the damage field $\alpha = .5, .4, .3, .2, .1, 0$.

If damage nucleates as soon as the loading begins it is confined to a single point, the tip of the notch. As the loading t increases (Fig. 2.5), the size of the damage zone increases and it's maximal value taken in $\mathbf{0}$ increases. The isovalues in the damage are very close to circles centered in $\mathbf{0}$. This evolution is stable until K_c.

Figure 2.6 reports the zoom at the tip of the notch for the loading K_c and the previous time step. Just before the loss of stability, the damage field at the tip of the notch (Fig. 2.7) decreases from its maximal value towards 0 on a range which does not depend much from the notches angle. Table 2.1 reports the values of the critical loading at localization as well as the maximum value of the damage and the radius. As the singularity decreases, the critical stress is a loading order above (Tab. 2.1). The initial length of the crack (Fig. 2.6) is a global property and depends on the geometry of the structure.

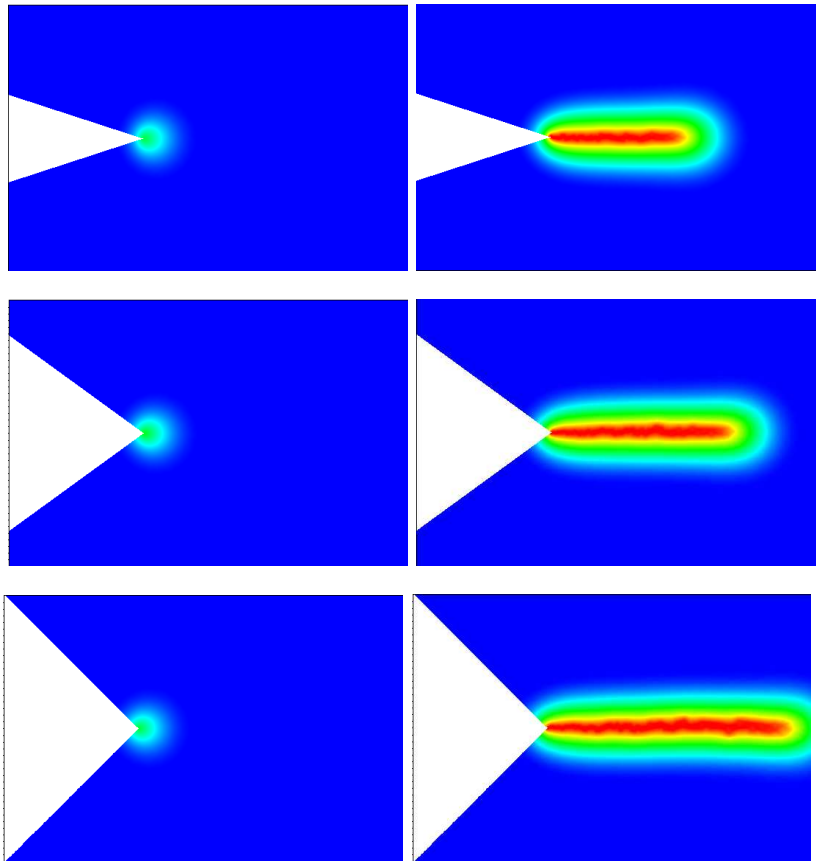

Figure 2.6: Damage field in the vicinity of the notch for two consecutive time steps at K_c. The notch is defined by the angle $\{.9\pi, .8\pi, .75\pi\}$ (top to bottom). Blue sound material ($\alpha = 0$), red totally damage ($\alpha = 1$).

The special case where $\omega = \pi$ is considered and thus the notch degenerates into a crack. As in the case of a notch damage increases progressively with the loading in a diffuse matter near the tip. At a given time this damage evolution is unstable and a crack with $\alpha = 1$ nucleates brutally. Thus the damage band nucleation appears for a loading $K_c = .191$

The construction of the damage field, in the direction of the previous crack set, is progressive till the nucleation of a continuous set of points such that $\alpha = 1$. Orthogonal to the direction of propagation (Fig. 2.9), the damage is maximal in the extension of the preexisting crack, and becomes the optimal profile from a one dimensional analysis at the critical loading.

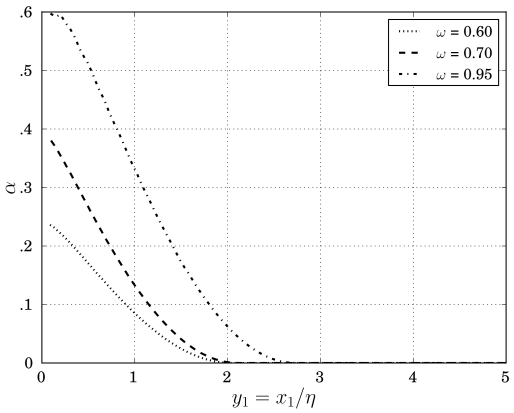

Figure 2.7: Damage profile at the tip of the notch at the time step prior to the bifurcation leading to the nucleation of a continuous set of points with no residual stress ($\alpha = 1$).

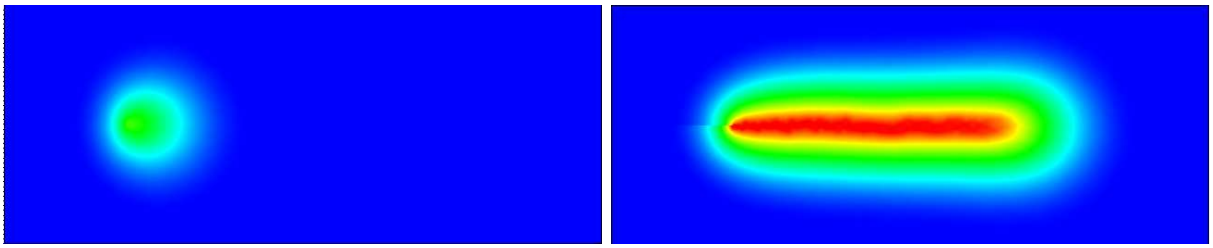

Figure 2.8: Damage field, Initiation of damage at a crack tip for two consecutive time steps at the loading $K_c = .191$.

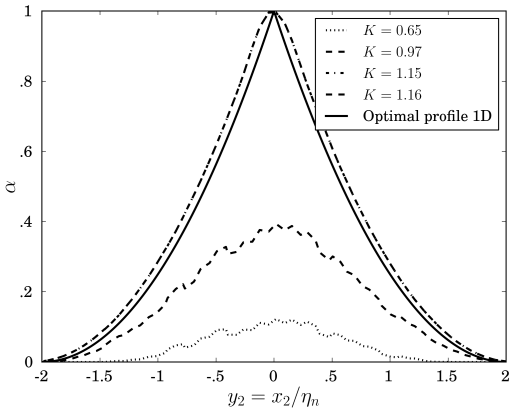

Figure 2.9: Damage field orthogonal to the tip of the crack at $y_1 = x_1/\eta_n = 1$.

2.2 Convergence of non local damage models towards Griffith

In the variational approach to fracture [Bourdin *et al.* 2008] the regularized functional introduced to approximate the total energy associated with Griffith's assumption on the surface energy can be interpreted as a non local damage model in the spirit of those developed by [Pham & Marigo 2010b]. These damage gradient models contain an internal length η which can be considered as a material characteristic. Whenever this length is small by comparison with the dimensions of the body, it can be proven by Gamma-convergence arguments [Ambrosio & Tortorelli 1990, Braides 2002] that the global minimum of the regularized functional converges to the global minimum of Griffith's functional. This result can be considered as a fundamental link between damage and fracture mechanics. However it deserves to be improved and generalized by removing the concept of global minimization of the energy which cannot be considered as a good physical principle. Indeed, this type of global minimization allows jumps from one state to the other without considering the presence of energy barriers. Therefore, the *global* minimization principle is replaced by a *stability* condition which can be considered as a *local* minimization principle. One is then interested whether the evolution of damage governed by such a weaker condition remains close to the one prescribed by Griffith's law when the internal length is small. The same question appears when considering numerical tests based on an alternate minimization algorithm [Bourdin 2007]. Indeed, such an algorithm does not converge necessarily to a global minimizer of the energy, but only to a stationary state. The issue is to compare the evolution given by the numerical computations with Griffith's law. Practically all the numerical simulations show that, after a stage of nucleation, the damage concentrates in bands whose width is of the order of the characteristic length η of the material. Moreover, except at the tip of the damage zone, the damage profile in the direction orthogonal to the band is practically the one given by a one-dimensional analysis [Pham & Marigo 2013]. These two properties (a thin damage band with an optimal profile) are the basic assumptions of our analysis. The last major issue in order to achieve this task is to give a sense to the concepts of energy release rate and of critical energy release rate, that is to say, to introduce correctly the basic quantities G and $\mathsf{G_c}$ entering in Griffith's law in the setting of our damage law. Specifically, in Griffith's theory, G is defined by assuming that the material has a purely elastic behavior. Then by virtue of Irwin's formula one can relate the energy release rate to the singularity at the tip of the crack and therefore to the stress intensity factors. In the context of the present damage law, there is no more singularities of the stresses (but the gradient of damage can be singular!), the stresses remain bounded. Besides, in Griffith's theory, $\mathsf{G_c}$ is a given material constant characterizing the energy associated with surfaces of discontinuity whereas in our damage approach the parameters characterizing the inelastic behavior of the material are the critical stress σ_c and the internal length η. Accordingly, G will be defined with the help of a two-scale approach and $\mathsf{G_c}$ will be defined as the energy dissipated by creating the optimal damage profile.

Specifically this section is organized as follows. After introducing fundamental assumptions, some general properties of the damage evolution are established in Section 2.2.1. Then, in Section 2.2.2, the separation of scales is performed by assuming that the internal length η is small by comparison with the length of the damage band and any other structural dimension. The damage problem, is first studied, far from the crack band and the crack tip. That allows us to define G, see Section 2.2.3. In Section 2.2.4,

after studying the damage problem in the damage band (far enough from its tip), $\mathsf{G_c}$ is identified with the dissipated energy in any unit of length of the damage band. In Section 2.2.5, the damage problem is analyzed in the neighborhood of the crack tip. That leads to the introduction of a generalized Rice path-integral which is studied in Section 2.2.6. In particular some properties relative to its path dependence are established. We are then in a position to conclude and to make the link between the propagation law of the damage band and Griffith's law (Section 2.2.7). The following results have been published in [Sicsic & Marigo 2013].

2.2.1 Consequences of the first order stability conditions and of the energy balance with an evolving totally damage set

In the Chapter 1, the Section 1.2.1 of the construction of the damage model, the set of points such that $\alpha = 1$ was considered fix. This hypothesis is dropped here. To simplify the presentation, the imposed loading is suppose to vanish but the results would remain even it were not the case. As previously stated, the stability condition (1.10) is satisfied *only if*, at each time, the body is at equilibrium and the damage criterion is satisfied. Specifically, they respectively read in a variational form (1.14)-(1.15) as

$$\int_\Omega \boldsymbol{\sigma}_t \cdot \boldsymbol{\varepsilon}(\mathbf{v} - \mathbf{u}_t)\,\mathrm{d}x = \mathcal{W}_t^e(\mathbf{v} - \mathbf{u}_t), \quad \forall \mathbf{v} \in \mathcal{C}_t$$

$$\int_\Omega \left(-\mathsf{Y}_t \cdot (\beta - \alpha_t) + \mathbf{q}_t \cdot \nabla(\beta - \alpha_t)\right)\,\mathrm{d}x \geq 0, \quad \forall \beta \in \mathcal{D} \ : \ \beta \geq \alpha_t,$$

where $\boldsymbol{\sigma}_t$, Y_t and $\mathbf{q}_t$ denote respectively the stress tensor, the energy release rate density and damage flux vector which are given in terms of the current state by the constitutive relations (1.1). These two conditions can be seen as the *first order stability conditions*. From the numerical point of view [Bourdin 2007], one uses an algorithm of alternate minimization in order to find the state of the body at each time step. In such a case it converges to a state $(\mathbf{u}_{t_i}, \alpha_{t_i})$ which satisfies the first order stability conditions (1.14)–(1.15) at time step t_i. A typical example of numerical results which can be obtained by this type of damage models with the alternate minimization algorithm is illustrated in Figure 1. In other words, the damage bands are assumed to have been previously created so that their width is of the order of η whereas their length is much greater than η such that the core of these bands is totally damaged. The evolution of these bands is our primerly interest. The propagation of such a *crack band* is studied by assuming that the path is given. The periodicity distribution will be the object of the following chapters. This leads to the following:

Hypothesis 5 (The structuration in crack bands). *Let Γ_t be the set of totally damaged points and let γ_t be the set of damage points at time t, i.e.*

$$\Gamma_t = \{\mathbf{x} \in \Omega \ : \ \alpha(\mathbf{x}, t) = 1\} \quad \subset \quad \gamma_t = \{\mathbf{x} \in \Omega \ : \ 0 < \alpha(\mathbf{x}, t) \leq 1\}.$$

The former set will be called the crack *whereas the latter will be called* the crack band. *The follow assumptions are made*

1. *Γ_t is a smooth curve whose end $\mathbf{P}_t$ (the* crack tip*) is moving such that the length of the curve be a smooth increasing function of time, say ℓ_t;*
2. *The stage of the evolution is such that ℓ_t is much larger that the material length η;*
3. *γ_t is contained in a thin band included in Ω, whose length differs from ℓ_t by a term of the order of η and whose cross-section has a width of the order of η;*
4. *The damage evolution is smooth both in time and space.*

Note that only the case where there is *one* crack band are considered, but since our analysis is essentially local the procedure could be easily extended to the case of a family of crack bands like in the example of the thermal shock. By standard arguments of the calculus of variations and By virtue of the hypothesis of regularity of the fields, one easily deduces from the first order stability conditions (1.14)–(1.15) that Proposition 3 reads in the current context:

Proposition 4. *The first order stability conditions are satisfied if and only if the following local conditions hold:*

$$\operatorname{div}\boldsymbol{\sigma}_t + \mathbf{f}_t = \mathbf{0} \text{ in } \Omega\setminus\Gamma_t, \qquad \boldsymbol{\sigma}_t\mathbf{n} = \mathbf{F}_t \text{ on } \partial_N\Omega, \qquad \boldsymbol{\sigma}_t\mathbf{n} = \mathbf{0} \text{ on } \Gamma_t, \tag{2.13}$$

$$\mathsf{Y}_t + \operatorname{div}\mathbf{q}_t \le 0 \text{ in } \Omega\setminus\Gamma_t, \qquad \mathbf{q}_t\cdot\mathbf{n} \ge 0 \text{ on } \partial\Omega. \tag{2.14}$$

Note that the two bulk conditions hold only in the uncracked part of the body.

It remains to use the energy balance (1.11). Owing to the smoothness assumption on the time evolution, one can take the derivative of (1.11) with respect to t and that leads to (2.15)

$$\begin{aligned} 0 &= \frac{d}{dt}\mathcal{P}_t(\mathbf{u}_t,\alpha_t) - \int_{\Omega\setminus\Gamma_t}\boldsymbol{\sigma}_t\cdot\boldsymbol{\varepsilon}(\dot{\mathbf{U}}_t)\,\mathrm{d}x + \mathcal{W}_t^e(\dot{\mathbf{U}}_t) + \dot{\mathcal{W}}_t^e(\mathbf{u}_t) \\ &= \frac{d}{dt}\left(\int_{\Omega\setminus\Gamma_t} W_t\,\mathrm{d}x\right) - \int_{\Omega\setminus\Gamma_t}\boldsymbol{\sigma}_t\cdot\boldsymbol{\varepsilon}(\dot{\mathbf{U}}_t)\,\mathrm{d}x - \mathcal{W}_t^e(\dot{\mathbf{u}}_t - \dot{\mathbf{U}}_t) \end{aligned}$$

where $W_t = W(\boldsymbol{\varepsilon}(\mathbf{u}_t),\alpha_t,\nabla\alpha_t)$. The main difficulty is to evaluate the rate of the bulk energy near the tip of the crack when the crack tip moves because of the possible presence of singularities. Accordingly, Ω is partitioned to isolate the (moving) tip of the crack. Let $\mathbb{B}_r(t)$ be the ball of radius r centered at $\mathbf{P}_t$, let $\mathbb{C}_r(t)$ be its boundary (a circle of radius r) and let $\Omega_r(t)$ be the uncracked part of the body outside the ball $\mathbb{B}_r(t)$: $\Omega_r(t) = \Omega\setminus(\Gamma_t\cup\mathbb{B}_r(t))$. The unit vector tangent to Γ_t at $\mathbf{P}_t$ is denoted $\boldsymbol{\tau}_t$ (Fig. 2.10). Let us evaluate the derivative with respect to t of the bulk energy included in $\Omega_r(t)$. Using classical results for the derivative of integrals over time dependent domains and by virtue of the regularity assumption, one gets

$$\frac{d}{dt}\left(\int_{\Omega_r(t)} W_t\,\mathrm{d}x\right) = \int_{\Omega_r(t)}\left(\boldsymbol{\sigma}_t\cdot\boldsymbol{\varepsilon}(\dot{\mathbf{u}}_t) - \mathsf{Y}_t\cdot\dot{\alpha}_t + \mathbf{q}_t\cdot\nabla\dot{\alpha}_t\right)\mathrm{d}x - \dot{\ell}_t\int_{\mathbb{C}_r(t)} W_t\boldsymbol{\tau}_t\cdot\mathbf{n}\,\mathrm{d}s \tag{2.15}$$

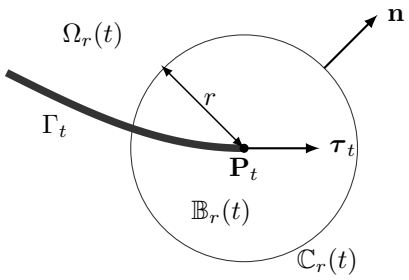

Figure 2.10: The crack tip moving with the speed $\dot{\ell}_t$. The contour $\mathbb{C}_r(t)$ translates with the crack tip.

where $\mathbf{n}$ denotes the outer unit normal to $\mathbb{B}_r(t)$. Inserting (2.15) into (2.15) leads to

$$\begin{aligned} 0 \;=\; & \int_{\Omega_r(t)} \Big(\boldsymbol{\sigma}_t \cdot \boldsymbol{\varepsilon}(\dot{\mathbf{u}}_t - \dot{\mathbf{U}}_t) - \mathbf{f}_t \cdot (\dot{\mathbf{u}}_t - \dot{\mathbf{U}}_t) - \mathsf{Y}_t \cdot \dot{\alpha}_t + \mathbf{q}_t \cdot \nabla \dot{\alpha}_t\Big)\, \mathrm{d}x - \int_{\partial_N \Omega} \mathbf{F}_t \cdot (\dot{\mathbf{u}}_t - \dot{\mathbf{U}}_t)\, \mathrm{d}s \\ & -\dot{\ell}_t \int_{\mathbb{C}_r(t)} W_t\, \mathbf{n} \cdot \boldsymbol{\tau}_t \; \mathrm{d}s + \frac{d}{dt}\left(\int_{\mathbb{B}_r(t)} W_t \, \mathrm{d}x\right) - \int_{\mathbb{B}_r(t)} \Big(\boldsymbol{\sigma}_t \cdot \boldsymbol{\varepsilon}(\dot{\mathbf{U}}_t) + \mathbf{f}_t \cdot (\dot{\mathbf{u}}_t - \dot{\mathbf{U}}_t)\Big)\, \mathrm{d}x. \end{aligned} \tag{2.16}$$

Integrating by parts the gradient terms in the integral over $\Omega_r(t)$ in (2.16) and using the equilibrium equations of (2.14) allow for simplifying the energy balance which can read now

$$\begin{aligned} 0 \;=\; & \int_{\Omega_r(t)} (\mathsf{Y}_t + \operatorname{div} \mathbf{q}_t) \cdot \dot{\alpha}_t \, \mathrm{d}x + \int_{\mathbb{C}_r(t)} \Big(W_t\, \mathbf{n} \cdot \boldsymbol{\tau}_t\, \dot{\ell}_t + \boldsymbol{\sigma}_t \mathbf{n} \cdot \dot{\mathbf{u}}_t + \mathbf{q}_t \cdot \mathbf{n}\, \dot{\alpha}_t\Big)\, \mathrm{d}s \\ & -\frac{d}{dt}\left(\int_{\mathbb{B}_r(t)} W_t \, \mathrm{d}x\right) + \int_{\mathbb{B}_r(t)} \Big(\boldsymbol{\sigma}_t \cdot \boldsymbol{\varepsilon}(\dot{\mathbf{U}}_t) + \mathbf{f}_t \cdot (\dot{\mathbf{u}}_t - \dot{\mathbf{U}}_t)\Big)\, \mathrm{d}x. \end{aligned} \tag{2.17}$$

To conclude one must pass to the limit when r goes to 0. The integrals over $\mathbb{B}_r(t)$ will not give a contribution to the limit because their integrand cannot be sufficiently singular. On the other hand, the integral over $\mathbb{C}_r(t)$ can give a non null limit. Its study will be made in the next section. For that purpose, it is more convenient to make a change of coordinates by taking the tip of the crack $\mathbf{P}_t$ as the (moving) origin of the coordinates and $(\hat{x}_1, \hat{x}_2)$ as the new cartesian coordinates with $\hat{x}_1 = (\mathbf{x} - \mathbf{P}_t) \cdot \boldsymbol{\tau}_t$. Specifically, one sets $\hat{\mathbf{x}} = (\mathbf{x} - \mathbf{P}_t)$ and any field f is transformed into $\hat{f}$ so that $\hat{f}(\hat{\mathbf{x}}, t) = f(\mathbf{P}_t + \hat{\mathbf{x}}, t)$. By the chain rule one gets

$$\dot{f}(\mathbf{x}, t) = \frac{\partial \hat{f}}{\partial t}(\hat{\mathbf{x}}, t) - \dot{\ell}_t \frac{\partial \hat{f}}{\partial \hat{x}_1}(\hat{\mathbf{x}}, t).$$

Inserting this change into the integral over $\mathbb{C}_r(t)$ which becomes an integral over $\tilde{\mathbb{C}}_r$, (2.17) can read as

$$0 = \int_{\Omega_r(t)} (\mathsf{Y}_t + \operatorname{div} \mathbf{q}_t) \cdot \dot{\alpha}_t \, \mathrm{d}x + \mathsf{J}_r(t) \dot{\ell}_t + \mathsf{I}_r(t) \tag{2.18}$$

with

$$\mathsf{J}_r(t) = \int_{\tilde{\mathbb{C}}_r} \left(\hat{W}_t\, \hat{n}_1 - \hat{\boldsymbol{\sigma}}_t \hat{\mathbf{n}} \cdot \frac{\partial \hat{\mathbf{u}}_t}{\partial \hat{x}_1} - \hat{\mathbf{q}}_t \cdot \hat{\mathbf{n}}\, \frac{\partial \hat{\alpha}_t}{\partial \hat{x}_1}\right) \mathrm{d}\hat{s} \tag{2.19}$$

and

$$\mathsf{I}_r(t) = \int_{\tilde{\mathbb{C}}_r} \left(\hat{\boldsymbol{\sigma}}_t \hat{\mathbf{n}} \cdot \frac{\partial \hat{\mathbf{u}}_t}{\partial t} + \hat{\mathbf{q}}_t \cdot \hat{\mathbf{n}} \, \frac{\partial \hat{\alpha}_t}{\partial t} \right) \mathrm{d}\hat{s} - \frac{d}{dt} \left(\int_{\mathbb{B}_r(t)} W_t \, \mathrm{d}x \right) + \int_{\mathbb{B}_r(t)} \Big(\boldsymbol{\sigma}_t \cdot \boldsymbol{\varepsilon}(\dot{\mathbf{U}}_t) + \mathbf{f}_t \cdot (\dot{\mathbf{u}}_t - \dot{\mathbf{U}}_t) \Big) \, \mathrm{d}x.$$

The second fundamental result can now be established

Proposition 5. *From a careful analysis of the singularities at the tip of the crack, one first proves that*

$$\lim_{r \to 0} \mathsf{I}_r(t) = 0, \qquad \lim_{r \to 0} \mathsf{J}_r(t) = \mathsf{J}_0(t) \leq 0. \tag{2.20}$$

Then, from the first order stability conditions and the global energy balance, one deduces that

$$(\mathsf{Y}_t + \operatorname{div} \mathbf{q}_t) \cdot \dot{\alpha}_t = 0 \text{ in } \Omega \setminus \Gamma_t, \qquad \mathsf{J}_0(t) \dot{\ell}_t = 0 \tag{2.21}$$

which can be seen as the local energy balances.

Proof. The complete proof of the property (2.20) is out of the scope of this work. A sketch of the proof is merely given in B.3. Accordingly, let us assume that (2.20) holds. Since $\lim_{r \to 0} \mathsf{I}_r(t) = 0$, passing to the limit when r goes to 0 in (2.18) gives

$$0 = \int_{\Omega \setminus \Gamma_t} (\mathsf{Y}_t + \operatorname{div} \mathbf{q}_t) \cdot \dot{\alpha}_t \, \mathrm{d}x + \mathsf{J}_0(t) \dot{\ell}_t. \tag{2.22}$$

Since $\mathsf{Y}_t + \operatorname{div} \mathbf{q}_t \leq 0$ by virtue of the first order stability conditions and since $\dot{\alpha}_t \geq 0$ by virtue of the irreversibility condition, the integral over $\Omega_r(t)$ in (2.18) is non positive. Since $\mathsf{J}_0(t) \leq 0$ and since $\dot{\ell}_t \geq 0$ by virtue of the irreversibility condition, $\mathsf{J}_0(t) \dot{\ell}_t \leq 0$. Therefore, each term in (2.22) is non positive while their sum must be zero, hence each term vanishes which is precisely (2.21). □

Remark 6. *By virtue of Proposition 5, $\mathsf{J}_0 \dot{\ell} = 0$. That means that the gradient of damage can be singular only when the crack does not propagate. Its singular part is then given by*

$$\nabla \alpha = \frac{K}{2\sqrt{r}} \left(-\cos \frac{\theta}{2} \mathbf{e}_r + \sin \frac{\theta}{2} \mathbf{e}_\theta \right) + \textit{regular terms}, \quad K \geq 0.$$

But K must vanish and hence the singularity disappears when the crack propagates.

2.2.2 Separation of scale

All the results of the previous section have been obtained without using the assumption that the internal length of the material η is small by comparison with the length of the crack and the dimensions of the body. In particular the property that $\mathsf{J}_0(t) \dot{\ell}_t = 0$ does not require such an assumption. On the other hand, the link with Griffith's law can only be made in this asymptotic context. Therefore, this assumption is adopted henceforth. To rigorously make a separation of scale requires the use of asymptotic methods like matched asymptotic expansions [Lagerstrom 1988]. We merely present here its great lines. Throughout the end of this section, η is considered as a small parameter and the dependence on it of any quantity is indicated by a superscript like $\mathbf{u}^\eta$ for the displacement field. On the contrary, the explicit time dependence is now removed.

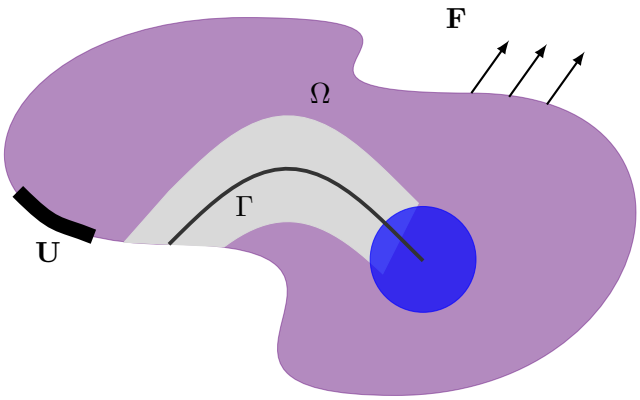

Figure 2.11: Shematic positons of the outer (purple), crack (gray) and tip (blue) problem

1. The damage evolution problem can be decomposed into three problems: (i) the *outer problem* which gives the behavior of the fields far enough from the crack band and the crack tip; (ii) the *crack band problem* which gives the behavior of the fields in or near the crack band but far enough from the crack tip; (iii) the *crack tip problem* which gives the behavior of the fields in the neighborhood of the crack tip.

2. The order of magnitude of the fields with respect to the small parameter η depends first on the order of magnitude of the loading and then on the zone where they are evaluated. It turns out that it is sufficient to prescribe a loading ($\mathbf{f}^\eta$, $\mathbf{F}^\eta$, $\mathbf{U}^\eta$ or $\boldsymbol{\varepsilon}^{0\eta}$) with a magnitude the order of $\sqrt{\eta}$ for propagating the crack. This is essentially due to the stress concentration which is automatically induced by the presence of the tip of the crack and to the fact that the dissipated energy for creating the crack band is of the order of η. The amplitude of the loading is assumed to be of the order of $\sqrt{\eta}$:

$$\mathbf{f}^\eta = \sqrt{\eta}\,\mathbf{f}, \quad \mathbf{F}^\eta = \sqrt{\eta}\,\mathbf{F}, \quad \mathbf{U}^\eta = \sqrt{\eta}\,\mathbf{U}, \quad \boldsymbol{\varepsilon}^{0\eta} = \sqrt{\eta}\,\boldsymbol{\varepsilon}^0.$$

This can be established as in Section 2.1. The only difference is that the small parameter is the internal length η which will allow to highlight the linearity to this quantity.

2.2.3 The outer problem and definition of Griffith's energy release rate

At a macroscale the thin process zone around the crack can be neglected and the associated outer problem is a purely elastic problem posed on the cracked domain $\Omega \setminus \Gamma$. Its solution depends linearly on the loading parameters. Since the magnitude of the loading is of the order of $\sqrt{\eta}$, the real displacement and stress fields can read

$$\mathbf{u}^\eta = \sqrt{\eta}\,\mathbf{u} + \cdots, \qquad \boldsymbol{\sigma}^\eta = \sqrt{\eta}\,\boldsymbol{\sigma} + \cdots$$

where $\mathbf{u}$ and $\boldsymbol{\sigma}$ satisfy

$$\operatorname{div}\boldsymbol{\sigma}+\mathbf{f}=0,\quad \boldsymbol{\sigma}=\mathsf{A}(\boldsymbol{\varepsilon}(\mathbf{u})-\boldsymbol{\varepsilon}^0)\quad \text{in}\quad \Omega\setminus\Gamma$$
$$\boldsymbol{\sigma}\mathbf{n}=\mathbf{F}\text{ on }\partial_N\Omega,\qquad \boldsymbol{\sigma}\mathbf{n}=\mathbf{0}\text{ on }\Gamma,\qquad \mathbf{u}=\mathbf{U}\text{ on }\partial_D\Omega.$$

The fields $\mathbf{u}$ and $\boldsymbol{\sigma}$ are singular near the tip of the crack (but of course these fields are not a good approximation of the real fields in that zone). In the case of an isotropic material, the singular part of $\boldsymbol{\sigma}$ is

$$\boldsymbol{\sigma}(\mathbf{x})=\frac{\bar K_I}{\sqrt{r}}\boldsymbol{\Sigma}_I(\theta)+\frac{\bar K_{II}}{\sqrt{r}}\boldsymbol{\Sigma}_{II}(\theta)+\cdots$$

where $\bar K_I$, $\bar K_{II}$ are the (rescaled) stress intensity factors and $\boldsymbol{\Sigma}_I$, $\boldsymbol{\Sigma}_{II}$ the usual angular functions corresponding to the opening and sliding modes [Leblond 2000].

The potential energy release rate G^η can also define in this fictitious elastic problem. It is related to the stress intensity factors by Irwin's formula [Leblond 2000]. By linearity, one gets

$$G^\eta=\eta\bar G,\qquad \bar G=\frac{1-\nu^2}{\mathsf{E}}(\bar K_I^2+\bar K_{II}^2) \tag{2.23}$$

where E and ν are the Young modulus and the Poisson ratio of the sound material. Note that G^η is of the order of η by virtue of the assumption on the loading magnitude. In the same manner the real stress intensity factors $K^\eta_{I,II}$ are of order $\sqrt{\eta}$: $K^\eta_{I,II}=\sqrt{\eta}\,\bar K_{I,II}$.

2.2.4 The damage field inside the crack band and definition of $\mathsf{G_c}$

In the crack band or in its neighborhood but far enough of the crack tip, the displacement and stress fields are matched to those of the outer problem. It follows in particular that the stresses are still of order $\sqrt{\eta}$. Let s be the arclength and $s\mapsto\boldsymbol{\chi}(s)$ be a parameterization of Γ. A point $\mathbf{x}$ in the crack band is represented by the system of curvilinear coordinates (s,ζ) such that $\mathbf{x}=\boldsymbol{\chi}(s)+\zeta\eta\boldsymbol{\nu}(s)$ where $\boldsymbol{\nu}(s)$ is unit normal vector to Γ at $\boldsymbol{\chi}(s)$ (Fig. 2.12). The damage field α^η in the crack band and its neighborhood is searched under the form

$$\alpha^\eta(\mathbf{x})=\alpha_*(s,\zeta)+\text{higher order terms}\quad\text{with}\quad \alpha_*(s,0)=1\quad\text{and}\quad \alpha_*(s,\zeta)=0\text{ for }|\zeta|\geq\bar L_c(s).$$

Hence $2\bar L_c(s)\eta$ represents the width of the crack band at s. Since $\frac12\mathsf{C}'(\alpha^\eta)\boldsymbol{\sigma}^\eta\cdot\boldsymbol{\sigma}^\eta$ is of the order of η whereas $\mathsf{w}'(\alpha^\eta)$ and $\operatorname{div}\mathbf{q}^\eta=\mathsf{w}_1\eta^2\Delta\alpha^\eta$ are of the order of 1. Since the gradient of α^η in the tangential direction is negligible by comparison with its gradient in the normal direction, the damage criterion (1.27) in the crack band can read at the first order as

$$\mathsf{w}'(\alpha_*)-\mathsf{w}_1\frac{\partial^2\alpha_*}{\partial\zeta^2}=0.$$

This autonomous second order ordinary differential equation admits a first integral. Indeed, multiplying it by $\partial\alpha_*/\partial\zeta$, it appears that $\mathsf{w}(\alpha_*)-\frac12\mathsf{w}_1\Big(\frac{\partial\alpha_*}{\partial\zeta}\Big)^2$ is independent of ζ. Using the boundary conditions at

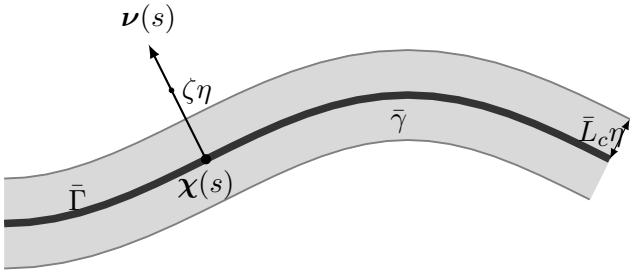

Figure 2.12: The damage band

$\zeta = \pm\bar{L}_c(s)$, one gets that this constant is 0 and hence

$$\sqrt{\frac{\mathsf{w}_1}{2\mathsf{w}(\alpha_*)}}\frac{\partial\alpha_*}{\partial\zeta} = \mathrm{sign}(\zeta). \tag{2.24}$$

Using the boundary condition at $\zeta = 0$ one finally obtains

$$\bar{L}_c = \int_0^1 \sqrt{\frac{\mathsf{w}_1}{2\mathsf{w}(\beta)}}\,\mathrm{d}\beta, \qquad |\zeta| = \int_{\alpha_*(\zeta)}^1 \sqrt{\frac{\mathsf{w}_1}{2\mathsf{w}(\beta)}}\,\mathrm{d}\beta, \tag{2.25}$$

$\alpha_*(\zeta)$ being given implicitly. It turns out that $\bar{L}_c$ and α_* are independent of s, which means that the damage profile is the same all along the crack band (except at its ends).

Let us calculate now the energy by unit length dissipated during the creation of the crack band. It is given by the integral over the crack band cross-section of $\mathsf{w}(\alpha^\eta) + \frac{1}{2}\mathsf{w}_1\eta^2\nabla\alpha^\eta\cdot\nabla\alpha^\eta$. Both terms in that sum are of the order of η and by virtue of (2.24) give the same contribution to the integral. Denoting by $\mathsf{G}_\mathsf{c}^\eta$ the leading term of the dissipated energy, after an easy calculation one obtains

$$\mathsf{G}_\mathsf{c}^\eta = \eta\bar{\mathsf{G}}_\mathsf{c}, \qquad \bar{\mathsf{G}}_\mathsf{c} = 2\sqrt{2}\int_0^1 \sqrt{\mathsf{w}_1\mathsf{w}(\beta)}\,\mathrm{d}\beta. \tag{2.26}$$

Note that $\mathsf{G}_\mathsf{c}^\eta$ is of the order of η, intrinsic to the material and independent of the crack path and how the crack band was created. It will play the role of the surface energy density in Griffith's law.

Example 3. *In the case of the constitutive law of Example 1 where* $\mathsf{A}(\alpha) = (1-\alpha)^2\mathsf{A}$ *and* $\mathsf{w}(\alpha) = \mathsf{w}_1\alpha$*, one gets* $\bar{L}_c = \sqrt{2}$ *(hence the width of the crack band is* $2\sqrt{2}\eta$*),* $\mathsf{G}_\mathsf{c}^\eta = 4\sqrt{2}\mathsf{w}_1\eta/3$ *whereas the critical stress* σ_c *in a uniaxial tensile test is independent of* η *and given by* $\sigma_c = \sqrt{\mathsf{w}_1\mathsf{E}}$*. Moreover the damage profile in the crack band is a parabola:* $\alpha_*(\zeta) = (1 - |\zeta|/\sqrt{2})^2$*.*

2.2.5 The damage problem near the tip of the crack

Near the tip of the crack, η is the natural length scale. On that account let us rescale the system of coordinates in the neighborhood of the crack tip $\mathbf{P} = \boldsymbol{\chi}(\ell)$ by setting

$$\mathbf{y} = \frac{\mathbf{x}-\mathbf{P}}{\eta} = y_1\mathbf{e}_1 + y_2\mathbf{e}_2, \qquad \rho = \|\mathbf{y}\| = \frac{r}{\eta}.$$

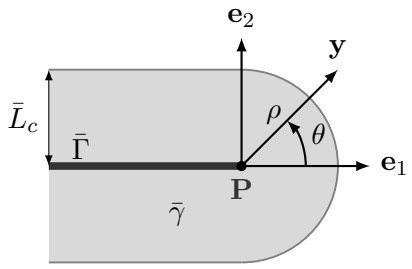

Figure 2.13: The crack tip with the damage zone

This crack tip problem is posed in the entire plane $\mathbb{R}^2$, the crack corresponding to the half-line $\bar{\Gamma} = (-\infty, 0) \times \{0\}$ and the crack band to $\bar{\gamma}$ (Fig. 2.13). One searches for the displacement, stress and damage fields under the form

$$\mathbf{u}^\eta(\mathbf{x}) = \sqrt{\eta}\mathbf{u}(\mathbf{P}) + \eta\bar{\mathbf{u}}(\mathbf{y}) + \cdots, \qquad \boldsymbol{\sigma}^\eta(\mathbf{x}) = \bar{\boldsymbol{\sigma}}(\mathbf{y}) + \cdots, \qquad \alpha^\eta(\mathbf{x}) = \bar{\alpha}(\mathbf{y}) + \cdots$$

where $\mathbf{u}(\mathbf{P})$ represents the displacement of the crack tip given by the outer problem. By virtue of a stress concentration effect due to the presence of the crack tip, the stresses are of the order of 1 in this region while they are of the order of $\sqrt{\eta}$ in the outer domain. Therefore, by matching the two expansions one gets the following behavior of $\bar{\boldsymbol{\sigma}}$ at infinity:

$$\lim_{\rho\to\infty}\left(\bar{\boldsymbol{\sigma}}(\mathbf{y}) - \frac{\bar{K}_I}{\sqrt{\rho}}\boldsymbol{\Sigma}_I(\theta) - \frac{\bar{K}_{II}}{\sqrt{\rho}}\boldsymbol{\Sigma}_{II}(\theta)\right) = \mathbf{0} \tag{2.27}$$

and hence the rescaled stress intensity factors $\bar{K}_I$ and $\bar{K}_{II}$ given by the outer problem will play the role of the time-dependent loading parameters for the crack tip problem. The equilibrium equations, the stress-strain relations and the boundary conditions read

$$\operatorname{div}\bar{\boldsymbol{\sigma}} = \mathbf{0} \quad \text{and} \quad \bar{\boldsymbol{\sigma}} = \mathsf{A}(\bar{\alpha})\boldsymbol{\varepsilon}(\bar{\mathbf{u}}) \quad \text{in} \quad \mathbb{R}^2 \setminus \bar{\Gamma}, \qquad \bar{\boldsymbol{\sigma}}\mathbf{e}_2 = \mathbf{0} \quad \text{and} \quad \bar{\alpha} = 1 \quad \text{on} \quad \bar{\Gamma} \tag{2.28}$$

where all the spatial derivatives are now taken with respect to $\mathbf{y}$. Note that the loadings $\mathbf{f}^\eta$ and $\boldsymbol{\varepsilon}^{0\eta}$ do not appear because they are of higher order. Since all terms in $Y^\eta + \operatorname{div}\mathbf{q}^\eta$ are of the order of 1, the damage criterion (1.27) reads at the first order as

$$\frac{1}{2}\mathsf{C}'(\bar{\alpha})\bar{\boldsymbol{\sigma}}\cdot\bar{\boldsymbol{\sigma}} - \mathsf{w}'(\bar{\alpha}) + \mathsf{w}_1\Delta\bar{\alpha} \le 0 \quad \text{in} \quad \mathbb{R}^2 \setminus \bar{\Gamma}. \tag{2.29}$$

From the chain rule, the rate of damage is of order of $1/\eta$ and reads

$$\dot{\alpha}^\eta(\mathbf{x}) = -\frac{\dot{\ell}}{\eta}\frac{\partial\bar{\alpha}}{\partial y_1}(\mathbf{y}) + \cdots. \tag{2.30}$$

Accordingly, the local energy balance (1.28) reads at the first order

$$\Big(\frac{1}{2}\mathsf{C}'(\bar{\alpha})\bar{\boldsymbol{\sigma}}\cdot\bar{\boldsymbol{\sigma}} - \mathsf{w}'(\bar{\alpha}) + \mathsf{w}_1\Delta\bar{\alpha}\Big)\frac{\partial\bar{\alpha}}{\partial y_1}\dot{\ell} = 0 \quad \text{in} \quad \mathbb{R}^2 \setminus \bar{\Gamma}. \tag{2.31}$$

The damage field expansion of the crack tip problem must be matched to the damage field expansions of the outer and crack band problems. Therefore $\bar{\alpha}$ must vanish at infinity except in the direction of the crack where it must correspond to the field α_* given by (2.25). Specifically, these matching conditions read

$$\lim_{\|y\|\to\infty,\ y_2\neq 0} \bar{\alpha}(\mathbf{y}) = 0, \qquad \lim_{y_1\to-\infty} \bar{\alpha}(\mathbf{y}) = \alpha_*(y_2). \tag{2.32}$$

Remark 7. *In current and previous section the same dimensioning path have not been used. Yet the notation are coherent. Especially the figures 2.1.3 and 2.13 and are at the same scale*

2.2.6 The generalized Rice integral and its properties

In the analysis of the global energy balance, the flux of energy $\mathsf{J}_r(t)$ defined in (2.19) is a path integral which generalizes Rice's integral used in brittle fracture to calculate the potential energy release rate. This path integral will be studied for paths which are very close to the tip of the crack. Using the rescaled system of coordinates (y_1, y_2), let us consider such a path $\bar{\mathcal{C}}$ whose ends are located on the lips of the crack and which circumvents the crack tip (Fig. 2.14). It appears that the associated path integral $J^\eta_{\bar{\mathcal{C}}}$ is of the order of η, $J^\eta_{\bar{\mathcal{C}}} = \eta \bar{J}_{\bar{\mathcal{C}}} + \cdots$ and $\bar{J}_{\bar{\mathcal{C}}}$ reads as

$$\bar{J}_{\bar{\mathcal{C}}} = \int_{\bar{\mathcal{C}}} \left(\bar{W}(\boldsymbol{\varepsilon}(\bar{\mathbf{u}}), \bar{\alpha}, \nabla\bar{\alpha}) n_1 - \frac{\partial \bar{W}}{\partial \bar{\boldsymbol{\varepsilon}}_{ij}}(\boldsymbol{\varepsilon}(\bar{\mathbf{u}}), \bar{\alpha}, \nabla\bar{\alpha}) n_j \frac{\partial \bar{u}_i}{\partial y_1} - \frac{\partial \bar{W}}{\partial \bar{g}_j}(\boldsymbol{\varepsilon}(\bar{\mathbf{u}}), \bar{\alpha}, \nabla\bar{\alpha}) n_j \frac{\partial \bar{\alpha}}{\partial y_1} \right) \mathrm{d}\bar{s} \tag{2.33}$$

where $\bar{s}$ denotes the arclength of $\bar{\mathcal{C}}$. In (2.33) $\bar{W}$ represents the rescaled bulk energy density, *i.e.*

$$\bar{W}(\bar{\boldsymbol{\varepsilon}}, \bar{\alpha}, \bar{\mathbf{g}}) = \frac{1}{2}\mathsf{A}(\bar{\alpha})\bar{\boldsymbol{\varepsilon}} \cdot \bar{\boldsymbol{\varepsilon}} + \mathsf{w}(\bar{\alpha}) + \frac{1}{2}\mathsf{w}_1 \bar{\mathbf{g}} \cdot \bar{\mathbf{g}} \tag{2.34}$$

and one sets $\bar{\mathbf{q}} = \dfrac{\partial \bar{W}}{\partial \bar{\mathbf{g}}} = \mathsf{w}_1 \bar{\mathbf{g}}$. One fundamental property of the path integral is its monotonicity with

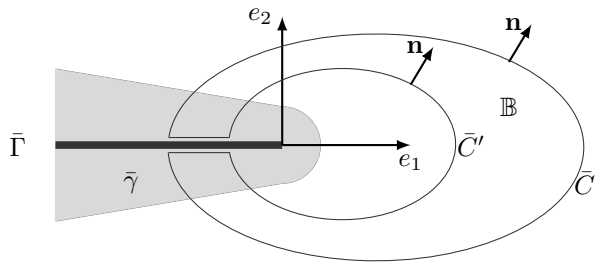

Figure 2.14: Two ordered paths in the neighborhood of the crack tip.

respect to the path. This requires to define the following partial order relation between the paths

Definition 3. *One says that the path $\bar{\mathcal{C}}$ is greater than the path $\bar{\mathcal{C}}'$, if $\bar{\mathcal{C}}'$ is included in the domain delimited by the path $\bar{\mathcal{C}}$ and the crack $\bar{\Gamma}$.*

Let us prove the first fundamental property of this path integral.

Proposition 6. *When the crack propagates, i.e. when $\dot{\ell} > 0$, then the path integral $\bar{J}_{\bar{\mathcal{C}}}$ is path independent.*

Proof. Let us consider two paths $\bar{\mathcal{C}}$ and $\bar{\mathcal{C}}'$ such that $\bar{\mathcal{C}} \geq \bar{\mathcal{C}}'$ in the sense of Definition 3 (Fig 2.14). Let $\mathbb{B}$ be the domain delimited by theses two paths and the crack line. It is easy to check that

$$\bar{J}_{\bar{\mathcal{C}}} - \bar{J}_{\bar{\mathcal{C}}'} = \int_{\partial\mathbb{B}} \left(\bar{W} n_1 - \bar{\sigma}_{ij} n_j \frac{\partial \bar{u}_i}{\partial y_1} - \bar{q}_j n_j \frac{\partial \bar{\alpha}}{\partial y_1} \right) \mathrm{d}\bar{s}$$

because $n_1 = 0$, $\bar{\boldsymbol{\sigma}}\mathbf{n} = \mathbf{0}$ and $\partial\bar{\alpha}/\partial y_1 = 0$ on $\bar{\Gamma}$. By Green's formula one gets

$$\begin{aligned} \bar{J}_{\bar{\mathcal{C}}} - \bar{J}_{\bar{\mathcal{C}}'} &= \int_{\mathbb{B}} \left(\frac{\partial \bar{W}}{\partial y_1} - \frac{\partial}{\partial y_j} \left(\bar{\sigma}_{ij} \frac{\partial \bar{u}_i}{\partial y_1} + \bar{q}_j \frac{\partial \bar{\alpha}}{\partial y_1} \right) \right) \mathrm{d}\bar{s} \\ &= \int_{\mathbb{B}} \left(\frac{\partial \bar{W}}{\partial \bar{\alpha}} \frac{\partial \bar{\alpha}}{\partial y_1} - \frac{\partial \bar{\sigma}_{ij}}{\partial y_j} \frac{\partial \bar{u}_i}{\partial y_1} - \operatorname{div} \bar{q} \frac{\partial \bar{\alpha}}{\partial y_1} \right) \mathrm{d}\bar{s} \end{aligned}$$

Using the equilibrium equation $\operatorname{div} \bar{\boldsymbol{\sigma}} = \mathbf{0}$ and the definitions of $\bar{W}$ leads to

$$\bar{J}_{\bar{\mathcal{C}}} - \bar{J}_{\bar{\mathcal{C}}'} = - \int_{\mathbb{B}} \left(\tfrac{1}{2} \mathsf{C}'(\bar{\alpha}) \bar{\boldsymbol{\sigma}} \cdot \bar{\boldsymbol{\sigma}} - \mathsf{w}'(\bar{\alpha}) + \mathsf{w}_1 \Delta\bar{\alpha} \right) \frac{\partial \bar{\alpha}}{\partial y_1} \, \mathrm{d}\bar{s} \tag{2.35}$$

and one concludes by the local energy balance (2.31) that $\bar{J}_{\bar{\mathcal{C}}} = \bar{J}_{\bar{\mathcal{C}}'}$. The proof that the equality remains true even if the path are not well ordered is left to the reader. Let us note that this invariance property remains true for more general bulk energy density than (2.34) because the proof is essentially based on the variational character of the damage evolution law. □

The second fundamental property requires an extra assumption which is stated here for future reference.

Hypothesis 6. *At each time and almost everywhere, the damage evolution is assumed to follow $\partial\bar{\alpha}/\partial y_1 \leq 0$.*

Remark 8. *The condition $\partial\bar{\alpha}/\partial y_1 \leq 0$ is automatically satisfied when the crack propagates by virtue of the irreversibility condition and* (2.30)*. Therefore it is sufficient that the damage remains constant in the neighborhood of the crack tip when the crack does not propagate in order that the condition remains true at every time.*

That leads to the

Proposition 7. *Under Hypothesis 6, the path integral is a decreasing function of the path, i.e.*

$$\bar{\mathcal{C}} \geq \bar{\mathcal{C}}' \quad \Longrightarrow \quad \bar{J}_{\bar{\mathcal{C}}} \leq \bar{J}_{\bar{\mathcal{C}}'}.$$

Proof. It suffices to start from (2.35). Then the inner damage criterion (2.29) and Hypothesis 6 give the desired inequality. □

The last property consists in calculating the path integral for large paths.

Proposition 8. *Let $\bar{\mathcal{C}}_\rho$ be the circle of radius ρ and centered at $(0,0)$. Then when ρ goes to infinity, one obtains the following limit for $\bar{J}_{\bar{\mathcal{C}}_\rho}$:*

$$\bar{J}_\infty := \lim_{\rho\to\infty} \bar{J}_{\bar{\mathcal{C}}_\rho} = \bar{G} - \bar{\mathsf{G}}_\mathsf{c} \tag{2.36}$$

where $\bar{G}$ and $\bar{\mathsf{G}}_\mathsf{c}$ are the rescaled energy release rate and the rescaled dissipated energy given in (2.23) *and* (2.26).

Proof. The circle $\bar{\mathcal{C}}_\rho$ is divided into two complementary parts $\bar{\mathcal{C}}^o_\rho$ and $\bar{\mathcal{C}}^b_\rho$, the former corresponding to $\theta \in [\pi - 1/\sqrt{\rho}, -\pi + 1/\sqrt{\rho}]$ and the latter to $\theta \in (-\pi, -\pi + 1/\sqrt{\rho}) \cup (\pi - 1/\sqrt{\rho}, \pi)$. Accordingly, for large values of ρ, the damage field is nil on $\bar{\mathcal{C}}^o_\rho$ and the contribution of this part to the path integral reads

$$\bar{J}_{\bar{\mathcal{C}}^o_\rho} = \int_{\bar{\mathcal{C}}^o_\rho} \left(\frac{1}{2} \mathsf{C}_0 \bar{\boldsymbol{\sigma}} \cdot \bar{\boldsymbol{\sigma}} n_1 - \bar{\sigma}_{ij} n_j \frac{\partial \bar{u}_i}{\partial y_1} \right) \mathrm{d}\bar{s}.$$

That corresponds to the usual Rice integral in a pure linear elastic setting [Leblond 2000]. Using the asymptotic behavior (2.27) of $\bar{\boldsymbol{\sigma}}$ at infinity and the fact that the missing angular sector tends to 0 when ρ goes to infinity, one obtains at the limit

$$\lim_{\rho\to\infty} \bar{J}_{\bar{\mathcal{C}}^o_\rho} = \frac{1-\nu^2}{\mathsf{E}} (\bar{K}_I^2 + \bar{K}_{II}^2) = \bar{G}.$$

On the complementary part $\bar{\mathcal{C}}^b_\rho$, for large values of ρ, one has:

$$\mathbf{n} \approx -\mathbf{e}_1, \quad \bar{\boldsymbol{\sigma}} \approx \mathbf{0}, \qquad \bar{\alpha} \approx \alpha_*.$$

Using (2.24)–(2.26), one gets at the limit

$$\lim_{\rho\to\infty} \bar{J}_{\bar{\mathcal{C}}^b_\rho} = -\int_{-\infty}^{\infty} \left(\mathsf{w}(\alpha_*(\zeta)) + \tfrac{1}{2}\mathsf{w}_1 \alpha_*'(\zeta)^2 \right) \mathrm{d}\zeta = -\bar{\mathsf{G}}_\mathsf{c}.$$

Hence $\lim_{\rho\to\infty} \bar{J}_{\bar{\mathcal{C}}_\rho} = \bar{G} - \bar{\mathsf{G}}_\mathsf{c}$. □

2.2.7 The link with Griffith's law

We are now in a position to conclude by the

Proposition 9. *As long as the internal length of the material is small by comparison with the dimensions of the cracked body and provided that the evolution of damage satisfies Hypotheses 4–6, the evolution of the tip of the crack is governed by Griffith's law, i.e. the following conditions hold*

$$\begin{cases} \textit{Irreversibility} & \dot{\ell} \geq 0 \\ \textit{Stability} & G^\eta \leq \mathsf{G}_\mathsf{c}^\eta \\ \textit{Energy balance} & (G^\eta - \mathsf{G}_\mathsf{c}^\eta)\,\dot{\ell} = 0 \end{cases} \tag{2.37}$$

Proof. Let us prove each item of Griffith's law.

1. The irreversibility condition for ℓ is a consequence of that for α.
2. From Proposition 5, one knows that $J_0^\eta = \eta \bar{J}_0 \leq 0$ where $\bar{J}_0 = \lim_{\rho\to 0} \bar{J}_{\bar{\mathcal{C}}_\rho}$. By Proposition 7, one knows that $\bar{J}_\infty \leq \bar{J}_0$. From Proposition 8, one knows that $\bar{J}_\infty = \bar{G} - \bar{\mathsf{G}}_\mathsf{c}$. Hence $G^\eta = \eta \bar{G} \leq \eta \bar{\mathsf{G}}_\mathsf{c} = \mathsf{G}_\mathsf{c}^\eta$.
3. From Proposition 5, one knows that $J_0^\eta \dot{\ell} = 0$. By Proposition 6, one knows that $\bar{J}_\infty \dot{\ell} = \bar{J}_0 \dot{\ell}$. From Proposition 8, one knows that $\bar{J}_\infty = \bar{G} - \bar{\mathsf{G}}_\mathsf{c}$. Hence $G^\eta \dot{\ell} = \mathsf{G}_\mathsf{c}^\eta \dot{\ell}$.

The proof is complete. □

2.3 Numerical investigation of the propagation of the damage tip

In Section 2.1 cracks have been initiated when the stress is singular. Other initiation process with no singularity are possible as the one proposed in the case of homogeneous stress in a bar in traction [Pham & Marigo 2013] of for stress concentration due to a diffusion process [Sicsic *et al.* 2013]. What ever, the nucleation type observed, numerically (*e.g.* Figs. 2.1, 2.6, 2.8), that the damage localizes in bands of width η_n. In this section, we are interested in the stationary propagation of these damage band. The first implementations [Bourdin *et al.* 2000] the length η_n was considered as a numerical parameter had no physical meaning. In an asymptotic analysis, we still consider that this parameters is small, but it that it's value has a meaning. And example of the meaning of such a length can be found on the stability of uniaxial answers [Pham *et al.* 2011] or in the thermal shock setting [Sicsic *et al.* 2013]. Although it is a small parameter it remains strictly positive. The material length η_n is small in front of the size of the structure and all the other dimensions of the structures (*e.g.* heterogeneities, the cracks length). This allows for a separation of scale as in the previous sections. Thus only a stationary problem near the tip of the damage band $\mathbf{P}_t$ is studied. Let us stress that regarding the stationary evolution of the damage phase is different then initiation around a notch even when this notch has an angle of π and is then assimilated to a crack. Indeed the displacement, damage and stress field take remarkable values.

We consider that the previous evolution of the the structure has lead to the construction of a damage band and assume that the localization of damage allows for Hypothesis 5 to hold. Once again the separation

of scale is based on the use of matched asymptotic expansions as in Section 2.1. Les us repeat that ϵ is considered as a small parameter. The damage evolution problem can be decomposed into three problems: (i) the *outer problem* which gives the behavior of the fields far enough from the crack band and the crack tip; (ii) the *crack band problem* which gives the behavior of the fields in or near the crack band but far enough from the crack tip; (iii) the *crack tip problem* which gives the behavior of the fields in the neighborhood of the crack tip.

The outer problem. The order of magnitude of the fields with respect to the small parameter ϵ depends first on the order of magnitude of the loading and then on the zone where they are evaluated. The amplitude of the loading is assumed to be of the order of $\sqrt{\epsilon}$:

$$\mathbf{f}^\epsilon = \sqrt{\epsilon}\,\mathbf{f}, \mathbf{F}^\epsilon = \sqrt{\epsilon}\,\mathbf{F}, \mathbf{U}^\epsilon = \sqrt{\epsilon}\,\mathbf{U}, \boldsymbol{\varepsilon}^{0\epsilon} = \sqrt{\epsilon}\,\boldsymbol{\varepsilon}^0.$$

At a macroscale the thin process zone around the crack can be neglected and the associated outer problem is a purely elastic problem posed on the cracked domain $\Omega\backslash\Gamma$. Its solution depends linearly on the loading parameters. Since the magnitude of the loading is of the order of $\sqrt{\eta_n}$, the real displacement and stress fields can read

$$\mathbf{u}^\epsilon = \sqrt{\epsilon}\,\mathbf{u} + \cdots, \qquad \boldsymbol{\sigma}^\epsilon = \sqrt{\epsilon}\,\boldsymbol{\sigma} + \cdots$$

where $\mathbf{u}$ and $\boldsymbol{\sigma}$ satisfy in $\Omega\backslash\Gamma$ the equilibrium $\operatorname{div}\boldsymbol{\sigma}+\mathbf{f}=0$ and the constitutive relation $\boldsymbol{\sigma} = \mathsf{A}(\boldsymbol{\varepsilon}(\mathbf{u})-\boldsymbol{\varepsilon}^0)$. The boundary conditions read $\boldsymbol{\sigma}\mathbf{n} = \mathbf{F}$ on $\partial_N\Omega$, $\boldsymbol{\sigma}\mathbf{n} = \mathbf{0}$ on Γ and $\mathbf{u} = \mathbf{U}$ on $\partial_D\Omega$.

The fields $\mathbf{u}$ and $\boldsymbol{\sigma}$ are singular near the tip of the crack. In the case of an isotropic material, the singular part of $\mathbf{U}$ is

$$\mathbf{U}(\mathbf{x}) = \bar{K}_I\sqrt{r}\mathbf{U}_I(\theta) + \bar{K}_{II}\sqrt{r}\mathbf{U}_{II}(\theta) + \cdots$$

where $\bar{K}_I$, $\bar{K}_{II}$ are the (rescaled) stress intensity factors and $\mathbf{U}_I$, $\mathbf{U}_{II}$ the usual angular functions corresponding to the opening and sliding modes [Leblond 2000] and $\mathbf{U}_I(\theta) = H^\pi(\theta)$.

The crack band problem. The displacement, stress and damage are assumed to vary slowly in the direction of the band. Thus the analysis is essentially one dimensional and the damage evolution follows that of the optimal profile (2.38).

The crack tip problem. The separation of scale justifies the existence of *tip problem* as soon as η is small in front of all the other dimensions. Therefore, in the sequel, a dimensionless problem is considered and always keeping in mind that this is due to a licit rescaling. Let us fix the notations for the study of the stable propagation of a damage band. The crack is oriented following $\tilde{\mathbf{e}}_1$ therefore, $y_1 = x_1/\eta_n$ is the coordinate in the direction to the crack and $y_2 = x_2/\eta_n$ orthogonal to it. The damage field is still denoted α and the optimal profile

$$\alpha(y_2) = \left(1 - \frac{|y_2 - y_0|}{2}\right)^2, \tag{2.38}$$

where y_0 is the position of the center of the damage band and the half width of the damage zone is 2, therefore for $|y_2| > 2$ damage vanishes in the band. The only loading parameter is the stress intensity factor K_g. (r,θ) are the polar coordinates from the tip of the crack $\mathbf{P}_t$. The study of the *crack tip problem* is the goal of this section.

2.3.1 Geometry and loading of the rescaled problem at the tip of a damage band

The tip domain $\bar{\Omega}_\infty$ (Fig. 2.15) is restricted to a large circle

$$\bar{\Omega}_R = \{(\rho, \theta) \in [0, R] \times (-\pi, \pi)\}$$

the crack

$$\bar{\Gamma} = \{(\rho, \theta) \in [0, R] \times \{-\pi\}\}$$

is straight due to the hypothesis of separation of scale. Thus one can work in the basis defined by $\bar{\mathbf{e}}_1$ following the crack and $\bar{\mathbf{e}}_2$ orthogonal to it. The domain $\bar{\Omega}_R$ is considered as a disk of radius 10 whose contour is the circle $\partial\Omega = \bar{\partial_0^-\Omega} \cup \bar{\partial_\gamma^-\Omega}$. The *outer problem* has given the behavior of the fields far enough from the crack band and the crack tip. Thus the loading is that of the singularity from LE.F.M. and the damage field is equal to 0 in all other direction then that of the crack. The *crack band problem*, that $\partial\alpha/\partial\mathbf{n}$ in the direction of the crack band vanishes. Thus in the case of the tip problem. One can consider a coin with a loading the singularity of the crack tip. On which the boundary conditions in damage are prescribed

$$\alpha = 0 \text{ on } \bar{\partial_0^-\Omega} \qquad \frac{\partial\alpha}{\partial\mathbf{n}} = 0 \text{ on } \bar{\partial_\gamma^-\Omega},$$

and for the displacement:

$$\mathbf{u} = \mathbf{U}(r, \theta) \text{ on } \partial\Omega$$

where the usual angular functions read

$$U_1 = \frac{K}{2}\sqrt{\frac{\rho}{2\pi}}(\kappa - \cos\theta)\cos\frac{\theta}{2}, \quad U_2 = \frac{K}{2}\sqrt{\frac{\rho}{2\pi}}(\kappa - \cos\theta)\sin\frac{\theta}{2}$$

where $\kappa = \frac{3-\nu}{1+\nu}$. These boundary conditions are those prescribed by the first order matched asymptotic expansions. In the disk we consider the crack Γ_t, a set of points such that $\alpha = 1$, thus this imposes the boundary conditions:

$$\alpha = 1 \qquad \frac{\partial\mathbf{u}}{\partial\mathbf{n}} = u_{,2} = 0 \text{ on } \Gamma$$

In the center of the domain $\tilde{\Omega}$, an ellipse of minor and major radius $5\eta_n$ and $10\eta_n$ centered on the point of coordinates $(1, 0)$ is defined. The inner mesh size of the ellipse is h_{in}. The mesh size on the outer ring varies progressively from $h_{in}/\eta_n = 20$ to $h_{out}/\eta_n = 1$. The inner coin has 159,766 elements and the outer ring 163,675 for a total number of 323,441 elements. The total number of nodes is 161,918. Three degree of freedom (d.o.f.) are declared at each node: the two coordinates of the displacement u_1, u_2 and the damage field α.

The initial Young modulus for a sound material $\mathsf{E} = 1$, the Poisson coefficient $\nu = 0$ and the material's Toughness is normalized $\mathsf{G_c} = 1$. A monotonically increasing boundary displacement obtained from the crack-tip field for a mode-I crack on an isotropic material, scaled by a factor t, is applied. The loading parameter t evolves between 0 and 1.3 in 200 time steps. The residual rigidity $k_{\eta_n} = 10^{-6}$ and the characteristic size of the domain $R/\eta_n = 50$

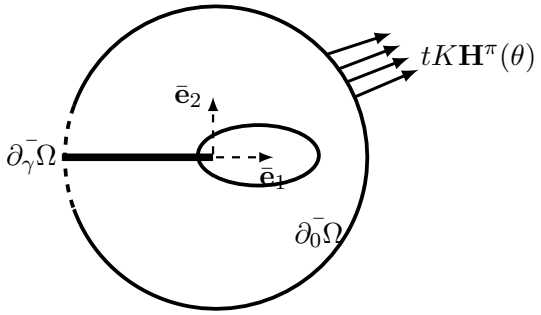

Figure 2.15: Geometry of the mesh simulating the loading at the tip pf a damage band. Ellipse at the time with a mesh size of $h = .1$

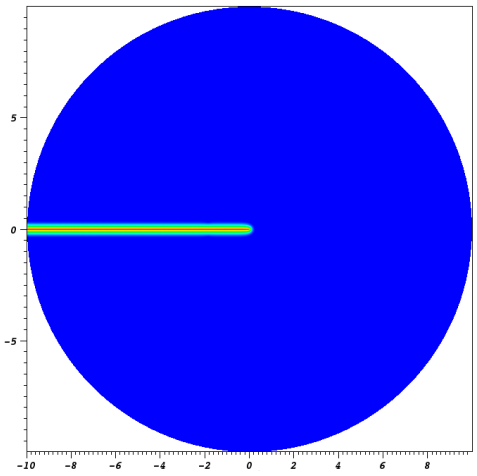

Figure 2.16: Damage field at the first time step $K = 0$. Red totally damaged field $\alpha = 1$ blue sound material $\alpha = 0$. The domain is a disc of radius 10.

2.3.2 The first time step and the optimal profile

During the first time step, the loading is nil $K = 0$. The alternate minimization algorithm captures the solution of the Laplacien with Neumann boundary conditions. Indeed as there is no loading $\mathbf{u} = 0$ the damage criteria and consistency condition (Eq. 2.11) become:

$$\mathsf{w}_1^{\mathsf{n}} + 2\mathsf{w}_1^{\mathsf{n}}\tilde{\Delta}\alpha = 0, \quad \left(\mathsf{w}_1^{\mathsf{n}} + 2\mathsf{w}_1^{\mathsf{n}}\tilde{\Delta}\alpha\right)\dot{\alpha} = 0$$

with the boundary condition $\alpha = 1$ on Γ_0. Plotting the damage field at the tip of the crack and zooming on a domain of size 1×1 we see the continuous phase of the damage (Fig. 2.17). This continuity is a consequence of the introduction of the damage of gradient.

The optimal damage profile is captures in most of the damage band except the very extremity (Fig. 2.18). Here for $y_1 = x_1/\eta_n < -1$ the damage profile in the damage zone is already that of the one dimensional study (2.38). Thus even in the tip problem, the influence of the band problem is observed, where the damage evolution follows the optimal profile.

Using polar coordinates shows that the damage profile is flatter and that as the tip the damage profile is flatten (Fig. 2.19). Thus when it is not loaded, as damage the tip of the damage band fades as quickly as possible. Let us stress, that this construction is artificial in the sens that $\alpha = 1$ is directly set. A progressive loading through α on $\bar{\Gamma}$ is not considered.

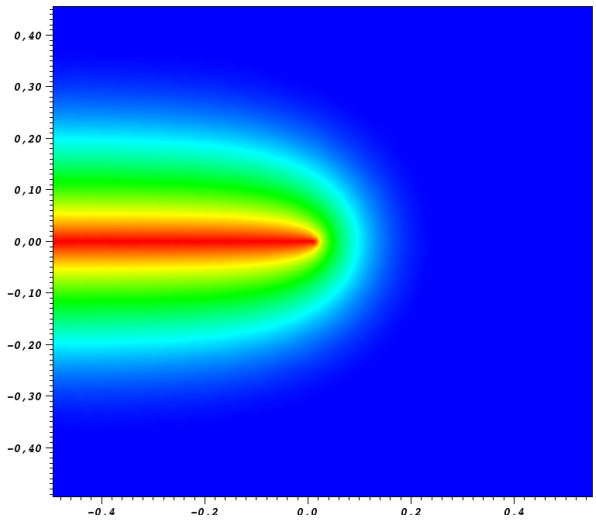

Figure 2.17: Zoom of Fig. 2.16 on the tip of the damage band ($5\eta \times 5\eta$)

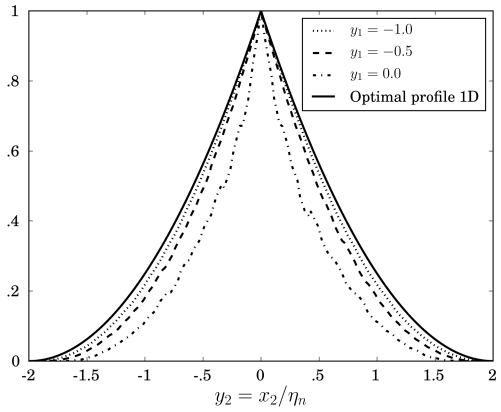

Figure 2.18: The damage profile for different distance $y_1 = \{-1, -.5, 0\}$ from the tip at the first time step for $\eta_n = .05$ compared to the optimal profile

2.3.3 Damage and stress building up to the crack propagation

The crack propagation is defined by the time step where the set of points Γ_t where the damage has reached the value 1 increases. From the first time step where there is no loading. While comparing the stress and damage in front of the crack Γ_t, (Fig. 2.23) stress grows progressively so that the zone on which the damage descents from 1 to 0. For $K = 1.02$, which corresponds to $t_i = 158$, the set of damage points such that $\alpha = 1$ grows *i.e.* the crack Γ_t propagates. This corresponds to the critical stress intensity factor of $K_{Ic} = \sqrt{\mathsf{EG_c}} = 1$ from Irwin's formula in the rescaled tip problem.

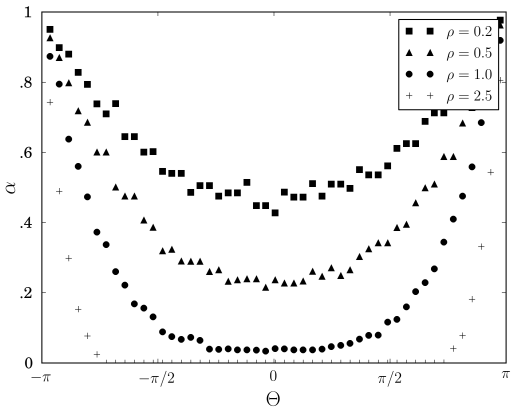

Figure 2.19: Damage profile following the angle coordinate $\theta \in [-\pi, \pi]$ for different radius $\rho = \{.2, .5, 1, 2.5\}$

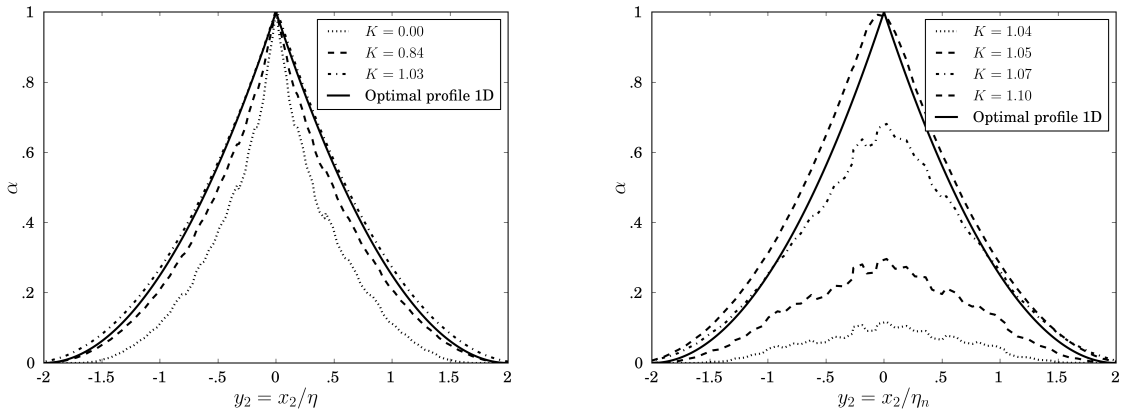

(a) Distance $y_1 = x_1 = 0$ from the tip

(b) Distance $y_1 = x_1/\eta_n = 2.5$ from the tip

Figure 2.20: The damage profile orthogonal to the crack propagation compared to the optimal profile at the tip of the crack and in the process zone

Figure 2.20 depicts the damage field orthogonal to the direction of the crack. Looking at the cross section to the tip of the crack (*i.e.* $x_1 = 0$), the damage profile with the optimal profile (2.38) for the loading corresponding to crack propagation (Fig. 2.20(a)). In front of the crack, the damage increases progressively. At a given distance from the crack (Fig. 2.20(b)) the damage only increases once the crack propagates and the optimal profile is once again captured with a certain delay. The loading has not been adapted to the propagation of the crack which explains the shift of the damage at $t_i = 170$ with the optimal profile. The entire construction of the damage profile in a crack band and thus the amount of energy dissipated happens at in front of the crack tip $\mathbf{P}_t$. Thus when the crack propagates, for any $x_1 < 0$, the cross section is that of the optimal profile and no more energy dissipation occurs.

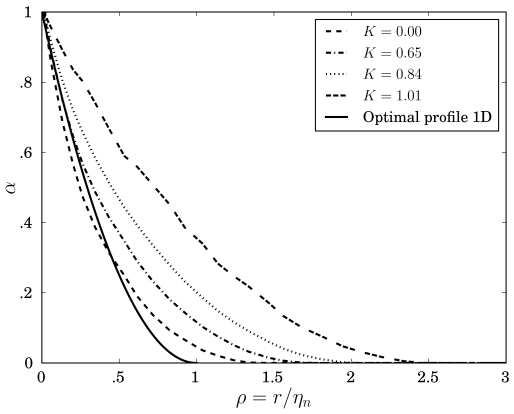

Figure 2.21: Damage profile for $\theta = 45$, at different time steps

The two privileges directions, that of the crack and its orthogonal, give us a good description of the construction of the crack tip. Yet other direction are now investigated. Figure 2.21 the damage field following a radius of angle $\theta = 45$ with the direction of the crack, illustrates the construction of the damage profile. When the crack propagates the damage profile is above the optimal profile. Thus, at propagation, we do not have isovalues following a given radius.

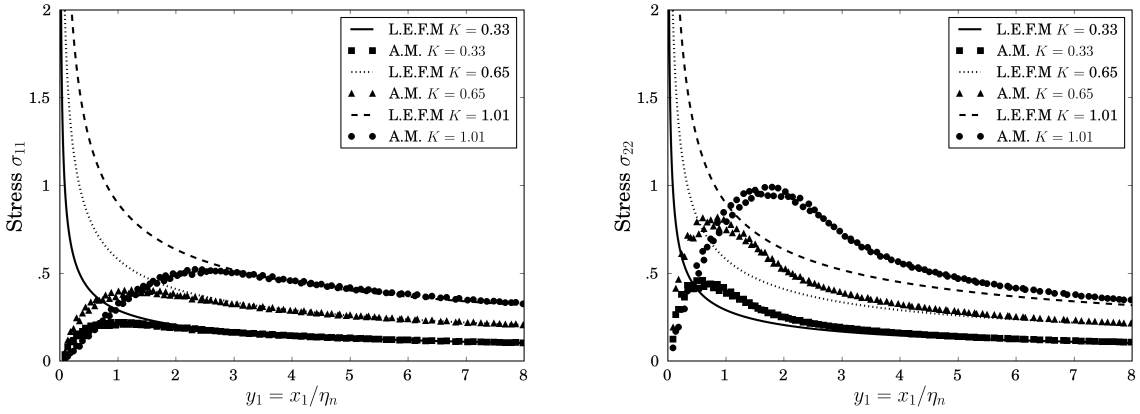

Figure 2.22: Stress evolution at the crack tip for different loading K, Comparison with the theoretical results from L.E.F.M

The stress computed by the alternate minimization algorithm is compared (Fig. 2.22) with that from L.E.F.M. The influence zone is larger in the case of σ_{22} then for the component σ_{11}. Out of this zone of influence, the two stress field coincide. For the former the zone is up to 4 times L_c where as the latter influence zone is restricted to $1.5L_c$.

2.3.4 Crack Propagation

The evolution of this damage band and that the tip problem really corresponds to a steady state (Fig. 2.23). It is remarkable how locally the stress field and the damage field coincide in their evolution.

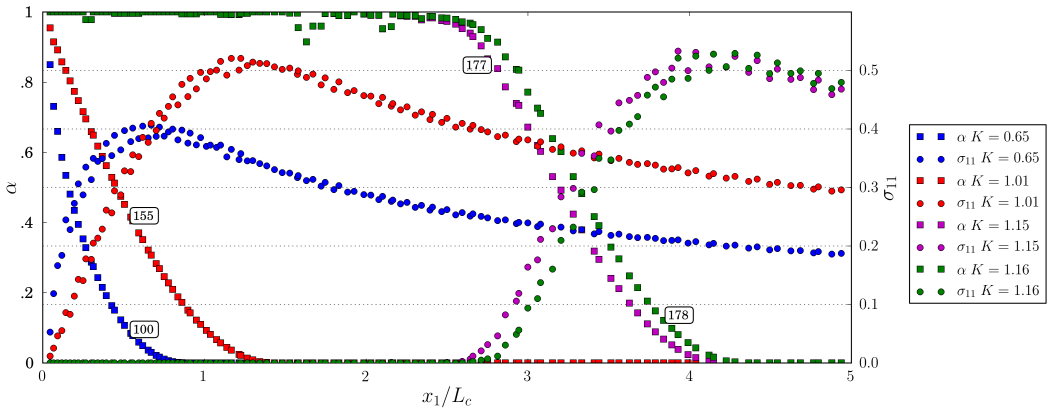

Figure 2.23: Damage and stress evolution at the crack tip for different loading K as a function of the distance from the tip of the initial crack. Although the loading (*i.e.* the singularity) is as if the crack has not propagated, one observes a translation of the stress and damage field.

The crack starts propagation at the time step $t_i = 158$, which corresponds to a loading $K = 1.03$. Study the state of the damage field for this particular loading. When the crack propagates the damage field (Fig. 2.24(a)) is very close to the optimal one in all directions. Yet the length of the process zone is one and half time the half width of the crack band, *i.e.* in the physical space three times the internal length η_n.

The stress field is no more singular because of the damage. Yet the damage field becomes singular (Remark 6). The numerical simulation captures this singularity, which is most visible when plotting the gradient of the damage for different loadings (Fig. 2.25). This singularity vanishes as predicted when the crack propagates the damage field becomes regular (Fig. 2.25).

In the one dimensional setting, the stress is always smaller then the critical stress (1.29) at any point during the entire evolution phase [Pham & Marigo 2013]. In a multidimensional context this condition is replaced by the damage criteria, which defined the state of admissible stress as a function of the current damage state. The variational evolution states that if the criteria is not reached damage can not evolve. Indeed, the damage field only starts to evolve when the criteria Figure 2.26 is reached, although the computation of the criteria (2.11) is noisy due to the laplacian of the damage field computed from linear elements.

In the numerical evolution, the alternate minimization captures a local minimum and no guarantee are given that the irreversibility condition and damage criteria are valid at all points (see *e.g.* Figs. 2.21,

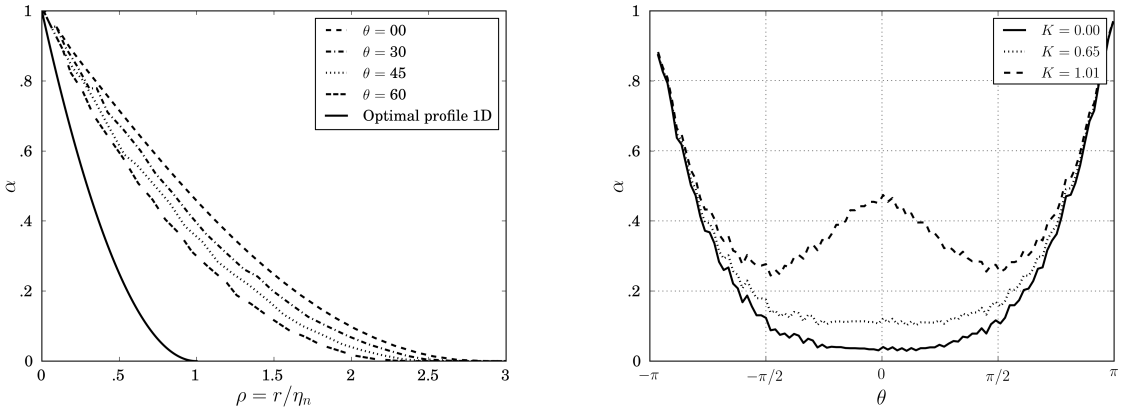

(a) Damage field for different angles at the critical time step

(b) Damage field as a function of the angle θ for a radius $\rho = r/\eta_n = 1$ for different loadings

Figure 2.24: Damage field following the Radius

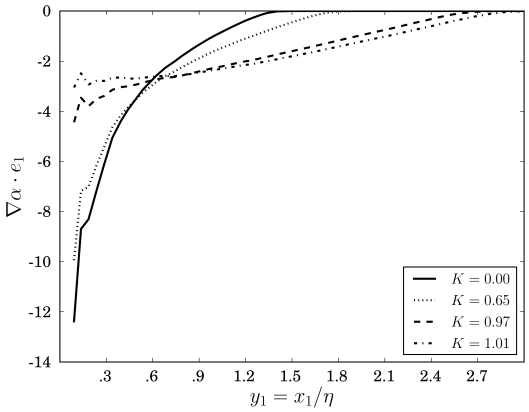

Figure 2.25: Gradient of the damage as a function of the distance from $\mathbf{P}_t$. The singularity of the damage vanishes when the crack propagates

2.24). Here, in this particular setting and as the loading in monotonically increasing, the irreversibility is automatically fulfilled. Thus enforcing or not the irreversibility condition in the numerical simulations gives the same results. The criterion is maximum at the tip of the crack and not a little away as it has been noticed [Simone *et al.* 2004] for other regularization.

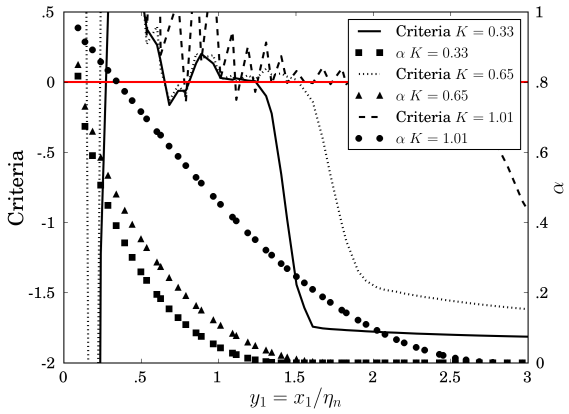

Figure 2.26: Damage field and damage criteria (2.11) at the tip of the damage band for the loading $K = \{.26, .65, 1.01\}$

2.3.5 Cohesive interpretation of the tip of the crack

Non local damage models and cohesive crack models enjoy very similar properties. Especially both present as threshold under the form of a critical stress before nucleation of damage or cracks. Yet the uses of damage on large structures is very costly in terms of computation. On the other hand cohesive model to not capture properly the position of cracks nucleation. Therefore many others [Cazes *et al.* 2009] have intended to link both formulations and build a transition from non local damage to cohesive models. Here we claim that in some sens the damage process zones in the damage band ban be viewed as a regularization of a cohesive crack model which is an intermediate step between damage and Griffith's surface energy.

The computation of the crack opening, is based on the fact that for any field ψ:

$$\int_\Omega \nabla \alpha_{\eta_n} \psi \, \mathrm{d}x \underset{\eta_n \to 0}{\to} \int \left[\psi^+ - \psi^-\right] \cdot \nu_u \, \mathrm{d}s$$

Therefore the integration of $\nabla\alpha \cdot \mathbf{u}$ over a cross section of the damage band converges towards the crack opening as η_n tends towards zero.

The theoretical profile for cohesive cracks [see Abdelmoula *et al.* 2010, Appendix], for $\nu = 0$ reads

$$[\![\mathbf{u}]\!](\mathbf{x}) = V\left(\frac{x - L}{D_c}\right) \frac{8}{\pi} \frac{\sigma_c}{\mathsf{E}} D_c$$

where σ_c is the critical stress of the cohesive model, E the young modulus D_c is the length of the cohesive process zone and $V(\zeta)$ is the dimensionless function defined by

$$V(\zeta) = \sqrt{1-\zeta} - \zeta \ln(1 + \sqrt{1-\zeta}) + \zeta \ln \sqrt{|\zeta|}$$

if $\zeta \leq 1,\ \zeta \neq 0$, $V(0) = 1$ and $V(\zeta) = 0$ otherwise.

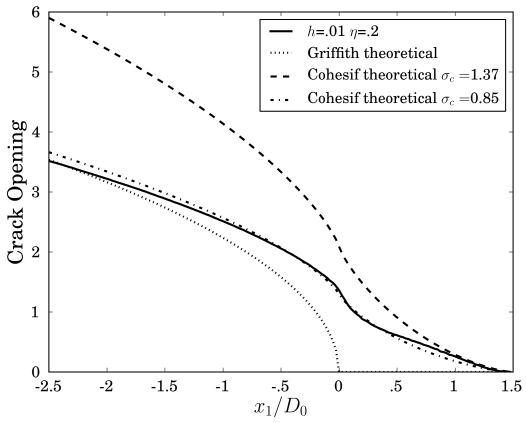

Figure 2.27: Crack Opening as distance from the tip for our damage model, two critical stress for the cohesive model and that from L.E.F.M.

Taking the critical stress $\sigma_c = 1.37$ computed from (1.29) overestimates the jump. The shape of the crack opening between the damage simulation and that from cohesive theory are very close with a concave phase for $x_1 \leq 0$ and convex phase for $0 < x_1 < D_t$. The limit of this analysis is that the distance of the process zone is the same as that at the tip of the crack. There is no physical justification for these two distances to be of the same order. Especially a damage process zone much longer then wide could be expected. Interpretation of the thickness of the damage band as that of the thickness of the process zone.

However, as the thickness and the width of the damage process zone have no reason of being of the same width, the current model is unable to truly represent a cohesive model. Adding plasticity [Alessi *et al.* 2013] seems a much promising bet as it adds the ability to predict real jumps of the displacement.

2.3.6 The case of branching under mode II loading

Here, the damage process at the tip under the loading of a mode II is investigated. Thus the damage band is considered established as in Section 2.3.2 and submitted to the mode II loading of L.E.F.M. Yet the secondary crack does not leave from the tip of the crack in $y_1 = 0$ but rather in this simulation from $y_1 = -2$. Let us state that the correct angle predicted in [Amestoy & Leblond 1992] is found (Fig. 2.28) and other angles are not investigated. The difference with [Bourdin *et al.* 2000] is that the inital state here is an established damage band and not a crack.

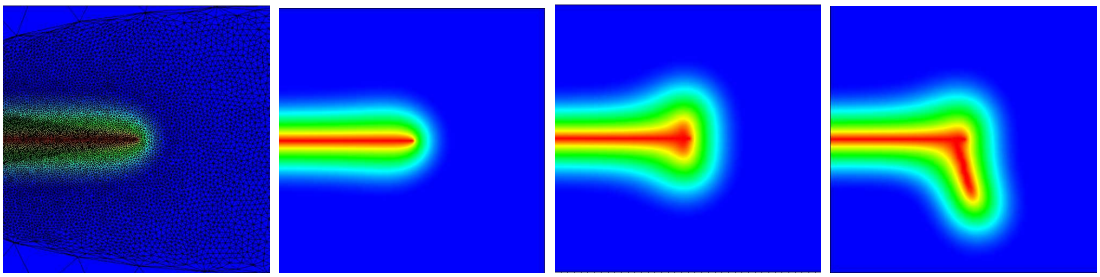

Figure 2.28: Branching on Mode II loading: Damage field for the time step {0, 100, 148, 149}

Conclusion of the chapter

Let us mention that the fundamental results of this chapter are asymptotic properties. In the case of nucleation if the size of the structure is of the same size the results would not hold *e.g.* for a plate with a notch. In Proposition 9, the crack band behaves like a Griffith crack only when the internal length η is small compared to any other length. For instance, the result is not true any more during the nucleation stage of the crack. Our result does not hold when the tip of the crack reaches the boundary of the body or is close to an inclusion. In particular, the "effective" propagation of crack bands in composite materials where the distance between the heterogeneities is of the same order as the internal length cannot be obtained with the asymptotic method proposed here.

The construction of the critical loading for crack nucleation (for instance, at the tip of a notch) with this type of gradient damage model is a very important task. Here it has been treated with a separation of scales method. First, the dimensionless problem has a scale effect appear as a competition between the size of the structure and the internal length. This means that all things being equal (geometry and material), the crack will not nucleate for the same loading as the size of the structure increases. Then the outer problem, far from the notch, is only elastic and geometric stress intensity factor is constructed. Then in the inner problem, in the vicinity of the notch, the problem is generic in the sens that it does not depend nor on the size of the structure nor on its geometry. This allows to compute a material stress intensity factor. The product of all three terms allows to determine the critical loading. Accurate results on the length of the initial cracks, at this loading, can not be established in the current framework as they are a global property. Indeed, the initial length would depend on the entire structure and is much more difficult to establish in a general sens.

Let us emphasize that the variational character of the damage evolution law is fundamental to make the link with Griffith's law. All the properties (and the definition itself) of the generalized Rice integral are based on the first order stability conditions and the energy balance. Therefore one can suspect that such a result is no more true if one adopts constitutive laws which are not connected with these energy principles. Especially in our approach, the construction of the surface energy density $\mathsf{G_c}$ as an intrinsic material parameter is a consequence of the characteristic damage profile not being history dependent. Several proofs are given here in a simplified context but one can expect that they could be extended to a

more general one. In particular, an interesting challenge would be to consider anisotropic materials and to find the dependence of the surface energy density on the orientation of the crack.

The link with Griffith's law is made with the sole help of the *first* order stability conditions and not with the complete stability condition. It is an advantage by comparison with the Gamma-convergence result based on global minimization. One can consider that our analysis reinforces this convergence result. On the other hand, it is interesting to explore all the consequences of the stability condition. In particular, one notes in the numerical simulations of the thermal shock that the cracks are periodically distributed. An interesting challenge is to give a theoretical proof of this *global* property of periodicity and even to give a method for calculating the period in terms of the parameters of the problem. This will be achieved by considering *second* order stability conditions in Chapter 3.

The alternate minimization captures the evolution in the tip of the damage band problem which is a very subtle phenomenon. The construction of the first state, for a vanishing loading, is artificial. The optimal profile can be found very near the crack tip. The stress is obviously bounded. The crack propagates for the expected loading from linear elastic fracture mechanics. The displacement field in the process zone is identical as that a cohesive zone crack model but with a different critical stress.

Chapter 3

Thermal Shock

Contents

This chapter studies the initiation of cracks in the thermal shock problem through the variational analysis of the quasi-static evolution of the gradient damage model. A two-dimensional semi-infinite slab is considered with an imposed temperature drop on its free surface. The damage model is formulated in the framework of the variational theory of rate-independent processes based on the principles of irreversibility, stability and energy balance. In the case of a sufficiently severe shock, we show that damage immediately occurs and that its evolution follows first a fundamental branch without localization. Then it bifurcates into another branch in which damage localization will take place to finally generate cracks. The determination of the time and mode of that bifurcation allows us to explain the periodic distribution of the so-initiated cracks and to calculate the crack spacing in terms of the material and loading parameters. Especially, the notions of bifurcation and loss of stability must be distinguished as unlike in elastic buckling where they often coincide, as in plasticity [Nguyen 1984, Nguyen 1987] it is not the case here. Numerical investigations complete and quantify the analytical results.

Specifically the chapter is organized as follows. Section 3.2 formalizes the thermal shock problem in a two dimensional setting and recalls the formulation of the gradient damage model. Section 3.3 establishes the fundamental solution in the elastic and damaged case. The following section is devoted to the bifurcation and loss of stability of this fundamental branch. In Section 3.4.1 we formalize the rate problem, then we characterize bifurcation and stability by Rayleigh's ratio minimization (Section 3.4.2) and give the main properties of the Rayleigh ratio (Section 3.4.3). We then characterize the first bifurcation (Section 3.4.4). The numerical computation are gathered in Section 3.5, dealing first with the fundamental solution and then with the bifurcation problem. The key results are resumed and commented in Section 3.6.

3.1 Introduction: the model problem of the thermal shock

The shrinkage of materials, induced by cooling or drying, may lead to arrays of regularly spaced cracks in a range of phenomena. Examples of such a situation come from various fields: civil engineering with the drying of concrete [Bisschop & Wittel 2011], mechanical engineering with the exposure of glass [Geyer & Nemat-Nasser 1982] or ceramics to a thermal shock [Bahr *et al.* 2010, Shao *et al.* 2010], geomaterials with the drying of soils [Morris *et al.* 1992, Chertkov 2002, Goehring *et al.* 2009] or colloidal suspensions [Gauthier *et al.* 2010], and the thermal shocks in overexploited gas storage caverns [Bérest *et al.* 2012]. These cracks are of importance as they can weaken the body or govern future diffusion process, modify the strength of the material [Shao *et al.* 2011] or compromise the safety of the structure. The thermal shock setting, that is a body at uniform setting temperature suddenly exposed to a different temperature is often used as a generic problem for the drying and cooling of materials.

Figure 3.1: Crack pattern in a slab after a thermal shock [Jiang *et al.* 2012]

The theoretical and numerical aspects of multiple cracking under thermal shock have been studied by many authors using classical tools of the Griffith theory of fracture mechanics [Hasselman 1969, Bazant *et al.* 1979, Bahr *et al.* 1988, Lu & Fleck 1998, Jagla 2002, Jenkins 2005, Bahr *et al.* 2010, Jiang *et al.* 2012]. The most intriguing phenomena are the period doubling in the crack spacing during the propagation inside the body and the crack initiation. The existing studies assume *a priori* that the cracks are straight, parallel to each other, and periodically distributed. Hence, they usually perform energetic analyses based on numerical or semi-analytical calculations of the strain energy associated to uniform or alternate crack propagation modes. In this context, [Bazant *et al.* 1979] explain selective crack arrest using a bifurcation analysis based on the change of sign of the second derivative of the strain energy with respect to the crack penetration. [Bahr *et al.* 1988] performs a similar analysis with numerical boundary element calculations and discuss crack initiation assuming periodicity and

the presence of initial flaws. [Jagla 2002] discusses the initiation and propagation of the periodic crack pattern using a stress criterion for initiation and energy minimality for optimal spacing. More recently, [Jenkins 2005] and [Jiang *et al.* 2012] study spacing and initiation by global minimization of the Griffith energy. [Bahr *et al.* 2010] derives semi-analytical scale laws for the spacing of the cracks as a function of the penetration and the severity of the thermal shock.

Differently from previous works on thermal shocks, where initiation is obtained by introducing initial flows or assuming the topology of the crack pattern, here we start with a truly sound and uniform material. By assuming a perfect conductivity at the surface of the thermal shock, we consider a Dirichlet boundary condition on the temperature and use the analytically calculated temperature field, function of space and time, to evaluate the mechanical loading in the form of thermally induced inelastic strains. The loading is controlled by the thermal shock mildness parameter $\Theta = \sigma_c/(\mathsf{E}\,\mathsf{a}\vartheta)$, where σ_c is the critical stress of the material, ϑ the temperature drop at the surface, a the thermal expansion coefficient and E the Young modulus. For mild shocks ($\Theta \geq 1$), one trivially obtains that the solution remains purely elastic and the damage is null at any time. For sufficiently severe shock ($\Theta < 1$), the damage criterion is reached at the beginning of the evolution. Looking for a solution invariant in the direction x_1 parallel to the surface of thermal shock, we show the existence of a fundamental solution with diffused damage localized in a finite strip (Proposition 11), where the damage field monotonically decreases from a maximum value at the surface to zero at a finite depth D_t^*.

Hence, we formulate the rate problem (Proposition 13) and the second-order stability conditions about this fundamental solution, whose uniqueness and stability are determined through the minimization of a Rayleigh ratio on linear spaces or convex cones (Proposition 16). The main result of this chapter is the solution of this bifurcation and stability problem (Proposition 18), which is obtained by adopting a partial Fourier decomposition in the direction parallel to the surface of the slab. We prove the existence of a finite time t_b from which a bifurcation from the fundamental branch can occur, the fundamental branch becoming unstable at a later time t_s. Moreover we show that the bifurcated solution is stable (Proposition 15) and characterized by a finite wavelength λ_b proportional to the internal length η of the material. This bifurcated solution represents the onset of the localization phenomena leading to the establishment of the periodic crack pattern observed in the experiments. Quantitative results are obtained through the numerical solution of a one-dimensional boundary value problem for the fundamental branch and of a parametric one-dimensional eigenvalue problem for establishing the key properties of the bifurcated solution as a function of the loading parameter Θ and the Poisson ratio.

3.2 Setting of the problem: the body and its thermal loading

The natural reference configuration of the plate is the semi-infinite strip $\Omega = (0, +\mathsf{L}) \times (0, +\infty)$. The length L is assumed to be much greater than the internal length η of the material. This assumption plays a role in the bifurcation and stability analyses (Section 3.4). The body forces are neglected. The sides $x_1 = 0$ or L are submitted to boundary conditions so that the normal displacement and the shear stress

vanish, whereas the side $x_2 = 0$ is free. Accordingly, the mechanical boundary conditions read as

$$u_1|_{x_1=0 \text{ or } \mathsf{L}} = 0, \quad \sigma_{21}|_{x_1=0 \text{ or } \mathsf{L}} = 0, \tag{3.1}$$

$$\sigma_{22}|_{x_2=0} = \sigma_{12}|_{x_2=0} = 0. \tag{3.2}$$

In $x_1 = 0$ or L and $x_2 = 0$ no boundary condition are imposed on the damage field, which can thus freely evolve. Up to time 0, the plate is at the reference uniform temperature T_0 and hence in its reference configuration, stress free and undamaged:

$$\mathbf{u}_t(\mathbf{x}) = \mathbf{0}, \quad \boldsymbol{\varepsilon}^e_t(\mathbf{x}) = \mathbf{0}, \quad \alpha_t(\mathbf{x}) = 0, \quad \boldsymbol{\sigma}_t(\mathbf{x}) = \mathbf{0}, \quad \forall \mathbf{x} \in \Omega, \quad \forall t \leq 0.$$

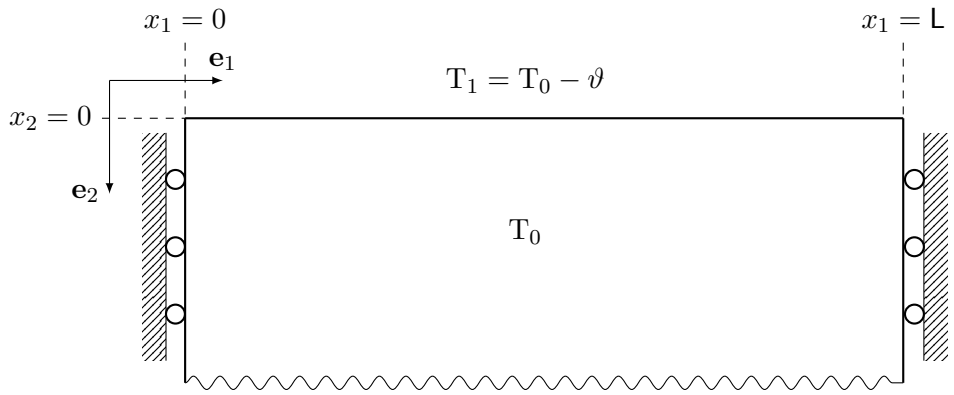

Figure 3.2: Thermal shock problem statement: Mechanical and thermal boundary conditions of a plate with an intial homogeneous temperature T_0

The plate is constituted of a material whose behavior law is that of Example 1. A is the stiffness tensor of the sound material. Thus, $(1-\alpha)^2\mathsf{A}$ represents the stiffness tensor of the material in the damage state α, it decreases from A to $\mathsf{0}$ when α grows from 0 to 1. The material being isotropic and by virtue of the plane stress assumption, the in-plane stiffness coefficients read for $i, j, k, l \in \{1, 2\}$ as

$$\mathsf{A}_{ijkl} = \frac{\nu \mathsf{E}}{1-\nu^2}\delta_{ij}\delta_{kl} + \frac{\mathsf{E}}{2(1+\nu)}(\delta_{ik}\delta_{jl} + \delta_{il}\delta_{jk}), \tag{3.3}$$

where E represents the Young modulus of the sound material and ν is the Poisson ratio, which does not change throughout the damage process.

From time 0, a colder temperature $\mathrm{T}_1 = \mathrm{T}_0 - \vartheta$ is prescribed on the side $x_2 = 0$. Assuming that the temperature field is not influenced by the damage evolution and that the sides $x_1 = 0$ or L are thermally insulated, the diffusion of the temperature inside the body is governed by the classical heat equation. Therefore, assuming the temperature boundary condition in $x_2 = 0$ is of Dirichlet type, the temperature field at time $t > 0$ is given by

$$\mathrm{T}_t(\mathbf{x}) = \mathrm{T}_0 - \vartheta\, \mathsf{f_c}\Big(\frac{x_2}{2\sqrt{\mathsf{k_c} t}}\Big) \tag{3.4}$$

where $\mathsf{f_c}$ it the complementary error function, strictly decreasing from 1 in zero (*i.e.* at the surface) to 0 at infinity, *i.e.*

$$\mathsf{f_c}(x) = \frac{2}{\sqrt{\pi}} \int_x^\infty e^{-s^2}\, \mathrm{d}s,$$

and $\mathsf{k_c}$ is the thermal diffusivity, a material constant. Thus the temperature field is uniform with respect to the x_1 direction. The influence of the damage where the permeability can change of order of magnitude has been studied by homogenization in [Dormieux & Kondo 2004, Dormieux *et al.* 2006], but this phenomena is not considered here.

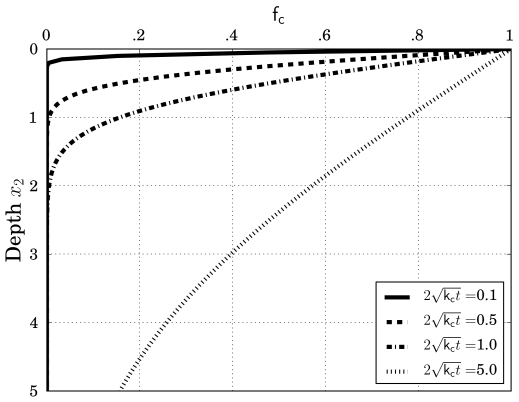

Figure 3.3: The complementary error function

At every time t, the elastic strain field $\boldsymbol{\varepsilon}_t^e$ is the difference between the total strain field $\boldsymbol{\varepsilon}_t$ and the thermal strain field $\boldsymbol{\varepsilon}_t^{\mathrm{th}}$. Since the material is isotropic, assuming that the shrinkage is linear, this latter one reads as $\boldsymbol{\varepsilon}_t^{\mathrm{th}}(\mathbf{x}) = \mathsf{a}(\mathrm{T}_t(\mathbf{x}) - \mathrm{T}_0)\mathbf{I}$, where a denotes the thermal dilatation coefficient of the material and $\mathbf{I}$ is the identity tensor of $\mathbb{M}_s$. Accordingly, the thermal and elastic strain fields read as

$$\boldsymbol{\varepsilon}_t^{\mathrm{th}}(\mathbf{x}) = -\mathsf{a}\vartheta\, \mathsf{f_c}\Big(\frac{x_2}{2\sqrt{\mathsf{k_c}t}}\Big)\, \mathbf{I}, \qquad \boldsymbol{\varepsilon}_t^e(\mathbf{x}) = \boldsymbol{\varepsilon}(\mathbf{u}_t)(\mathbf{x}) + \mathsf{a}\vartheta\, \mathsf{f_c}\Big(\frac{x_2}{2\sqrt{\mathsf{k_c}t}}\Big)\, \mathbf{I}, \tag{3.5}$$

where $\boldsymbol{\varepsilon}(\mathbf{u}_t)$ is the symmetrized part of the gradient of $\mathbf{u}_t$.

Only the first stage of the damage process will be considered in this chapter, so that α reaches nowhere the critical value 1 corresponding to the loss of rigidity of the material. Accordingly, the set of admissible damage fields $\mathcal{D}$ and the set of kinematically admissible displacement fields $\mathcal{C}$ are defined as

$$\mathcal{D} := \{\beta \in H^1(\Omega) \,:\, 0 \le \beta < 1 \text{ in } \Omega\}, \qquad \mathcal{C} := \{\mathbf{v} \in H^1(\Omega)^2 \,:\, v_1 = 0 \text{ on } x_1 = 0 \text{ or } \mathsf{L}\} \tag{3.6}$$

where $H^1(\Omega)$ denotes the usual Sobolev space of functions which are square integrable over Ω and whose distributional gradient is also square integrable. The spaces $\mathcal{D}$ and $\mathcal{C}$ are time independent and are equipped with the natural norm of $H^1(\Omega)$. With every pair of admissible displacement and damage fields,

i.e. with every $(\mathbf{v},\beta)\in\mathcal{C}\times\mathcal{D}$, is associated the total energy of the body at time t in this state, that is

$$\begin{aligned}\mathcal{P}_t(\mathbf{v},\beta) &:= \int_\Omega W(\boldsymbol{\varepsilon}(\mathbf{v})-\boldsymbol{\varepsilon}_t^{\mathrm{th}},\beta,\nabla\beta)\,\mathrm{d}\mathbf{x}\\ &= \int_\Omega\Big(\frac{1}{2}(1-\beta)^2\mathsf{A}(\boldsymbol{\varepsilon}(\mathbf{v})-\boldsymbol{\varepsilon}_t^{\mathrm{th}})\cdot(\boldsymbol{\varepsilon}(\mathbf{v})-\boldsymbol{\varepsilon}_t^{\mathrm{th}})+\mathsf{w}_1\beta+\frac{\mathsf{w}_1\eta^2}{2}\nabla\beta\cdot\nabla\beta\Big)\,\mathrm{d}\mathbf{x}. \qquad (3.7)\end{aligned}$$

where $\boldsymbol{\varepsilon}(\mathbf{v})$ denotes the symmetrized gradient of $\mathbf{v}$.

Throughout the chapter an extensive use of the directional derivatives of $\mathcal{P}_t$ and its partial derivatives with respect to time are made. All these derivatives up to the second order are defined below.

Definition 4 (Derivatives of the total energy)**.**

1. *First partial derivative with respect to t:*

$$\dot{\mathcal{P}}_t(\mathbf{v},\beta)=-\int_\Omega(1-\beta)^2\mathsf{A}(\boldsymbol{\varepsilon}(\mathbf{v})-\boldsymbol{\varepsilon}_t^{\mathrm{th}})\cdot\dot{\boldsymbol{\varepsilon}}_t^{\mathrm{th}}\,\mathrm{d}\mathbf{x}; \qquad (3.8)$$

2. *Second partial derivative with respect to t:*

$$\ddot{\mathcal{P}}_t(\mathbf{v},\beta)=\int_\Omega\Big((1-\beta)^2\mathsf{A}\dot{\boldsymbol{\varepsilon}}_t^{\mathrm{th}}\cdot\dot{\boldsymbol{\varepsilon}}_t^{\mathrm{th}}-(1-\beta)^2\mathsf{A}(\boldsymbol{\varepsilon}(\mathbf{v})-\boldsymbol{\varepsilon}_t^{\mathrm{th}})\cdot\ddot{\boldsymbol{\varepsilon}}_t^{\mathrm{th}}\Big)\,\mathrm{d}\mathbf{x}; \qquad (3.9)$$

3. *First directional derivative of $\mathcal{P}_t$ at $(\mathbf{u},\alpha)$ in the direction $(\mathbf{v},\beta)$:*

$$\begin{aligned}\mathcal{P}_t'(\mathbf{u},\alpha)(\mathbf{v},\beta) &= \int_\Omega\Big((1-\alpha)^2\mathsf{A}(\boldsymbol{\varepsilon}(\mathbf{u})-\boldsymbol{\varepsilon}_t^{\mathrm{th}})\cdot\boldsymbol{\varepsilon}(\mathbf{v})\\ &\quad+\Big(\mathsf{w}_1-(1-\alpha)\mathsf{A}(\boldsymbol{\varepsilon}(\mathbf{u})-\boldsymbol{\varepsilon}_t^{\mathrm{th}})\cdot(\boldsymbol{\varepsilon}(\mathbf{u})-\boldsymbol{\varepsilon}_t^{\mathrm{th}})\Big)\beta+\mathsf{w}_1\eta^2\nabla\alpha\cdot\nabla\beta\Big)\,\mathrm{d}\mathbf{x}; \qquad (3.10)\end{aligned}$$

4. *Second directional derivative of $\mathcal{P}_t$ at $(\mathbf{u},\alpha)$ in the direction $(\mathbf{v},\beta)$:*

$$\begin{aligned}\mathcal{P}_t''(\mathbf{u},\alpha)(\mathbf{v},\beta) &= \int_\Omega\Big((1-\alpha)^2\mathsf{A}\boldsymbol{\varepsilon}(\mathbf{v})\cdot\boldsymbol{\varepsilon}(\mathbf{v})-4(1-\alpha)\mathsf{A}(\boldsymbol{\varepsilon}(\mathbf{u})-\boldsymbol{\varepsilon}_t^{\mathrm{th}})\cdot\boldsymbol{\varepsilon}(\mathbf{v})\beta\\ &\quad+\mathsf{A}(\boldsymbol{\varepsilon}(\mathbf{u})-\boldsymbol{\varepsilon}_t^{\mathrm{th}})\cdot(\boldsymbol{\varepsilon}(\mathbf{u})-\boldsymbol{\varepsilon}_t^{\mathrm{th}})\beta^2+\mathsf{w}_1\eta^2\nabla\beta\cdot\nabla\beta\Big)\,\mathrm{d}\mathbf{x}; \qquad (3.11)\end{aligned}$$

   In (3.11), $\mathcal{P}_t''(\mathbf{u},\alpha)$ is considered as a quadratic form. The associated symmetric bilinear form is still denoted by $\mathcal{P}_t''(\mathbf{u},\alpha)$, but is discriminated by denoting $\mathcal{P}_t''(\mathbf{u},\alpha)\,\big\langle(\mathbf{v},\beta),(\bar{\mathbf{v}},\bar{\beta})\big\rangle$ its application to a pair of directions. Accordingly, one has $\mathcal{P}_t''(\mathbf{u},\alpha)(\mathbf{v},\beta)=\mathcal{P}_t''(\mathbf{u},\alpha)\,\langle(\mathbf{v},\beta),(\mathbf{v},\beta)\rangle$.

5. *Second order cross term:*

$$\dot{\mathcal{P}}_t'(\mathbf{u},\alpha)(\mathbf{v},\beta)=\int_\Omega\Big(-(1-\alpha)^2\mathsf{A}\dot{\boldsymbol{\varepsilon}}_t^{\mathrm{th}}\cdot\boldsymbol{\varepsilon}(\mathbf{v})+2(1-\alpha)\mathsf{A}(\boldsymbol{\varepsilon}(\mathbf{u})-\boldsymbol{\varepsilon}_t^{\mathrm{th}})\cdot\dot{\boldsymbol{\varepsilon}}_t^{\mathrm{th}}\beta\Big)\,\mathrm{d}\mathbf{x}. \qquad (3.12)$$

To simplify the presentation, only evolutions smooth both in space and time will be considered. It is not really a restrictive assumption. Indeed, the main interest is the loss of uniqueness and of stability of the "fundamental branch" which is smooth as seen in the next section. Specifically, the following smoothness assumption is made

Hypothesis 7. *The only evolutions considered are those such that*

1. *Each component of* $\mathbf{u}_t$ *and* α_t *are continuously differentiable in* Ω *and belong to* $H^2(\Omega)$ *at every* $t \geq 0$*;*
2. $t \mapsto \mathbf{u}_t$ *and* $t \mapsto \alpha_t$ *are continuous and piecewise continuous differentiable. The right and the left time derivatives* $\dot{\mathbf{u}}_t^{\pm}$ *and* $\dot{\alpha}_t^{\pm}$ *exist at every time,* $\dot{\mathbf{u}}_t^{\pm}$ *belongs to* $\mathcal{C}$ *and* $\dot{\alpha}_t^{\pm}$ *belongs to* $\mathcal{D}^+$*, where*

$$\mathcal{D}^+ := H^1(\Omega) \cap \{\beta \geq 0\}.$$

From the damage evolution law (Hypothesis 4) and specifically Proposition 3, the first order stability conditions (1.14)–(1.15)are satisfied if and only if:

$$\operatorname{div} \boldsymbol{\sigma}_t = \mathbf{0} \text{ in } \Omega, \qquad \boldsymbol{\sigma}_t \mathbf{e}_2 = \mathbf{0} \text{ on } x_2 = 0, \qquad \boldsymbol{\sigma}_t \mathbf{e}_1 \cdot \mathbf{e}_2 = 0 \text{ on } x_1 = 0 \text{ or } \mathsf{L}, \tag{3.13}$$

$$(1-\alpha_t)\mathsf{A}\boldsymbol{\varepsilon}_t^e \cdot \boldsymbol{\varepsilon}_t^e - \mathsf{w}_1 + \mathsf{w}_1 \eta^2 \Delta \alpha_t \leq 0 \text{ in } \Omega, \qquad \frac{\partial \alpha_t}{\partial n} \geq 0 \text{ on } \partial\Omega. \tag{3.14}$$

Let us use the energy balance (1.11) which reads in the current setting as

$$\mathcal{P}_t(\mathbf{u}_t, \alpha_t) + \int_0^t \left(\int_\Omega \boldsymbol{\sigma}_s \cdot \dot{\boldsymbol{\varepsilon}^{\text{th}}}_t \, \mathrm{d}\mathbf{x} \right) \mathrm{d}s = 0.$$

Owing to the smoothness assumption on the time evolution, taking the derivative of (1.11) with respect to t leads to

$$\begin{aligned} 0 &= \frac{d}{dt} \int_\Omega W(\boldsymbol{\varepsilon}(\mathbf{u}_t) - \boldsymbol{\varepsilon}_t^{\text{th}}, \alpha_t, \nabla \alpha_t) \, \mathrm{d}\mathbf{x} + \int_\Omega \boldsymbol{\sigma}_t \cdot \dot{\boldsymbol{\varepsilon}}_t^{\text{th}} \, \mathrm{d}\mathbf{x} \\ &= \int_\Omega \left(\boldsymbol{\sigma}_t \cdot \boldsymbol{\varepsilon}(\dot{\mathbf{u}}_t) - \mathsf{Y}_t \dot{\alpha}_t + \mathbf{q}_t \cdot \nabla \dot{\alpha}_t \right) \mathrm{d}\mathbf{x} \\ &= -\int_\Omega \Big(\operatorname{div} \boldsymbol{\sigma}_t \cdot \dot{\mathbf{u}}_t + (\mathsf{Y}_t + \operatorname{div} \mathbf{q}_t) \dot{\alpha}_t \Big) \, \mathrm{d}\mathbf{x} + \int_{\partial\Omega} \Big(\boldsymbol{\sigma}_t \mathbf{n} \cdot \dot{\mathbf{u}}_t + \mathbf{q}_t \cdot \mathbf{n} \dot{\alpha}_t \Big) \, \mathrm{d}s. \end{aligned} \tag{3.15}$$

Taking into account the equilibrium and the boundary conditions (3.13), the terms containing $\boldsymbol{\sigma}_t$ vanish in (3.15). By virtue of the irreversibility conditions and the inequalities (3.14), the equality (3.15) holds if an only if the following pointwise equalities hold

$$\Big((1-\alpha_t)\mathsf{A}\boldsymbol{\varepsilon}_t^e \cdot \boldsymbol{\varepsilon}_t^e - \mathsf{w}_1 + \mathsf{w}_1 \eta^2 \Delta \alpha_t \Big) \dot{\alpha}_t = 0 \text{ in } \Omega, \qquad \frac{\partial \alpha_t}{\partial n} \dot{\alpha}_t = 0 \text{ on } \partial\Omega. \tag{3.16}$$

These equalities can be seen as the local energy balances. They correspond also to what is generally called the consistency relations in Kuhn-Tucker conditions. (1.16) becomes

Proposition 10. *A smooth stable evolution $t \mapsto (\mathbf{u}_t, \alpha_t) \in \mathcal{C} \times \mathcal{D}$ must satisfy the following set of local conditions at every time $t \geq 0$ (with the convention that at any time when $t \mapsto \alpha_t$ is not differentiable, the relations hold both for $\dot\alpha_t^-$ and $\dot\alpha_t^+$):*

1. **The Kuhn-Tucker conditions in the bulk**

$$\text{In } \Omega: \qquad \begin{cases} \dot\alpha_t \geq 0, \\ (1-\alpha_t)\mathsf{A}(\boldsymbol{\varepsilon}(\mathbf{u}_t) - \boldsymbol{\varepsilon}_t^{\mathrm{th}}) \cdot (\boldsymbol{\varepsilon}(\mathbf{u}_t) - \boldsymbol{\varepsilon}_t^{\mathrm{th}}) - \mathsf{w}_1 + \mathsf{w}_1 \eta^2 \Delta\alpha_t \leq 0, \\ \Big((1-\alpha_t)\mathsf{A}(\boldsymbol{\varepsilon}(\mathbf{u}_t) - \boldsymbol{\varepsilon}_t^{\mathrm{th}}) \cdot (\boldsymbol{\varepsilon}(\mathbf{u}_t) - \boldsymbol{\varepsilon}_t^{\mathrm{th}}) - \mathsf{w}_1 + \mathsf{w}_1 \eta^2 \Delta\alpha_t\Big)\dot\alpha_t = 0. \end{cases}$$

2. **The Kuhn-Tucker conditions on the boundary**

$$\text{On } \partial\Omega: \qquad \dot\alpha_t \geq 0, \quad \frac{\partial \alpha_t}{\partial n} \geq 0, \quad \frac{\partial \alpha_t}{\partial n}\dot\alpha_t = 0.$$

3. **The equilibrium equations and the static boundary conditions**

$$\operatorname{div} \boldsymbol{\sigma}_t = \mathbf{0} \text{ in } \Omega, \qquad \boldsymbol{\sigma}_t \mathbf{e}_2 = \mathbf{0} \text{ on } x_2 = 0, \qquad \boldsymbol{\sigma}_t \mathbf{e}_1 \cdot \mathbf{e}_2 = 0 \text{ on } x_1 = 0 \text{ or } \mathsf{L}.$$

4. **The stress-strain relation**

$$\boldsymbol{\sigma}_t = (1-\alpha_t)^2 \mathsf{A}(\boldsymbol{\varepsilon}(\mathbf{u}_t) - \boldsymbol{\varepsilon}_t^{\mathrm{th}}) \text{ in } \Omega.$$

These conditions are sufficient in order for the irreversibility condition and the energy balance be satisfied, but not sufficient to verify the full stability condition (1.10)*. Accordingly, a smooth evolution which satisfies only the four conditions above will be called a* stationary *evolution.*

3.3 The fundamental branch

3.3.1 The elastic response

Let us consider the elastic response of the plate, *i.e.* the response such that $\alpha_t = 0$ at every t. The stress and strain fields are given by

$$\boldsymbol{\sigma}_t(\mathbf{x}) = \mathsf{E}\mathsf{a}\vartheta\, \mathsf{f}_{\mathsf{c}}\Big(\frac{x_2}{2\sqrt{\mathsf{k}_{\mathsf{c}} t}}\Big)\mathbf{e}_1 \otimes \mathbf{e}_1, \qquad \boldsymbol{\varepsilon}(\mathbf{u}_t)(\mathbf{x}) = -(1+\nu)a\vartheta\, \mathsf{f}_{\mathsf{c}}\Big(\frac{x_2}{2\sqrt{\mathsf{k}_{\mathsf{c}} t}}\Big)\mathbf{e}_2 \otimes \mathbf{e}_2, \tag{3.17}$$

from which one easily deduces $\mathbf{u}_t$ (in particular $\mathbf{u}_t \cdot \mathbf{e}_1 = 0$ and $\mathbf{u}_t \cdot \mathbf{e}_2$ only depends on x_2). Since $|\sigma_{t11}|$ is maximal on the side $x_2 = 0$ where it takes the value $\mathsf{E}\mathsf{a}\vartheta$ at every $t \geq 0$, the damage criterion (3.14) is satisfied everywhere in Ω at every time if and only if $\mathsf{a}\vartheta \leq \sigma_c/\mathsf{E}$ with $\sigma_c = \sqrt{\mathsf{w}_1 \mathsf{E}}$ given by (1.29). Specifically, one has

1. If $\mathsf{E}\mathsf{a}^2\vartheta^2 \leq \mathsf{w}_1$, then inserting (3.17) into (3.10) leads to

$$\mathcal{P}'_t(\mathbf{u}_t,0)(\mathbf{v}-\mathbf{u}_t,\beta) = \int_\Omega \left(\mathsf{w}_1 - \mathsf{E}\mathsf{a}^2\vartheta^2\,\mathsf{f}_\mathsf{c}\Big(\frac{x_2}{2\sqrt{\mathsf{k}_\mathsf{c} t}}\Big)^2\right)\beta\,\mathrm{d}\mathbf{x}, \qquad \forall t>0, \forall(\mathbf{v},\beta)\in\mathcal{C}\times\mathcal{D}.$$

   Since $\mathsf{f}_\mathsf{c}(x)$ decreases from 1 to 0 when x grows from 0 to ∞, $\mathcal{P}'_t(\mathbf{u}_t,\alpha_t)(\mathbf{v}-\mathbf{u}_t,\beta) \geq 0$ and the equality holds if and only if $\beta = 0$ everywhere in Ω. Moreover, by virtue of (3.11), in such directions the second derivative reads as

$$\mathcal{P}''_t(\mathbf{u}_t,0)(\mathbf{v}-\mathbf{u}_t,0) = \int_\Omega \mathsf{A}\boldsymbol{\varepsilon}(\mathbf{v})\cdot\boldsymbol{\varepsilon}(\mathbf{v})\,\mathrm{d}\mathbf{x}.$$

   Therefore $\mathcal{P}''_t(\mathbf{u}_t,0)(\mathbf{v}-\mathbf{u}_t,0) > 0$ for every $\mathbf{v}\in\mathcal{C}\setminus\{0\}$ and hence *the elastic response is stable* at every time $t \geq 0$ in all directions by virtue of Proposition 2.

2. If $\mathsf{E}\mathsf{a}^2\vartheta^2 > \mathsf{w}_1$, then at every time $t>0$ there exists a subdomain of Ω where the damage criterion (3.14) is not satisfied. Hence, *the elastic response is never stable.* Damage occurs as soon as $t>0$.

3.3.2 The fundamental *damage* branch

From now on only the case when $\mathsf{a}\vartheta\mathsf{E} > \sigma_c$ will be considered. The dimensionless loading parameter Θ which characterizes the mildness of the thermal shock

$$\Theta = \frac{\sigma_c}{\mathsf{a}\vartheta\mathsf{E}} < 1 \tag{3.18}$$

is introduced. If the elastic response is considered, one sees that the damage criterion (3.14) is violated in the strip $0 < x_2 < 2\mathsf{f}_\mathsf{c}^{-1}(\Theta)\sqrt{\mathsf{k}_\mathsf{c} t}$ which grows progressively with time. One can suspect that damage occurs in this strip. Moreover, since the loading and the geometry are invariant with respect to the x_1 direction, one can seek first for an evolution which only depends on x_2 and t. Accordingly, a stationary evolution $(\mathbf{u}^*_t,\alpha^*_t)$ such that α^*_t is of the form

$$\alpha^*_t(\mathbf{x}) = \bar\alpha_\tau(y), \quad \tau = \frac{2\sqrt{\mathsf{k}_\mathsf{c} t}}{\Theta\eta}, \quad y = \frac{x_2}{2\sqrt{\mathsf{k}_\mathsf{c} t}} \tag{3.19}$$

is treated. Where new spatial and time variables inspired by the thermal diffusion process have been introduced. Inserting this form into (3.13), it is easy to see that the displacement field is the same as the elastic one and hence

$$\boldsymbol{\varepsilon}(\mathbf{u}^*_t)(\mathbf{x}) = \bar{\boldsymbol{\varepsilon}}_\tau(y) := -(1+\nu)a\vartheta\,\mathsf{f}_\mathsf{c}(y)\mathbf{e}_2\otimes\mathbf{e}_2. \tag{3.20}$$

The stress field is different because of the damage evolution

$$\boldsymbol{\sigma}^*_t(\mathbf{x}) = \bar{\boldsymbol{\sigma}}_\tau(y) := (1-\bar\alpha_\tau(y))^2\mathsf{E}\mathsf{a}\vartheta\,\mathsf{f}_\mathsf{c}(y)\mathbf{e}_1\otimes\mathbf{e}_1. \tag{3.21}$$

It remains to find the evolution of the damage $\bar\alpha_\tau$ in the coordinates $(y,\ \tau)$. Assuming that the support of $\bar\alpha_\tau$ is the interval $[0,\delta_\tau)$ where δ_τ has to be determined, by virtue of (3.14) and (3.16), $\bar\alpha_\tau$ must satisfy the following differential equation in this interval

$$\frac{1}{\tau^2}\frac{d^2\bar\alpha_\tau}{dy^2}(y) + \mathsf{f}_\mathsf{c}(y)^2(1-\bar\alpha_\tau(y)) = \Theta^2 \qquad \forall y\in(0,\delta_\tau). \tag{3.22}$$

The Kuhn-Tucker condition at $x_2 = 0$ requires that the first derivative of $\bar{\alpha}_\tau$ vanishes at $y = 0$. The continuity of $\bar{\alpha}_\tau$ and of its first derivative at $y = \delta_\tau$ require that both quantities vanish. Therefore the boundary conditions read

$$\frac{d\bar{\alpha}_\tau}{dy}(0) = 0, \qquad \bar{\alpha}_\tau(\delta_\tau) = 0, \qquad \frac{d\bar{\alpha}_\tau}{dy}(\delta_\tau) = 0. \tag{3.23}$$

Moreover, the damage criterion is satisfied for $y \geq \delta_\tau$ if and only if $\mathsf{f_c}(\delta_\tau) \leq \Theta$ and hence if and only if

$$\delta_\tau \geq \mathsf{f_c}^{-1}(\Theta). \tag{3.24}$$

The existence and the uniqueness of $\bar{\alpha}_\tau$ and δ_τ as a solution of (3.22)–(3.24) is a consequence of the following

Proposition 11. *At each time $\tau > 0$ the damage field $\bar{\alpha}_\tau$ is necessarily the unique minimizer of $\bar{\mathcal{P}}_\tau$ over $\{\beta \in H^1(0,\infty) \,:\, 0 \leq \beta \leq 1\}$, where*

$$\bar{\mathcal{P}}_\tau(\beta) := \int_0^\infty \left(\frac{1}{2\tau^2}\beta'(y)^2 + \frac{1}{2}\mathsf{f_c}(y)^2(1-\beta(y))^2 + \Theta^2\beta(y) \right) \mathrm{d}y. \tag{3.25}$$

Accordingly, the support of $\bar{\alpha}_\tau$ is really a finite interval $[0,\delta_\tau)$ and $(\bar{\alpha}_\tau, \delta_\tau)$ satisfy (3.22)–(3.24). Moreover $\bar{\alpha}_\tau$ is monotonically decreasing in $[0,\delta_\tau)$ from $\bar{\alpha}_\tau(0) < 1$ to 0.

Proof. The proof goes as follows. First the existence and uniqueness of minimizers is established. Then 0 is proven not to be a minimizer. The regularity of $\bar{\alpha}_\tau$ and its support are established. The proof is given in Appendix C.1. □

From the characterization of $\bar{\alpha}_\tau$, it is easy to obtain its asymptotic behavior at small times and at large times. This leads to the

Proposition 12 (Asymptotic behaviors of $\bar{\alpha}_\tau$)**.**

1. *When τ tends to 0, $(\bar{\alpha}_\tau/\tau^2, \delta_\tau)$ strongly converges in $H^1(0,\infty)\times\mathbb{R}$ to $(\bar{\alpha}_0, \delta_0)$ given by*

$$\delta_0 \text{ is the unique positive number such that } \Theta^2\delta_0 = \textstyle\int_0^{\delta_0} \mathsf{f_c}(y)^2 \,\mathrm{d}y, \tag{3.26}$$

$$\begin{cases} \bar{\alpha}_0''(y) = \Theta^2 - \mathsf{f_c}(y)^2 & \text{if} \quad y \in [0,\delta_0) \\ \bar{\alpha}_0(y) = 0 & \text{if} \quad y > \delta_0 \end{cases}, \qquad \bar{\alpha}_0(\delta_0) = \bar{\alpha}_0'(\delta_0) = 0. \tag{3.27}$$

2. *When τ tends to ∞, $(\bar{\alpha}_\tau, \delta_\tau)$ strongly converges in $L^2(0,\infty)\times\mathbb{R}$ to $(\bar{\alpha}_\infty, \delta_\infty)$ given by*

$$\delta_\infty = \mathsf{f_c}^{-1}(\Theta), \qquad \bar{\alpha}_\infty(y) = \begin{cases} 1 - \dfrac{\Theta^2}{\mathsf{f_c}(y)^2} & \text{if} \quad y \in [0,\delta_\infty) \\ 0 & \text{if} \quad y \geq \delta_\infty \end{cases}. \tag{3.28}$$

Proof. This result is quite natural in view of (3.22)-(3.23). It can be rigorously proved by virtue of Proposition 11 and using classical arguments of functional analysis based on first estimates, weak and strong convergences. The proof is given in Appendix C.2. □

Thus Proposition 12 gives the typical behavior for short and long times. The impact of Θ easily be illustrated on positioning Θ, δ_0 and δ_∞ on the graph of $\mathsf{f_c}^2$ (Fig. 3.4) and mild loading will lead to very close initial and final diffusivity whereas for severe loading the initial diffusivity which be much higher.

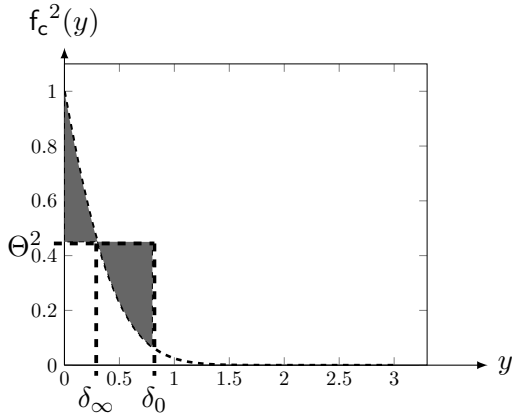

Figure 3.4: Geometrical interpretation of the initial δ_0 and final δ_∞ diffusivity. δ_0 verifies Maxwell line: the two gray area are equal.

In order that $t \mapsto (\mathbf{u}_t^*, \alpha_t^*)$ be an admissible evolution (at least a stationary evolution), it remains to verify that $t \mapsto \alpha_t^*$ satisfies the irreversibility condition, *i.e.* is monotonically increasing. Unfortunately, this property cannot be proven analytically and will be only checked numerically. Indeed, using the chain rule, $\dot{\alpha}_t^*(\mathbf{x})$ reads as

$$\dot{\alpha}_t^*(\mathbf{x}) = \frac{d\bar{\alpha}_\tau}{dy}(y)\frac{\partial y}{\partial t} + \dot{\bar{\alpha}}_\tau(y)\frac{d\tau}{dt}.$$

The first term in the right hand side above is positive because $y \mapsto \bar{\alpha}_\tau(y)$ is monotonically decreasing at given time and y is a decreasing function of t at given x_2. Yet, $\tau \mapsto \bar{\alpha}_\tau$ is not monotonically increasing. Indeed, $\tau \mapsto \delta_\tau$ is in fact *monotonically decreasing*. (In particular one immediately deduces from (3.26) and (3.28) that $\delta_0 > \delta_\infty$.) Consequently, the second term in the right hand side above is not always positive and one cannot conclude. Accordingly, one adopts the following

Hypothesis 8 (Monotonicity of $t \mapsto \alpha_t^*$). *Throughout the next section $t \mapsto \alpha_t^*$ is assumed to be monotonically increasing and hence that the depth $\mathsf{D}_t^* := 2\delta_\tau\sqrt{\mathsf{k_c}t}$ of the damage zone associated with the fundamental branch is an increasing function of time. Those properties will be checked numerically in Section 3.5.*

3.4 Bifurcation from and instability of the fundamental branch

In the wake of [Nguyen 1994, Nguyen 2000] bifurcation and stability theory is used. It has been introduced in the case of non local damage for the selection of solutions in [Benallal & Marigo 2007]. The response can follow the fundamental branch only as long as the associated state is stable. But the evolution can bifurcate on another branch before the loss of stability of the fundamental branch, whenever such a branch exists and is itself stable (at least in a neighborhood of the bifurcation point). Accordingly, it is important to identify the possible points of bifurcation on the fundamental branch. It is the aim of this section.

3.4.1 Setting of the rate problem

Let $t > 0$ be a given time and $(\mathbf{u}_t^*, \alpha_t^*)$ be the associated state of the fundamental branch, given by (3.19)–(3.24). Let us study the evolution problem in the time interval $[t, t+t')$, with $t' > 0$ and small enough, assuming that the state of the body is the fundamental one $(\mathbf{u}_t^*, \alpha_t^*)$ at time t. Let $\{(\mathbf{u}_s, \alpha_s)\}_{s\in[t,t+t')}$ be a possible solution of the evolution problem during the time interval $[t, t+t')$. One assumes that the evolution is sufficiently smooth so that the right derivative exists at t. This derivative denoted $(\dot{\mathbf{u}}, \dot{\alpha})$ is defined by

$$\dot{\mathbf{u}} = \lim_{h\downarrow 0} \frac{1}{h}(\mathbf{u}_{t+h} - \mathbf{u}_t^*), \qquad \dot{\alpha} = \lim_{h\downarrow 0} \frac{1}{h}(\alpha_{t+h} - \alpha_t^*), \tag{3.29}$$

these limits being understood in the sense of the natural norm of $\mathcal{C}\times\mathcal{D}$. Moreover, the construction of the rate problem giving $(\dot{\mathbf{u}}, \dot{\alpha})$ needs an additional smoothness assumption relative to the growth of the damage zone. Specifically, one adopts the following

Hypothesis 9 (Smooth growth of the damage zone)**.** *Let Ω_s^d be the damage zone at time $s \in [t, t+t')$ in the evolution $\{(\mathbf{u}_s, \alpha_s)\}_{s\in[t,t+t')}$, i.e.*

$$\Omega_s^d = \{\mathbf{x} \in \Omega \ : \ \alpha_s(\mathbf{x}) > 0\}. \tag{3.30}$$

Thus $\Omega_t^d = (0,\mathsf{L})\times[0,\mathsf{D}_t^*)$. By virtue of the irreversibility condition and Hypothesis 8, $s \mapsto \Omega_s^d$ is increasing. One assumes that this growth is smooth in the sense that there exists $C > 0$ such that

$$\Omega_s^d \setminus \Omega_t^d \subset (0,\mathsf{L})\times[\mathsf{D}_t^*, \mathsf{D}_t^* + C(s-t)).$$

Thus, the new damaging points in the time interval (t, s) are included in a strip of width $C(s-t)$.

Of course, if the evolution follows the fundamental branch, then $(\dot{\mathbf{u}}, \dot{\alpha}) = (\dot{\mathbf{u}}_t^*, \dot{\alpha}_t^*)$ and Hypothesis 9 is satisfied because $\tau \mapsto \delta_\tau$ is smooth.

Our purpose is to find whether another rate is possible, recalling that only the case $\Theta < 1$ is considered. Imposing the evolution to satisfy the three items (IR), (ST) and (EB) and Hypothesis 7, one deduces the following variational formulation for the rate problem.

Proposition 13 (The rate problem)**.** *Let $t > 0$ be a given time. At this time, the rate $(\dot{\mathbf{u}}, \dot{\alpha})$ of any branch which is solution of the evolution problem and follows the fundamental branch up to time t is such that*

$$\begin{aligned} \dot{\boldsymbol{\chi}} = (\dot{\mathbf{u}}, \dot{\alpha}) \in \mathcal{C}\times\dot{\mathcal{D}}_t^+, \qquad \forall \boldsymbol{\xi} = (\mathbf{v}, \beta) \in \mathcal{C}\times\dot{\mathcal{D}}_t^+ \\ \mathcal{P}_t''(\boldsymbol{\chi}_t^*)\langle\dot{\boldsymbol{\chi}}, \boldsymbol{\xi} - \dot{\boldsymbol{\chi}}\rangle + \dot{\mathcal{P}}_t'(\boldsymbol{\chi}_t^*)(\boldsymbol{\xi} - \dot{\boldsymbol{\chi}}) \geq 0. \end{aligned} \tag{3.31}$$

In (3.31) *$\dot{\mathcal{D}}_t^+$ is the set of admissible damage rate fields at time t, i.e.*

$$\dot{\mathcal{D}}_t^+ = \{\beta \in H^1(\Omega) : \beta \geq 0 \text{ in } \Omega_t^d,\ \beta = 0 \text{ in } \Omega \setminus \Omega_t^d\}, \qquad \Omega_t^d = (0, \mathsf{L})\times[0, \mathsf{D}_t^*).$$

Proof. The proof given in C.3 is based on the derivation of the first order stability condition and the expansion of the energy balance at $t + h$ The regularity assumptions of Hypotheses 7 and 9 are key. □

$\dot{\mathcal{D}}_t^+$ is time dependent unlike $\mathcal{D}$ as Ω_s^d (3.30) evolves with time as the fundamental solution penetrates into the body.

3.4.2 Characterization of bifurcation and stability by Rayleigh's ratio minimization

The rate $\dot{\boldsymbol{\chi}}_t^* = (\dot{\mathbf{u}}_t^*, \dot{\alpha}_t^*)$ is solution of (3.31). The question is to know whether another solution exists. The uniqueness is guaranteed when the quadratic form $\mathcal{P}_t''(\boldsymbol{\chi}_t^*)$ is positive definite on the linear space $\mathcal{C}\times\dot{\mathcal{D}}_t$, $\dot{\mathcal{D}}_t$ denoting the linear space generated by $\dot{\mathcal{D}}_t^+$, *i.e.*

$$\dot{\mathcal{D}}_t = \{\beta \in H^1(\Omega) : \beta = 0 \text{ in } \Omega \setminus \Omega_t^d\}. \tag{3.32}$$

Indeed, in such a case, let us consider another solution $\dot{\boldsymbol{\chi}}$. Making $\boldsymbol{\xi} = \dot{\boldsymbol{\chi}}_t^*$ in (3.31):

$$\mathcal{P}_t''(\boldsymbol{\chi}_t^*)\langle\dot{\boldsymbol{\chi}}, \dot{\boldsymbol{\chi}}_t^* - \dot{\boldsymbol{\chi}}\rangle + \dot{\mathcal{P}}_t'(\boldsymbol{\chi}_t^*)(\dot{\boldsymbol{\chi}}_t^* - \dot{\boldsymbol{\chi}}) \geq 0. \tag{3.33}$$

Making $\boldsymbol{\xi} = \dot{\boldsymbol{\chi}}$ in the variational inequality satisfied by $\dot{\boldsymbol{\chi}}_t^*$, gives

$$\mathcal{P}_t''(\boldsymbol{\chi}_t^*)\langle\dot{\boldsymbol{\chi}}_t^*, \dot{\boldsymbol{\chi}} - \dot{\boldsymbol{\chi}}_t^*\rangle + \dot{\mathcal{P}}_t'(\boldsymbol{\chi}_t^*)(\dot{\boldsymbol{\chi}} - \dot{\boldsymbol{\chi}}_t^*) \geq 0. \tag{3.34}$$

The addition of the two inequalities (3.33)-(3.34) leads to $\mathcal{P}_t''(\boldsymbol{\chi}_t^*)(\dot{\boldsymbol{\chi}} - \dot{\boldsymbol{\chi}}_t^*) \leq 0$ which is possible only if $\dot{\boldsymbol{\chi}} = \dot{\boldsymbol{\chi}}_t^*$ when $\mathcal{P}_t''(\boldsymbol{\chi}_t^*)$ is positive definite.

Let us now consider the question of the stability of $(\dot{\mathbf{u}}_t^*, \dot{\alpha}_t^*)$. By virtue of Proposition 2, this fundamental state is stable *only if* $\mathcal{P}_t''(\boldsymbol{\chi}_t^*)(\dot{\boldsymbol{\xi}}) \geq 0$, for all $\boldsymbol{\xi} \in \mathcal{C}\times\dot{\mathcal{D}}_t^+$, and *if* $\mathcal{P}_t''(\boldsymbol{\chi}_t^*)(\dot{\boldsymbol{\xi}}) > 0$ for all rates $\dot{\boldsymbol{\xi}} \neq \mathbf{0}$ in $\mathcal{C}\times\dot{\mathcal{D}}_t^+$. Accordingly, the stability is governed by the positivity of $\mathcal{P}_t''(\boldsymbol{\chi}_t^*)$ on $\mathcal{C}\times\dot{\mathcal{D}}_t^+$.

By virtue of (3.11), $\mathcal{P}_t''(\boldsymbol{\chi}_t^*)$ can read as the difference of two definite positive quadratic forms on $\mathcal{C}\times\dot{\mathcal{D}}_t$, *i.e.*

$$\mathcal{P}_t''(\boldsymbol{\chi}_t^*) = \mathcal{A}_t^* - \mathcal{B}_t^*$$

with

$$\mathcal{A}_t^*(\mathbf{v},\beta) = \int_\Omega \Big(\mathsf{A}\big((1-\alpha_t^*)\boldsymbol{\varepsilon}(\mathbf{v}) - 2\boldsymbol{\varepsilon}_t^{e*}\beta\big)\cdot\big((1-\alpha_t^*)\boldsymbol{\varepsilon}(\mathbf{v}) - 2\boldsymbol{\varepsilon}_t^{e*}\beta\big) + \mathsf{w}_1\eta^2\nabla\beta\cdot\nabla\beta\Big)\,\mathrm{d}\mathbf{x}, \quad (3.35)$$

$$\mathcal{B}_t^*(\beta) = \int_\Omega 3\mathsf{A}\boldsymbol{\varepsilon}_t^{e*}\cdot\boldsymbol{\varepsilon}_t^{e*}\ \beta^2\,\mathrm{d}\mathbf{x}, \qquad \boldsymbol{\varepsilon}_t^{e*}(\mathbf{x}) = \mathsf{a}\vartheta\,\mathsf{f}_\mathsf{c}\Big(\frac{x_2}{2\sqrt{\mathsf{k}_\mathsf{c}t}}\Big)(\mathbf{e}_1\otimes\mathbf{e}_1 - \nu\mathbf{e}_2\otimes\mathbf{e}_2). \quad (3.36)$$

where $\boldsymbol{\varepsilon}_t^{e*}(\mathbf{x})$ comes from (3.5) and (3.17). Accordingly, one has:

Proposition 14. *The study of the positivity of $\mathcal{P}_t''$ is equivalent to compare the following Rayleigh ratio $\mathcal{R}_t^*$ with 1:*

$$\mathcal{R}_t^*(\mathbf{v},\beta) = \begin{cases} \dfrac{\mathcal{A}_t^*(\mathbf{v},\beta)}{\mathcal{B}_t^*(\beta)} & \text{if } \beta\neq 0 \\ +\infty & \text{otherwise} \end{cases}. \quad (3.37)$$

Specifically, the possibility of bifurcation from the fundamental state is given by

$$\mathsf{R}_t^b := \min_{\mathcal{C}\times\dot{\mathcal{D}}_t}\mathcal{R}_t^*, \qquad \begin{cases} \mathsf{R}_t^b > 1 & \Longrightarrow \quad \text{no bifurcation} \\ \mathsf{R}_t^b \le 1 & \Longrightarrow \quad \text{bifurcation possible} \end{cases} \quad (3.38)$$

while for the stability of the fundamental state one gets

$$\mathsf{R}_t^s := \min_{\mathcal{C}\times\dot{\mathcal{D}}_t^+}\mathcal{R}_t^*, \qquad \begin{cases} \mathsf{R}_t^s > 1 & \Longrightarrow \quad \text{stability} \\ \mathsf{R}_t^s < 1 & \Longrightarrow \quad \text{instability} \end{cases} \quad (3.39)$$

Remark 9. *By standard arguments one can prove that both minimization problems admit a solution. Since the dependence on time of the fundamental state is smooth, so is the dependence on time of the minima R_t^b and R_t^s. Since $\dot{\mathcal{D}}_t^+ \subset \dot{\mathcal{D}}_t$, one immediately gets $\mathsf{R}_t^b \le \mathsf{R}_t^s$ and hence one can suspect that a bifurcation occurs before the instability. The proof of that result as well as the determination of the times t_b and t_s when the bifurcation and the loss of stability occur are the aim of the next subsections.*

The bifurcated branch is only observed if it corresponds to stable states. Thus the following result characterizes the neighboring states after bifurcation from the stable fundamental branch.

Proposition 15. *Let $(\mathbf{u}_t^*,\alpha_t^*)$ be the state of the fundamental branch at time $t<t_s$. Let $s\mapsto(\mathbf{u}_s,\alpha_s)$ be a stationary evolution (as defined in Proposition 10) in the time interval $[t,t+t')$ which starts from $(\mathbf{u}_t^*,\alpha_t^*)$ at time t. Then for t' sufficiently small, all the states of this branch satisfy* (ST) *and are thus stable.*

Proof. The proof is given in C.4 and uses a continuity argument. □

3.4.3 Some properties of Rayleigh's ratio minimizations

Let $\hat{\boldsymbol{\xi}} = (\hat{\mathbf{v}},\hat{\beta})$ be a minimizer of $\mathcal{R}_t^*$ over $\mathcal{C}\times\dot{\mathcal{D}}_t$. It satisfies the following optimal conditions which involve the symmetric bilinear forms $\mathcal{A}_t^*\langle\cdot,\cdot\rangle$ and $\mathcal{B}_t^*\langle\cdot,\cdot\rangle$ associated with the quadratic forms $\mathcal{A}_t^*(\cdot)$ and $\mathcal{B}_t^*(\cdot)$:

$$\mathcal{A}_t^*\langle\hat{\boldsymbol{\xi}},\boldsymbol{\xi}\rangle = \mathsf{R}_t^b\ \mathcal{B}_t^*\langle\hat{\beta},\beta\rangle, \qquad \forall\boldsymbol{\xi}=(\mathbf{v},\beta)\in\mathcal{C}\times\dot{\mathcal{D}}_t. \quad (3.40)$$

By standard arguments, one deduces the natural boundary conditions $\partial\hat{\beta}/\partial x_1 = 0$ on $x_1 = 0$ or L. Therefore, as it is suggested by the x_1 independence of the fundamental state, one can decompose $\hat{\beta}$ into the following Fourier series:

$$\hat{\beta}(\mathbf{x}) = \sum_{k\in\mathbb{N}} \hat{\beta}^k(\zeta)\cos\left(k\pi\frac{x_1}{\mathsf{L}}\right), \qquad \zeta = \frac{x_2}{\mathsf{D}_t^*}, \tag{3.41}$$

where one introduces the change of coordinate $x_2 \mapsto \zeta$ in order that the support of the functions $\hat{\beta}^k$ be the fix interval $[0,1)$. Accordingly, the $\hat{\beta}^k$'s can be seen as elements of $\mathcal{H}_0$,

$$\mathcal{H}_0 = \{\beta \in H^1(0,1) : \beta(1) = 0\}.$$

In the same way, using the boundary conditions $\hat{v}_1 = 0$, $\varepsilon_{12}(\hat{\mathbf{v}}) = 0$ and hence $\partial\hat{v}_2/\partial x_1 = 0$ on $x_1 = 0$ or L, $\hat{\mathbf{v}}$ can be decomposed as follows:

$$\hat{\mathbf{v}}(\mathbf{x}) = \sum_{k\in\mathbb{N}} 2\mathsf{a}\vartheta\delta_\tau\sqrt{\mathsf{k_c}t}\left(\hat{V}_1^k(\zeta)\sin\left(k\pi\frac{x_1}{\mathsf{L}}\right)\mathbf{e}_1 + \hat{V}_2^k(\zeta)\cos\left(k\pi\frac{x_1}{\mathsf{L}}\right)\mathbf{e}_2\right) \tag{3.42}$$

where the $\hat{\mathbf{V}}^k$'s are normalized to simplify future expressions and belong to $\mathbf{H}$,

$$\mathbf{H} = H^1(0,\infty)^2.$$

Considering only the rates $(\mathbf{v},\beta)$ in $\mathcal{C}\times\dot{\mathcal{D}}_t$ which can be decomposed in the same manner and using the orthogonality between the trigonometric functions of x_1 entering in the expansions of $(\mathbf{v},\beta)$, the different modes $(\mathbf{V}^k,\beta^k)$ are uncoupled from each other. Specifically $\mathcal{A}_t^*$ and $\mathcal{B}_t^*$ can read as

$$\mathcal{A}_t^*(\mathbf{v},\beta) = \sum_{k\in\mathbb{N}} \mathcal{A}_t^k(\mathbf{V}^k,\beta^k) \qquad \mathcal{B}_t^*(\beta) = \sum_{k\in\mathbb{N}} \mathcal{B}_t^k(\beta^k).$$

Therefore, if one introduces the Rayleigh ratios $\mathcal{R}_t^k(\mathbf{V},\beta) = \mathcal{A}_t^k(\mathbf{V},\beta)/\mathcal{B}_t^k(\beta)$ for $k\in\mathbb{N}$, then

$$\mathsf{R}_t^b = \min_{k\in\mathbb{N}}\min_{\mathbf{H}\times\mathcal{H}_0} \mathcal{R}_t^k. \tag{3.43}$$

Indeed, let $\hat{\mathsf{R}}_t^k$ be the minimum of $\mathcal{R}_t^k$ over $\mathbf{H}\times\mathcal{H}_0$ and let $(\hat{V}_t^k,\hat{\beta}_t^k)$ be a minimizer. Let $\hat{k}_t$ be a minimizer of $k\mapsto\hat{\mathsf{R}}_t^k$. All these minimizers exist. Then $\mathcal{A}_t^k(\mathbf{V},\beta) \geq \hat{\mathsf{R}}_t^{\hat{k}_t}\mathcal{B}_t^k(\beta)$ for all $k\in\mathbb{N}$ and all $(\mathbf{V},\beta)\in\mathbf{H}\times\mathcal{H}_0$. Therefore, $\mathsf{R}_t^b \geq \hat{\mathsf{R}}_t^{\hat{k}_t}$. But since $\hat{\mathsf{R}}_t^{\hat{k}_t} = \mathcal{R}_t^*(\hat{V}_t^{\hat{k}_t},\hat{\beta}_t^{\hat{k}_t})$, one gets $\hat{\mathsf{R}}_t^{\hat{k}_t} \geq \mathsf{R}_t^b$ and hence $\hat{\mathsf{R}}_t^{\hat{k}_t} = \mathsf{R}_t^b$.

Finally, after a last change of variable (3.47) and introducing the assumption that the internal length η is small by comparison with the width of the body L, the following proposition holds:

Proposition 16. *Assuming that $\eta \ll \mathsf{L}$, at a given time $t > 0$, the minimum of the Rayleigh ratio $\mathcal{R}_t^*$ over $\mathcal{C}\times\dot{\mathcal{D}}_t$ is given by*

$$\mathsf{R}_t^b = \min_{\kappa\geq 0}\min_{\mathbf{H}\times\mathcal{H}_0} \bar{\mathcal{R}}_\tau^\kappa, \qquad \bar{\mathcal{R}}_\tau^\kappa(\mathbf{V},\beta) = \begin{cases} \dfrac{\bar{\mathcal{A}}_\tau^\kappa(\mathbf{V},\beta)}{\bar{\mathcal{B}}_\tau(\beta)} & \text{if } \beta \neq 0 \\ +\infty & \text{otherwise} \end{cases}, \tag{3.44}$$

where the dimensionless quadratic forms $\bar{\mathcal{A}}_\tau^\kappa$ and $\bar{\mathcal{B}}_\tau$ are given by

$$\begin{aligned} \bar{\mathcal{A}}_\tau^\kappa(\mathbf{V},\beta) &= \int_0^\infty \frac{(1-\bar{\alpha}_\tau(\delta_\tau\zeta))^2}{1-\nu^2}\Big(\kappa^2 V_1(\zeta)^2 + V_2'(\zeta)^2 + 2\nu\kappa V_1(\zeta)V_2'(\zeta) + \frac{1-\nu}{2}\Big(V_1'(\zeta)+\kappa V_2(\zeta)\Big)^2\Big)\,\mathrm{d}\zeta \\ &\quad + \int_0^1 \Big(-4(1-\bar{\alpha}_\tau(\delta_\tau\zeta))\mathsf{f_c}(\delta_\tau\zeta)\kappa V_1(\zeta)\beta(\zeta) + 4\mathsf{f_c}(\delta_\tau\zeta)^2\beta(\zeta)^2\Big)\,\mathrm{d}\zeta \\ &\quad + \frac{1}{\delta_\tau^2\tau^2}\int_0^1 \Big(\kappa^2\beta(\zeta)^2 + \beta'(\zeta)^2\Big)\,\mathrm{d}\zeta, \end{aligned} \tag{3.45}$$

$$\bar{\mathcal{B}}_\tau(\beta) = \int_0^1 3\mathsf{f_c}(\delta_\tau\zeta)^2\beta(\zeta)^2\,\mathrm{d}\zeta. \tag{3.46}$$

The optimal "wave number" $\hat{k}_t$ is related to the optimal dimensionless "wave number" $\hat{\kappa}_\tau$ (minimizer of $\bar{\mathcal{R}}_\tau^\kappa$) by

$$\hat{k}_t = \frac{\hat{\kappa}_\tau}{\pi\Theta\delta_\tau\tau}\frac{\mathsf{L}}{\eta}, \quad \tau = \frac{2\sqrt{\mathsf{k_c}t}}{\Theta\eta}, \tag{3.47}$$

and, since $\eta \ll \mathsf{L}$, the discrete minimization problem over $\mathbb{N}$ for k can be replaced by a continuous minimization problem over $\mathbb{R}^+$ for κ.

Proof. The change of variable $\zeta = x_2/\mathsf{D}_t^*$ reduces the support of β to $[0,1)$. By virtue of (3.43), it suffices to insert (3.41) and (3.42) into (3.35)–(3.37) to obtain after some calculations (3.44)–(3.47). □

The next Proposition gives some useful estimates of the Rayleigh ratio minima.

Proposition 17 (Some estimates of R_t^b, $\min_{\mathbf{H}\times\mathcal{H}_0}\bar{\mathcal{R}}_\tau^\kappa$ and R_t^s)**.**

1. *There exists $C>0$ such that $\min_{\mathbf{H}\times\mathcal{H}_0}\bar{\mathcal{R}}_\tau^\kappa \geq \dfrac{C}{\tau^2}$ for all $\tau>0$ and all $\kappa\geq 0$;*
2. $\lim_{t\to 0}\mathsf{R}_t^b = \lim_{\tau\to 0}\Big(\min_{\mathbf{H}\times\mathcal{H}_0}\bar{\mathcal{R}}_\tau^\kappa\Big) = +\infty$, $\forall\kappa\geq 0$;
3. $\lim_{t\to\infty}\mathsf{R}_t^b \leq \lim_{t\to\infty}\mathsf{R}_t^s < 1$;
4. $\min_{\mathbf{H}\times\mathcal{H}_0}\mathcal{R}_\tau^0 \geq 4/3$, $\forall\tau>0$. *Moreover,* $\lim_{\tau\to\infty}\min_{\mathbf{H}\times\mathcal{H}_0}\mathcal{R}_\tau^0 = 4/3$.
5. *For given $\tau>0$,*
$$\lim_{\kappa\to\infty}\frac{\min_{\mathbf{H}\times\mathcal{H}_0}\bar{\mathcal{R}}_\tau^\kappa}{\kappa^2} = \frac{1}{3\delta_\tau^2\tau^2}.$$

Proof. The proof is given in C.5. □

3.4.4 Determination of the first bifurcation

The major result of this chapter can now be established

Proposition 18. *There exists a time $t_b > 0$ such that $\mathsf{R}_t^b > 1, \forall t < t_b$ and $\mathsf{R}_{t_b}^b = 1$. Therefore t_b is the first time at which a bifurcation from the fundamental branch can occur. The fundamental branch is still stable at this time but becomes definitively unstable at a time t_s such that $t_b < t_s < +\infty$.*

Moreover, at time t_b, the rate problem admits other solutions than the rate $(\dot{\mathbf{u}}_{t_b}^*, \dot{\alpha}_{t_b}^*)$ corresponding to the fundamental branch. Such bifurcation rates $(\dot{\mathbf{u}}, \dot{\alpha})$ are necessarily of the following form

$$(\dot{\mathbf{u}}, \dot{\alpha}) = (\dot{\mathbf{u}}_{t_b}^*, \dot{\alpha}_{t_b}^*) + c\,(\mathbf{v}^b, \beta^b) \tag{3.48}$$

where $(\mathbf{v}^b, \beta^b)$ is a minimizer of $\mathcal{R}_{t_b}^*$ over $\mathcal{C} \times \dot{\mathcal{D}}_{t_b}$ while c is an arbitrary (but non-zero) constant whose absolute value is sufficiently small so that $\dot{\alpha}_{t_b}^* + c\,\beta^b \geq 0$. Conversely, if $(\mathbf{v}^b, \beta^b)$ is a minimizer of $\mathcal{R}_{t_b}^*$ over $\mathcal{C} \times \dot{\mathcal{D}}_{t_b}$, then there exists $\bar{c} > 0$ such that, for every c with $|c| \leq \bar{c}$, $(\dot{\mathbf{u}}, \dot{\alpha})$ given by (3.48) is really solution of the rate problem at t_b.

Specifically, the time t_b and the mode of bifurcation $(\mathbf{v}^b, \beta^b)$ are given by

$$t_b = \frac{\Theta^2 \tau_b^2 \eta^2}{4\mathsf{k_c}}, \tag{3.49}$$

$$\mathbf{v}^b(\mathbf{x}) = \mathsf{a}\vartheta \mathsf{D}_b \left(\hat{V}_1^b\Big(\frac{x_2}{\mathsf{D}_b}\Big) \sin\left(2\pi \frac{x_1}{\lambda_b}\right) \mathbf{e}_1 + \hat{V}_2^b\Big(\frac{x_2}{\mathsf{D}_b}\Big) \cos\left(2\pi \frac{x_1}{\lambda_b}\right) \mathbf{e}_2 \right), \tag{3.50}$$

$$\beta^b(\mathbf{x}) = \hat{\beta}^b\Big(\frac{x_2}{\mathsf{D}_b}\Big) \cos\left(2\pi \frac{x_1}{\lambda_b}\right). \tag{3.51}$$

In (3.49)–(3.51) the wave number κ_b and the modes $(\hat{\mathbf{V}}^b, \hat{\beta}^b)$ are (normalized) minimizers of $\bar{\mathcal{R}}_{\tau_b}^{\kappa}(\mathbf{V}, \beta)$ over all $\kappa \geq 0$ and all $(\mathbf{V}, \beta) \in \mathbf{H} \times \mathcal{H}_0$ while τ_b is such that $\bar{\mathcal{R}}_{\tau_b}^{\kappa_b}(\hat{\mathbf{V}}^b, \hat{\beta}^b) = 1$. Since $0 < \kappa_b < +\infty$, the damage mode of bifurcation is a sinusoid with respect to x_1 whose wavelength λ_b is finite and given by

$$\lambda_b = 2\pi \frac{\Theta \delta_{\tau_b} \tau_b}{\kappa_b} \eta. \tag{3.52}$$

In (3.50)-(3.51), D_b represents the depth of the damage zone at time t_b, i.e.

$$\mathsf{D}_b := 2\delta_{\tau_b} \sqrt{\mathsf{k_c} t_b} = \Theta \delta_{\tau_b} \tau_b \eta. \tag{3.53}$$

Hence, λ_b and D_b are proportional to the internal length η of the material. The coefficients of proportionality only depend on the Poisson ratio ν and on the dimensionless parameter Θ characterizing the amplitude of the thermal shock.

Proof. The proof is divided into 3 steps.

(i) : *Definitions of t_b and t_s.* By virtue of Proposition 17 (Properties 2 and 3), R_t^b varies continuously from a value less than 1 to $+\infty$ when t goes from 0 to $+\infty$. Hence, there exists at least one time s such

that $\mathsf{R}^b_s = 1$. Any such time is necessarily non-zero and finite, *i.e.* $0 < s < +\infty$. Defining t_b as the smallest of such times, one gets $\mathsf{R}^b_t > 1$ for all $t < t_b$ by virtue of Property 2. Therefore, by virtue of (3.38), t_b is the first time when a bifurcation can occur.

In the same way, since $\mathsf{R}^s_t \geq \mathsf{R}^b_t$ and by virtue of the Properties 2 and 3, R^s_t varies continuously from a value less than 1 to $+\infty$ when t goes from 0 to $+\infty$. Hence there exists at least one time σ such that $\mathsf{R}^s_\sigma = 1$. Any such time is necessarily non-zero and finite, *i.e.* $0 < \sigma < +\infty$. Defining t_s as the largest of such times, one gets $\mathsf{R}^s_t < 1$ for all $t > t_s$ by virtue of Property 3. Therefore, by virtue of (3.39), the fundamental branch is never stable after t_s. Hence, these critical times are such that $0 < t_b \leq t_s < +\infty$. The inequality $t_b < t_s$ will be proved in the next step. $\triangleleft$

(ii) : *Necessary form of a bifurcation rate.* Let us consider the rate problem at time t_b and let $\dot{\boldsymbol{\chi}}$ be a solution. Inserting into (3.31) and taking into account that $\dot{\boldsymbol{\chi}}^*_{t_b}$ itself satisfies (3.31) at time t_b gives $\mathcal{A}^*_{t_b}(\dot{\boldsymbol{\chi}} - \dot{\boldsymbol{\chi}}^*_{t_b}) \leq \mathcal{B}^*_{t_b}(\dot{\boldsymbol{\chi}} - \dot{\boldsymbol{\chi}}^*_{t_b})$, see (3.33)-(3.34). But since $\mathsf{R}^s_{t_b} := \min_{\mathcal{C}\times\dot{\mathcal{D}}_{t_b}} \mathcal{R}^*_{t_b} = 1$, one has also the converse inequality and hence the equality

$$\mathcal{A}^*_{t_b}(\dot{\boldsymbol{\chi}} - \dot{\boldsymbol{\chi}}^*_{t_b}) = \mathcal{B}^*_{t_b}(\dot{\boldsymbol{\chi}} - \dot{\boldsymbol{\chi}}^*_{t_b}).$$

Therefore, if $\dot{\boldsymbol{\chi}} \neq \dot{\boldsymbol{\chi}}^*_{t_b}$, then $\dot{\boldsymbol{\chi}} - \dot{\boldsymbol{\chi}}^*_{t_b}$ must be a minimizer of $\mathcal{R}^*_{t_b}$ over $\mathcal{C}\times\dot{\mathcal{D}}_{t_b}$. Therefore, by virtue of the analysis of the previous subsection and Proposition 16, $\dot{\boldsymbol{\chi}}$ must take the form given by (3.48)–(3.53). Indeed, $(\kappa_b, \hat{V}^b, \hat{\beta}^b)$ is a minimizer of $(\kappa, \mathbf{V}, \beta) \mapsto \bar{\mathcal{R}}^\kappa_{\tau_b}(\mathbf{V}, \beta)$ over $\mathbb{R}^+\times\mathbf{H}\times\mathcal{H}_0$ and $1 = \bar{\mathcal{R}}^{\kappa_b}_{\tau_b}(\kappa_b, \hat{V}^b, \hat{\beta}^b)$. By virtue of the properties 4 and 5 of Proposition 17, $0 < \kappa_b < +\infty$ and hence the wave length λ_b is non-zero and finite. By using (3.47) at time t_b, one obtains (3.49) and (3.52). Since, at a given τ, $\bar{\alpha}_\tau$ depends only on Θ, so does δ_τ. Therefore $\bar{\mathcal{R}}^\kappa_\tau$ depends only on ν and Θ. Accordingly, κ_b and τ_b depend only on ν and Θ.

Since $\lambda_b < +\infty$, the dependence of β^b on x_1 is really sinusoidal and hence β^b does not belong to $\dot{\mathcal{D}}^+_{t_b}$. Accordingly $(\mathbf{v}^b, \beta^b)$ cannot be a minimizer of $\mathcal{R}^*_{t_b}$ over $\mathcal{C}\times\dot{\mathcal{D}}^+_{t_b}$. Therefore $\mathsf{R}^s_{t_b} > 1 = \mathsf{R}^b_{t_b}$ and hence $t_s > t_b$. The fundamental branch is still stable at t_b. $\triangleleft$

(iii) : *Existence of a bifurcation rate.* It remains to prove that non trivial solutions for the rate problem really exist at time t_b. So, let $(\kappa_b, \hat{V}^b, \hat{\beta}^b)$ be a minimizer of $(\kappa, \mathbf{V}, \beta) \mapsto \bar{\mathcal{R}}^\kappa_{\tau_b}(\mathbf{V}, \beta)$ over $\mathbb{R}^+\times\mathbf{H}\times\mathcal{H}_0$. Since $(\kappa_b, c\hat{V}^b, c\hat{\beta}^b)$ is also a minimizer for any $c \neq 0$ and since $\hat{\beta}^b \neq 0$, one can normalize the minimizer for instance by $\int_0^1 \hat{\beta}^b(\zeta)^2\,\mathrm{d}\zeta = 1$. Let us consider the rate $\dot{\boldsymbol{\chi}} = \dot{\boldsymbol{\chi}}^*_{t_b} + c\boldsymbol{\xi}^b$ with $\boldsymbol{\xi}^b = (\mathbf{v}^b, \beta^b)$ given by (3.50)-(3.51) and $c \neq 0$. Since $\boldsymbol{\xi}^b$ is a minimizer of $\mathcal{R}^*_{t_b}$ over $\mathcal{C}\times\dot{\mathcal{D}}_{t_b}$ and since $\mathsf{R}^b_{t_b} = 1$, $\boldsymbol{\xi}^b$ satisfies the variational equality

$$\mathcal{P}''_{t_b}(\boldsymbol{\chi}^*_{t_b})\langle\boldsymbol{\xi}^b, \boldsymbol{\xi}\rangle = 0, \quad \forall\boldsymbol{\xi} \in \mathcal{C}\times\dot{\mathcal{D}}_{t_b}. \tag{3.54}$$

Since $\dot{\boldsymbol{\chi}}^*_{t_b}$ is solution of the rate problem, it satisfies (3.31) which reads at time t_b as

$$\mathcal{P}''_{t_b}(\boldsymbol{\chi}^*_{t_b})\langle\dot{\boldsymbol{\chi}}^*_{t_b}, \boldsymbol{\xi} - \dot{\boldsymbol{\chi}}^*_{t_b}\rangle + \dot{\mathcal{P}}'_{t_b}(\boldsymbol{\chi}^*_{t_b})(\boldsymbol{\xi} - \dot{\boldsymbol{\chi}}^*_{t_b}) \geq 0, \quad \forall\boldsymbol{\xi} \in \mathcal{C}\times\dot{\mathcal{D}}^+_{t_b}. \tag{3.55}$$

Using (3.12), (3.50) and (3.51), it turns out that $\dot{\mathcal{P}}'_{t_b}(\boldsymbol{\chi}^*_{t_b})(\boldsymbol{\xi}^b) = 0$. Indeed, by virtue of the independence of $\boldsymbol{\varepsilon}^{\mathrm{th}}_t$ and α^*_t on x_1, one gets

$$\dot{\mathcal{P}}'_{t_b}(\boldsymbol{\chi}^*_{t_b})(\boldsymbol{\xi}^b) = \int_0^\infty \int_0^L \phi(\zeta)\cos\left(k_b\pi\frac{x_1}{L}\right)\mathrm{d}x_1\,\mathrm{d}\zeta = 0. \tag{3.56}$$

Therefore, after calculations based on (3.54)–(3.56), one obtains $\forall \boldsymbol{\xi} \in \mathcal{C} \times \dot{\mathcal{D}}^+_{t_b}$:

$$\mathcal{P}''_{t_b}(\boldsymbol{\chi}^*_{t_b})\langle \dot{\boldsymbol{\chi}}, \boldsymbol{\xi} - \dot{\boldsymbol{\chi}} \rangle + \dot{\mathcal{P}}'_{t_b}(\boldsymbol{\chi}^*_{t_b})(\boldsymbol{\xi} - \dot{\boldsymbol{\chi}}) = \mathcal{P}''_{t_b}(\boldsymbol{\chi}^*_{t_b})\langle \dot{\boldsymbol{\chi}}^*_{t_b}, \boldsymbol{\xi} - \dot{\boldsymbol{\chi}}^*_{t_b} \rangle + \dot{\mathcal{P}}'_{t_b}(\boldsymbol{\chi}^*_{t_b})(\boldsymbol{\xi} - \dot{\boldsymbol{\chi}}^*_{t_b}) \geq 0, \tag{3.57}$$

and hence $\dot{\boldsymbol{\chi}}$ satisfies (3.31) at t_b. In order that $\dot{\boldsymbol{\chi}}$ be a solution of the rate problem, it remains to verify that $\dot{\alpha}^*_{t_b} + c\beta^b \geq 0$. Since it is true for sufficiently small $|c|$ (one has to prove that $\dot{\alpha}'$ is non zero and that β' is finite. This proof is left to the reader), one has constructed a family of non trivial solutions of the rate problem at time t_b. ◁ The proof of the Proposition is complete. □

3.5 Numerical results

This section is devoted to the numerical exploration of the equations of the minimization problem. These results can be classified in three families: illustration, hypothesis validation and quantification. Some results are illustrated by plotting the solutions. The validation of hypothesis can be made numerically such as the irreversibility. The main interest is to quantify the results especially those of Proposition 18 with the wavelength at the first bifurcation. This numerical implementation is based on two aspects: solving (3.22) by a shoot method and minimizing (3.44). Before starting, let us recall that the loading parameter reads $\Theta = \sigma_c/(\mathsf{a}\vartheta\mathsf{E})$, and thus $\Theta \to 0$ corresponds to a strong thermal shock and $\Theta \to 1$ to a very light loading.

3.5.1 The fundamental branch

The fundamental branch is a solution with homogeneous damage in the direction parallel to the surface of the thermal shock. It exists for any positive time $t > 0$ and has non-zero damage in a strip within a positive distance D^*_t from the surface. Using the time and space variables τ and y adapted to the thermal problem, the value of the damage field in the region $0 < y < \delta_\tau = D^*_t/2\sqrt{\mathsf{k_c}t}$ is found by solving the second order non-autonomous linear differential equation (3.22) with the boundary conditions (3.23). The existence and uniqueness of the solution of this boundary value problem is guaranteed by Proposition 12. To solve it, for a given time τ and mildness of thermal shock Θ, a shooting method is applied, which, after solving the initial value problem for $\bar{\alpha}_\tau(\delta_\tau) = \bar{\alpha}'_\tau(\delta_\tau) = 0$, searches for the length of the damaged domain δ_τ such that $\bar{\alpha}'_\tau(0) = 0$. The corresponding solution for δ_τ is checked against the asymptotic results for δ_0 and δ_∞ obtained in Proposition 12 (Fig. 3.5). For large values of τ, the numerical problem becomes ill-conditioned and differential solver and root finding algorithms show convergence issues.

Figure 3.6 reports the damage field obtained for different times and thermal shock intensities. The left and right columns show the results in the scaled (y,τ) and physical ($\mathbf{x}$,t) coordinates, respectively. This fundamental solution is independent of the Poisson ratio ν, being characterized by null displacements in the x_1-direction.

The damage is non null for any positive time. For severe thermal shocks (see the plots at the top for

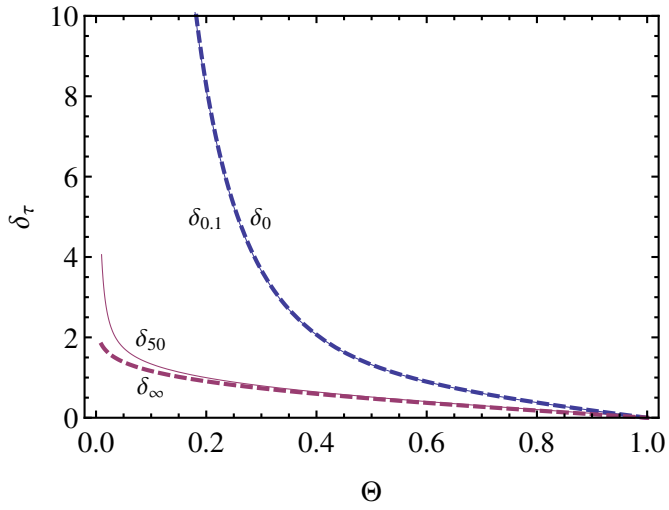

Figure 3.5: Asymptotic result for the scaled depth of the damage strip δ_τ as a function of the mildness thermal shock Θ. The dashed lines are the results for $\tau \to 0$, δ_0, and for $\tau \to \infty$, δ_∞. The continuous lines are the results of the numerical root finding in the shooting method for short ($\tau = 0.1$) and long ($\tau = 50$) times.

$\Theta = 0.01$ in Figure 3.6), the solution in the physical space is characterized by an almost fully damaged zone close to the boundary, which propagates inside the domain with increasing time. For mild thermal shock ($\Theta = 0.5, 0.9$) the solution is with smaller space and time gradients. Note that δ_τ is decreasing with τ, whilst D_t^* is increasing with t. For any value of Θ and τ, the solution is monotonically decreasing in space, varying from a maximum value $\alpha_t^*(0)$ at the boundary to 0 at $x = D_t^*$, as proven in Proposition 11. Hence, its behavior as a function of Θ and t can be globally resumed by the contour-plots of the damage at the surface, $\alpha_t^*(0)$, and the length of the damaged domain, D_t^*, see Figure 3.7. Both the maximal value of the damage field and the damage penetration depth increase monotonically with the severity of the thermal shock and the time. The limit value of the maximal value of the damage field for $t, \tau \to \infty$ is $\alpha_\infty^*(0) = 1 - \Theta^2 < 1$ (see Proposition 12, Eq. (3.28)). To check numerically that the solution $\alpha_t^*(x_2)$ respects the irreversibility condition for a fixed loading Θ, $\dot{\alpha}_t^*(x_2)$ is reported in Figure 3.8 as a function of x_2 and t for $\Theta = \{0.01,\ \ 0.2,\ 0.5,\ 0.9\}$. Similar results are found for any other tested value of Θ. In particular, for any value of Θ, whenever the numerical ODE solver converges, the minimum value of $\dot{\alpha}_t^*(x_2)$ over $t > 0, x_2 > 0$ is 0. The numerical tests seem to corroborate the validity of Hypothesis 8 on the irreversibility of the fundamental branch.

3.5.2 Bifurcation from the fundamental branch: critical times, critical damage penetration and optimal wavelength

The goal of this Section is to quantify numerically the first possible bifurcation from the fundamental branch. Starting from the result of Proposition 16, the problem is solved using the partial Fourier series in

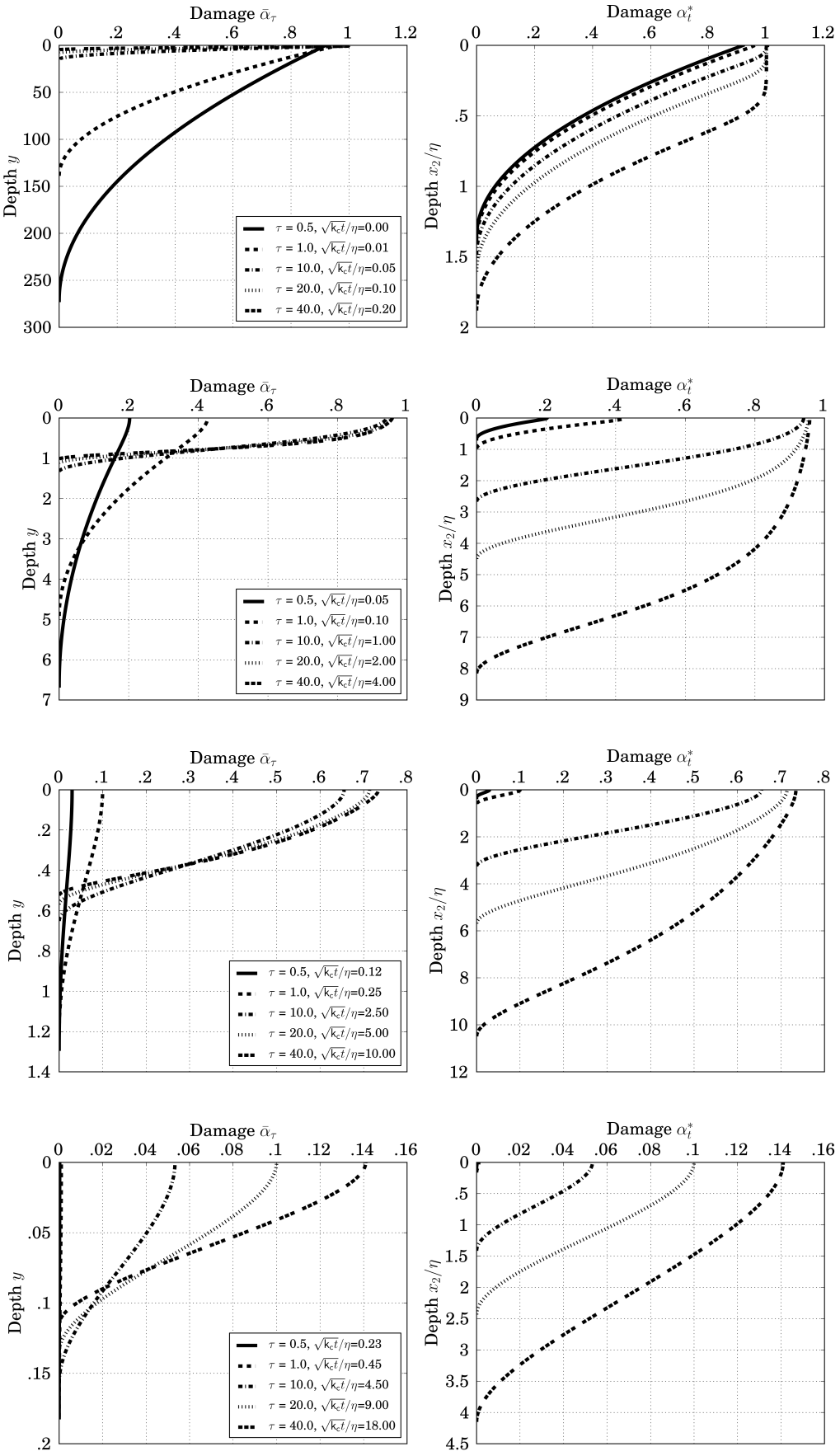
Damage $\bar{\alpha}_\tau$
Depth y
τ = 0.5, $\sqrt{k_c t}/\eta$=0.00
τ = 1.0, $\sqrt{k_c t}/\eta$=0.01
τ = 10.0, $\sqrt{k_c t}/\eta$=0.05
τ = 20.0, $\sqrt{k_c t}/\eta$=0.10
τ = 40.0, $\sqrt{k_c t}/\eta$=0.20
Damage α_t^*
Depth x_2/η
Damage $\bar{\alpha}_\tau$
Depth y
τ = 0.5, $\sqrt{k_c t}/\eta$=0.05
τ = 1.0, $\sqrt{k_c t}/\eta$=0.10
τ = 10.0, $\sqrt{k_c t}/\eta$=1.00
τ = 20.0, $\sqrt{k_c t}/\eta$=2.00
τ = 40.0, $\sqrt{k_c t}/\eta$=4.00
Damage α_t^*
Depth x_2/η
Damage $\bar{\alpha}_\tau$
Depth y
τ = 0.5, $\sqrt{k_c t}/\eta$=0.12
τ = 1.0, $\sqrt{k_c t}/\eta$=0.25
τ = 10.0, $\sqrt{k_c t}/\eta$=2.50
τ = 20.0, $\sqrt{k_c t}/\eta$=5.00
τ = 40.0, $\sqrt{k_c t}/\eta$=10.00
Damage α_t^*
Depth x_2/η
Damage $\bar{\alpha}_\tau$
Depth y
τ = 0.5, $\sqrt{k_c t}/\eta$=0.23
τ = 1.0, $\sqrt{k_c t}/\eta$=0.45
τ = 10.0, $\sqrt{k_c t}/\eta$=4.50
τ = 20.0, $\sqrt{k_c t}/\eta$=9.00
τ = 40.0, $\sqrt{k_c t}/\eta$=18.00
Damage α_t^*
Depth x_2/η

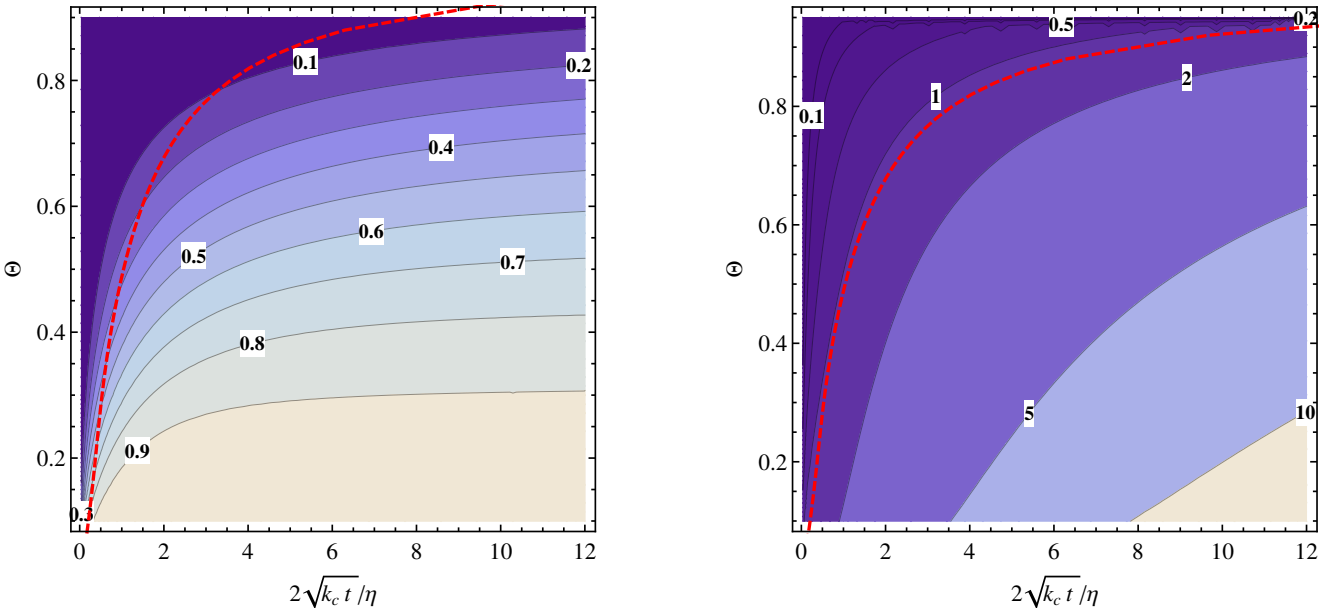

(a) $\alpha_t^*(0)$ (b) D_t^*/η

Figure 3.7: Fundamental solution: damage at the surface $\alpha_t^*(0)$ and penetration of the damage D_t^* as a function of the thermal shock mildness (Θ) and time. The red dashed line indicates the bifurcation time as a function Θ and separate the parameter space in regions where the fundamental solution is unique or not.

the x_1-variable and the associated wave number κ introduced in Section 3.4.3, Eqns. (3.41)-(3.42). For the x_2-direction, the dimensionless variables $\zeta = x_2/\mathsf{D}_t^*$, are used, so that the support of the damaged strip of the fundamental solution is $[0,1)$ for any loading parameter Θ. Hence, the sign of the second derivative of the energy $\mathcal{P}_t''(\boldsymbol{\chi}_t^*)$ is studied numerically, which below is referred to as $\mathcal{P}_t''$ for brevity, and look for the critical bifurcation times τ_b, the critical wave numbers κ_b and the associated bifurcation modes as a function of the thermal shock mildness Θ.

In the numerical work, the study of the positive definiteness of $\mathcal{P}_t''$ is based on the following Proposition.

Proposition 19. *Let*

$$\left\{\mu_i, (\mathbf{V}^{(i)}, \beta^{(i)})\right\}_{i=1}^{\infty}, \qquad \mu_i \le \mu_{i+1}$$

be the eigenvalues and the eigenvectors of the following quadratic form defined on the finite interval $[0,1]$

$$\tilde{\mathcal{P}}_\tau''(\mathbf{V},\beta) = \tilde{\mathcal{A}}_\tau^\kappa(\mathbf{V},\beta) + \frac{\kappa}{1-\nu^2} C(\mathbf{V}(1)) - \bar{\mathcal{B}}_\tau(\beta), \quad (\mathbf{V},\beta) \in H^1(0,1)^2 \times \mathcal{H}_0 \tag{3.58}$$

where $\tilde{\mathcal{A}}_\tau^\kappa$ *is the restriction of* $\bar{\mathcal{A}}_\tau^\kappa$ *on* $[0,1]$ *and* $C(\mathbf{V}(1)) = \frac{c_{11}}{2}V_1(1)^2 + c_{12}V_1(1)V_2(1) + \frac{c_{22}}{2}V_2(1)^2$ *is defined by*

$$C(\mathbf{V}(1)) = \min_{\mathbf{W}\in\mathbf{H}_{\mathbf{V}(1)}} \tilde{\bar{\mathcal{A}}}_\tau^\kappa(\mathbf{W}), \qquad \mathbf{H}_{\mathbf{V}(1)} = \left\{W \in H^1(0,\infty)^2 : \mathbf{W}(0) = \mathbf{V}(1)\right\} \tag{3.59}$$

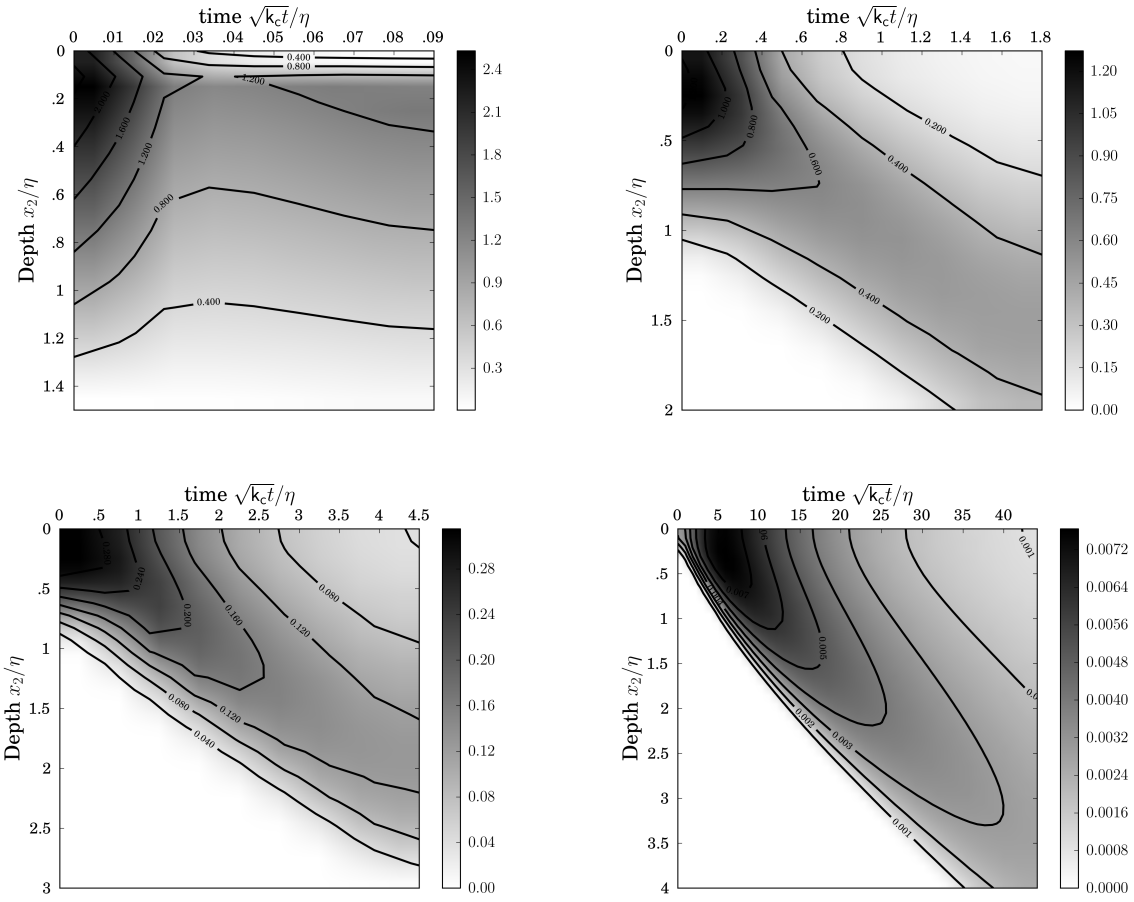

Figure 3.8: Check of the irreversibility condition: Total time derivative of the damage field of the fundamental branch α_t^* with respect to time, $\dot{\alpha}_t^*$, for the loading $\Theta = \{.01, .2, .5, .9\}$.

with

$$\tilde{\bar{\mathcal{A}}}_\tau^\kappa(\mathbf{W}) = \int_0^{+\infty} \left(W_1(\tilde{\zeta})^2 + W_2'(\tilde{\zeta})^2 + 2\nu W_1(\tilde{\zeta}) W_2'(\tilde{\zeta}) + \frac{1-\nu}{2}(W_1'(\tilde{\zeta}) + W_2(\tilde{\zeta}))^2 \right) \mathrm{d}\tilde{\zeta}$$

The study of the positivity of $\mathcal{P}_t''$ *is equivalent to compare the smallest eigenvalue* μ_1 *with zero and* $\mathsf{R}_t^b >$ (resp. $<$)1 *if and only if* $\mu_1 >$ (resp. $<$)0. *The possibility of bifurcation from the fundamental solution is given by*

$$\begin{cases} \mu_1 > 0 \implies & \textit{no bifurcation} \\ \mu_1 \leq 0 \implies & \textit{bifurcation possible} \end{cases} \tag{3.60}$$

Moreover, $(\mathbf{V}^{(1)}, \beta^{(1)})$ *is the restriction on* $[0,1]$ *of the first eigenvector of* $\mathcal{P}_t''$.

Proof. Being $\bar{\mathcal{A}}_\tau^\kappa$ and $\bar{\mathcal{B}}_\tau$ positive definite and $\bar{\mathcal{B}}_\tau$ defined on $[0,1]$, the positive definiteness of the quadratic

form $\mathcal{P}_t''$ is equivalent to the positive definiteness of

$$\tilde{\mathcal{P}}_\tau''(\mathbf{V},\beta) = \min_{\mathbf{V}\in H^1(1,\infty)^2} \mathcal{P}_\tau''(\mathbf{V},\beta).$$

The expression (3.58) is obtained by decomposing $\bar{\mathcal{A}}_\tau^\kappa$ in the contributions coming from the integral over $[0,1]$ and $[1,\infty]$. The latter contribution is given by

$$\int_1^\infty \frac{(1-\bar{\alpha}_\tau(\delta_\tau\zeta))^2}{1-\nu^2}\left(\kappa^2 V_1(\zeta)^2 + V_2'(\zeta)^2 + 2\nu\kappa V_1(\zeta)V_2'(\zeta) + \frac{1-\nu}{2}\Big(V_1'(\zeta)+\kappa V_2(\zeta)\Big)^2\right)\mathrm{d}\zeta \qquad (3.61)$$

which, using the change of variable $\zeta \to 1+\tilde{\zeta}/\kappa$ and that $\bar{\alpha}_\tau = 0$ in $[1,\infty)$, may be rewritten as $\frac{\kappa}{1-\nu^2}\tilde{\bar{\mathcal{A}}}_\tau^\kappa$.

The criterion for assessing the positivity of the quadratic form $\tilde{\mathcal{P}}_t''$ on the basis of the sign of its smallest eigenvalue is a classical result of the spectral decomposition theorem for a continuous self-joint linear operator on a real Hilbert space and is not discussed further here. □

The quadratic form (3.58) is a reduced version of the second derivative of the potential energy defined on the finite interval $[0,1]$, instead of on the semi-infinite space $[0,\infty)$. The formulation above is more convenient for the numerical analysis than the Rayleigh ratio bifurcation criterion of Proposition 14 for two main reasons: (i) the availability of efficient numerical methods for the calculation of the smallest eigenvalue of a symmetric matrix; (ii) the formulation of the eigenvalue problem on a finite interval is better suited for the discretization. The effect of the subdomain $[1,\infty]$ is accounted for by an equivalent stiffness localized in $\zeta = 1$ ($C(\mathbf{V}(1)$), which implies a boundary condition of the Robin type in $\zeta = 1$. The coefficients of the quadratic form C are evaluated by solving the linear differential equations obtained as Euler-Lagrange equations for (3.59). An easy analytical solution is possible for the case $\nu = 0$, giving

$$c_{11} = 2/3 \qquad c_{12} = -1/3 \qquad c_{22} = 2/3.$$

For $\nu \neq 0$ the analytical solution becomes cumbersome and the coefficients must be computed numerically, once for all. The corresponding results obtained through a finite element solver are reported in Figure 3.9. They are obtained on a domain long enough to obtain a result almost independent of its length (the solutions of (3.59) are decaying exponentially with ζ). Note that $c_{11} = c_{22}$.

For the numerical analysis of the sign of (3.58), the problem is discretized using linear 1d Lagrange finite elements and a uniform mesh. Hence, for given values of the parameters τ, Θ, ν and the wave number κ in the x_1-direction, the smallest eigenvalue $\mu_1(\tau,\kappa,\Theta,\nu)$ of the matrix corresponding to the discrete version of (3.58) is computed. The numerical code for this purpose is based on the use of the finite element library `FEniCS` [Logg *et al.* 2012] and the eigensolvers provided in `SLEPC` [Hernandez *et al.* 2005].

To find the shortest bifurcation time τ_b for which $\mu_1 = 0$ and the associated wave number κ_b the following steps are used:

1. *Initialization.* Set the values of (ν,Θ).

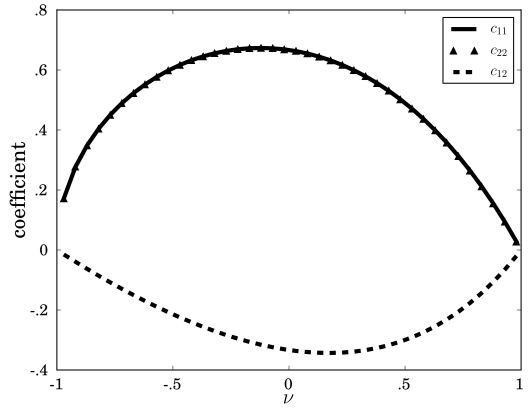

Figure 3.9: Evolution of the coefficients c_{11}, c_{12}, c_{22} with respect to the Poisson ratio ν

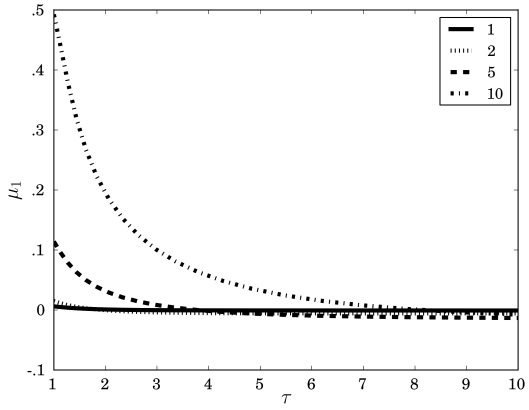

Figure 3.10: Decreasing of the first eigenvalue μ_1 with respect to τ of the quadratic form (3.58) for $\Theta = .4$, $\nu = 0$ for $\kappa = \{1, 2, 5, 10\}$

2. *Define the critical curve.* Given κ, find $\tau(\kappa)$ such that $\mu_1(\tau, \kappa, \Theta, \nu) = 0$, using a bisection algorithm on τ. This gives the *critical curve* in the $\tau - \kappa$ space.

3. *Find the bifurcation point* given by $\kappa_b = \text{argmin}_\kappa \, \mu_1(\tau(\kappa), \kappa, \Theta, \nu)$ and $\tau_b = \tau(\kappa_b)$. To this end a numerical minimization routine using the downhill simplex algorithm (`fmin` function provided in the optimization toolbox of `SciPy` [Jones *et al.* 01]) is used.

For step 2, neither existence nor uniqueness of a solution for the critical τ for a given κ can be established. The $\mu_1(\tau, \kappa, \Theta, \nu)$ is numerically found to be a monotonically decreasing function of τ (Fig. 3.10), which gives us the convergence of the bisection algorithm if a solution exists in the selected initial interval. However, for small values of κ a solution may not exist at all, in agreement with the Property 4 of Proposition 17.

Figure 3.11 illustrates the critical curves obtained for $\nu = 0$ and different Θ. For a given loading Θ the critical curve partitions the space (κ, τ) in the region below the curve, where the fundamental solution is the unique solution of the rate problem, and in the region above the curve, where other solutions may exist. During the evolution problem, the first time for which another solution may exist (and indeed it does exist, as stated in Proposition 18), is the minimum point on the critical curve $\kappa \mapsto \tau(\kappa)$. This point is the bifurcation point corresponding to the critical time τ_b and the wave number κ_b (see Proposition 18). The numerical solution provided in Figure 3.11 may be checked against the qualitative properties of the Rayleigh ratio proved in Proposition 17. Namely, one observes that: (i) the fundamental solution is unique for τ sufficiently small (Properties 1-2); (ii) the fundamental solution is unique for sufficiently small wave numbers even for very long times (Property 4); (iii) for $\kappa \to \infty$, $\tau(\kappa)$ is approximately linear in κ (Property 5).

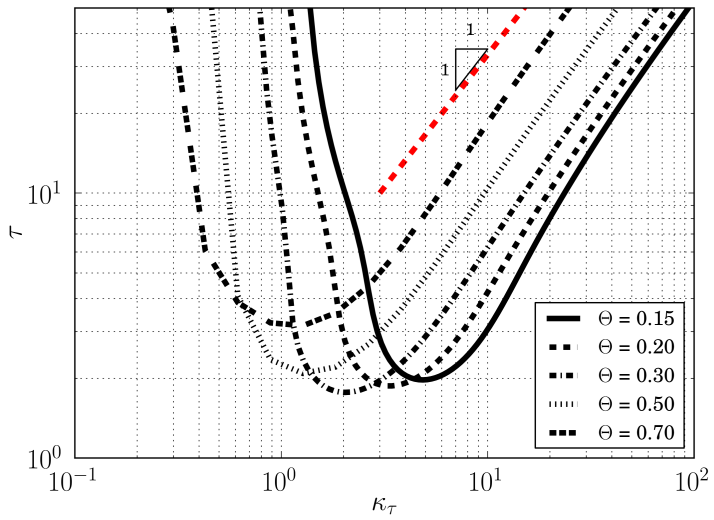

Figure 3.11: Critical curves separating the states (κ_τ, τ) unique and those where bifurcation can occur for different values of the loading parameter Θ

For the case $\nu = 0$, the critical time τ_b and wave number κ_b at the bifurcation as a function of Θ are reported in Figure 3.12. Figure 3.13 shows the shape of the damage rate β^b as a function of ζ for the eigenvector associated to the eigenvalue $\mu_1 = 0$.

The key numerical results of this chapter are condensed in Figure 3.14. It shows as a function of Θ (and $\nu = 0$) the plots of the critical bifurcation time t_b, wave length $\lambda_b = 2\pi \frac{\Theta \delta_{\tau_b} \tau_b}{\kappa_b} \eta$ and penetration of the damage D_b in the physical space and time variables, x_2 and t. The critical time at the bifurcation is reported also as dashed lines in Figure 3.7, which partitions the $\Theta - t$ space in the regions where the fundamental solution is unique or not.

Figure 3.15 shows the influence of the Poisson ratio on the results for a fixed value of Θ, showing that the critical wavelength, time and damage depth have a relevant dependence on the Poisson ratio only for ν close to -1. Recall that in plane stress elasticity thermodynamically admissible values of the Poisson ratio are in the interval $(-1, 1)$.

3.6 Final remarks: the genesis of periodic crack patterns

The initiation of a periodic solution in a gradient damage model under a thermal shock loading has been studied. The quasi-static evolution problem for a semi-infinite slab has been formulated in the framework of the variational theory of rate-independent processes. From the first order stability conditions and energy

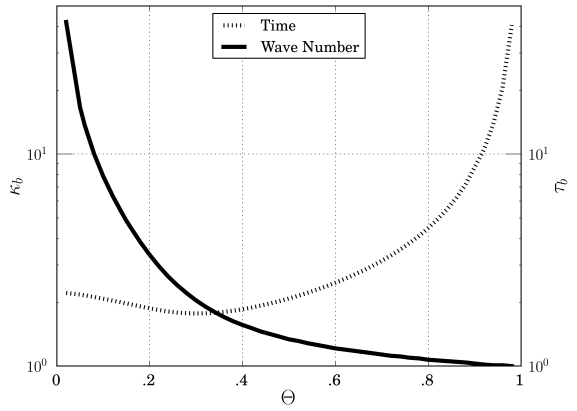

Figure 3.12: Wave number and rescaled time at the first bifurcation point κ_b, τ_b defined by (3.41) and (3.47) for a vanishing Poisson ratio $\nu = 0$

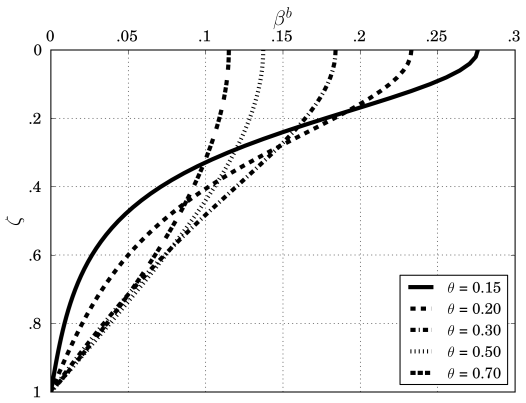

Figure 3.13: Characterization of damage rate at bifurcation through the eigenvector β^b (3.48)

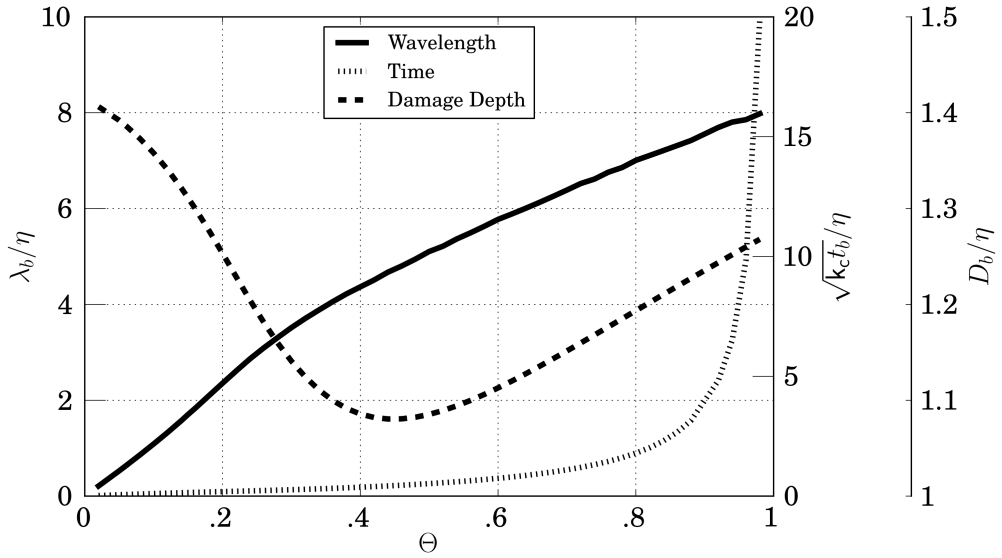

Figure 3.14: Wavelength λ_b, time t_b and penetration of the damage zone D_b at the first possible bifurcation (given by (3.49), (3.52)) for a vanishing Poisson ratio $\nu = 0$ as a function of the loading parameter Θ

balance, it has been proven that, for sufficiently severe thermal shocks, damage initiates at $t = 0$ with non-zero damage diffused in a strip parallel to the surface of the shock. The analysis of the rate problem about this fundamental solution shows the existence of a bifurcation at a finite time t_b towards a stable

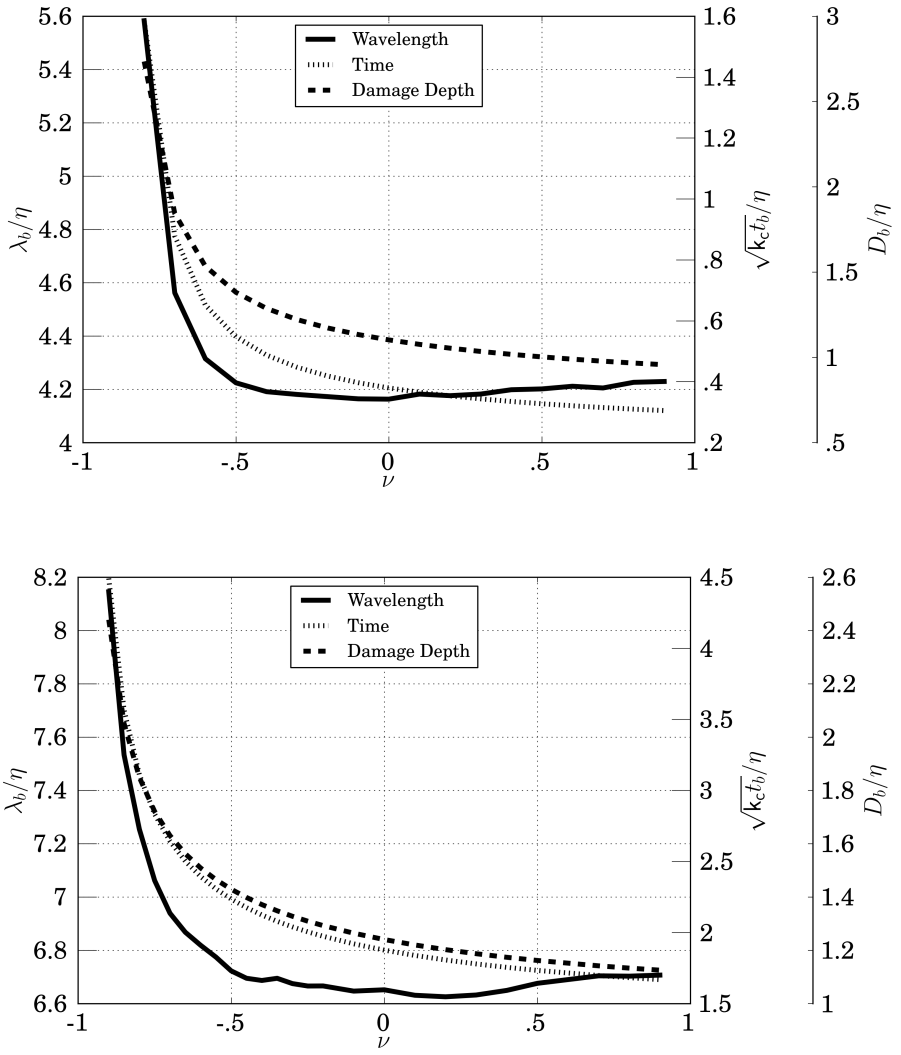

Figure 3.15: Influence of the Poisson ratio on the characteristic of the first bifurcation point as a function of the loading parameter $\Theta = \{.4,\ .8\}$.

solution with periodic damage. The fundamental solution becomes unstable at a later time $t_s > t_b$. The bifurcation and stability analysis is based on the study of the sign of the second derivative of the energy in an infinite dimensional setting. The analytical results are obtained by the minimization of a Rayleigh ratio and the decomposition of the solution with a partial Fourier series. Further quantitative results about the time, damage penetration and wavelength at the bifurcation are obtained numerically by solving a one-dimensional eigenvalue problem.

The analysis of gradient damage models of the previous sections quantitatively predicts the estab-

lishment of a fundamental solution with diffuse damage and its bifurcation at a finite time t_b towards a periodic solution. Let us resume and comment below the main results, coming from our analytical and numerical approaches on a semi-infinite slab.

- *Loading parameter.* The solution of the problem depends on a single dimensionless parameter, the mildness of the thermal shock $\Theta = \sigma_c/\mathsf{a}\mathsf{E}\vartheta$, defined as the ratio between the critical stress of the material and the thermal stresses induced by the temperature drop ϑ at the surface, and the Poisson ratio ν. The dependence on the internal length of the damage model η is almost trivial and given explicitly (see below).

- *Existence of a critical severity of the thermal shock.* For mild shocks with $\Theta \geq 1$ the solution remains purely elastic at any time and there is not damage at all.

- *Fundamental solution.* If $\Theta < 1$ there exists, for any $t > 0$ a solution with diffused damage in a strip, varying monotonically from a maximum damage value $\alpha_t^*(0)$ at the surface to zero at a depth D_t^*. The values of $\alpha_t^*(0)$ and D_t^* as a function of time and the mildness of the thermal shock can be read in Figure 3.7, where the dashed red line critical time t_b for the first bifurcation toward the periodic solution. This fundamental solution becomes unstable at a finite time $t_s > t_b$ (Proposition 18).

- *Bifurcated solution.* At a finite time t_b there exists a bifurcation from the fundamental solution toward a periodic solution with a wavelength λ_b in the x_1 variable. This bifurcated branch is stable for t sufficiently close to t_b (Proposition 15).

- *Bifurcation time.* The bifurcation time t_b is monotonically increasing with the mildness of the thermal shock. The numerical results of Figure 3.14 for $\nu = 0$ indicate that it varies from very small values for $\Theta \to 0$ to very large values for $\Theta \to 1$. Proposition 18 states that t_b is always a strictly positive time.

- *Bifurcation wavelength.* The wavelength of the bifurcated solution is increasing with the mildness of the thermal shock Θ . The numerical results of Figure 3.14 for $\nu = 0$ indicate that it goes to zero for $\Theta \to 0^+$. For $\Theta \to 1$, it has finite limit which is of about eight times the internal length, (numerical result for $\Theta = .96$).

- *Damage penetration.* The damage penetration at the bifurcation, D_b, is almost independent of the loading (it varies only between η and $1.5\,\eta$), as evident also from Figure 3.7(b), where the dashed line corresponding to the bifurcation almost coincides with an iso-depth line. The penetration of the damage band seems to be the parameter triggering the bifurcation and not the maximal value of damage or time which vary with the loading.

- *Influence of the internal length.* The damage penetration in the homogeneous solution D_t and the wavelength λ_b of the bifurcated solution are simply proportional to the internal length η of the damage model. This fact does not really come as surprise, because η is the only characteristic length of the problem for a semi-infinite slab (the characteristic length of the diffusion process associated to the material constant k_c can be eliminated by a trivial rescaling of the time variable). The bifurcation time t_b is proportional to η^2.

- *Influence of the Poisson ratio.* The fundamental solution is independent of the Poisson ratio. The numerical results of Figure 3.15 show a weak dependence of the key properties of the bifurcated solution of the Poisson ratio ν, except for $\nu \to -1$.

Our work relies on many simplifying hypotheses, which allow us to reach an almost complete analytical treatment of the initiation problem. First, the geometry and the loading are highly idealized. More realistic settings will include the effect of the finite dimension of the slab and a full two-dimensional solution of the thermal problem, eventually accounting for boundary condition of the Robin type on the temperature (Newtonian cooling) and the localized changes in the thermal conductivity due to cracks. Three dimensional effects may play a crucial role as soon as the thickness of the slab increases. Further generalization should consider the effect of choice of the damage law, as done in a 1d setting by [Pham & Marigo 2013]. The existence of a critical stress assures the existence of a purely elastic response. The numerical values of Section 3.5 will depend on the specific damage model. Here a specific choice has been made (see Example 1) which assures an easy numerical treatment.

Chapter 4

Morphogenis of cracks

Contents

In the previous chapter the nucleation process of the thermal shock problem has been studied in a semi-analytical manner. The behavior at the exposed surface for short times has been examined, leading to the nucleation of a periodic set of localized damage zones. In the second chapter, it has been established that when the length of the damage is long in front of the dimension of the internal length, the damage band follows Griffith's evolution law. In this chapter, the entire evolution process from the nucleation to crack selection mechanisms is addressed in a mostly numerical matter. The model problem of the thermal shock

is once again considered. The results will also be compared to experiments. Furthermore the behavior of the model is a three-dimensional setting is illustrated. Some insight on the engineering answers that can be exploited will be given, making explicit the material parameters. This chapter, although using the results from the previous one, can be read independently.

Specifically, in Section 4.1 the dimensionless energy is re-investigated and two regimes governed respectively by σ_c and $\mathsf{G_c}$ are established. Then (Section 4.2) the nucleation phase is investigated comparing the alternate minimization solution with those of Chapter 3. The next phase, the nucleation of cracks is discussed in Section 4.3. Once the cracks are established, the propagation phase and the crack selection mechanisms are studied (Section 4.4) and comparison to experimental results (on the nucleation and propagation phases) are performed. The three-dimensional simulations (Sec. 4.5) exhibit a hexagonal crack patterns when the domain is very large. The limit case of thin slabs justifies the two-dimensional assumption. Finally two applications are investigated (Sections 4.6-4.7).

4.1 The two loading parameters Θ and ℓ_0 in the thermal shock setting

The natural configuration of the plate is $\Omega = (0, L_x) \times (0, L_y)$ and is at a uniform temperature T_0. As in Chapter 3 a perfect conductivity of the temperature is assumed. Therefore, the temperature boundary condition in $x_2 = 0$ is of Dirichlet type, the temperature field at time $t > 0$ is

$$\mathrm{T}_t(\mathbf{x}) = \mathrm{T}_0 - \vartheta\, \mathsf{f_c}\Big(\frac{x_2}{2\sqrt{\mathsf{k_c} t}}\Big), \quad \forall t > 0, \text{ with } \mathsf{f_c}(x) = \frac{2}{\sqrt{\pi}} \int_x^\infty e^{-s^2}\, \mathrm{d}s,$$

where $\mathsf{f_c}$ it the complementary error function, strictly decreasing from 1 to 0 at infinity. The material constant $\mathsf{k_c}$ characterizes its thermal conductivity. Thus the temperature field is uniform with respect to the x_2 direction. The body forces are neglected. The depth of numerical specimen L_y is large in front of the characteristic length of the diffusion process $\sqrt{\mathsf{k_c} t_b}$, where t_b is the first bifurcation time. The shear stress and the normal displacement vanish on $x_1 = 0$ and $x_1 = L_x$. The surfaces $x_2 = 0$ and $x_2 = L_y$ are stress free. The damage field evolution is left free of any constraint on all boundaries. Thus the boundary conditions read:

$$\begin{gathered} u_1|_{x_1=0 \text{ or } L_x} = 0 \\ \sigma_{22}|_{x_2=0 \text{ or } L_x} = \sigma_{12}|_{x_2=0 \text{ or } L_x} = 0 \\ \sigma_{11}|_{x_2=0 \text{ or } L_y} = \sigma_{22}|_{x_2=0 \text{ or } L_y} = \sigma_{12}|_{x_2=0 \text{ or } L_y} = 0. \end{gathered} \tag{4.1}$$

The plate is constituted of a material whose constitutive relation is that of Example 1. In the numerical simulation, whose study is the goal of the first sections of this chapter, the main stages of the damage evolution are as follows. Damage nucleates (Fig. 4.1(a)) on the surface exposed to the temperature change at $t = 0$. Then it propagates in the depth of the structure (Fig. 4.1(b)) remaining homogeneous parallel to exposed surface, the maximal damage value remains at the surface and increases. At a given time, a

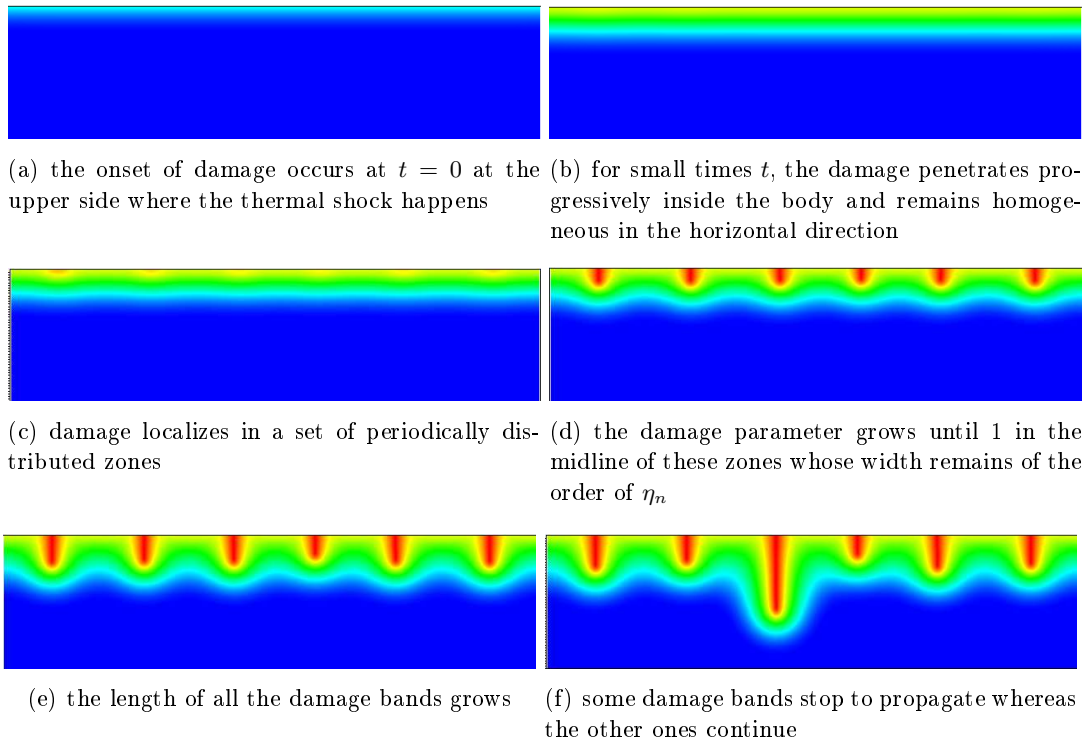

(a) the onset of damage occurs at $t = 0$ at the upper side where the thermal shock happens

(b) for small times t, the damage penetrates progressively inside the body and remains homogeneous in the horizontal direction

(c) damage localizes in a set of periodically distributed zones

(d) the damage parameter grows until 1 in the midline of these zones whose width remains of the order of η_n

(e) the length of all the damage bands grows

(f) some damage bands stop to propagate whereas the other ones continue

Figure 4.1: Main stages captured by the alternate minimization algorithm with no assumption on the topology. Illustrates the singularity in time, the loss of uniqueness and the localization process. A damage band with $\alpha = 1$ at its center is assimilated to a crack.

bifurcation (Fig. 4.1(c)) from this initial solution is observed, a periodic solution arises. The localizing process has begun which terminates with the construction of a crack (Fig. 4.1(d)). Then these cracks propagate (Fig. 4.1(e)). The last phase is a mechanism of crack selection (Fig. 4.1(f)), where every other cracks stops. This is the general overview and some steps might be skipped for severe of mild loading.

Before elaborating a more precise description of the numerical results from the thermal problem, the relevant quantities are identified. In experiments parallel arrays of cracks are observed (Fig. 3.1). Assuming that the dissipative corresponds to Griffith surface energy, a dimensionless analysis introduces the length [Jagla 2002, Jenkins 2005, Bahr *et al.* 2010]:

$$\ell_0 = \frac{\mathsf{G_c}}{\mathsf{E}(\mathsf{a}\vartheta)^2}, \tag{4.2}$$

which is called the *Griffith length*. Thus the total energy (1.33) of the system reads in a dimensionless form

$$\bar{\mathcal{P}}^G(\mathbf{u}, \mathrm{T}, \ell) = \int_{\Omega\setminus\Gamma_t} \bar{\psi}_0(\bar{\boldsymbol{\varepsilon}}(\mathbf{u})(\mathbf{x}), \bar{\boldsymbol{\varepsilon}^0}) \, \mathrm{d}\mathbf{x} + \ell_0 \mathcal{S}_\ell \tag{4.3}$$

where ψ_0 is normalized by the volumic elastic energy induced by the maximum shrinkage $\mathsf{E}(\mathsf{a}\vartheta)^2$. This length ℓ_0 is the ratio between the crack surface energy density and the volumic stored elastic energy.

Thereby an other loading parameter than the one introduced in Chapter 4 appears when considering the Griffith surface energy. However the gradient damage model converges towards Griffith surface energy for small internal length η. How can we explain these two quantifications of the loading the *Griffith length* ℓ_0 and the *mildness of the thermal shock* Θ?

This problem has a multiple of length: Griffith's length ℓ_0, the dimensions of the structure L_x, L_y, the internal length η_n, the diffusion penetration $2\sqrt{\mathsf{k_c}t}$. At the exception of the diffusion one, all these length are fixed for a given problem. Two regimes are going to be identified according to the length $2\sqrt{\mathsf{k_c}t}$. Using the energy density of Example 2 and writing the regularized functional (1.34) in a dimensionless setting:

$$\bar{\mathcal{P}}(\mathbf{u}, \mathrm{T}, \alpha) := \int_{\bar{\Omega}} \frac{1}{2}(1-\alpha_t)^2 \bar{\mathsf{A}}\bar{\boldsymbol{\varepsilon}}^e(y) \cdot \bar{\boldsymbol{\varepsilon}}^e(y) + \frac{\mathsf{w_1^n}}{\mathsf{E}(\mathsf{a}\vartheta)^2}\left(\frac{\alpha}{\eta_n} + \frac{\eta_n}{4\mathsf{k_c}t}\bar{\nabla}\alpha_t \cdot \bar{\nabla}\alpha_t\right) \mathrm{d}\bar{\mathbf{x}} \tag{4.4}$$

where $\bar{\nabla} = 2\sqrt{\mathsf{k_c}t}\nabla$, $\bar{\mathsf{A}} = \mathsf{A}/\mathsf{E}$, $\bar{\boldsymbol{\varepsilon}}_t^e = \boldsymbol{\varepsilon}_t^e/(\mathsf{a}\vartheta)$, and $\bar{\mathbf{x}} = \mathbf{x}/(2\sqrt{\mathsf{k_c}t})$. From (4.4), two choices are possible. Introducing a loading parameter Θ and a rescaled time τ:

$$\Theta = \frac{\sigma_c}{\mathsf{a}\vartheta\mathsf{E}} \qquad \tau = \frac{\sqrt{2}\sqrt{\mathsf{k_c}t}}{\Theta\eta_n}, \tag{4.5}$$

where one recalls that (1.29) $\sigma_c = \sqrt{\mathsf{w_1^n}\mathsf{E}/\eta_n}$, and thus the loading parameter is the ratio between the material's critical stress and the maximum stress imposed by the thermal shock. The dimensionless regularized energy[1] (4.4) reads:

$$\int_{\bar{\Omega}} \frac{1}{2}(1-\alpha_\tau)^2 \bar{\mathsf{A}}\bar{\boldsymbol{\varepsilon}}^e(y) \cdot \bar{\boldsymbol{\varepsilon}}^e(y) + \Theta^2\alpha_\tau + \frac{1}{2\tau^2}\bar{\nabla}\alpha_\tau \cdot \bar{\nabla}\alpha_\tau \, \mathrm{d}\bar{\mathbf{x}}$$

The other choice, is to explicit the *Griffith length* ℓ_0. The dimensionless quantity $\bar{\eta}_n = \eta_n/(2\sqrt{\mathsf{k_c}t})$, ratio between the materials internal length and the penetration of the diffusion is introduced, and (4.4) reads:

$$\int_{\bar{\Omega}} \frac{1}{2}(1-\alpha)^2 \bar{\mathsf{A}}\bar{\boldsymbol{\varepsilon}}^e(y) \cdot \bar{\boldsymbol{\varepsilon}}^e(y) + \frac{8}{3}\ell_0\left(\frac{\alpha}{\bar{\eta}_n} + \bar{\eta}_n\bar{\nabla}\alpha \cdot \bar{\nabla}\alpha\right) \mathrm{d}\bar{\mathbf{x}}. \tag{4.6}$$

What is the meaning of these two transcriptions of $\bar{\mathcal{P}}$? First, in (4.6) the structure is the same as in (1.34), and thus when $\bar{\eta}_n \to 0$ one can expect the integral of the gradient term to converge towards the measure of the crack set. But this is valid for a given time t. And thus for any length η_n there will always exist a time $\tilde{t}$ where $\bar{\eta}_n$ can not be considered small. Indeed, if the regularized approach to fracture was used one would have to use a variable (with time) internal length which verifies

$$\eta_n(t) << 2\sqrt{\mathsf{k_c}t}, \qquad \forall t \in (0, +\infty(.$$

Not only would the introduce numerical difficulties but it contradicts the physical meaning given in this work to the internal length. In the physical space, η_n should be small in front of all the other dimensions and especially the penetration of the temperature field $2\sqrt{\mathsf{k_c}t}$ for the *Griffith length* to have a meaning. Otherwise, the gradient damage remains the valid model, and $\Theta = \sigma_c/(\mathsf{a}\mathsf{E}\vartheta)$ captures the loading. Finally, both interpretations are valid, depending on the time in our problem:

[1] The choice made in Chapter 3 let to a different definition of σ_c and τ but consistent with the one proposed here taking $\eta = \sqrt{2}\eta_n$

1. For short times, the *mildness parameter* Θ, the ratio between the critical stress and the imposed thermal stress, governs the evolution.
2. For longer times t such that $2\sqrt{\mathsf{k_c}t} >> \eta_n$, the *Griffith length* ℓ_0 is the sole parameter governing the evolution.

Before investigating at length the numerical evolution of the crack set in the thermal shock problem it is useful to come back to the material parameters and especially those of damage and fracture, $\mathsf{G_c}, \sigma_c, \eta_n$. These material constants are linked coherently (1.32) due to the framework proposed by the gradient damage model. The intensity of the thermal shock (4.2) and (4.5) can be formulated depending on the choice of material parameters:

- The material is characterized by $(\sigma_c, \mathsf{G_c})$, the two most current macroscopic quantities for brittle fracture
$$\Theta = \frac{\sigma_c}{\mathsf{a}\vartheta\mathsf{E}} \qquad \ell_0 = \frac{\mathsf{G_c}}{\mathsf{E}(\mathsf{a}\vartheta)^2}$$
The loading Θ which gives the mildness of the thermals shock does not depend on the internal length η_n. The internal length can be figured out from (1.32) as $\eta_n = 8\sigma_c^2/(3\mathsf{E}\mathsf{G_c})$.
- The material is characterized by (σ_c, η_n) which define the damage model
$$\Theta = \frac{\sigma_c}{\mathsf{a}\vartheta\mathsf{E}} \qquad \ell_0 = \frac{4\sqrt{2}}{3}\frac{\sigma_c^2\eta_n}{(\mathsf{E}\mathsf{a}\vartheta)^2} = \frac{4\sqrt{2}}{3}\Theta^2\eta_n$$
- The material is characterized by $(\eta_n, \mathsf{G_c})$ corresponding to a Griffith evolution law which is regularized with a parameter η_n, which possibly has no physical meaning
$$\Theta = \sqrt{\frac{3}{8}}\frac{\sqrt{\mathsf{G_c}}}{\sqrt{\mathsf{E}\eta_n}\mathsf{a}\vartheta} = \sqrt{\frac{3}{8}}\sqrt{\frac{\ell_0}{\eta_n}} \qquad \ell_0 = \frac{\mathsf{G_c}}{\mathsf{E}(\mathsf{a}\vartheta)^2}$$
this illustrates that Θ is a competition between the materials internal length η_n and that of the Griffith problem ℓ_0.

The *mildness parameter* and *Griffith's length* being characterized depending on the choice of material parameters (a direct consequence of (1.32)). Let us discuss their evolution:

- for a given material, when the loading (*i.e.* the gradient of the thermal shock ϑ) increases, then Θ and ℓ_0 decrease
- for a given loading $\mathsf{a}\vartheta$, and critical stress σ_c: Θ is invariant to η_n and ℓ_0 is proportional to η_n (because the toughness is proportional to η_n (1.32) $\mathsf{G_c} = 8\sigma_c\eta/(3\mathsf{E})$)
- for a given loading $\mathsf{a}\vartheta$, and toughness $\mathsf{G_c}$ then ℓ_0 is invariant and Θ increases with σ_c or decreases with η_n.

The reader is now well aware that using the bulk energy density from Example 1 would just change a few numerical coefficient but in no case the interpretations which have just been given. These few paragraphs have: (i) exhibited two regimes depending on the time from the damage model, (ii) linked the parameters quantifying the loading two the material available. They should be kept in mind as browsing through the chapter as many results are based on the different interpretations.

4.2 Nucleation phase: comparison between analytical and numerical results

Here the first steps of the evolution are studied (Figs. 4.1(a), 4.1(b) 4.1(c)), corresponding to the nucleation phase of localized damage zones. Does the numerical implementation, through the alternate minimization (Chapter 1) capture the fundamental solution and the bifurcation to localized states ?

4.2.1 Main results from the analytical damage at nucleation

In Chapter 3 the same setting has been studied using the variational formulation of the non local damage model based on irreversibility, stability and energy balance. Using conventional techniques of calculus of variations we proved

1. The state of the system depends on the loading parameter Θ.
2. If $\Theta > 1$ the elastic solution remains stable for any time.
3. If $\Theta < 1$ damage starts at $t = 0$. First the state only depends on the depth $\alpha_t^*(\mathbf{x}) = \bar{\alpha}_\tau(y)$ where the change of variable $y = x_2/(2\sqrt{\mathsf{k_c}t})$ is suggested by the diffusion process. It has been proven that the damage fields fundamental branch is governed by:

$$\begin{cases} \frac{1}{\tau^2}\frac{d^2\bar{\alpha}_\tau}{dy^2}(y) + \mathsf{f_c}(y)^2(1-\bar{\alpha}_\tau(y)) = \Theta^2 & \forall y \in (0,\delta_\tau) \\ \frac{d\bar{\alpha}_\tau}{dy}(0) = 0, \qquad \bar{\alpha}_\tau(\delta_\tau) = 0, & \frac{d\bar{\alpha}_\tau}{dy}(\delta_\tau) = 0. \end{cases} \tag{4.7}$$

   The damage profile can been computed by numerical integration of (4.7). The displacement field is the same as the elastic one but the stress field is different because of the damage evolution

$$\boldsymbol{\varepsilon}(\mathbf{u}_t^*)(\mathbf{x}) = \bar{\boldsymbol{\varepsilon}}_\tau(y) := -(1+\nu)a\vartheta\,\mathsf{f_c}(y)\mathbf{e}_2\otimes\mathbf{e}_2, \quad \boldsymbol{\sigma}_t^*(\mathbf{x}) = \bar{\boldsymbol{\sigma}}_\tau(y) := (1-\bar{\alpha}_\tau(y))^2\mathsf{E}a\vartheta\,\mathsf{f_c}(y)\mathbf{e}_1\otimes\mathbf{e}_1.$$

4. The uniqueness and stability of this fundamental branch are then studied in Section 3.4. The homogeneous phase is unique and stable for a strictly positive time.
5. At a critical time t_b there is a loss of uniqueness of the homogeneous solution and a bifurcation of finite periodicity arises. The time and periodicity at bifurcation are given by:

$$t_b = \frac{\Theta^2\tau_b^2\eta_n^2}{4\mathsf{k_c}}, \quad \lambda_b = 2\pi\frac{\Theta\delta_{\tau_b}\tau_b}{\kappa_b}\eta_n.$$

where (κ_b, τ_b) only depend on the loading Θ and the Poisson ratio ν. They are solution of a minimization problem (Fig. 3.14). The bifurcation solution $(\sqrt{t_b}, \lambda_b)$ varies linearly to the internal length η_n. Therefore t_b is the first time at which a bifurcation from the fundamental branch can occur. The fundamental branch is still stable at this time but becomes definitively unstable at a time t_s such that $t_b < t_s < +\infty$.

The bifurcation towards a periodic solution is the onset of the localization process leading to the formation of periodic crack patterns.

4.2.2 The fundamental solution: invariant parallel to the exposed surface

For short times, the damage and displacement field depend only on the second space variable (x_2 in the physical space). The analytical solution of the fundamental branch $\mathbf{x} \mapsto \alpha_t^*(\mathbf{x})$ is computed from (4.7) and leads to (Fig. 3.6). For the alternate minimization implementation, a domain of size $L_x = 200$ $L_y = 50$ of elements of size $h = .2$ is considered. The numerical parameters are set at $\nu = 0$, $\mathsf{E} = 1$, $\mathsf{G_c} = 1$:

- For two different internal length $\eta_n = 10$ and $\eta_n = 20$ (Fig. 4.2) which correspond to loadings $\Theta = 0.194$ and $\Theta = 0.137$. Thus this internal length
- Fixing $\eta_n = 10$ (Fig. 4.3) a severe $\Theta = .01$ and a mild loading $\Theta = .5$ are considered.

These results are totally independent of the mesh size. There is not even an error introduced for the evaluation of the toughness $\mathsf{G_c}$. As the numerical algorithm includes the first order stability condition (1.35) which is used to compute the semi-analytical solution. For any time step belonging to this fundamental branch, it is very *easy* to capture the solution with respect to the next section. It will not be discussed any further, indeed the fundamental solution has been extensively studied in (Fig. 3.6).

4.2.3 Bifurcation and loss of stability: the periodic solution

The alternate minimization algorithm allows to capture properly the horizontal homogeneous solution. We concentrate on the step of Fig. 4.1(c) where the numerical algorithm bifurcates from the fundamental branch and a periodic solutions arises. At a given depth a, the evolution of the damage field (Fig. 4.4) bifurcates in a single time step from the constant value $\alpha_t^*(a, \cdot)$ to a periodic damage solution of minimum $\alpha_t^*(a, \cdot)$. This time step is the beginning of the localizing process. All the periods evolve in cracks on a few time steps.Note that some sorts of boundary effects is observed and that the solution is not entirely periodic, in the sense that the amplitude of the damage is not the same for each "wave". These are numerical aspects which are not relevant to the general process but will become relevant for certain loading parameters. In this section, the bifurcation time step is studied, whereas the construction of cracks, for which no analytical results exist are studied in Section 4.3.

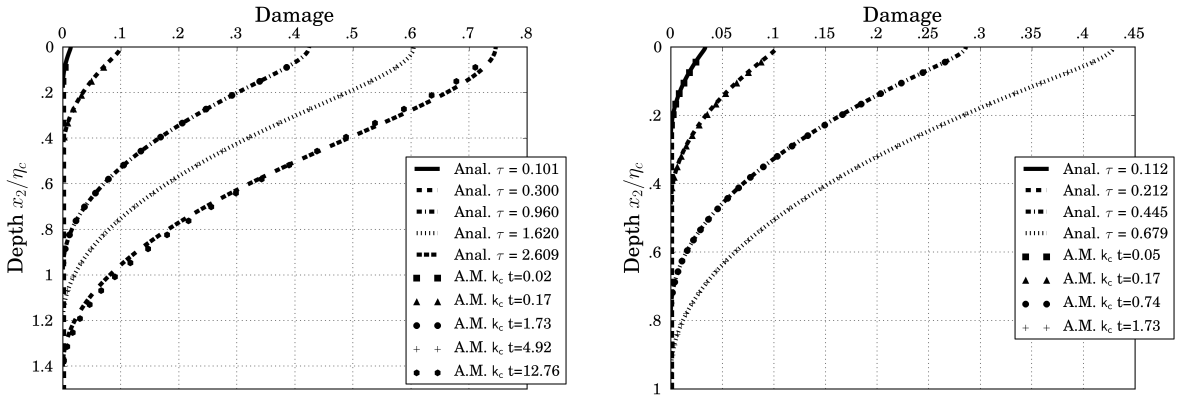

Figure 4.2: The fundamental solution damage field in function of the depth from the semi-analytical solution (Anal.) and the alternate minimization algorithm (A.M.) $\eta_n = 10$ (left) and $\eta_n = 20$ (right). The semi-analytical results come from Chap. 3, Sec. 3.3.

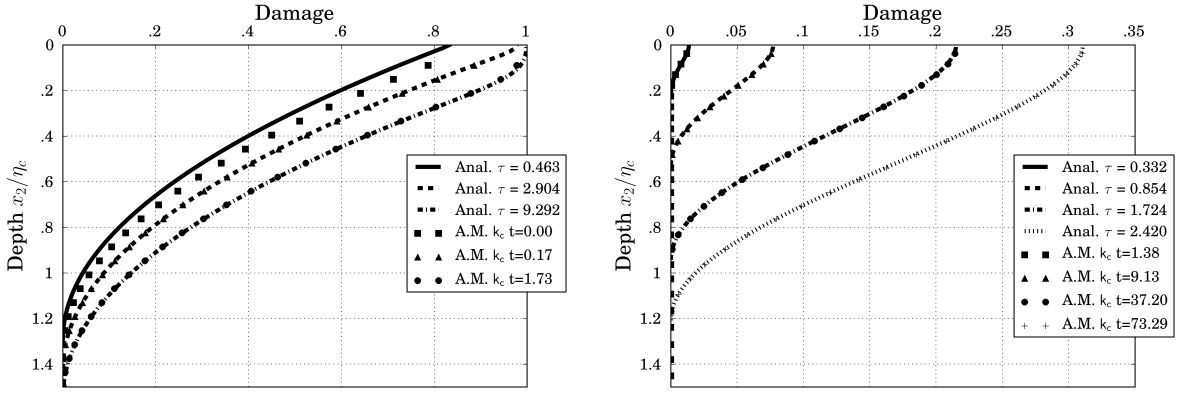

Figure 4.3: The fundamental solution damage field in function of the depth from the semi-analytical solution (Anal.) and the alternate minimization algorithm (A.M.) for a severe $\Theta = .01$ (left) and mild $\Theta = .5$ (right) loading. The semi-analytical results come from Chap. 3, Sec. 3.3.

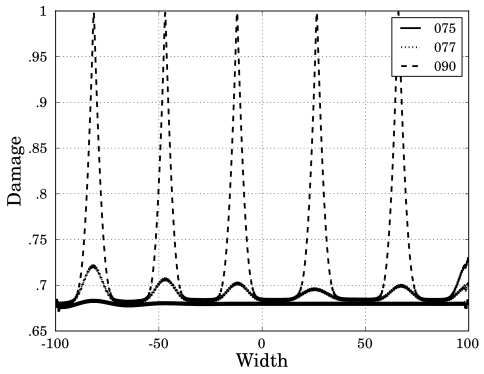

Figure 4.4: Evolution of the damage profile at a given distance from the surface. The damage is constant following the x direction for small times. Then the periodicity arises.

Once the solution bifurcates from the fundamental branch no more analytical solution exists any more. We therefore would like to compare the time and wavelength of the bifurcation from the fundamental branch. In the wake of Chapter 3 - Section 3.5 where the influence of the Poisson ratio is seen as negligible this parameter is not studied fixed at $\nu = 0$. The periodicity and the critical time of this loss of stability are extracted (Table 4.1). The error estimation is due to the time discretization and the finite width of the domain. The wavelength window is related to the fact that the number of periods in the domain is given up to a half period, as the boundary condition is such that $\frac{\partial \alpha}{\partial \mathbf{n}}$. Thus for n periods of width λ_b the error of the finite dimension is given at $\lambda_b/(2n)$. The same error estimates are used in Tables 4.4-4.5. When the load decreases, and thus the periodicity increases, less and less localization zones appear for a given width of the slab. The wavelength is computed on the 6 or 7 periods at the center of the slab.

The results (Table 4.1) are compared to those of Chapter 3 in the physical space. Figure 4.5 reports for the various loadings Θ the numerical results from the alternate minimization algorithm and those from the semi analytical work. Thus the relation in the periodicity λ_b between the alternate minimization computation and those from the analytical (Fig. 4.5) are a good match. The bifurcation from the alternate minimization computation is systematically above. As that computed in Chapter 3 was a first bifurcation time. Indeed no estimate of the loss of stability of the fundamental branch exist. The penetration of the damage is once again constant for any loading. The periodicity for $.7 < \Theta < 1$ is not investigated for two linked reason. As the bifurcation occurs, its amplitude is of the order of the variations on the elements. Furthermore the system evolves directly towards cracks.

Remark 10. *The computation cost of the bifurcation time step is much higher than during the evolution of the fundamental solution where the number of iterations for a given time step jumps (typically the number of iterations is multiplied by 7). Furthermore, the numerical noise due to the mesh is a sufficient imperfection for the bifurcation to occur. The fact that the localization comes from a lost of stability or a bifurcation has not been investigated and would require to compare the eigenvalues of the Hessian during the computation.*

Θ	.02	.1	.2	.3	.4	.5	.6	.7
$\mathsf{a}\vartheta$	9.68	1.93	.968	.645	.484	.387	.323	.277
ℓ_0/η_n	.0011	.0267	.107	.24	.427	.667	.96	1.307
λ_b	3.28	18 $\pm$.12	37$\pm$ .6	50$\pm$1.86	55.8$\pm$1.94	74.65 $\pm$3.48	81.8 $\pm$ 3.2	86.3 $\pm$ 3.7
$\mathsf{k_c}t_b$	.25	4.15$\pm$.18	12.4 $\pm$.3	22 $\pm$.29	43$\pm$.5	69.8$\pm$.7	147 $\pm$ 1	307 $\pm$ 2
D_b	20	20.21	19.34	17.78	18.18	16.48	17.32	17.32
λ_c	3.04	16.7	41.1	96.6	160	198	352	713
$\mathsf{k_c}t_{cracks}$	.37	7.87	25.5	40.8	76.5	124	224	649
D_c	20.4	21.92	20.99	19.79	19.2	16.7	16.7	16.7
$\mathcal{S}_\ell(\alpha = 1)$	Nan	1.76	4.5	5.99	9.70	12.5	21	42
$\mathcal{S}_\ell(\alpha > 0)$	Nan	21.5	22	24.83	22.32	39.7	49	72
$\mathcal{S}_\ell(\alpha = 1)/\ell_0$	Nan	6.59	4.2	2.5	2.27	1.87	2.2	3.2
λ_c/ℓ_0	276	62.5	41.1	40.25	37.47	29.7	36.7	54.6
$\mathsf{k_c}t_{cracks}/\ell_0^2$	3057	110	22.2	7.08	4.19	2.8	2.4	3.8

Table 4.1: Wavelength, bifurcation time and damage depth for different loading parameters Θ. Numerical parameters $h = .2$, $\eta_n = 10$, $\nu = 0$. The domain size varies from $L_x, L_y = 800, 50$ to $L_x, L_y = 5000, 2000$. The loading is adapted through the variation of the thermal expansion coefficient.

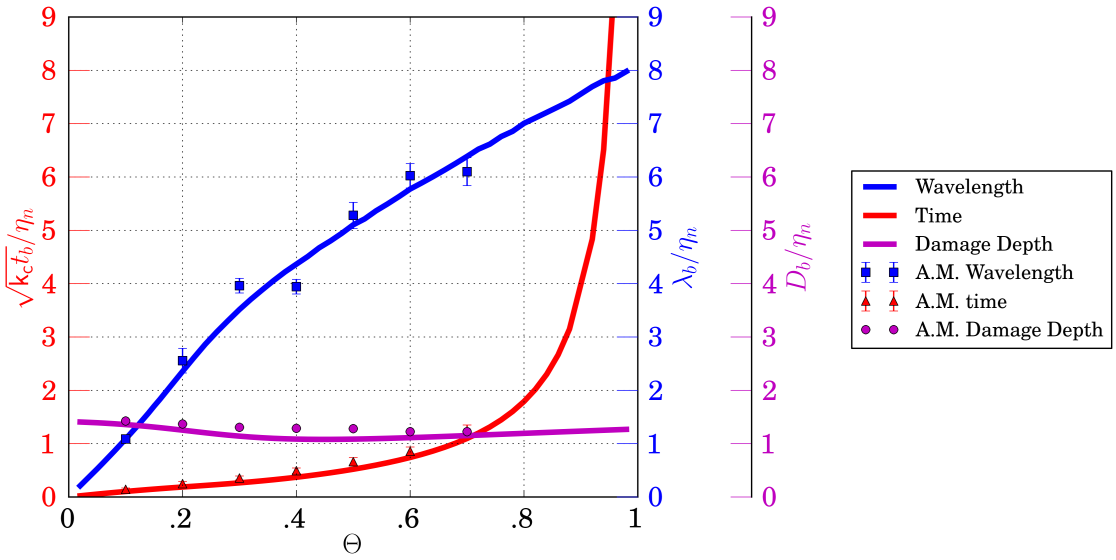

(a) Θ and linear space. Going rights corresponds to an increase of the critical stress σ_c or to a decrease of the loading $\mathbf{a}\vartheta$ and thus to a milder loading.

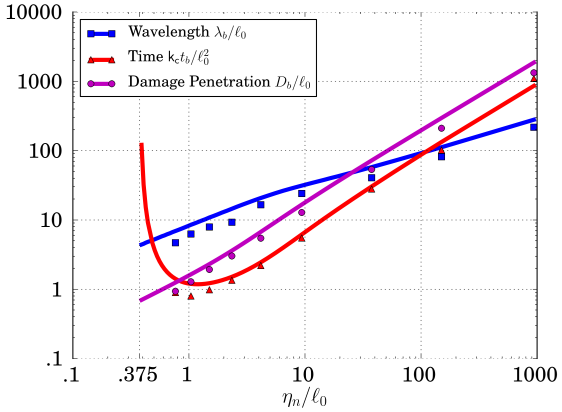

(b) For a given "propagation" loading ℓ_0 change in the internal length. $\eta/\ell_0 = .375$ corresponds to $\Theta = 1$.

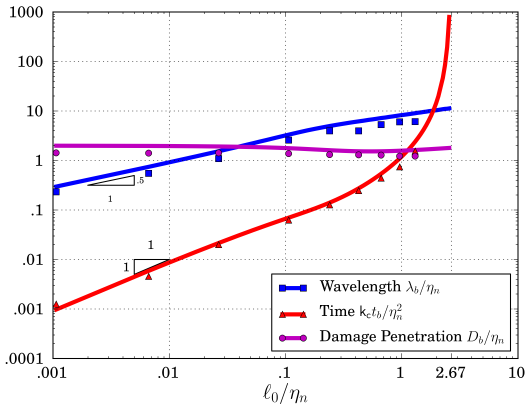

(c) For a given material parameter η_n change in the loading ℓ_0. $\ell_0/\eta = 2.67$ corresponds to $\Theta = 1$

Figure 4.5: Comparison of the bifurcation spacing and given by the damage formulation and those of the alternate minimization process in function of the loading parameter Θ. Data from Table 4.1 and Figure 3.14 correspond to the first bifurcation possible.

For severe loadings, the asymptotic behavior of (Fig. 4.5) can be quantified

$$\left(\log\frac{\lambda_b}{\ell_0}, \log\frac{\mathsf{k_c}t_b}{\ell_0^2}, \log\frac{D_b}{\ell_0}\right) = A_{\ell_0}\log\left(\frac{\eta_n}{\ell_0}\right) + B_{\ell_0} \qquad \left(\log\frac{\lambda_b}{\eta_n}, \log\frac{\mathsf{k_c}t_b}{\eta_n^2}, \log\frac{D_b}{\eta_n}\right) = A_{\eta_n}\log\left(\frac{\ell_0}{\eta_n}\right) + B_{\eta_n}$$

where the coefficients $(A_{\ell_0},\ B_{\ell_0})$ and $(A_{\eta_n},\ B_{\eta_n})$ are given by Tables 4.2-4.3

	A_{ℓ_0}	B_{ℓ_0}
λ_b/ℓ_0	0.4758	1.0204
$\mathsf{k_c}t_b/\ell_0^2$	1.0976	-0.2729
D_b/ℓ_0	1.0487	0.1913

Table 4.2: For large η_n/ℓ_0 *i.e.* $\eta_n/\ell_0 > 2$.

	A_{η_n}	B_{η_n}
λ_b/η_n	0.5241	1.0205
$\mathsf{k_c}t_b/\eta_n^2$	0.9024	-0.2729
D_b/η_n	-0.0487	0.1913

Table 4.3: For small ℓ_0/η_n *i.e.* $\ell_0/\eta_n < .5$.

Of course Figure 4.5 is just a question of formatting which allows to see the evolution of the bifurcates solution as the materials internal length increases (Fig. 4.5(b)), or for a given material as the loading increases (Fig. 4.5(c)).

4.2.4 Study of the influences of the material's internal length η_n

In the previous section the characteristics of the numerical bifurcation have been compared with those of Chapter 3 using the thermal expansion coefficient $\mathsf{a}\vartheta$ to change the loading parameter. The internal length has been kept constant although claim were made on its impact. Does the numerical simulation capture properly the linearity of the solution with respect to the internal length? On a domain of same size and for a giving loading the damage profile seems to follow an homothetic transformation (Fig. 4.6) as η_n increases.

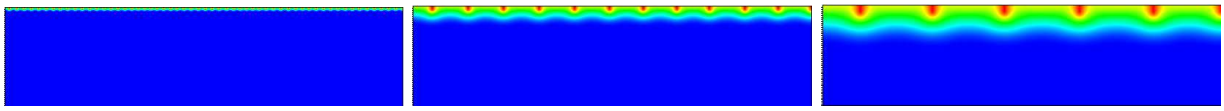

Figure 4.6: Initial crack distribution for different internal length. $\eta_n = (1, 5, 10)$ for L_x=200 and L_y=50 for a constant thermal loading $\Theta = .2$.

Let us check it more precisely. A given loading Θ is considered, and the materials internal length varies, thus considering a family of materials where the internal length varies but the critical stress σ_c is kept constant (Fig. 4.6).

Tables 4.4 and 4.5 investigate the linearity of λ_b for $\Theta = .1$ and $\Theta = .2$. The last line of each table corresponds to the first two columns of Table 4.1. In Table 4.4 * corresponds to a domain size of $L_x = 800$. In the same manner, the semi analytical results where computed for an infinite domain L_x/η_n. In the present case the slab takes a finite value which is a function of the internal length. As η_n increases less and less periods nucleate on a given domain challenging the hypothesis of large domains.

Remark 11. *These tables are at fix Θ and have η_n vary, consequently ℓ_0 is not constant. A dimensional analysis gives that the parameters are $\Theta, L_x/\eta_n, L_y/\eta_n$. The semi analytical study is run when $L_x/\eta_n \to \infty$ and $L_y/\eta_n \to \infty$. Thus, Tables 4.4 and 4.5 also investigate the impact of the finite size on the domain.*

4.3 From lost of uniqueness to an array of cracks

Here, the process leading to cracks (Fig. 4.1(d)) is shed some light on, this section is purely numerical as no analytical results exist. The description from the bifurcation to a set of parallel initial cracks is given. Their spacing is discussed in the light of the convergence towards Griffith's theory. Although their length is of the same dimension as their width, a continuous set of points have reached $\alpha = 1$ leading to no residual stress, this set of points is called a crack, even if the surrounding points are already heavily damaged. Once again, the material's toughness will not be corrected for the numerical error $\mathsf{G_c}(1 + 3h/8\eta_n)$.

The linearity with respect to the internal length η_n is now extended to the periodicity of cracks. Table 4.6 for a fix value of Θ the number of cracks is inversely proportional to the internal length. However, the *Griffith length* ℓ_0 is not constant even though it is suppose to control the crack evolution. This section investigates this matter.

4.3.1 Construction of the optimal Profile

From a one-dimensonal study [Pham & Marigo 2013] one can construct the entire phase from the bifurcation of the fundamental solution to cracks. Here this is not a continuous evolution. The evolution of a single period is considered (Fig. 4.7) which is the zoom of Figure 4.4 on a single localization zone. Up to time step 79, the fundamental solution is unique and thus at a given depth the solution is homogeneous with respect to x_1.

Is the periodicity that arises sufficiently large such that a crack can develop in each wave ? to answer this question, the periodicity of the bifurcated solution is compared to that necessary for a crack to develop from $\alpha^*(0)$ (Fig. 4.8). At the surface, there is always enough room for a crack to appear, whatever the loading and thus the internal length. As in [Pham & Marigo 2013] a first integral arises and by integration this leads to the width of the localization and to the optimal profile of center $x_1|_0$:

$$|x_1 - x_1|_0| = \eta_n \int_{\alpha^*(0)}^{\alpha(\sigma)} \beta^{-1/2}\, \mathrm{d}\beta, \tag{4.8}$$

from which we deduce the width of a localization and an optimal profile from a state α^*

$$L_c^* = 4\eta_n\sqrt{1-\alpha^*(0)}, \qquad \alpha(x_1,0) = \alpha^*(0) + \left(\sqrt{1-\alpha^*(0)} - \frac{|x_1 - x_1|_0\,|}{\eta_n}\right)^2$$

Whether the loading is severe (and $\alpha^*(0)$ is close to one) or very mild ($\alpha^*(0)$ remains small), by comparing

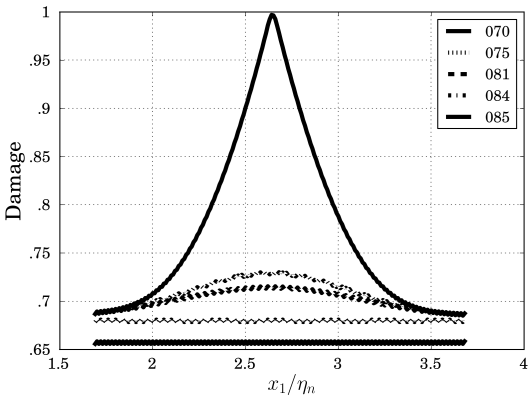

Figure 4.7: Localization process *i.e.* Construction of a crack in the thermal shock problem. At a depth of $2\eta_n$ from the surface for the time steps $\{70, 75, 81, 84, 85\}$.

the periodicity of the bifurcated solution λ_b/η_n to the width of a damage localization $2L_c^*/\eta_n$ we observe that their is always *enough space* (Fig. 4.8).

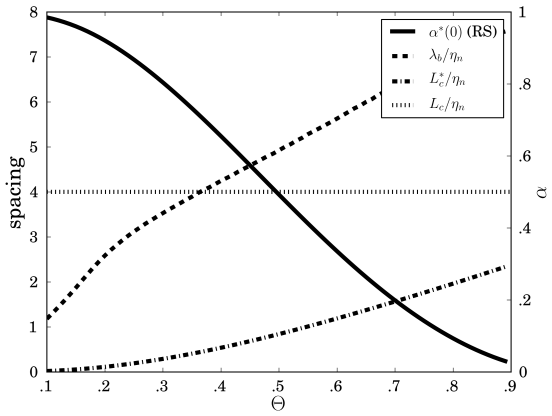

Figure 4.8: Comparison between the bifurcation periodicity and the space $2L_c^*$ to create an optimal profile from $\alpha^*(0)$.

When considering the global picture of the evolution (Fig. 4.9) from the homogeneous damage field to the apparition of cracks ($\alpha = 1$), the evolution is always as follows. The bifurcation happens in one time-step and a periodic solution appears as already described. Then the bifurcated solution evolves, the value of damage increases, and suddenly a crack can form in some periods. As the loading increases, more and more periods switch to cracks. At a given time the cracks that have formed propagate (Fig. 4.1(e)).

But when do these cracks appear ? Table 4.1 reports an estimate of the time between the lost of

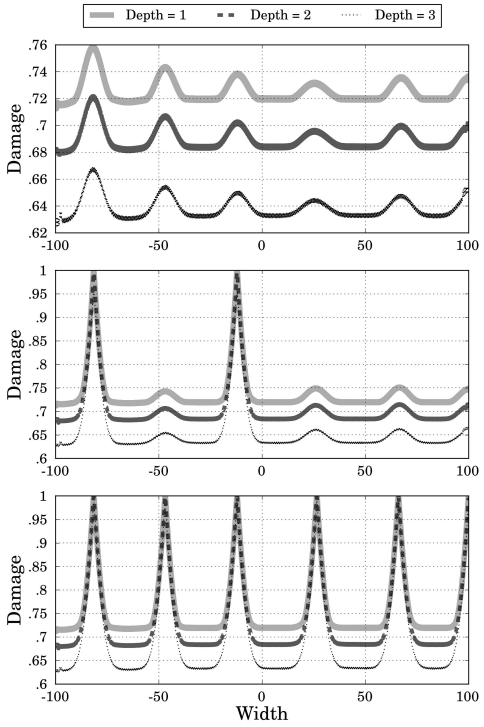

Figure 4.9: Damage evolution for different depth at three non consequential time steps. The depth correspond to $\{.1\eta_n,\ .2\eta_n,\ .3\eta_n\}$.

stability and that where all the cracks are formed step 4.1(d). Once all these cracks are created the last step, which is the propagation or arrest of some cracks will be the subject of Section 4.4. Obviously the growth of all cracks simultaneously together at the beginning, which is the first step of this evolution, depends on the initial length of these cracks.

4.3.2 The initial crack spacing

The fist step of the localization does not guarantee that for each wave, a real crack will appear. Thus the initial periodicity of *real* cracks can not be established. Numerically for $\Theta < .3$ it is observed that it is always possible with a depth of the domain large enough and sufficiently small time steps to initiate a real crack in each wave. As Θ increases less and less waves evolves towards cracks. Let us define the critical loading Θ^* where all localized zone does not become cracks, numerically it seams to lie in the range $.3 < \Theta^* < .5$. For mild loading $\Theta > .5$ cracks do not initiate in each period. No definitive answer is proposed on how many cracks appear. Three interpretations are proposed:

1. the competition between the *Griffith length* ℓ_0 and the internal length η_n (Fig. 4.10),

For severe loading $\Theta = .2$ the penetration of temperature is small in front of the internal length. For milder loading $\Theta = .7$, the penetration of the diffusion and the internal length are of the same order.

2. the length of the initial crack with respect to the penetration of damage at bifurcation D_b (Fig. 4.11).

   For severe loadings, *i.e.* small Θ values the length of the initial cracks are much larger then ℓ_0 Tab. 4.1, where as for less severe thermal shocks the length of initials cracks are of the order of ℓ_0

3. the dissipated energy at the time of bifurcation with respect to the elastic energy.

Griffith global Minimization A very close setting has been studied with Griffith's surface energy using global minimization [Jenkins 2005]. The data is extracted from [Jenkins 2005, Fig. 10], where $L_y/\ell_0 = 16$ which seem to have reached an asymptotic regime from the initial crack spacing as the behavior is the same as for $L_y/\ell_0 = \{10, 12, 14\}$. The length of initial cracks is ℓ_0 and their spacing evolves from $40\,\ell_0$ for the first cracks to $18\,\ell_0$ for the minimal spacing at the surface for times which are respectively $t_c^{gri}/\ell_0^2 = .1$ and $t/\ell_0^2 = .8$. For $\Theta > 1$ and large enough domains cracks appear with no previous damage zone in the case of global minimization. But the alternate minimization algorithm is a local minimization algorithm and thus those solutions are not captured. In comparing local and global minimum it is obvious that the local minimum will always lead to a bifurcation before.

Mesh sensitivity. The non-local damage model is said to mesh independent. However, this statement requires clarification. Bifurcation and stability are sensitive to imperfections and especially those introduced by the mesh. The solution is sensible to the size of the mesh and a thorough analysis of the second Hessian of the total energy in the numerical implementation would be of great interest to understand the bifurcation.

4.3.3 The impact of irreversibility on the nucleation of localized zones

The different solutions given by the alternate minimization according to the implementation of the irreversibility condition are discussed. The numerical observation is that whithout the irreversibility condition the cracks all appear at the same time whereas when the irreversibility is implemented the apparition of cracks is a sequential evolution between t_b and t_{cracks} (Fig. 4.13).

In the case with no irreverisibility, an unloading (Fig. 4.12) of the damage between the cracks is observed. Yet the periodicity is the same. Furthermore in the case of no irreversibility (Fig. 4.13) all the cracks are created in one single time step. The implementation of irreverisiblity on the damage field through a projection for any positive damage value not only for those who have developed a crack is mandatory. Indeed, a too light condition on irreversibility, as would be only considering is for established cracks, is equivalent to its absence. The Back-Tracking algorithm [Bourdin 2007] has no impact on theses simulation as the total energy is always increasing (Fig. 4.13).

η_n	a	λ_b	t_b	D_b	λ_b/η_n	t_b/η_n^2	D_b/η_n
1	6,124	1.96 ± .01	.09 ± .01	2.19	1.9 ± .01	.09 ± .01	2.2
2	4,330	3.52 ± .03	0.19 ± .01	3.93	1.75 ± .015	.05 ± .002	1.97
5	2,739	11.45 ± .33	1.38 ± .05	9.64	2.29 ± .066	.05 ± .002	1.92
7	2,315	12.65 ± 1.60	2.17 ± .1	13.8	1.8 ±.23	.051 ± .002	1.97
10	1,936	36.15 ±3.27	12.13 ± .32	19.51	3.6 ± .32	.12± .003	1.9
10*	1,936	15.34 ±.12	3.97 ± .18	20.14	1.15 ± .01	.04 ± .002	2.01
Semi-Analytical Section 3.5.2					1.53	.21	1.92

Table 4.4: Numerical simulation for different internal lengths. Loading parameters $\Theta = .1$. Slab of dimension L_x=200, L_y=50 $\nu = 0$.

η_n	a	λ_b	t_b	D_b	λ_b/η_n	t_b/η_n^2	D_b/η_n
1	3.062	3.56 ± .03	.13 ± .04	1.85	3.56 ± .03	.13 ± .04	1.85
2	2.165	6.17 ± .1	.38± .01	3.75	3.09 ± .05	.09 ± .003	1.87
5	1.369	17.02 ± .72	2.65 ± .07	9.47	3.40 ± .14	.11 ± .003	1.89
7	1.157	22.4 ± 1.25	5.75 ± .15	13.45	3.2 ± .18	.12 ± .003	1.92
10	0.968	37.33 ± 3.48	12.45 ± .32	19.34	3.73 ± .35	.12 ± .003	1.93
Semi-Analytical Section 3.5.2					3.33	.07	1.77

Table 4.5: Numerical simulation for different numerical length parameters $\Theta = .2$ L_x=200, L_y=50.

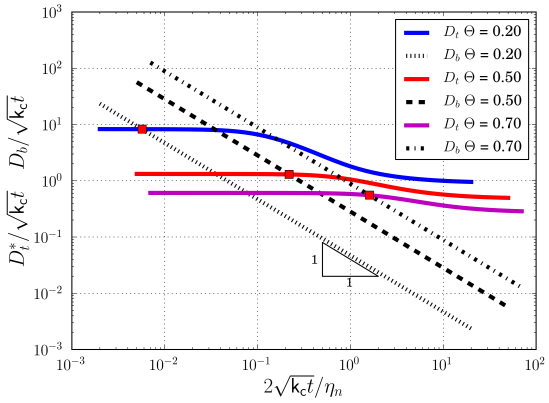

Figure 4.10: Damage penetration rescaled by the diffusion penetration. The penetration of the fundamental damage solution is constant with the penetration of the temperature field. The red dots correspond to the first bifurcation state t_b. For severe loading $\Theta = .2$ the penetration of temperature is small in front of the internal length. For milder loading $\Theta = .7$, the penetration of the diffusion and the internal length are of the same order.

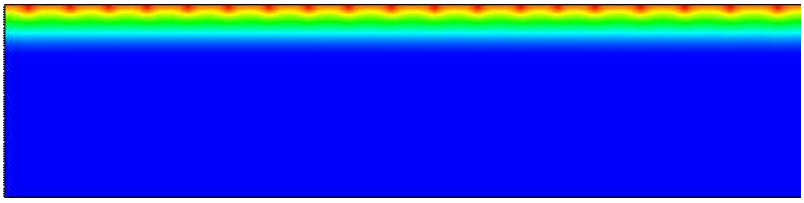

(a) Almost continuously evolution from the bifurcation and thus very short cracks $\Theta = .1$ height $.1\ell_0$

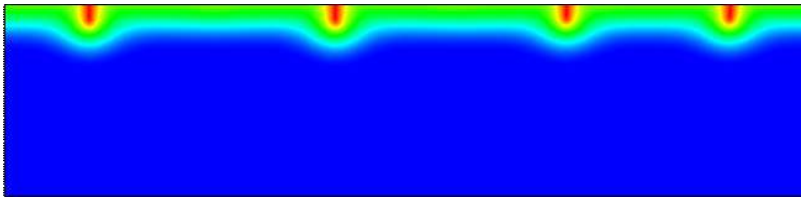

(b) Cracks of the length of the damage band appear $\Theta = .3$ height $1\ell_0$

(c) Cracks longer then the damage band appear, thus necessarily a strong discontinuity in the evolution of the damage field $\Theta = .6.$ height $3.3\ell_0$. On the left of the crack one observes 3 other beginning of localization which have not evolved into cracks

Figure 4.11: Different type of initial cracks. Let us recall that the depth of the damage is a constant for any loading $\Theta < 1$ dimension of the capture $5\eta_n \times 40\eta_n$.

η_n	a	Nb cracks	t_b	t_{cracks}
1	3.062	58	.13	.169
2	2.165	30	0.38	0.671
5	1.369	12	2.65	4.33
7	1.157	8	5.75	8.63
10	0.968	6	12.45	18.84

Table 4.6: Numerical simulation for different numerical length parameters for a constant loading $\Theta = .2$. Domain size L_x=200, L_y=50.

ℓ_0/η_n	t_c^{gri}	Elastic E.	Dissipated E.	Ratio
.0267	1.4	.085	.35	4
.107	.08	0.15	.065	.44
.24	.01	.035	.00035	.009
.427	.005	.005	8e-7	1.7e-4

Table 4.7: Surface and Elastic energy at Griffith time for crack nucleation such that $t_c^{gri}/\ell_0^2 = .1$ depending on the loading.

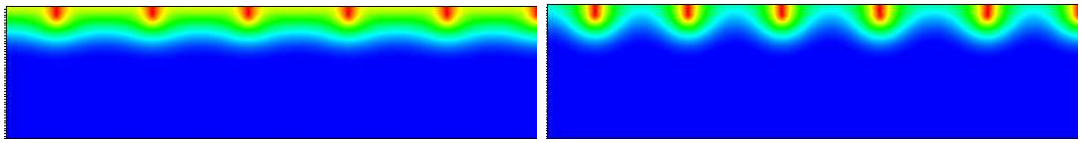

Figure 4.12: Domain size 200×50 $\Theta = .2, \eta_n = 10$ All cracks created. Left no irreversibility, right irreversibility. Note how even if the crack periodicity is the same, damage release appears between the cracks when the irreversibility is not implemented.

4.4 The scale law and comparison with experimental results

When considering domain size large in front of the internal length η_n, the characteristic pattern is the one reproduced in Figure 4.14 for large times. An array of cracks, the spacing of which increases with depth, is observed. This is exactly the same simulation as given in the problem statement (Fig. 4.1) but for a larger domain. Actually considering only the surface of the domain exposed to the thermal shock, Figure 4.14 would give Figure 4.1. In this section, the crack selection mechanism resulting in the arrest of every other crack each time a characteristic period doubles is investigated.

As η_n becomes small in front of all other length in the structure, these damage bands behave like cracks (Chapter 2) for a local minimum. Thus the scale law from [Bahr *et al.* 2010] is expected to be valid. This scale law gives a relation between the crack spacing d as a function of the distance a from the surface (Fig. 4.4).

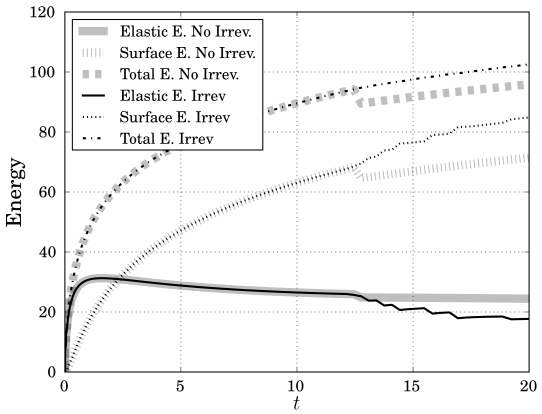

Figure 4.13: Evolution with time (*i.e.* the loading parameter) fd the elastic and dissipated (surface) energy in the case of irreverisibility and no irreversibility $\Theta = .2,\ \eta_n = 10,\ L_x \times L_y = 200 \times 50$.

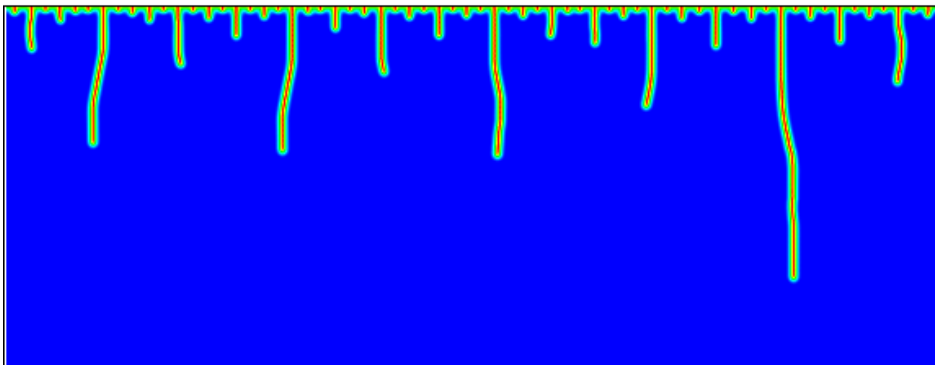

Figure 4.14: Damage distribution obtained at a large time. The spacing increases with the depth

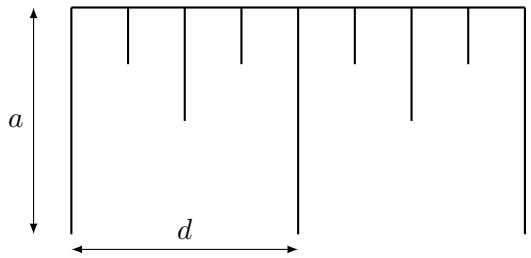

Figure 4.15: Spacing between crack d at a given depth a. Assuming that the cracks are straight orthogonal to the surface and equally spaced.

The experiments considered are thin slabs which are heated before being quenched into water. The states of the cracks at the end of the diffusion process is studied. Many slabs are put together such that heat only diffuses by the small faces. A complete description of the experimental set up can be found in

[Bahr *et al.* 1986, Jiang *et al.* 2012]. The two dimensional hypothesis will be challenged in the following section. All material parameters come from the published papers and the data sets from the experiments, giving the spacing as a function of the distance from the surface, have directly been communicated by the authors.

4.4.1 A first experimental set

The slab considered is 5 mm$\times$10 mm$\times$60 mm. The material parameters are $K_{Ic} = 1.89$ MPa.$\sqrt{\text{m}}$, $\mathsf{a} = 1.15 \times 10^{-5}$ and $\mathsf{E} = 60$ GPa. Thus from Irwin formula and taking $\nu = .22$ one deduces $\mathsf{G_c} = 57.5$ J.m^{-2}. No reference have been found, for a specific critical stress σ_c for this material. Thus, from the observation of [Bahr *et al.* 1986] that states the existence of a critical temperature between $154°K$ and $159°K$, which we associate to the parameter loading $\Theta = 1$, from which is deduced that $\sigma_c = 110$ MPa and thus $\eta_n = .11$

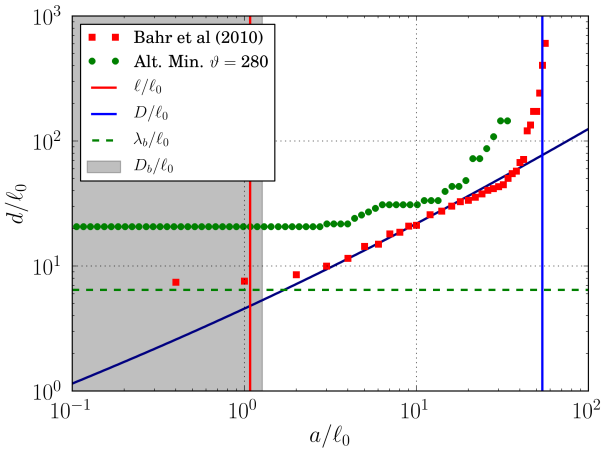

Figure 4.16: Scale law: Spacing between cracks d as a function of the distance a from the exposed surface (square experiments and circle simulation). Horizontal green line initial periodicity λ_b predicted in Chapter 3. Vertical lines: in red the internal length η_n, in blue D the depth of the slab. Full black line scale law from [Bahr *et al.* 2010]. The relevant dimensionless number is ℓ_0.

These results show room for improvement, especially because we have no guarantee that the same material is used in [Bahr *et al.* 1986] and [Bahr *et al.* 2010]. Let us turn towards a more complete data set.

4.4.2 Confrontation with experimental results from [Shao *et al.* 2011] on ceramics

This section is devoted to the study of an entire thermal shock problem. Comparing with the scale law from [Bahr *et al.* 2010] and using experiments partially reported in [Shao *et al.* 2011]. This numerical simulations has to goal of looking at three phases: (i) nucleation (ii) scale law (iii) crack arrest in a specific

case.

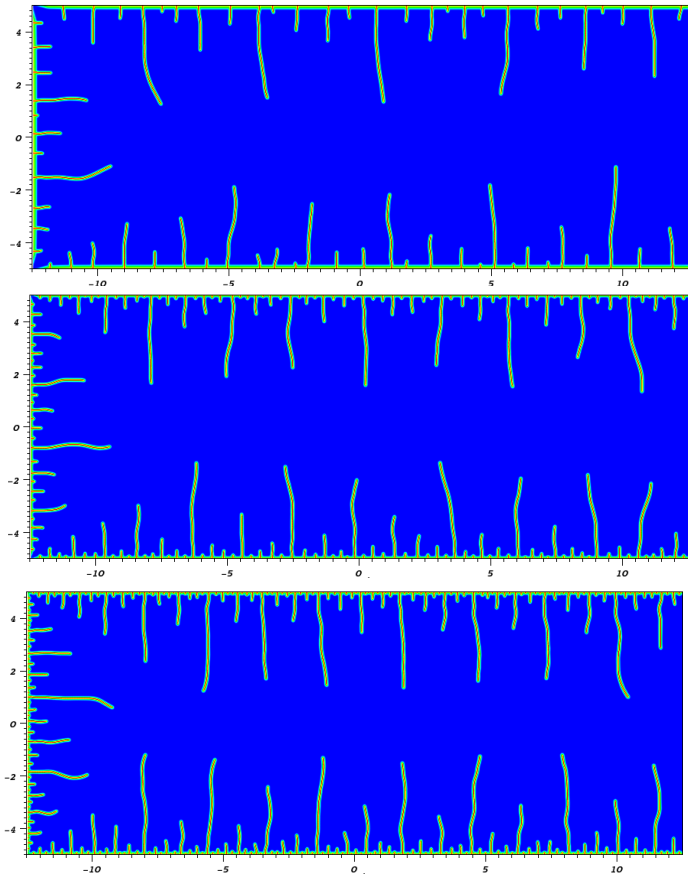

Figure 4.17: Half domain size corresponding to that experiments in [Shao *et al.* 2011] for temperatures $\vartheta = \{280, 380, 580\}$. S.I. unit is used except length that are in [mm].

In the numerical simulations, half a slab is considered (Domain size 10 mm $\times$ 25 mm). The material parameters $\mathsf{E} = 340$ GPa, $\mathsf{G_c} = 42.47$ J.m^{-2}, $\sigma_c = 342.4$ MPa (and also $\nu = .22$), give, using an internal length[2] $\eta_n = 46\mu$m. Which leads to the loading parameters from Table 4.8. Here from the couple $(\mathsf{G_c}, \sigma_c)$ as material parameter, the value of η_n is computed which is then used as material parameter for the numerical computation. Thus the mesh size is fixed at $h = .01$ mm, ensuring $h/\eta_n = 5$. Leading to a mesh with 5×10^6 elements and thus 20×10^6 degree of freedom (d.o.f.). The simulation are runned on half the test specimen and the boundary conditions $u_x = 0, \partial\alpha/\partial n = 0, \sigma_{12} = 0$ are enforced. The other boundaries are left free in displacement and damage. The intensivity of the thermal shock and the Griffith length are reported in Table 4.8.

The diffusion is simplified with respect to the modeling part of [Shao *et al.* 2011], as the material

[2]From [Shao *et al.* 2011] the limit temperature would be identified as $\vartheta = 230$ (thus $\ell_0 = 0.036895$ mm) which gives an internal length $\eta_n = 0.098$ mm

ϑ	Θ	$\ell_0\,[\mu m]$
280	0.4492	24.89
380	0.3308	13.51
580	0.2167	5.80

Table 4.8: Value of the loading parameters Θ and ℓ_0 corresponding to the experience from [Shao *et al.* 2011].

constant are assumed not to depend on the temperature. Solving the heat equation $\frac{\partial \mathrm{T}}{\partial t} - \mathsf{k_c}\frac{\partial^2 \mathrm{T}}{\partial \mathbf{x}^2} = 0$ with $\mathsf{k_c} = k/(\rho c_p)$ is the thermal diffusivity $[m^2/s]$. The thermal expansion coefficient is chosen constant to $\mathsf{a} = 8 \times 10^{-6}$ corresponding to a temperature of $600\,^\circ K$ in [Shao *et al.* 2011].

Figure 4.17 reports the final network of damage bands at the end of the simulation on the entire domain for different temperatures. As already mentioned no hypothesis on the crack set are made. Thus in the center part of the specimen, where the heat equation is unidirectional, the parallel array of cracks as in Figure 4.14 is a result of the minimization process. The number of cracks is computed for 100 depth points distributed on a log space on the upper side of the computation.

Figure 4.18 reports the comparison, in the thermal shock problem on ceramics, between experimental measures and the numerical simulation with alternate minimization algorithm. The first depth experimentally measured is well beyond the *damage zone* predicted from Chapter 3. For different loading, despite the simplification in the thermal process (heat equation and linear shrinkage), very good agreement is found.

In the center part of the domain the linear regressions of the simulations and the experimental data are compared

$$\log\left(\frac{d}{\ell_0}\right) = A \log\left(\frac{a}{\ell_0}\right) + B,$$

which quantify the impressive results for different loadings.

	Experiment		A.M.	
ϑ	A	B	A	B
280	.83	.61	.75	.67
380	.63	.90	.69	.79
580	.58	1.11	.68	.81

Table 4.9: Regression on the experimental and computed spacing as a function of the penetration in the crack selection regime.

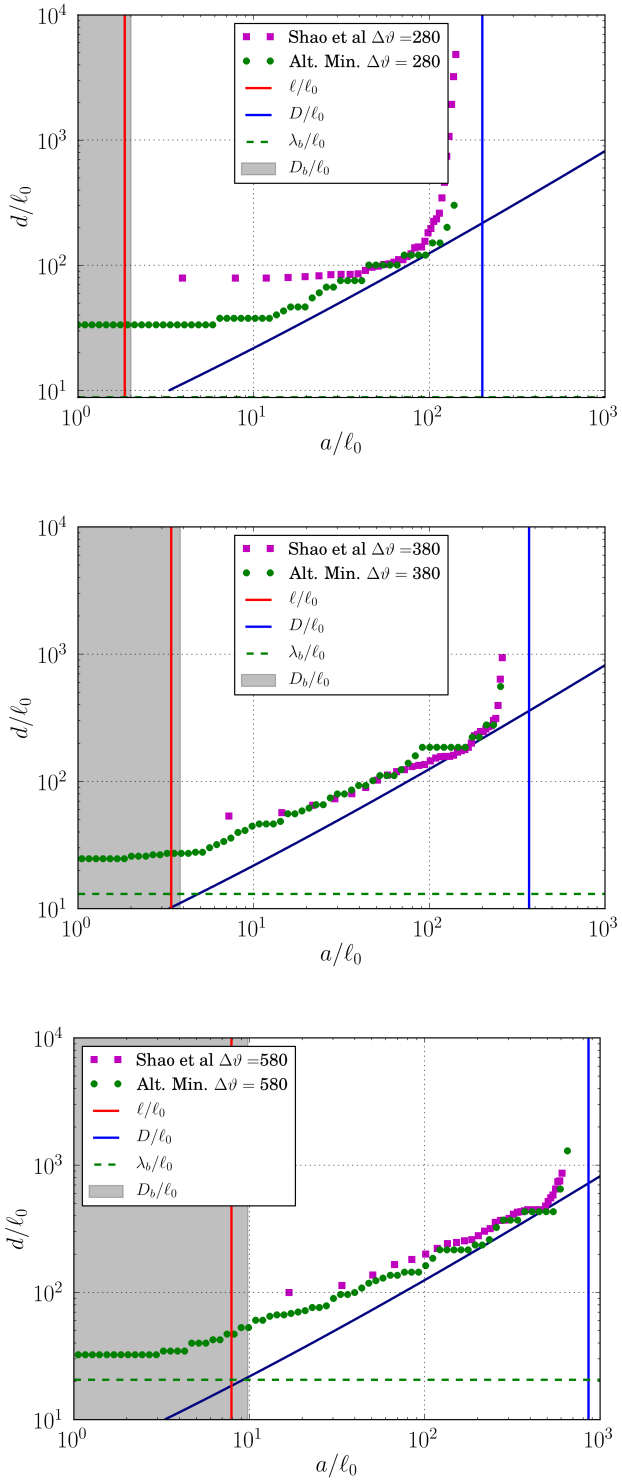

Figure 4.18: Scale law: Spacing between cracks d as a function of the distance a from the exposed surface (square experiments and circle simulation). Horizontal green line initial periodicity λ_b predicted in Chapter 3. Vertical lines: in red the internal length η_n, in blue $D = L_y/2$, the half of the depth of the slab. Full black line scale law from [Bahr *et al.* 2010]. The relevant dimensionless number is ℓ_0.

4.5 Three-dimensional numerical simulations

4.5.1 The scale-law on large domains

In three dimensions (Fig. 4.19) more complex morphology appear. Especially, hexagons of width increases when penetrating in the material are observed. In three-dimensions, it is not possible to perform full-domain numerical experiments while resolving the material's internal length for anything but the smallest structures. In order to study scaling properties of three-dimensional crack pattern, we considered an semi-infinite domain $\{z \geq 0\}$ subject to a thermal shock on the face $\{z = 0\}$. The elastic properties and experimental settings are the same as in the two-dimensional experiments of Section 4.4.2. A series of numerical experiments were performed on subdomains $(-L/2, L/2) \times (-L/2, L/2) \times (0, L)$, for increasing values of L from 2mm to 2m. Null normal displacement on all lateral and the upper faces was prescribed.

The number of elements in the mesh was kept constant by setting the critical size of the elements $h = L/200$, and an internal length to $\eta_n = 5h$. For $L = 2$mm, we get $\eta_n = 5e-2$, matching the considered material's internal length, and allowing us to capture crack nucleation. For larger domains, we do not claim to be able to capture the initial onset of fracture, but following the rationale developed in the two-dimensional case and validated in Figure 4.18, we claim that the selection mechanism is properly accounted for. The outcome of this series of simulation is shown in Figure 4.19 where the crack patter is highlighted by taking the isovolume $\alpha \geq .95$. The temperature field is projected on these surfaces representing the cracks.

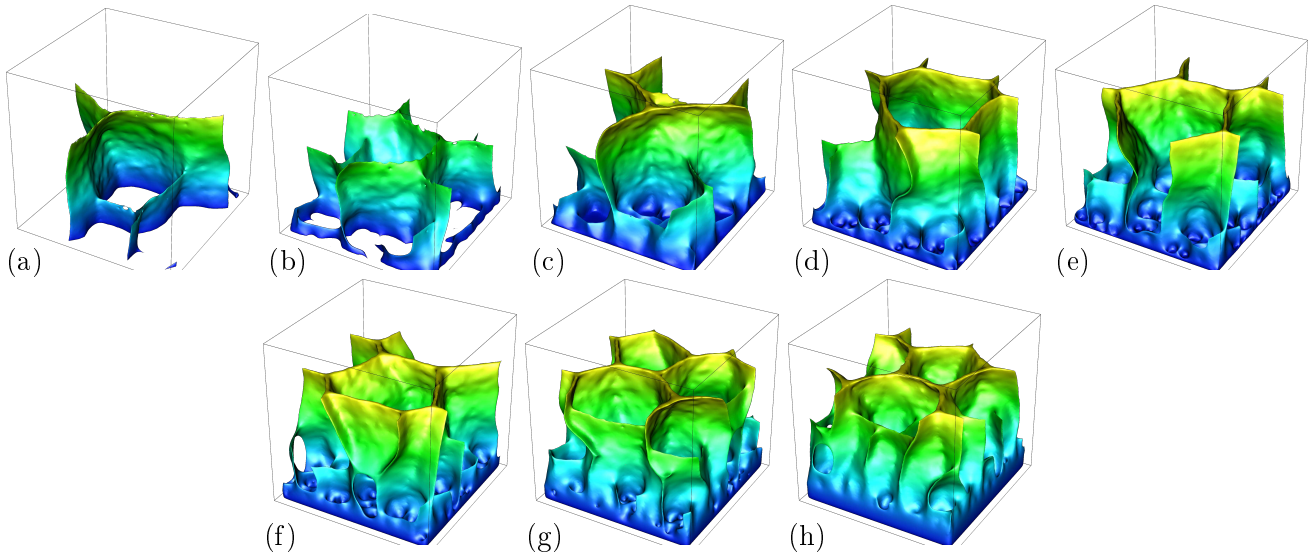

Figure 4.19: Three-dimensional crack patterns for domains with edge length (a) 2mm; (b) 10mm; (c) 20mm; (d) 40mm; (e) 63.2mm; (f) 200mm; (g) 632mm; (h)2m. [Bourdin *et al.* 2013].

Boundary effects for deep cracks are filtered out by showing the crack pattern only for $z \leq .75L$. The fracture patterns delimit polygonal cells, and a coarsening phenomenon similar to that of the two-

dimensional case is observed. Figure 4.19 is obtained by measuring the average cross-sectional area of the cells as a function of the penetration depth in numerical simulations. As in the two-dimensional case, the solid line is the scaling law from [Bahr *et al.* 2010]. In the Griffith regime (that is for crack size much larger than the material's internal length), our numerical simulations follow closely the two-dimensional scaling law, for a range of domain sizes spanning three orders of magnitude.

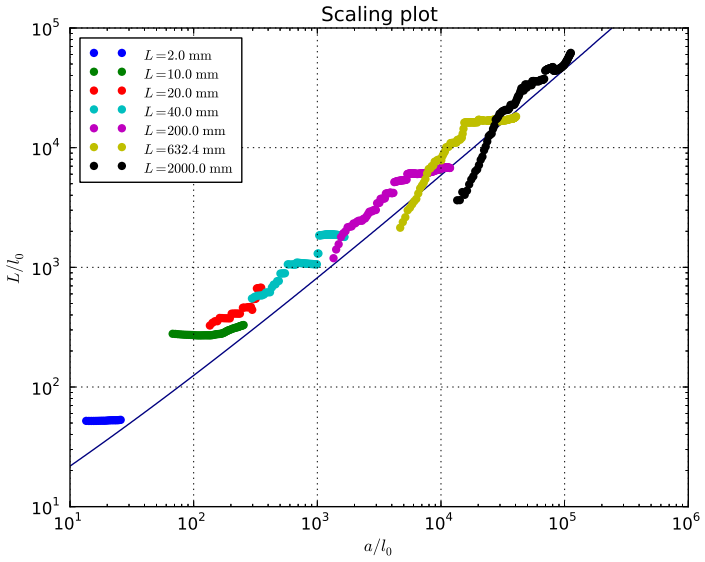

Figure 4.20: Scale law in the 3 dimensional case: Scale of the hexagons with respect to the penetration

4.5.2 Three-dimensional effects in thin slabs and transition to transverse cracks

In the case of simulations of width 1 mm two dimensional effects whereas 5 mm three dimensional effects (Fig. 4.21) appear. This correspond to the observations made in [Shao *et al.* 2010] for domains of width 5 mm and [Shao *et al.* 2011] for domains of 1 mm. In this sens these computation validate the hypothesis of a two dimensional in plane stress although the with of 1 mm is $20\eta_n$.

A second series of numerical simulations attempts at providing quantitative validation of our approach and its ability to capture complex fracture patterns by focusing on the transition from two-dimensional to three-dimensional crack patterns. Experiments suggest that for identical materials and environmental parameters, the sample can have a strong influence on the crack patterns at onset.

For "thin" domains, the solution is essentially two-dimensional while for domain of thickness comparable or larger than the initial crack spacing, three-dimensional polygonal crack patterns arise (compare for instance the crack patterns from Figure 7 in [Shao *et al.* 2011] to that of Figure 2 in [Shao *et al.* 2010].) In all cases, the domain is long enough and the cracks short enough in relation to the domain size to avoid boundary effects potentially arising from computations on a subdomain.

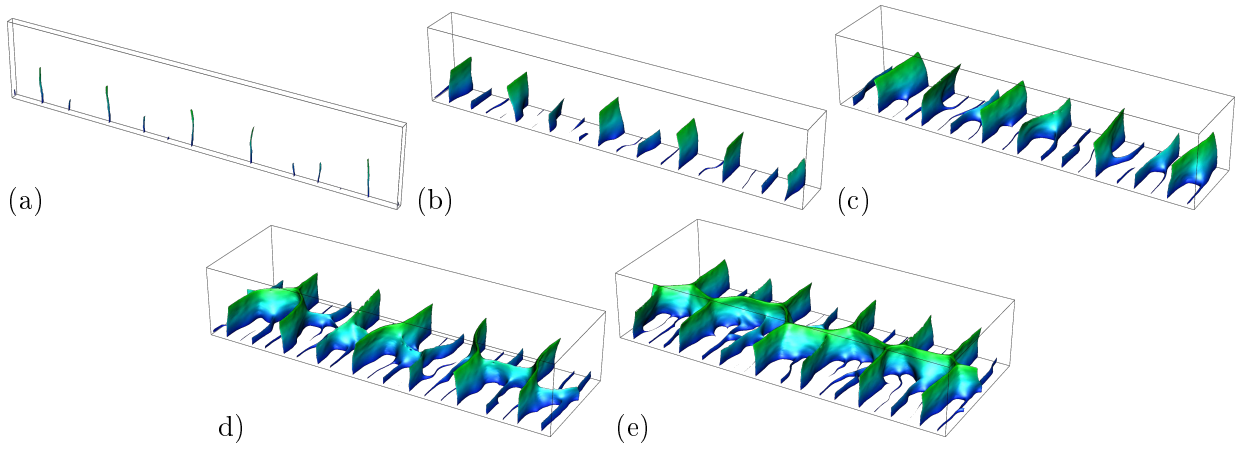

Figure 4.21: Three-dimensional version of the experiment from Figure 4.17(b) performed on a subset of dimension 5mm $\times$ L $\times$ 5mm of the full domain for L_y = (a) .1mm; (b) .5mm; (c) 1mm; (d) 1.5mm; (e) 2mm. [Bourdin *et al.* 2013]

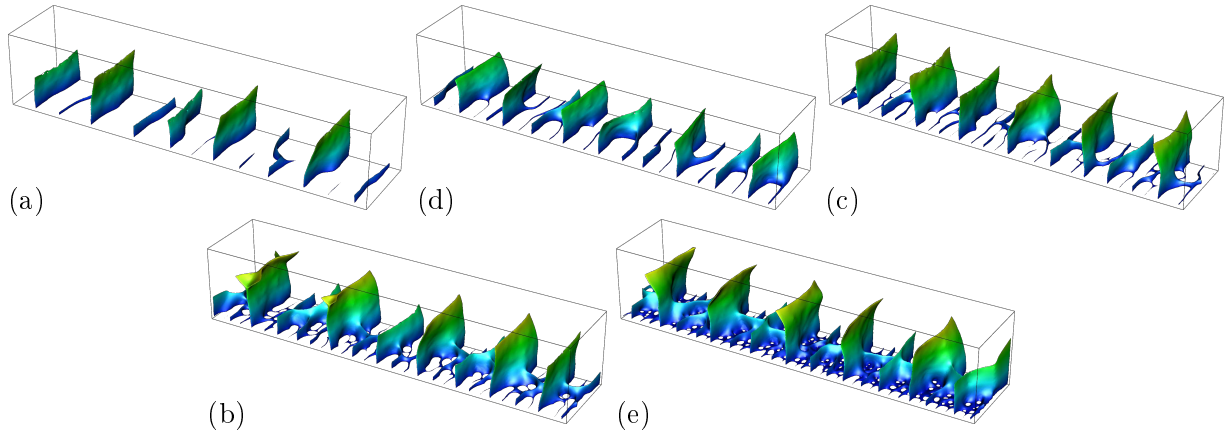

Figure 4.22: Three-dimensional version of the experiment from Figure 4.17 performed on a subset of dimension 5mm $\times$ 1mm $\times$ 5mm of the full domain for a temperature contrast (a) $280°C$; (b) $380°C$; (c) $480°C$; (d) $580°C$; (e) $680°C$. [Bourdin *et al.* 2013]

Finally, we focus on the two to three-dimensional crack transition as a function of the shock intensity. A careful look at Figure 5 in [Shao *et al.* 2011] suggests that for temperature contrasts below $380°C$, only transverse cracks are observed, that for $\vartheta = 580°C$, some three dimensional artifacts are observed, while for $\vartheta = 680°C$, full three-dimensional patterns are observed from the onset. Again, our numerical simulations matches experimental observations: for $\vartheta = 280°C$ and $\vartheta = 380°C$, cracks are essentially transverse. For $\vartheta = 480°C$, $\vartheta = 580°C$, some three-dimensional effects arise while for $\vartheta = 680°C$ full three-dimensional patterns are observed from the onset. Note that when they appear three-dimensional effects are limited to a shallow layer past which cracks become transverse.

4.6 Application to gas storage cavern

This work has initiated following question from the geo-mechanical group at LMS.

4.6.1 Moss Bluff cavern, general overview

A cavern initially filled with gas is considered, due to an accident or to normal running operation a drop of pressure occurs in the cavern. This drop of pressure induces a drop of temperature $\mathrm{T}_{\mathrm{drop}}$ in the cavern, eventually after the initial drop the temperature raises back to the initial temperature. Before, the gas release the salt is at an initial stress state at which one must add the effects of temperature variation in the well. They can be estimated by assuming that they are applied "instantaneously" and that the viscoelastic flow that follows has not time to propagate. This is a rough assumption, especially for the well, but which give the orders of magnitude. The viscoelastic behavior of brittle solids has been studied analytically in [Nguyen *et al.* 2013] and applied to sedimentary rocks. In any case the mechanical effect of the change of pressure in the gas in the cavern is neglected.

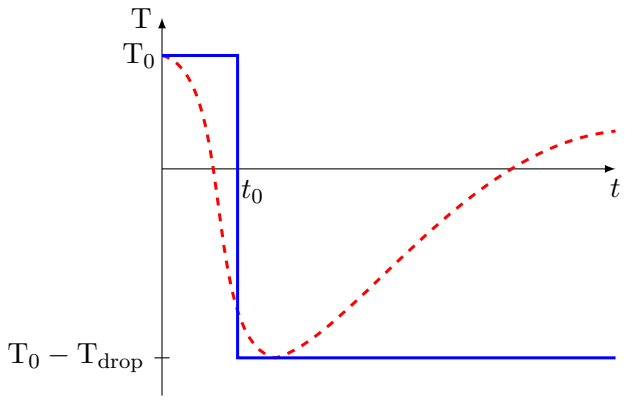

Figure 4.23: The temperature drop and thermal loading. Dashed-Red: profile of the real temperature [Bérest *et al.* 2013]. Blue: approximation with a thermal shock used in Section 4.6.2.

The material constitutive of the cavern is modelized by an homogeneous brittle material. The material properties are given in Table 4.10 and are those of the salt. The measured elastic moduli of natural rock salt from ten different locations in the US [Hansen *et al.* 1984] where mean values were found to be in the $24-32\,\mathrm{GPa}$ range. The material's toughness is computed from the critical stress intensity factor K_{Ic} varying between $8-25\,\mathrm{MPa.mm}^{-1/2}$ found in [Guosheng 1998]. Using Irwin's formula $\mathsf{G_c} = (1-\nu)^2 K_{Ic}^2/\mathsf{E}$ we determine the materials toughness varies between 2.4 $\mathrm{J.m}^{-2}$ and $23.4\,\mathrm{J.m}^{-2}$. The materials length η is given by (1.30) and will be discussed in the following section. Finally, its thermal diffusivity $\mathsf{k_c}$ is determined from a thermal conductivity of 6 $\mathrm{W.m}^{-1}.\mathrm{K}^{-1}$, a heat capacity of 921 $\mathrm{J.kg}^{-1}.\mathrm{K}^{-1}$ and a density of 2.19.

The cavern is supposed to be a cylinder whose cross section is the domain Ω (Fig. 4.24) the surface

E	ν	a	G_c	σ_c	η	k_c
25 GPa	.25	4.10^{-5}	$15\,J.m^{-2}$	1.35 MPa	.1 m	$1.76.10^{-6}m^2.s^{-1}$

Table 4.10: Average material parameters of the elasto-damageable salt constitutive of the cavern.

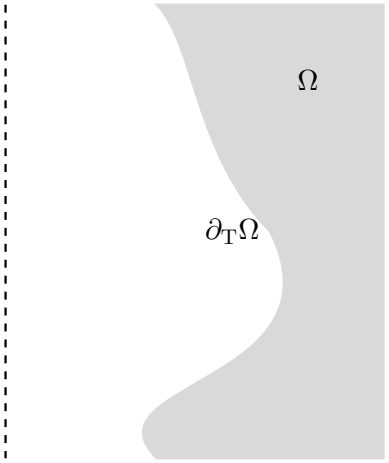

Figure 4.24: Schematic representation of a cavern: axis of revolution (Dashed line), the salt formation Ω (gray zone) and Rock wall $\partial_T\Omega$.

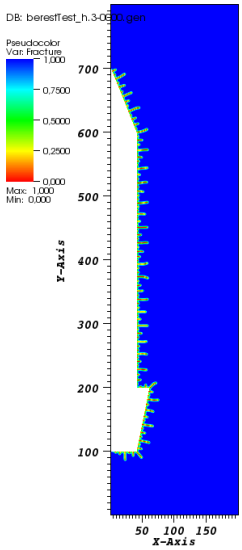

Figure 4.25: Representation of the Moss Bluff cavern at a damage state. Blue sound material. Red damage state with $\eta = 1.5$ m.

$\partial_T\Omega$ (*i.e.* the cavity wall) is exposed to the thermal shock. All boundaries are left stress free. The thermal loading imposes an linear shrinkage $\boldsymbol{\varepsilon}^{\text{th}} = a(T(\mathbf{x},t) - T_0)$ and we assume that the thermal diffusivity is independent of the materials states, thus the temperature field is solution of the heat equation

$$\frac{\partial T}{\partial t}(\mathbf{x},t) - k_c \Delta T(\mathbf{x},t) = 0 \quad \forall \mathbf{x} \in \Omega$$

with the boundary condition $T = T_0 - T_{\text{drop}}$ on the surface of the cavern $\partial_T\Omega$ and the initial condition $T(\mathbf{x},0) = T_0 \, \forall \mathbf{x} \in \Omega$. The thermal diffusivity is assumed to be constant in the entire material and independent of the temperature and the crack state.

The operating engineer is interested in the following questions: Will the fractures be arrested at a certain distance from the cavity wall ? Will the cavity be stable in spite of the fracture formation ? We are concerned with assessing the risk of cracking during the Moss Bluff accident [Bérest *et al.* 2013]. The cavern of height 700 m and of radius varying between 20 m and 40 m is filled with gas. Its total capacity is 1.291.766 m^3. The profile of $\partial_T\Omega$ is the average profile based on 4 orthogonal measures of the circumference made of 2800 points. The domain Ω is carved in a the domain $[0, 150] \times [-720, -1250]$ where the point $(0, 0)$ is taken as the point of the axis of revolution situated at the see level.

Temperature evolution in the cavity: The change of temperature can be precisely computed in [Bérest *et al.* 2013] where simplified state equations (ideal gas and Van der Waals gas) to allow getting closed-form solutions of the blow-out problem. These solutions are applied to the cases of compressed air storage and hydrogen storage in salt caverns. The minimal temperature is reached after 2 days and comes back to a normal temperature after 7 days. The drop in temperature is of $78°C$.

Initial state around the cavity: Around the well, before the blow, exists an initial stress field. Near the surface, the vertical stress component is dominant and takes value close to 20 MPa. As $\mathsf{Ea}/(1-\nu) = 1.33$ MPa.K^{-1}, As an approximation, we run a simulation with no initial stress but simulate a drop of temperature $20°C$ lower then the actual $\mathrm{T}_{\mathrm{drop}}$.

A computation on the entire cavern (Figure 4.25) is not realistic because of the internal length η is very small in front of the size of the structure. With an overestimated internal length, we see that the cavern can be study a cross section at a time. Thus we will restrict our analysis to the bottom part of the cavern to use the real material parameters.

4.6.2 Crack nucleation and propagation in Moss Bluff blow out

From Figure 4.25, cracks do not seem to propagate in a privileged region of the salt foundations, although the geometry induces stress singularities. Thus in the sequel, the computation will be restricted to a slice of the cavern. On the top and bottom of the domain normal displacement are blocked $u_y = 0$ and shear stress are assumed to vanish. Near the surface $\partial_{\mathrm{T}}\Omega$, up to a distance of 45 from the revolution axis the mesh is set to $h = .03$ the size of the mesh is then increases up to 5. Near the surface $\partial_{\mathrm{T}}\Omega$, we need a refined mesh as to approximate properly the energy dissipated one must respect the characteristic size of the mesh is small in front of η. Typically $h/\eta = 5$ allows the surface energy density to well approximate the materials toughness while minimizing the computation cost. Thus the computation are performed on meshes of 14 millions elements leading to 31 millions degrees of freedom (2 for displacement and 1 for damage field at each node). Furthermore, an unstructured mesh is used such that no favored direction be introduced and to avoid overestimating the energy [Negri 1999].

The goal is to quantify up to which depth the cavern can be damaged to evaluate the potential volume variation. In this case we consider the short time behavior for the total blast, the amplitude of the thermal shock is [Bérest *et al.* 2013]

$$\mathrm{T}_{\mathrm{drop}} = 78°C \qquad \mathrm{T}^{\mathrm{n}}_{\mathrm{drop}} = 58°C\,.$$

The damage state at 3 different dates after the beginning of the loading is reported in Figure 4.26. At the beginning a totally damage zone diffuses in the bulk of the material (Fig. 4.26(a)). This zone has no residual consistence and would lead to a disintegration of the rock wall. Then after a certain time (a little more than a day) cracks nucleate (Fig. 4.26(b)). These cracks progressively penetrate the bulk of the salt formation. Then around the third day, a periodic array of cracks is created. The periodicity arises despite the roughness of the surface and despite the initially totally damage zone. This property is noteworthy. Let us stress once again that we have made no assumption on the topology of cracks. Thus the evolution

principle, automatically selects the localization into cracks.

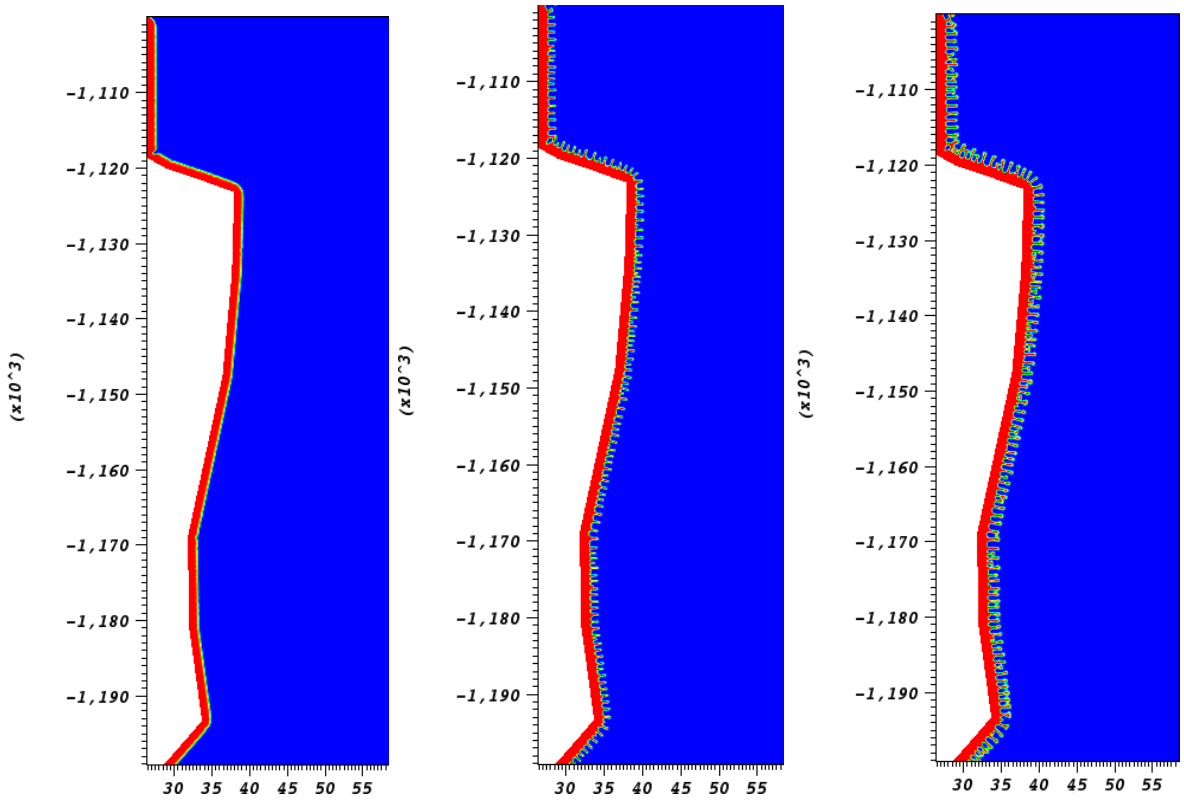

(a) 1 day (b) 3 days (c) 7 days

Figure 4.26: Damage field after a thermal shock as in the Moss Bluff cavern. Very Severe blow up $\mathrm{T}_{\mathrm{drop}} = 78°C$ on 7 days. Blue sound material point $\alpha(\mathbf{x}) = 0$, Red totally damage point $\alpha(\mathbf{x}) = 1$. Distance in meters.

Thus we observe that during the first day (Fig. 4.26(a)), a zone of depth 40 cm totally damaged is created all along $\partial_{\mathrm{T}}\Omega$. The consequence is that in this zone could lead to the fall of rocks of volume $2\pi \times 30\mathrm{m} \times 700\mathrm{m} \times 40\mathrm{cm}$. ($52000\mathrm{m}^3$) which is 4 percent of the cavern. The crack spacing, for the current loading is of no specific interest as the loading is very severe, except that its existence confirms that a disintegrate zone will always localize into a set of cracks. We are now interested in the evolution of this array on a longer period, which is the concern of the following section.

The same analysis is reproduced but for an amplitude of the thermal shock of $\mathrm{T}_{\mathrm{drop}} = 40$ and over on a period of 6 months. This temperature drop is more realistic over a "long" period. Thus the loading is given by

$$\mathrm{T}_{\mathrm{drop}} = 40°C \qquad \mathrm{T}^{\mathrm{n}}_{\mathrm{drop}} = 20°C\,.$$

The goal is primely to determine how far and with which spacing the cracks propagate. The length of crack increases as time goes by (Fig. 4.27). Unlike, for the severe loading, cracks nucleate periodically at

the surface. After 3 days, one can observe a set of periodically cracks of the order of the meter. After 7 days, only every other cracks has continued its propagation. This crack arrest and period doubling continues over the six first months.

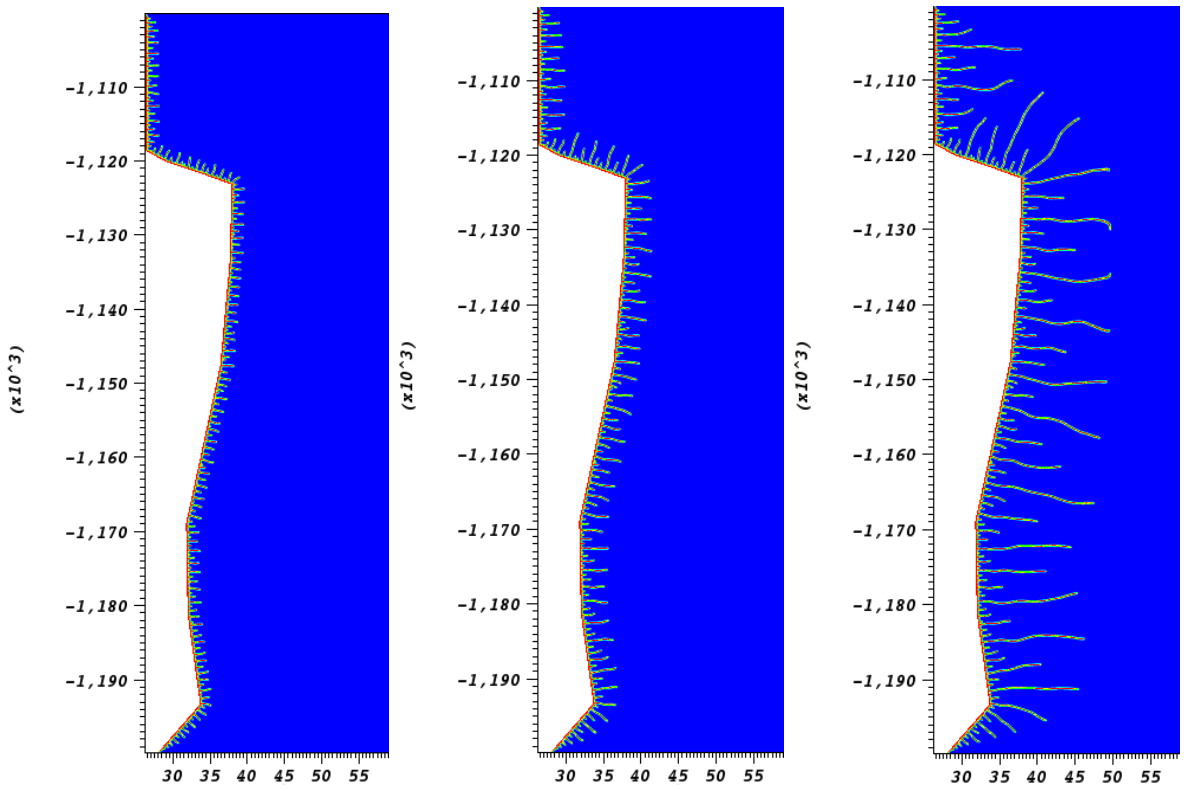

(a) 3 days (b) 7 days (c) 6 months

Figure 4.27: Damage field after a long exposure to a thermal field $\mathrm{T}_{\mathrm{drop}} = 40°C$. Evolution on a long period. Blue sound material point $\alpha(\mathbf{x}) = 0$, Red totally damage point $\alpha(\mathbf{x}) = 1$.

The crack spacing as a function of the average depth is reported in Figure 4.28, where ℓ_0 is a length characterizing the intensity of the loading. In the case of a half-plane, [Bahr *et al.* 2010] have predicted the crack spacing of a parallel array of cracks following Griffith's law. Thus, when considering the entire range of -1130 m to -1190 m below the see level, the relation between the penetration and the crack spacing follows the scale law from Griffith's theory. The geometry has very little influence on the position and spacing of cracks. Albeit the surface of the rock wall is not regular, the global picture is a parallel array of cracks. If we were to add a few heterogeneities, these would not modify the global picture, albeit some individuals cracks would follow a different path.

The results of Figure 4.27 shows little influence of the geometry of the cavern on the crack pattern. This allows to use the results from a thermal shock on a semi infinite slab.

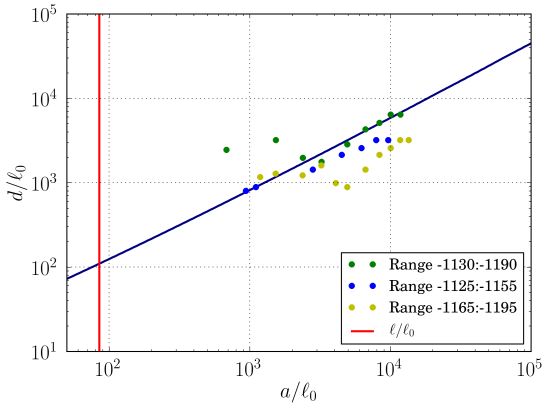

Figure 4.28: Crack spacing d as a function of the distance a from the average of the radius of the rock face for 3 different ranges from the see level. Blue diagonal scale law from [Bahr *et al.* 2010]. The red vertical fixes the scale of the internal length of the material.

	Θ	ℓ_0
$T^n_{drop} = 58°C$	.023	.11 mm
$T^n_{drop} = 20°C$	.068	.94 mm

Table 4.11: Loading parameters for two different temperatures based on the material parameters of Table 4.10.

4.6.3 Conclusion on the Moss Bluff Application

On the one hand, we have performed a simplified analysis especially: (i) the behavior of the material has been considered rate independent and thus the viscoelastic nature of the material has been neglected, (ii) the initial pre-stress of the material has only been taken into account through a change of the loading (iii) We have considered two simplified temperature profile, compared with the real profile (Fig. 4.23), with respectively a drop of temperature $T_{drop} = 60°C$ and $T_{drop} = 40°C$; (iv) The initial temperature field is assumed to be constant and at the temperature of the gas before the blow. On the other hand, the damage model used is very versatile. The identification of material parameters of the model is given from (1.30) and is thus very simple from quantities well know in fracture mechanics, the Young modulus, the toughness and the critical stress. Furthermore, this work benefits from the theoretical work on thermal shock setting done in the previous chapter.

However, these assumptions do not reassess the main conclusions. Thus the damage based fracture model allows to capture the topology of the crack setting. Although, notches and angles are Thus the geometry of the cavern plays a small role in front of the intensity of the thermal loading. The consequence is that when cracks propagate, the simplifies approach [Bahr *et al.* 2010] related the spacing of cracks as a function of their penetration: (i) If the thermal shock is extremely severe, the rock wall is totally damaged;

(ii) at a given time (or penetration) the gradient damage model always structures it self in bands which are the regularized version of cracks; (iii) These cracks propagates in the bulk of the material as long as the temperature drop propagates; (iv) as the cracks penetrate, their spacing increases, and they follow the scale law from Griffith's theory.

Thereby, very fine results can be established at a high computation cost. Perspectives are to consider real evolutions in temperature as well as precise initials stress states and the viscoelastic flow. This application also exhibit that the analysis in the case of half domains remains highly relevant, and thus those theoretical and analytical results can be used in many gas storage caverns submitted to a rapid change is temperature.

4.7 Application to non homogeneous materials

Many materials are not homogeneous, it is especially the case of concrete. Let us consider a simple composite material: a brittle phase in which are enclosed elastic inclusions. This specific case deserves to be studied in depth, yet here the previous results will merely be applied. In which sens the heterogeneities change the results ?

The inclusion do not participate to the transport. It easily conceivable for drying for example with glass inclusions in a cement paste [Bisschop & Van Mier 2002b, Bisschop & Van Mier 2002a, Bisschop 2002]. The inclusions and the matrix have the same rigidity $\mathsf{E} = 1$ and Poisson ratio $\nu = .2$. Considering fix positions of inclusion, but increasing their radius (Fig. 4.29) as their size increase the influence is greater. Here not only does the size of the inclusion change but also the ratio between inclusion and matrix. We try to separate both factor.

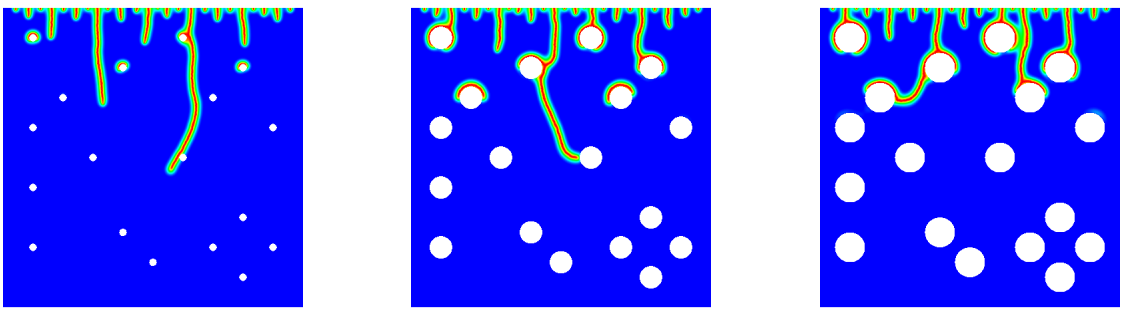

Figure 4.29: Drying in non homogeneous materials: Position of inclusions fix, radius increasing.

The inclusions are of radius r and the ratio of the surface of inclusions on the total surface is ϕ. The internal length of the material is kept constant $\eta_n = .5$ and is thus smaller (but of the same order)

as the inclusions[3]. Thus the size and the ratio have an impact on the damage properties (Fig. 4.32). Quantitatively, smaller inclusions tend to locate the damage on the surface, and this damage remains very diffuse, the localization into damage bands does not necessarily happen. For larger inclusions the array of cracks remains. The cracks are more or less parallel. The impact of the ratio is a expected, the amount of damage increases with the ratio of inclusions as the stress increases. This has a impact on the maximum penetration of cracks. These results are at the same drying time and more precise results as in [Bisschop 2002] related to the mass loss should be sought for.

For the considered loading, in the homogeneous case, all the localization develop into cracks. We consider one quantitative result, comparing the crack spacing at the surface as a function of the size of the inclusion and the ratio ϕ (Table 4.12). The deviation with the homogeneous case remain below 20 percents.

radius	.2	.3	.4
1	1.98	2.17	1.66
3	1.97	2.02	2.03

Table 4.12: Initial spacing of cracks for $\Theta = .2$ for different inclusion ratio to be compared with a $\lambda_b/\eta_n = 3.7$ (*i.e.* $\lambda_b = 1.85$ for $\eta_n * .5$) in the case of a homogeneous material (Tab. 4.1).

Conclusion

Nucleation of complex cracks morphology is still a difficult task. The ability of the numerical implementation of the variational approach to fracture to initiate a parallel sets of cracks has been illustrated. Theses numerical results are confronted to two semi-analytical results: the localized damage solution detailed in Chapter 3 and the scale law from [Bahr *et al.* 2010]. These two bounds give us some confidence in the numerical results which will thus be extended to more complex settings directly linked with industrial applications. These cracks emerge in a periodic localized damage solution which is the bifurcation of a fundamental branch homogeneous with respect to the horizontal direction. The periodicity is confronted with that of the bifurcated solution of gradient damage model and to that predicted by Griffith's theory. Many simplification are made in this work yet the essential elements remain the singularity in the evolution of the temperature field. Two extensions of this work are possible: to other diffusion process and to smaller domains (exhibit scale effects).

Different regimes arise depending on the value of the loading parameter, which is the ratio between the materials critical stress and the stress induced by the thermal shock. For severe loading, the non local damage interpretation explains the entire nucleation phase, whereas for milder loading the Griffith regime appears during the cracks nucleation phase. In the former the periodicity is well explained as a global property of the damage evolution, whereas is the latter, no mean to prove periodicity exist. Different

[3]This could typically be the case of a mortar with aggregates in the case of concrete

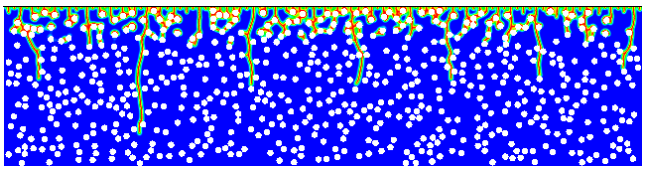

(a) $\phi = .2$

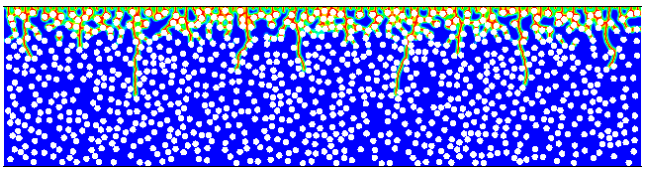

(b) $\phi = .3$

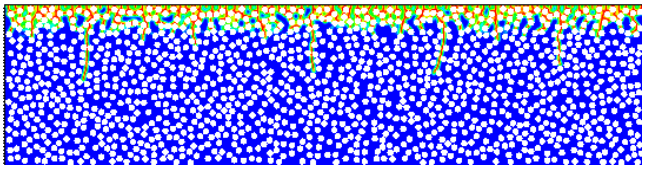

(c) $\phi = .4$

Figure 4.30: radius $r = .1$

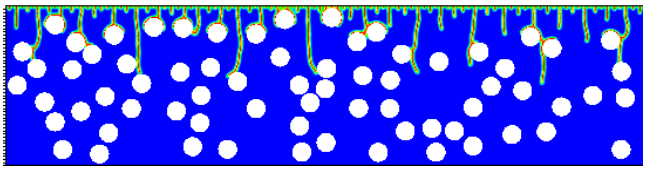

(a) $\phi = .2$

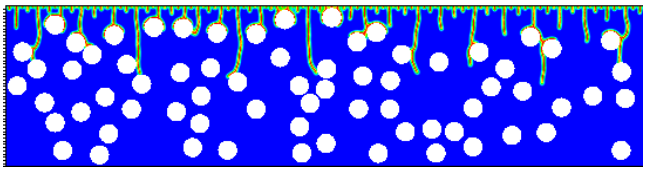

(b) $\phi = .3$

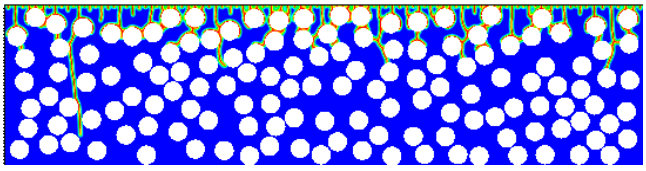

(c) $\phi = .4$

Figure 4.31: radius $r = .3$

Figure 4.32: Drying in non homogeneous materials. Depending on the size of the inclusions r and their density ϕ damage localizes in bands or remains diffuse.

interpretations are proposed on this aspect but with no definitive answer.

Finally the simulations are confronted to a real thermal shock experiment. The numerical implementation captures all three phases: nucleation, scale law and crack arrest. The influence of the physical parameter of the internal length is illustrated, although it is most important that it is compared with other experiments. These comparison are confronted to the difficulty to physically measure a crack and the definition of a crack in a continuous damage zone. This matter deserves further investigation. Both interpretation of damage and Griffith of a same formulation depending on the crack regime have been discussed.

The three-dimensional computation allows to exhibit an hexagonal crack pattern whose scale law is the same as in two dimensions. The emergence of three dimensional effects in the case of slabs when the thickness increases corresponds to the experimental observations. Then two applications are considered, both for severe loadings, from which we conclude that many results from the half plane thermal shock have a broad domain of validity.

To better understand of all the numerical results, the question of computation cost reducing techniques should be addressed. Either simple with evolving mesh size with the penetration or more complex with adaptive mesh and re-meshing. Indeed at the surface the mesh size is given by the materials critical stress which usually forces to have very fine meshes. As we penetrate in the material and that cracks have nucleated, the internal length has less physical meaning and its choice could be relaxed.

Conclusion and Perspectives

In this dissertation new results in the use of gradient damage models to capture brittle fracture are proposed. These results are based on the sound mathematical bases of calculus of variations. They stand at different levels in the construction of the theory. The construction of the variational approach to damage and fracture, for a rate-independent process, in a quasi-static setting, based on the three principles of: irreversibility, stability and energy balance, is recalled. The same damage models used in the regularized approach to fracture of the numerical simulations [Bourdin *et al.* 2000] are considered. This model fits into the family of models introduced in [Pham & Marigo 2010b], for which a general analysis of the one-dimensional traction problem has been reported in [Pham & Marigo 2013]. It is characterized by a scalar damage variable and a gradient term in the damage, which introduces an internal length η. Underlying to the variational approach is the choice of an energy, whose dissipative process is characterized by a critical stress σ_c and an internal length η. The one chosen in this thesis allows to capture brittle material: critical stress, finite dissipated energy and finite crack opening. The variational principal used in the one of directional stability. From the first order stability condition the equilibrium and damage criteria are devised. These are point-wise conditions. The second order condition give a global property. In the case of an evolution of a bar in traction, the evolution is as follows. There exists an elastic phase, when the stress reaches the threshold σ_c damage nucleates everywhere in the bar. As the behaviors studied are softening, the stress in the bar decreases. Then this solution localizes. The loading at which it happens depends on the size of the bar which underscores a size effect. From a single localization the material's toughness $\mathsf{G_c}$ can be identified, is it proportional to the internal length η. The main contributions of this work are summarized before opening on possible perspectives.

Nucleation of a crack at a notch singularity

A major issue that remains in fracture mechanics is how to model the nucleation of a crack in a sound material. Here, an intermediate step is introduced by using damage and to not directly nucleate a crack from a sound material. A separation of scales illustrates that damage only nucleates in the surrounding of the notch, and thus far away from the notch the behavior remains elastic. Thus, rescaling the family of problems brings up a first term which captures the size effect. Then on the rescaled problem, using the techniques of matched asymptotic methods on the outer part of the domain the stress intensity factor K_g due to the geometry is identified. This is a simple elastic computation. Finally in the vicinity of the notch the so called *inner problem* is studied, which only depends on the angle of the notch ω. On the one hand, the order of magnitude of the loading to nucleate a crack only depends on the notch angle. On the other hand, this allows to develop a simple approach for engineers to design at crack nucleation. Indeed, using Table 2.1 the problem is reduced to an elastic computation possible with any *F.E.M.* as detailed in Appendix B.2 to determine K_g.

Propagation of damage bands and convergence towards Griffith's evolution law

Whenever the length η is small by comparison with the dimensions of the body, one can prove by Gamma-convergence arguments that the global minimum of the regularized functional converges to the global minimum of Griffith's functional. This result is the base of the numerical implementation of the variational approach to fracture. This key result is viewed as a fundamental link between damage and fracture mechanics. However the concept of global minimization of the energy cannot be considered as a good physical principle. Indeed, not only does this type of global minimization allow for jumps from one state to an other without considering the presence of energy barriers, but in the case of prescribe forces it does not accept any solution. It deserves to be improved and generalized by replacing the *global* minimization principle by a *stability* condition used in this dissertation. One is then interested whether the evolution of damage governed by such a weaker condition remains close to the one prescribed by Griffith's law when the internal length η is small. The same question appears when considering numerical tests based on an alternate minimization algorithm. Indeed, such an algorithm does not converge necessarily to a global minimizer of the energy but only to a stationary state. The issue is to compare the evolution given by the numerical computations with Griffith's law.

Practically the numerical simulations show that, after a stage of nucleation, the damage concentrates in bands. Their width is of the order of the characteristic length η of the material. Moreover, except at the tip of the damage zone, the damage profile in the direction orthogonal to the band is practically the one given by a one-dimensional analysis. These two properties (a thin damage band with an optimal profile) are the basic assumptions (Hypothesis 5) of our analysis. The local energy balance conditions still hold even in the vicinity of the crack tip (Proposition 5). The last major issue in order to achieve this task is to give a sense to the concepts of energy release rate and of critical energy release rate, that is to say, to introduce correctly the basic quantities G and $\mathsf{G_c}$ entering in Griffith's law in the setting of our damage law. Specifically, in Griffith's theory, G is defined by assuming that the material has a purely elastic behavior. Then by virtue of Irwin's formula one can relate the energy release rate to the singularity at the tip of the crack and therefore to the stress intensity factors. In the context of the present damage law, the stresses remain bounded but the gradient of damage can be singular. Besides, in Griffith's theory, $\mathsf{G_c}$ is a given material constant characterizing the energy associated with surfaces of discontinuity whereas in our damage approach the parameters characterizing the inelastic behavior of the material are the critical stress σ_c and the internal length η. Accordingly, G is defined with the help of a two-scale approach and $\mathsf{G_c}$ as the energy dissipated by creating the optimal damage profile. From all these ingredients, in Proposition 9 is established that the damage bands follow Griffith's propagation law.

The numerical investigation of the tip problem gives a better understanding of the evolution of damage bands. Obviously there is no singularity in stress as the damage criteria induces a stress threshold. The crack propagates for the expected critical stress intensity factor. In this stationary phase (Fig. 2.23), the damage profile is almost invariant for any angle leaving from the tip (Fig. 2.24). As established analytically, the damage is singular at the tip of the damage band except when the crack propagates.

Nucleation for stress concentration in a thermal shock setting

When there is a singularity due to a notch the nucleation phase is localized in the vicinity of the notch. Yet cracks can also appear when the stress is much more diffuse, especially, in many situations cracks which a characteristic distance between them appear. This study aims at giving further insight on the initiation phenomenon in thermal shock fracture and, more generally, on the morphogenesis of complex crack patterns. It also provides a non-trivial example of the study of the evolution and bifurcation problem of gradient damage models in a two dimensional settings. The thermal shock problem for a semi-infinite two-dimensional slab is taken as a model problem. By assuming a perfect conductivity at the surface of the thermal shock, a Dirichlet boundary condition on the temperature is considered. The analytically calculated temperature field, function of space and time is used to evaluate the mechanical loading in the form of thermally induced inelastic strains.

Hence, the rate problem (Proposition 13) is formulated. The fundamental solution uniqueness and stability are determined through the minimization of a Rayleigh ratio on linear spaces or convex cones (Proposition 16). The main result of this chapter is the solution of this bifurcation and stability problem (Proposition 18), which is obtained by adopting a partial Fourier decomposition in the direction parallel to the surface of the slab. The existence of a finite time t_b from which a bifurcation from the fundamental branch can occur is proven, the fundamental branch becoming unstable at a later time t_s. Moreover the bifurcated solution is stable (Proposition 15) and characterized by a finite wavelength λ_b proportional to the internal length η of the material. This bifurcated solution represents the onset of the localization phenomena leading to the establishment of the periodic crack pattern observed in the experiments.

Quantitative results are obtained through the numerical solution of a one-dimensional boundary value problem for the fundamental branch and of a parametric one-dimensional eigenvalue problem for establishing the key properties of the bifurcated solution as a function of the loading parameter θ and the Poisson ratio. The main assumption is the perfect conductivity that implies that the maximal stress is reached on the surface at $t = 0$.

Morphogenesis of cracks under drying or cooling

This last chapter studies numerically the morphogenesis of cracks patterns in the thermal shock. The understanding of the variational damage models is leveraged to numerically study the morphogenis of complex crack patterns and their selective growth. These results illustrate the predictive and quantitative modeling of the complex fracture pattern evolution. Once again they are based on no a priori hypotheses on the crack set geometry. The loading comes from the cooling induced shrinkage. Nucleation is governed by both the critical stress σ_c and the internal length η_n where the propagation is governed by $\mathsf{G_c}$. Yet only two materials parameters are needed and they are related in our formulation.

Although this section is numerically based, one greatly benefits from the understanding of the nucle-

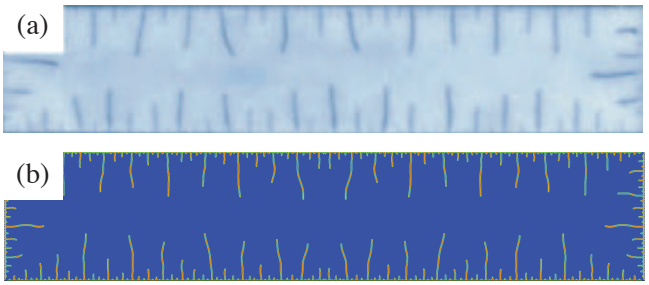

Figure 4.33: (a) Crack pattern in a slab of ceramic after thermal shock (b) numerical simulation. Damage field α indicating the location of cracks.

ation developed previously. Especially, the importance of the evolution of the damage and of the diffusion process, must not be neglected. As the cracks penetrate our model captures the scale law observed experimentally on a multitude of scales and which can be deducted from Griffith's evolution law. Very good qualitative (Fig. 4.33) and quantitative agreements are found.

This detailed study shows that the computation costs remain high as soon as material parameters are used. Indeed, from material parameters, the internal length is small in front of the size of the structures. Not only does this length appear in solutions as in the thermal shock setting, it also governs the link between the toughness $\mathsf{G_c}$ and the critical stress σ_c. Thus a change in the length will modify one of these key physical parameters. When cracks are established, σ_c is less relevant, but for nucleation, the relation between the mesh size, the internal length and the size of the structure leads to heavy computations.

The extension to three-dimensional simulations is natural and does not require new theoretical development. For large domains, cracks form a hexagonal pattern, which in the case of the thermal shock follows the same scale law as in two-dimensions. A very subtle behavior is captured for the transition between three and two dimensional crack patterns which corresponds to the experimental observations. Moreover non regular surfaces or heterogeneous materials can also be addressed in this framework, and illustrate the generality of the simplified framework studied.

Perspectives

There are many outlooks to this thesis. Following the order of the chapters let us give a few hints on what they could be. First, the justification of the gradient term through homogenization is still lacking in the construction of the model. The nucleation phase should be compared to other evolution law, surface energy densities such a Griffith or cohesive force models but also other bulk models such as plasticity or a coupled plastic damage model. Once the damage bands are established, the convergence of the evolution of their length towards a given evolution law in the case of non homogeneous materials, should be established. The result should depend of the size of heterogeneities compared to the internal length η. Especially the

effective propagation of crack bands in composite materials where the distance between the heterogeneities is of the same order as the internal length. Obviously rate dependent evolutions as well as dynamic loading are still open questions. The limit of the gradient in damage it is a very strong regularization which on the mathematical side a proper space for the damage field must be established.

In the case of the thermal shock, the investigation of size effects is an interesting extension, where the width of the slate as well as its height should influence the initial periodicity. A post buckling analysis which would allow to understand the selection mechanisms from bifurcated state to the crack setting. A litmus test is to compare the results to different class of materials, where other damage models in the same vain could be used. These results can be used as one, among other, selection mechanisms for the proper damage models. But, the present work is a step forwards as the internal length is linked to a macroscopic quantity. The evolution of damage with hydration or the alkali-silica reaction is a natural extension at least numerically.

Speaking of numerics, materials often are such that the internal length η is small in front of the dimension of structure. The numerical approximation of a characteristic mesh size small in front of η leads to problems with a great number of degree of freedoms. One can not overlook that this is an obstacle to the industrial diffusion of these methods. This issue could be addressed from a numerical perspective.

Appendix A

Appendix of Chapter 1

While reasoning on the underlying local damage model, the connexity Hypothesis 1 is justified through homogenization. The strain energy is linearized around the state $(0, \mathrm{T}_0, \alpha)$ up to the second order assuming small strains, and a small variation from the initial temperature

$$W_0(\boldsymbol{\varepsilon}, \mathrm{T}, \alpha) = W_0(0, \mathrm{T}_0, \alpha) + \boldsymbol{\sigma}_0(\alpha) \cdot \boldsymbol{\varepsilon} + \frac{1}{2}\mathsf{A}(\alpha)\boldsymbol{\varepsilon} \cdot \boldsymbol{\varepsilon} - \mathsf{A}(\alpha)\mathsf{a}(\alpha)\boldsymbol{\varepsilon}(\mathrm{T} - \mathrm{T}_0) + \frac{1}{2}\gamma(\alpha)(\mathrm{T} - \mathrm{T}_0)^2.$$

Physical interpretation of the different terms: $\sigma_0(\alpha)$ is the prestress, $\mathsf{a}(\alpha)$ is the thermal dilatation considered isotropic, $\mathsf{A}(\alpha)$ is the rigidity and $\gamma(\alpha)/\mathrm{T}_0$ is the specific heat capacity at constant strain. A priori these coefficients depend on the damage state. Choosing the reference state such that the prestress term vanishes and identifying $\mathsf{w}(\alpha) = W_0(0, \mathrm{T}_0, \alpha)$ and thus the elastic energy density is:

$$\psi(\boldsymbol{\varepsilon}, \mathrm{T}, \alpha) = \frac{1}{2}\mathsf{A}(\alpha)\boldsymbol{\varepsilon} \cdot \boldsymbol{\varepsilon} - \mathsf{A}(\alpha)\mathsf{a}(\alpha)\boldsymbol{\varepsilon}(\mathrm{T} - \mathrm{T}_0) + \frac{1}{2}\gamma(\alpha)(\mathrm{T} - \mathrm{T}_0)^2$$

$$\psi(\boldsymbol{\varepsilon}, \mathrm{T}, \alpha) = \frac{1}{2}\mathsf{A}(\alpha)\left(\boldsymbol{\varepsilon} - \mathsf{a}(\alpha)(\mathrm{T} - \mathrm{T}_0)\right) \cdot \left(\boldsymbol{\varepsilon} - \mathsf{a}(\alpha)(\mathrm{T} - \mathrm{T}_0)\right) - \frac{1}{2}c(\alpha)(\mathrm{T} - \mathrm{T}_0)^2$$

Proposition 1 and Hypothesis 1 lead to a yield surface of

$$-\psi_{,\alpha}(\boldsymbol{\varepsilon}, \mathrm{T}, \alpha) \leq \mathsf{w}(\alpha)$$

$$-\frac{1}{2}\mathsf{A}'(\alpha)\boldsymbol{\varepsilon} \cdot \boldsymbol{\varepsilon} + \left(\mathsf{A}'(\alpha)\mathsf{a}(\alpha) + \mathsf{A}(\alpha)\mathsf{a}'(\alpha)\right)\boldsymbol{\varepsilon}(\mathrm{T} - \mathrm{T}_0) - \frac{1}{2}\gamma(\alpha)(\mathrm{T} - \mathrm{T}_0)^2 \leq \mathsf{w}(\alpha) \tag{A.1}$$

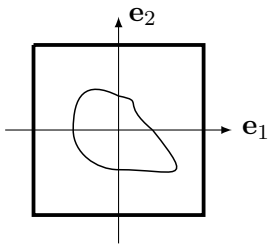

Figure A.1: Cell Y for the homogenization process of characteristic size ϵ

Justification of the convex domain in the temperature field (Hypothesis 1). Therefore a two scale homogenization asymptotic approach is considered. Let us consider a cell Y (Fig. A.1) of characteristic

size ϵ constituted of an inclusion Y_i in a matrix Y_m. The dependence of the displacement and temperature field on ϵ is made explicit. The solution is searched for in power series of the small parameter ϵ:

$$\mathrm{T}_\epsilon(\mathbf{x},\mathbf{y}) = \bar{\mathrm{T}}(\mathbf{x}) + \epsilon \mathrm{T}_1(\mathbf{x},\mathbf{y}) + \cdots \quad \text{and} \quad \mathbf{u}_\epsilon(\mathbf{x}) = \bar{\mathbf{u}}(\mathbf{x}) + \epsilon \mathbf{u}_1(\mathbf{x},\mathbf{y}) + \cdots,$$

where $\mathbf{y}$ is the fast variable $\mathbf{y} = \mathbf{x}/\epsilon$. In the mechanical problem, the temperature field only appears through it's average value on the cell $\bar{\mathrm{T}}$. The homogenized energy density for a macroscopic temperature $\bar{\mathrm{T}}$ is solution of the minimization problem

$$\bar{\psi}(\bar{\boldsymbol{\varepsilon}}, \bar{\mathrm{T}}) := \min_{v \in H^1_\sharp(Y)} \frac{1}{|Y|} \int_Y \frac{1}{2} \mathsf{A}(\mathbf{y}) \left(\boldsymbol{\varepsilon}(\mathbf{v}) - \mathsf{a}(\mathbf{y})\bar{\mathrm{T}}\right) \cdot \left(\boldsymbol{\varepsilon}(\mathbf{v}) - \mathsf{a}(\mathbf{y})\bar{\mathrm{T}}\right) - \frac{1}{2} c(\mathbf{y}) \bar{\mathrm{T}}^2 \, \mathrm{d}\mathbf{y}$$

where $H^1_\sharp(Y) = \left\{ v \in H^1(Y) \,|\quad v \,\text{periodic} \right\}$ which becomes at the first order in $\mathbf{u}_\epsilon$

$$\bar{\psi}(\bar{\boldsymbol{\varepsilon}}, \bar{\mathrm{T}}) = \min_{v \in H^1_\sharp(Y)} \frac{1}{|Y|} \int_Y \frac{1}{2} \mathsf{A}(\mathbf{y}) \left(\boldsymbol{\varepsilon}(\bar{\mathbf{u}}) + \boldsymbol{\varepsilon}(\mathbf{v}) - \mathsf{a}(\mathbf{y})\bar{\mathrm{T}}\right) \cdot \left(\boldsymbol{\varepsilon}(\bar{\mathbf{u}}) + \boldsymbol{\varepsilon}(\mathbf{v}) - \mathsf{a}(\mathbf{y})\bar{\mathrm{T}}\right) - \frac{1}{2} c(\mathbf{y}) \bar{\mathrm{T}}^2 \, \mathrm{d}\mathbf{y}.$$

The term χ is used to make reference to the solution of the minimization process, which by linearity reads $\chi(\mathbf{y}) = \bar{\boldsymbol{\varepsilon}}_{ij} \chi^{ij}(\mathbf{y}) + \bar{\mathrm{T}} \chi^0(\mathbf{y})$, where χ^{ij} and χ^0 are solution of the 7 elementary problems:

$$\int_Y \mathsf{A}_{ijkl}(\mathbf{y}) \left(\bar{\boldsymbol{\varepsilon}} + \boldsymbol{\varepsilon}_{kl}(\chi^{mh})\right) \boldsymbol{\varepsilon}_{ij}(\mathbf{v}) \, \mathrm{d}\mathbf{y} = 0 \qquad \forall v \in \bar{H}^1_\sharp(Y), \quad (m,h) \in \{1,2,3\}^2$$

$$\int_Y \mathsf{A}_{ijkl}(\mathbf{y}) \left(\bar{\boldsymbol{\varepsilon}} + \boldsymbol{\varepsilon}_{kl}(\chi^0)\right) \boldsymbol{\varepsilon}_{ij}(\mathbf{v}) \, \mathrm{d}\mathbf{y} = 0 \qquad \forall v \in \bar{H}^1_\sharp(Y)$$

where $\bar{H}^1$ of vanishing average. The derivative should be understood in the sense of distributions in the case of discontinuous fields. Finally, knowing χ^{ij} and χ^0 the homogenized energy density reads:

$$\begin{aligned} \bar{\psi}(\bar{\boldsymbol{\varepsilon}}, \bar{\mathrm{T}}) = \quad & \frac{1}{|Y|} \quad \int_Y \left(\frac{1}{2} \mathsf{A}(\mathbf{y}) \left(\boldsymbol{\varepsilon}(\bar{\mathbf{u}}) + \boldsymbol{\varepsilon}_{ij}(\bar{\mathbf{u}}) \boldsymbol{\varepsilon}(\chi^{ij}) + \boldsymbol{\varepsilon}(\chi^0)\bar{\mathrm{T}} - \mathsf{a}(\mathbf{y})\bar{\mathrm{T}}\right) \right. \\ & \left. \cdot \left(\boldsymbol{\varepsilon}(\bar{\mathbf{u}}) + \boldsymbol{\varepsilon}_{ij}(\bar{\mathbf{u}}) \boldsymbol{\varepsilon}(\chi^{ij}) + \boldsymbol{\varepsilon}(\chi^0)\bar{\mathrm{T}} - \mathsf{a}(\mathbf{y})\bar{\mathrm{T}}\right) - \frac{1}{2} c(\mathbf{y}) \bar{\mathrm{T}}^2 \right) \mathrm{d}\mathbf{y} \end{aligned}$$

Denoting δ_{kl} the Kronecker symbol, the homogenized Hooke tensor, prestress $\bar{\boldsymbol{\sigma}}^0$, and the homogenized coupling term read as:

$$\begin{aligned} \bar{\mathsf{A}}_{ijkl} &:= \frac{1}{|Y|} \int_Y \mathsf{A}_{ijkl} \left(\delta_{km}\delta_{lh} + \boldsymbol{\varepsilon}_{kl}(\chi^{mh}(\mathbf{y}))\right) \mathrm{d}\mathbf{y}, \\ \bar{\sigma}^0_{ij} &:= \bar{\mathsf{A}}\bar{\mathsf{a}} := \frac{1}{|Y|} \int_Y \mathsf{A}_{ijkl} \left(\delta_{km}\delta_{lh} + \boldsymbol{\varepsilon}_{kl}(\chi^{mh}(\mathbf{y}))\right) \cdot (\mathsf{a}\delta_{kl} - \boldsymbol{\varepsilon}_{kl}(\chi^0)) \, \mathrm{d}\mathbf{y}, \\ \bar{\mathsf{b}}_{ij} &:= \frac{1}{|Y|} \int_Y \mathsf{A}_{ijkl} (\mathsf{a}\delta_{kl} - \boldsymbol{\varepsilon}_{kl}(\chi^0)) \cdot (\mathsf{a}\delta_{kl} - \boldsymbol{\varepsilon}_{kl}(\chi^0)) \, \mathrm{d}\mathbf{y}. \end{aligned}$$

Finally, the elastic energy density reads:

$$\begin{aligned} \bar{\psi}(\bar{\boldsymbol{\varepsilon}}, \bar{\mathrm{T}}) &= \frac{1}{2} \bar{\mathsf{A}}\bar{\boldsymbol{\varepsilon}} \cdot \bar{\boldsymbol{\varepsilon}} - \bar{\sigma}^0 \bar{\boldsymbol{\varepsilon}} \bar{\mathrm{T}} + \frac{1}{2} (\bar{b} - < c >) \bar{\mathrm{T}}^2 \\ &= \frac{1}{2} \bar{\mathsf{A}} (\bar{\boldsymbol{\varepsilon}} - \bar{\mathsf{a}}\bar{\mathrm{T}}) \cdot (\bar{\boldsymbol{\varepsilon}} - \bar{\mathsf{a}}\bar{\mathrm{T}}) - \frac{1}{2} (-\bar{b} + \bar{\mathsf{A}}\bar{\mathsf{a}}\bar{\mathsf{a}} + < c >) \bar{\mathrm{T}}^2 \end{aligned}$$

combining (A.1) leads to $\bar{b}$ which must be decreasing with respect to the damage. This is the case as $\bar{b}$ is solution of a minimization problem on a space that increases with the damage. Thus Hypothesis 1 is justified.

Appendix B

Appendices of Chapter 2

B.1 The singular displacement field at the tip of the notch

A notch near an elastic material generates a singularity. To fix the notation let us mention the main steps to compute the displacement field at the tip of a notch. A solution is searched for as an Airy function of the shape:

$$\phi(\bar{r},\theta) = \sum_{i=1}^{N} K_i \bar{r}^{\varrho+1} F^i(\theta)$$

where $(\bar{r},\theta)$ are the polar coordinates (Fig. 2.3) defined from the tip of the notch. In the case where $\omega < \pi$, the first two singularities ϱ are solution of

$$\sin 2\varrho\omega = -\varrho \sin 2\omega \quad \text{and} \quad \sin 2\varrho\omega = \varrho \sin 2\omega \tag{B.1}$$

and are reported (Fig. B.1). For $\omega < \omega^* = 2.2467$ a single singularity exists. In the sequel only the strongest singularity will be considered, which could vanish for specific loading or geometries, in which case one should consider the following singularity. The first angular function $F^1(\theta)$ is even:

$$F^1(\theta) = (1-\varrho)\sin(1-\varrho)\omega\cos(1+\varrho)\theta - (1+\varrho)\sin(1+\varrho)\omega\cos(1-\varrho)\theta \tag{B.2}$$

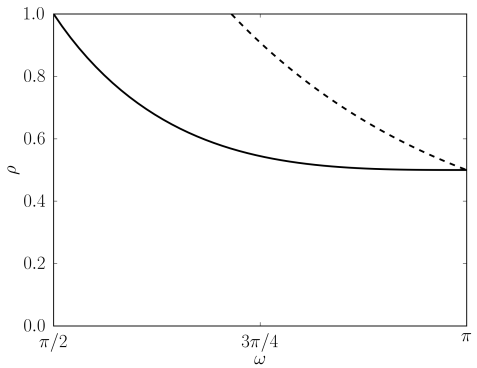

Figure B.1: Power of the singularity function on the angle of the notch

Then the strain is integrated up to the displacement (for $\nu = 0$), $U_r = 2r\boldsymbol{\varepsilon}_{rr}$ and $U_\theta = \frac{1}{\varrho}U'_r - 4\sqrt{r}\boldsymbol{\varepsilon}_{r\theta}$, with the stress

$$\sigma^0_{rr} = \frac{1}{r^2}\frac{\partial^2\phi}{\partial\theta^2} + \frac{1}{r}\frac{\partial\phi}{\partial r}, \quad \sigma^0_{r\theta} = -\frac{\partial}{\partial r}\left(\frac{1}{r}\frac{\partial\phi}{\partial\theta}\right)$$

$$\begin{aligned} H^\omega_1(\theta) &= (1-\varrho)\sin(\theta\varrho + (\varrho-1)\omega) + (\varrho-1)\sin[\theta\varrho + \omega - \varrho\omega] + 3\sin[\theta\varrho - (1+\varrho)\omega] \\ - &\quad 3\sin[\theta\varrho + \omega + \varrho\omega] - \varrho\sin[2\theta - \theta\varrho - (1+\varrho)\omega] + \varrho\sin[2\theta - \theta\varrho + \omega + \varrho\omega] \end{aligned} \tag{B.3}$$

$$\begin{aligned} H^\omega_2(\theta) &= (1-\varrho)\cos(\theta\varrho + (\varrho-1)\omega) + (\varrho-1)\cos[\theta\varrho + \omega - \varrho\omega] - 3\cos[\theta\varrho - (1+\varrho)\omega] \\ + &\quad 3\cos[\theta\varrho + \omega + \varrho\omega] + \varrho\cos[2\theta - \theta\varrho - (1+\varrho)\omega] - \varrho\cos[2\theta - \theta\varrho + \omega + \varrho\omega] \end{aligned} \tag{B.4}$$

Finally, denoting $\mathbf{H}^\omega(\theta) = (H^\omega_1(\theta), H^\omega_2(\theta))$ the first term of the outer expansion $\mathbf{u}^0$ can be written under the form (2.8)

B.2 Computation of K_g through the dual stress singularity method

As proven in Section 2.2.3, in the outer domain the behavior is elastic and thus the stress field is solution of the equilibrium

$$\operatorname{div}\boldsymbol{\sigma}^0 + \mathbf{f} = 0 \tag{B.5}$$

and the boundary conditions

$$\begin{cases} \mathbf{u}^0 = \mathbf{U} & \text{on } \partial_D\Omega_1 \\ \boldsymbol{\sigma}^0\mathbf{n} = \mathbf{F} & \text{on } \partial_N\Omega_1 \\ \boldsymbol{\sigma}^0\mathbf{n} = 0 & \text{on } \tilde{\Gamma}^\pm \end{cases} \tag{B.6}$$

And thus the first singular term (2.8) $\mathbf{u}^0 = K_g\tilde{r}^\varrho\mathbf{H}^\omega(\theta)$. To compute the stress intensity factor K_g we propose to use the dual stress singular method. For that, we note that for an angle ω if ϱ is solution of (B.1), then $\varrho^\star = -\varrho$ also is. Furthermore, the angular function associated reads $F^\star = -F$ and the airy function of the dual singularity is

$$\phi^\star = -r^{\varrho+1}F^i(\theta)$$

Thus the stress read

$$\sigma^\star_{rr} = -r^{-\varrho-1}\left(F''(\theta) + (1-\varrho)F(\theta)\right),$$
$$\sigma^\star_{r\theta} = -\varrho r^{-\varrho-1}F(\theta), \qquad \sigma^\star_{\theta\theta} = \varrho(1_\varrho)r^{-\varrho-1}F(\theta)$$

and the displacement

$$\mathbf{u}^* = r^\varrho \left(U_r^\star(\theta)\mathbf{e}_r + U_\theta^\star(\theta)\mathbf{e}_\theta\right)$$

with

$$U_r^\star(\theta) = \frac{1}{\varrho}\left(F''(\theta) + (1-\varrho)F^1(\theta)\right),$$

$$U_\theta^\star(\theta) = \frac{1}{(1+\varrho)\varrho}\left(F'''(\theta) + (2\varrho^2 - \varrho + 1)F'(\theta)\right).$$

The main difficulty is to evaluate near the tip of the notch. Accordingly, we partition Ω to isolate the tip of the notch. Let $\mathbb{B}_r$ be the ball of radius r centered at the tip of the notch, let $\mathbb{C}_r$ be its boundary (a circle of radius r) and let $\tilde{\Omega}_r$ be the uncracked part of the body outside the ball $\mathbb{B}_r$: $\tilde{\Omega}_r = \Omega_1 \setminus \mathbb{B}_r$.

Rewriting the equilibrium (B.5) under its weak form and using two integral by parts:

$$\begin{aligned}
0 &= \int_{\tilde{\Omega}_r} \left(\operatorname{div}\boldsymbol{\sigma}^0 + \mathbf{f}\right)\cdot\mathbf{u}^* \tilde{r}\,\mathrm{d}\tilde{r}\,\mathrm{d}\theta \\
&= \int_{\tilde{\Omega}_r} -\tilde{\nabla}\mathbf{u}^0\cdot\tilde{\nabla}\mathbf{u}^* + \mathbf{f}\mathbf{u}^* r\,\mathrm{d}\tilde{r}\,\mathrm{d}\theta + \int_{\partial\tilde{\Omega}_r} \frac{\partial \mathbf{u}^0}{\partial \mathbf{n}}\cdot\tilde{\nabla}\mathbf{u}^*\,\mathrm{d}\tilde{r}\,\mathrm{d}\theta \\
&= \int_{\tilde{\Omega}_r} \mathbf{u}^0\cdot\tilde{\Delta}\mathbf{u}^* + \mathbf{f}\mathbf{u}^* r\,\mathrm{d}\tilde{r}\,\mathrm{d}\theta + \int_{\partial\tilde{\Omega}_r} \left(\frac{\partial \mathbf{u}^0}{\partial \mathbf{n}}\cdot\mathbf{u}^* - \mathbf{u}^0\cdot\frac{\partial \mathbf{u}^*}{\partial \mathbf{n}}\right)\mathrm{d}\tilde{r}\,\mathrm{d}\theta
\end{aligned}$$

The term in $\mathbf{u}^0\cdot\tilde{\Delta}\mathbf{u}^*$ of the first integral vanishes as $\mathbf{u}^*$ is harmonic by construction. As the normal on the notch is $-\mathbf{e}_r$, and passing to the limit in $\tilde{r}$,

$$\int_{\mathbb{C}_r} \left(\frac{\partial \mathbf{u}^0}{\partial \mathbf{n}}\cdot\mathbf{u}^* - \mathbf{u}^0\cdot\frac{\partial \mathbf{u}^*}{\partial \mathbf{n}}\right)\mathrm{d}\tilde{r}\,\mathrm{d}\theta = 2\varrho K_g \int_0^\omega \left(\mathbf{H}^\varrho(\theta)\right)^2\,\mathrm{d}\theta$$

where the computation of the displacement field $\mathbf{u}$ can be done with any finite element software as it is solution of an elastic problem and $\mathbf{u}^*$ is a given function.

$$K_g = \frac{\int_{\tilde{\Omega}_r} \mathbf{f}\mathbf{u}^* \tilde{r}\,\mathrm{d}\tilde{r}\,\mathrm{d}\theta + \int_{\partial\tilde{\Omega}_r}\left(\frac{\partial \mathbf{u}^0}{\partial \mathbf{n}}\cdot\mathbf{u}^* - \mathbf{u}^0\cdot\frac{\partial \mathbf{u}^*}{\partial \mathbf{n}}\right)\mathrm{d}\tilde{r}\,\mathrm{d}\theta}{2\varrho\int_0^\omega \left(\mathbf{H}^\varrho(\theta)\right)^2\,\mathrm{d}\theta} \tag{B.7}$$

B.3 Sketch of the proof of Property 5

The proof of property (2.20) for the general class of strongly brittle materials needs a complete analysis of the singularities at the tip of the crack. Such an analysis requires additional hypotheses on the state function W. Consequently, a sketch of the proof is merely given in the particular case of the damage model in Example 1. The analysis of the singularities is made near the tip of the crack and hence a polar system of coordinates (r,θ) is used with pole the tip of the crack, $\theta = 0$ corresponding to the axis tangent

to the crack. Accordingly the lips of the crack correspond to $\theta = \pm\pi$. Since the time is fixed, the index t is removed from all fields.

Let us denote $v = 1 - \alpha$, only singular parts of the displacement are considered and damage fields of the following form:

$$v(r,\theta) = r^p V(\theta) + \cdots, \qquad \mathbf{u}(r,\theta) = r^q \left(U_r(\theta)e_r + U_\theta(\theta)e_\theta\right) + \cdots$$

where p and q will be called the order of the singularity. In order that the total energy be finite the orders p and q must be such that $p > 0$ and $p + q > 0$. The damage criterion $(2.14)_3$ reads

$$\frac{1}{2}v^{-3}\mathsf{C}_0\boldsymbol{\sigma}\cdot\boldsymbol{\sigma} - \mathsf{w}_1 - \mathsf{w}_1\eta^2\Delta v \leq 0. \tag{B.8}$$

The first term of (B.8), $\frac{1}{2}v^{-3}\mathsf{C}_0\boldsymbol{\sigma}\cdot\boldsymbol{\sigma}$, being non negative, it cannot be more singular than the two other terms of (B.8) whose orders are respectively 0 and at least $p-2$. p merely considered such that $p \leq 2$ because otherwise the proof is trivial. Therefore, the order of $\frac{1}{2}v^{-3}\mathsf{C}_0\boldsymbol{\sigma}\cdot\boldsymbol{\sigma}$ must be greater or equal to $p-2$. This condition is automatically satisfied when the singular field displacement field corresponds to a rigid displacement and in such a case $q \in \{0,1\}$. Otherwise $\frac{1}{2}v^{-3}\mathsf{C}_0\boldsymbol{\sigma}\cdot\boldsymbol{\sigma}$ is of order $p+2q-2$. Hence, in any case q must be non negative.

From the two inequalities $p > 0$ and $q \geq 0$, it is easy to check that $\lim_{r\to 0}\mathsf{l}_r = 0$. Moreover the only terms in J_r which can give a non null contribution are the gradient damage terms. Since $\nabla\alpha\cdot\nabla\alpha$ and $q_r\alpha_{,1}$ are both of order $2p-2$, $\mathsf{J}_0 = 0$ if $p > 1/2$. Therefore, it remains to consider the cases when $p \leq 1/2$.

Let us prove that even if $q = 0$, the order of $\frac{1}{2}v^{-3}\mathsf{C}_0\boldsymbol{\sigma}\cdot\boldsymbol{\sigma}$ is greater than $p-2$. It is true when $q > 0$. If $q = 0$, then the order of the strains is at least -1, the order of ε_{rr} is greater than -1 and the order of the stresses is at least $2p-1$. Since the stress field $\boldsymbol{\sigma}$ must satisfy the equilibrium equations, assuming that the body forces are not singular, the singular part of $\operatorname{div}\boldsymbol{\sigma}$ must vanish. This is equivalent to introduce an Airy function of order $2p+1$, say $\phi(r,\theta) = r^{2p+1}F(\theta)$, and to set

$$\sigma_{rr} = \frac{1}{r^2}\frac{\partial^2\phi}{\partial\theta^2} + \frac{1}{r}\frac{\partial\phi}{\partial r} + \cdots, \quad \sigma_{r\theta} = -\frac{\partial}{\partial r}\left(\frac{1}{r}\frac{\partial\phi}{\partial\theta}\right) + \cdots, \quad \sigma_{\theta\theta} = \frac{\partial^2\phi}{\partial r^2} + \cdots. \tag{B.9}$$

From the stress-strain relation $v^2\mathsf{E}\varepsilon_{rr} = (1-\nu^2)\sigma_{rr} - \nu(1+\nu)\sigma_{\theta\theta}$, where E is the Young modulus of the sound material and ν the (invariable) Poisson ratio, one deduces that $F(\theta)$ must satisfy

$$0 = (1-\nu)F''(\theta) + (1-\nu(2p+1))(2p+1)F(\theta).$$

Since the lips of the crack are stress free, F must satisfy the boundary conditions $F(\pm\pi) = F'(\pm\pi) = 0$. Therefore, the unique solution is $F = 0$, the order of the stresses is greater than $2p-1$ and hence the order of $\frac{1}{2}v^{-3}\mathsf{C}_0\boldsymbol{\sigma}\cdot\boldsymbol{\sigma}$ is greater than $p-2$.

Writing (B.8) at the order $p-2$, one deduces that V must be a non null function which satisfies

$$V'' + p^2V \geq 0 \quad \text{and} \quad V \geq 0 \text{ in } (-\pi,\pi), \qquad V(\pm\pi) = 0.$$

Let us prove that $p \geq 1/2$. Multiplying the inequality $V'' + p^2 V \geq 0$ by V, integrating over $(-\pi, \pi)$, integrating by parts the first term and taking into account the boundary conditions lead to

$$p^2 \geq \frac{\int_{-\pi}^{\pi} V'(\theta)^2 \, \mathrm{d}\theta}{\int_{-\pi}^{\pi} V(\theta)^2 \, \mathrm{d}\theta} \geq \min_{\substack{\varphi \geq 0 \\ \varphi(\pm\pi)=0}} \frac{\int_{-\pi}^{\pi} \varphi'(\theta)^2 \, \mathrm{d}\theta}{\int_{-\pi}^{\pi} \varphi(\theta)^2 \, \mathrm{d}\theta} = \frac{1}{4} \tag{B.10}$$

where the last equality is a classical result the proof of which is left to the reader. Moreover, all inequalities become equalities in (B.10) if and only if $p = 1/2$ and $V(\theta) = K \cos(\theta/2)$ with $K > 0$. This matches the classical singularity of the laplacian with Dirichlet boundary conditions on the lips of the crack. In such a case, a straightforward calculation gives

$$\mathsf{J}_0 = -\frac{\pi}{4} \mathsf{w}_1 \eta^2 K^2 < 0$$

which completes the sketch of the proof.

Appendix C

Appendices of Chapter 3

C.1 Proof of Proposition 11

Proof. The proof is divided into 8 steps. Throughout the proof τ is a given positive number. The functional spaces read

$$\mathcal{D}_0^1 := \{\beta \in H^1(0,\infty) \,:\, 0 \le \beta \le 1\} \quad \text{and} \quad \mathcal{D}_0 := \{\beta \in H^1(0,\infty) \,:\, 0 \le \beta\}.$$

(i) : *Existence and uniqueness of the minimizer.* Since $\bar{\mathcal{P}}_\tau$ is positive and lower semi-continuous and since $\mathcal{D}_0^1$ is closed in $H^1(0,\infty)$, a minimizer exists. Since $\bar{\mathcal{P}}_\tau$ is strictly convex, the minimizer is unique and is denoted by $\bar{\alpha}_\tau$. $\triangleleft$

(ii) : $\bar{\alpha}_\tau$ *is also the unique minimizer of* $\bar{\mathcal{P}}_\tau$ *over* $\mathcal{D}_0$. By the same arguments as for the minimization over $\mathcal{D}_0^1$, the minimizer exists and is unique, say $\hat{\alpha}_\tau$. Let us set $\check{\alpha}_\tau = \min\{\hat{\alpha}_\tau, 1\} \in \mathcal{D}_0^1 \subset \mathcal{D}_0$. One easily checks that $\bar{\mathcal{P}}_\tau(\check{\alpha}_\tau) \le \bar{\mathcal{P}}_\tau(\hat{\alpha}_\tau)$. Therefore $\hat{\alpha}_\tau = \check{\alpha}_\tau \in \mathcal{D}_0^1$ and hence $\hat{\alpha}_\tau = \bar{\alpha}_\tau$. $\triangleleft$

(iii) : 0 *is not the minimizer.* Since $\Theta < 1 = \mathsf{f_c}(0)$, there exists $h > 0$ such that $\Theta < \mathsf{f_c}(y)$ in $[0,h]$. Since

$$\bar{\mathcal{P}}_\tau'(0)(\beta) = \int_0^\infty (\Theta^2 - \mathsf{f_c}(y)^2)\beta(y)\,\mathrm{d}y,$$

if one chooses $\beta \in \mathcal{D}_0$ with its support included in $[0,h]$, then $\bar{\mathcal{P}}_\tau'(0)(\beta) < 0$ and hence 0 cannot be the minimizer. The (open) support of $\bar{\alpha}_\tau$ is denoted by I_τ, *i.e.* $I_\tau = \{y \ge 0 \,:\, \bar{\alpha}_\tau(y) > 0\}$. $\triangleleft$

(iv) : $\bar{\alpha}_\tau$ *is indefinitely continuously differentiable in* I_τ *and satisfies*

$$\frac{1}{\tau^2}\bar{\alpha}_\tau''(y) + \mathsf{f_c}(y)^2(1 - \bar{\alpha}_\tau(y)) = \Theta^2 \qquad \forall y \in I_\tau. \tag{C.1}$$

Since $\bar{\alpha}_\tau$ minimizes $\bar{\mathcal{P}}_\tau$ over $\mathcal{D}_0$, by standard arguments one gets that it satisfies

$$\int_0^\infty \left(\frac{1}{\tau^2}\bar{\alpha}_\tau'(y)\beta'(y) + \Big(\Theta^2 - \mathsf{f_c}(y)^2(1 - \bar{\alpha}_\tau(y))\Big)\beta(y)\right)\mathrm{d}y \ge 0, \quad \forall \beta \in \mathcal{D}_0, \tag{C.2}$$

and the equality holds when $\beta = \bar{\alpha}_\tau$. Let $\varphi \in C_0^\infty(I_\tau)$ (where $C_0^\infty(I_\tau)$ is the set of indefinitely differentiable functions with compact support in I_τ). For h small enough, $\beta := \bar{\alpha}_\tau + h\varphi \in \mathcal{D}_0$ and one gets from (C.2)

$$\int_{I_\tau} \left(\frac{1}{\tau^2} \bar{\alpha}'_\tau(y)\varphi'(y) + \Big(\Theta^2 - \mathsf{f_c}(y)^2(1-\bar{\alpha}_\tau(y))\Big)\varphi(y) \right) \mathrm{d}y \geq 0.$$

Changing φ in $-\varphi$ gives the opposite sign and the equality for every $\varphi \in C_0^\infty(I_\tau)$. Therefore $\bar{\alpha}_\tau$ satisfies (C.1) in I_τ. Since $\bar{\alpha}_\tau$ is continuous and since $\mathsf{f_c}$ is indefinitely continuously differentiable, one deduces by induction that $\bar{\alpha}_\tau$ is also indefinitely continuously differentiable in I_τ. $\triangleleft$

(v) : *The support I_τ is an interval of the form $[0, \delta_\tau)$ with $0 < \delta_\tau \leq \infty$.* Let us prove by contradiction that there does not exist a connected component (a, b) of I_τ such that $0 < a < b \leq \infty$. If such a component exists, then $\bar{\alpha}_\tau(a) = \bar{\alpha}_\tau(b) = 0$ (even if $b = \infty$ because $\bar{\alpha}_\tau$ must tend to 0 at infinity in order to belong to $H^1(0,\infty)$). Let us prove that $\bar{\alpha}'_\tau(a) = 0$ by using (C.2). For $h > 0$ and small enough, let us consider the family of test functions β_h defined by $\beta_h(y) = 1 - |y-a|/h$ when $|y-a| \leq h$ and $\beta_h(y) = 0$ otherwise. Then (C.2) gives

$$0 \leq \frac{\alpha_\tau(a-h)}{h} + \frac{\alpha_\tau(a+h)}{h} \leq \tau^2 \int_{a-h}^{a+h} \Big(\Theta^2 - \mathsf{f_c}(y)^2(1-\bar{\alpha}_\tau(y))\Big)\beta_h(y)\,\mathrm{d}y.$$

Passing to the limit when h goes to 0 gives $\bar{\alpha}'_\tau(a-) = \bar{\alpha}'_\tau(a+)$ and hence $\bar{\alpha}_\tau$ is differentiable at a. But since $\bar{\alpha}_\tau \geq 0$ and $\bar{\alpha}_\tau(a) = 0$, this is possible if and only if $\bar{\alpha}'_\tau(a) = 0$. Therefore $\bar{\alpha}''_\tau(a+)$ must be non negative so that $\bar{\alpha}_\tau$ be positive in a neighborhood of a. Since $\bar{\alpha}''_\tau(a+) = \tau^2(\Theta^2 - \mathsf{f_c}(a)^2)$ by (C.1), since $\mathsf{f_c}$ is decreasing and since $0 < \bar{\alpha}_\tau \leq 1$ in (a,b), one gets

$$\alpha''_\tau(y) = \tau^2(\Theta^2 - \mathsf{f_c}(y)^2(1-\bar{\alpha}_\tau(y)) > \tau^2(\Theta^2 - \mathsf{f_c}(a)^2) \geq 0, \quad \forall y \in I_\tau.$$

Consequently $\bar{\alpha}'_\tau$ is increasing and hence positive in I_τ. Hence $\bar{\alpha}_\tau$ must be increasing in I_τ which is incompatible with $\bar{\alpha}_\tau(b) = 0$. This is the contradiction and therefore $a = 0$. Consequently, there exists a unique connected component and I_τ is an interval of the form $[0, \delta_\tau)$. $\triangleleft$

(vi) : *$\bar{\alpha}_\tau$ satisfies the boundary conditions $\bar{\alpha}'_\tau(0) = \bar{\alpha}_\tau(\delta_\tau) = \bar{\alpha}'_\tau(\delta_\tau) = 0$ and δ_τ is finite.* Taking $\beta = \bar{\alpha}_\tau$ in (C.2) which is then an equality, integrating by parts the first term in the integral and using (C.1) give $\bar{\alpha}'_\tau(0)\bar{\alpha}_\tau(0) = 0$. Since $\bar{\alpha}_\tau(0) > 0$, one obtains $\bar{\alpha}'_\tau(0) = 0$. If $\delta_\tau = \infty$, then the boundary conditions at δ_τ are a consequence of $\bar{\alpha}_\tau$ belongs to $H^1(0,\infty)$ and is indefinitely continuously differentiable. If $\delta_\tau < \infty$, integrating by parts the first term in the integral of (C.2) and using (C.1) leads to

$$\bar{\alpha}'_\tau(\delta_\tau-)\beta(\delta_\tau) + \tau^2 \int_{\delta_\tau}^{\infty} (\Theta^2 - \mathsf{f_c}(y)^2)\beta(y)\,\mathrm{d}y \geq 0, \quad \forall \beta \in \mathcal{D}_0.$$

This is possible if and only if $\bar{\alpha}'_\tau(\delta_\tau-) \geq 0$ and $\Theta \geq \mathsf{f_c}(y)$ for all $y \geq \delta_\tau$. But since $\bar{\alpha}_\tau(\delta_\tau) = 0$ and $\bar{\alpha}_\tau \geq 0$, one also has $\bar{\alpha}'_\tau(\delta_\tau-) \leq 0$. Hence $\bar{\alpha}'_\tau(\delta_\tau-) = 0$ and since $\bar{\alpha}'_\tau(\delta_\tau+) = 0$ one finally has $\bar{\alpha}'_\tau(\delta_\tau) = 0$.

From the inequality $\Theta \geq \mathsf{f_c}(y)$ for all $y \geq \delta_\tau$ one deduces that $\delta_\tau \geq \mathsf{f_c}^{-1}(\Theta)$. Integrating (C.1) over I_τ gives

$$\Theta^2\delta_\tau = \int_0^{\delta_\tau} \mathsf{f_c}(y)^2(1-\bar{\alpha}_\tau(y))\,\mathrm{d}y \leq \int_0^{\infty} \mathsf{f_c}(y)^2\,\mathrm{d}y < \infty \tag{C.3}$$

and hence δ_τ is finite. $\triangleleft$

(vii) : $\bar\alpha_\tau(y)$ *is monotonically decreasing from* $\bar\alpha_\tau(0) < 1$ *to 0 when* y *goes from* 0 *to* δ_τ. If $\bar\alpha_\tau(0) = 1$, then one should have both $\bar\alpha'_\tau(0) = 0$ and $\bar\alpha''_\tau(0) = \Theta^2 > 0$. Hence $\bar\alpha_\tau(y)$ should be greater than 1 for small positive y which is impossible. So, $\bar\alpha_\tau(1) < 1$. Let us show that there does not exist a point y where $\bar\alpha'_\tau(y) > 0$, by contradiction. If such a point exists, then by continuity there should exist a connected component (a, b) where $\bar\alpha'_\tau > 0$. Since $\bar\alpha'_\tau(0) = \bar\alpha'_\tau(\delta_\tau) = 0$, one should have $\bar\alpha'_\tau(a) = \bar\alpha'_\tau(b) = 0$. Consequently $\bar\alpha''_\tau(a) \geq 0$. But, by (C.1), $\bar\alpha''_\tau$ should be increasing in (a, b) (because $\mathsf{f_c}$ and $1 - \bar\alpha_\tau$ are decreasing). Therefore $\bar\alpha''_\tau$ should be positive and hence $\bar\alpha'_\tau$ should be increasing in (a, b). That is impossible, hence $\bar\alpha'_\tau \leq 0$ everywhere. $\triangleleft$

(viii) : *There exists a unique pair* $(\bar\alpha_\tau, \delta_\tau)$ *in* $\mathcal{D}_0 \times (0, +\infty)$ *which satisfies* (3.22)–(3.24). Let us first remark that (3.24) with $\bar\alpha_\tau = 0$ in (δ_τ, ∞) implies that

$$\frac{1}{\tau^2}\bar\alpha''_\tau(y) + \mathsf{f_c}(y)^2(1 - \bar\alpha_\tau(y)) \leq \Theta^2 \qquad \forall y \in (\delta_\tau, \infty). \tag{C.4}$$

Multiplying (3.22) and (C.4) by $\beta \in \mathcal{D}_0$, integrating over $(0, \delta_\tau) \cup (\delta_\tau, \infty)$, integrating by parts and using (3.23) leads to (C.2). Moreover the equality holds when $\beta = \bar\alpha_\tau$. Therefore $\bar\alpha_\tau \in \mathcal{D}_0$ is such that $\bar{\mathcal{P}}'_\tau(\bar\alpha_\tau)(\beta - \bar\alpha_\tau) \geq 0$ for all $\beta \in \mathcal{D}_0$ which is a characterization of the unique minimizer of $\bar{\mathcal{P}}_\tau$ over $\mathcal{D}_0$. $\triangleleft$ $\square$

C.2 Proof of Proposition 12

Proof. The proof is divided into 4 steps. The case for small and large times τ are distinguished.

(i) : *limit* $\bar\alpha_0$. Considering the test fields $\beta = \tau^2 exp(-y)$ in (3.25) leads to the estimation $\bar{\mathcal{P}}_\tau(\bar\alpha_\tau) \leq C$ which implies $\|\bar\alpha_\tau\|^2_{L^1} \leq C$ and $\|\bar\alpha'_\tau\|^2_{L^2} \leq C\tau^2$. Substracting $\bar{\mathcal{P}}_\tau(0)$ from (3.25), $\|\bar\alpha_\tau\|^2_{L^2} \leq C\tau^2$ and $\|\bar\alpha'_\tau\|^2_{L^2} \leq C\tau^4$. Therefore up to a subsequence $\frac{\bar\alpha_\tau}{\tau^2}$ (respectively $\bar\alpha_\tau$) converges weakly towards $\bar\alpha_0$ (respectively 0) in $H^1(\mathbb{R})$. Let us fix β in (C.2) and let τ tend towards 0, then

$$\int_0^\infty \Big(\bar\alpha'_0(y)\beta'(y) + \Big(\Theta^2 - \mathsf{f_c}(y)^2\Big)\beta(y)\Big)\,\mathrm{d}y \geq 0, \quad \forall \beta \in \mathcal{D}_0. \tag{C.5}$$

and the equality holds for $\beta = \bar\alpha_0$. Thus $\bar\alpha_0$ is uniquely defined, and the entire sequence $\bar\alpha_\tau$ converges weakly towards $\bar\alpha_0$. The strong convergence is a consequence of the weak convergences and (C.2) and (C.5).

$\triangleleft$

(ii) : *Limit* δ_0. From (C.3) δ_τ is bounded, then up to a subsequence it weakly converges in $\mathbb{R}$ towards δ_0. Passing to the limit in (C.3), as

$$\Theta^2\delta_0 = \int_0^{\delta_0} \mathsf{f_c}(y)^2\,\mathrm{d}y,$$

gives that δ_0 is uniquely defined, and the entire sequence δ_τ converges weakly towards δ_0. Finally

$$c\|\delta_\tau - \delta_0\|_{\mathbb{R}}^2 \leq \int_0^{\delta_\tau} \mathsf{f_c}(y)^2(1-\bar{\alpha}_\tau(y))\,\mathrm{d}y - \int_0^{\delta_0} \mathsf{f_c}(y)^2\,\mathrm{d}y$$

which converges towards zero, and thus the convergence is strong. $\triangleleft$

(iii) : *Limit* $\bar{\alpha}_\infty$. Taking the test field $\beta = exp(-y)$, that vanishes as y tends towards infinity, leads to the following estimations Proposition 11 leads to :

$$\int_0^\infty \frac{1}{2}\mathsf{f_c}(y)^2(1-\bar{\alpha}_\tau(y))^2 + \Theta^2\bar{\alpha}_\tau(y)\,\mathrm{d}y \leq C$$

and thus $\int_0^\infty \mathsf{f_c}(y)^2\bar{\alpha}_\tau(y)^2\,\mathrm{d}y \leq C$ and $\int_0^\infty \bar{\alpha}_\tau(y)\,\mathrm{d}y \leq C$. Since $\mathsf{f_c}$ is indefinitely continuously differentiable $\|\bar{\alpha}_\tau\|_{L^2}^2 \leq C$ and thus up to a subsequence $\bar{\alpha}_\tau$ converges weekly towards $\bar{\alpha}_\infty$ in L^2. Fixing β in (C.2) and letting τ grow to infinity :

$$\int_0^\infty \Big(\Big(\Theta^2 - \mathsf{f_c}(y)^2(1-\bar{\alpha}_\infty(y))\Big)\beta(y)\Big)\,\mathrm{d}y \geq 0, \quad \forall \beta \in \{\beta \in L^2(0,\infty) \,:\, 0 \leq \beta\}, \tag{C.6}$$

where the equality holds $\beta = \bar{\alpha}_\infty$. Thus $\bar{\alpha}_\infty$ is uniquely (and given by (3.28)) defined and the entire sequence $\bar{\alpha}_\tau$ converges weakly towards it. The strong convergence is given by:

$$\begin{aligned} c\|\bar{\alpha}_\tau - \bar{\alpha}_\infty\|_{L^2}^2 &\leq \int_0^\infty \mathsf{f_c}(y)(\bar{\alpha}_\tau - \bar{\alpha}_\infty)^2\,\mathrm{d}y & \text{(C.7)}\\ &\leq \int_0^\infty \mathsf{f_c}(y)\left(\bar{\alpha}_\tau(y)^2 + \bar{\alpha}_\infty(y)^2 - 2\bar{\alpha}_\tau(y)\bar{\alpha}_\infty(y)\right)\,\mathrm{d}y + \int_0^\infty \frac{1}{\tau^2}\bar{\alpha}_\tau'(y)^2\,\mathrm{d}y & \text{(C.8)}\end{aligned}$$

using (C.2) with $\beta = \bar{\alpha}_\tau$ and (C.6) with $\beta = \bar{\alpha}_\tau$ and $\beta = \bar{\alpha}_\infty$.

$$c\|\bar{\alpha}_\tau - \bar{\alpha}_\infty\|_{L^2}^2 \leq \int_0^\infty (\Theta^2 - \mathsf{f_c}(y))(\bar{\alpha}_\tau(y) - \bar{\alpha}_\infty(y))\,\mathrm{d}y$$

where the second member tends towards zero by virtue of the weak convergence. $\triangleleft$

(iv) : *Limit* δ_∞. From (C.3) δ_τ is bounded, then up to a subsequence it converges weakly in $\mathbb{R}$ towards δ_∞. Passing to the limit in (C.3), as

$$\Theta^2\delta_\infty = \int_0^{\delta_\infty} \mathsf{f_c}(y)^2(1-\bar{\alpha}_\infty(y))\,\mathrm{d}y$$

δ_∞ is uniquely defined and the entire subsequence converges weakly in $\mathbb{R}$.$\triangleleft$ $\square$

C.3 Proof of Proposition 13

Proof. The three items (IR), (ST) and (EB) give the following necessary conditions for $(\dot{\mathbf{u}}, \dot{\alpha})$:

1. By (IR), $\dot\alpha \geq 0$ and hence $(\dot{\mathbf{u}}, \dot\alpha) \in \mathcal{C}\times\mathcal{D}_+$;

2. The stability condition (ST) implies the first order stability conditions which at time $t+h$ read as

$$\forall (\mathbf{v},\beta) \in \mathcal{C}\times\mathcal{D}_+, \qquad \mathcal{P}'_{t+h}(\mathbf{u}_{t+h},\alpha_{t+h})(\mathbf{v},\beta) \geq 0. \tag{C.9}$$

   Let us discriminate between two types of direction:

   (a) For the directions $(\mathbf{v},\beta)$ such that $\mathcal{P}'_t(\mathbf{u}^*_t,\alpha^*_t)(\mathbf{v},\beta) > 0$, by continuity the inequality (C.9) holds for h small enough and hence (ST) is satisfied.

   (b) Considering the directions $(\mathbf{v},\beta)$ such that $\mathcal{P}'_t(\mathbf{u}^*_t,\alpha^*_t)(\mathbf{v},\beta) = 0$. By virtue of (1.16)-(1.27) they correspond to the directions such that $\beta = 0$ in the undamaged domain at time t $\Omega^e_t = \Omega \setminus \Omega^d_t$. Dividing the inequality (C.9) by h and passing to the limit when h goes to 0 give the following inequality that the $(\dot{\mathbf{u}},\dot\alpha)$ rate must satisfy

$$\forall (\mathbf{v},\beta) \in \mathcal{C}\times\mathcal{D}_+ \quad \mathcal{P}''_t(\mathbf{u}^*_t,\alpha^*_t)\,\langle (\dot{\mathbf{u}},\dot\alpha),(\mathbf{v},\beta)\rangle + \dot{\mathcal{P}}'_t(\mathbf{u}^*_t,\alpha^*_t)(\mathbf{v},\beta) \geq 0. \tag{C.10}$$

   In (C.10), $\mathcal{P}''_t(\mathbf{u}^*_t,\alpha^*_t)$ represents the symmetric bilinear form associated with the quadratic form defined in (3.11), while $\dot{\mathcal{P}}'_t(\mathbf{u}^*_t,\alpha^*_t)$ is the linear form given by (3.12).

3. From the Kuhn-Tucker conditions in the bulk at time t, see Proposition 10, $\dot\alpha = 0$ in Ω^e_t. The energy balance (EB) reads at time $t+h$

$$\begin{aligned} 0 &= \mathcal{P}_{t+h}(\boldsymbol{\chi}_{t+h}) - \mathcal{P}_t(\boldsymbol{\chi}^*_t) + \int_t^{t+h}\int_\Omega \boldsymbol{\sigma}_s \cdot \dot{\boldsymbol{\varepsilon}}^{\rm th}_s \,\mathrm{d}\mathbf{x}\,\mathrm{d}s \\ &= \mathcal{P}_{t+h}(\boldsymbol{\chi}_{t+h}) - \mathcal{P}_{t+h}(\boldsymbol{\chi}^*_t) + \mathcal{P}_{t+h}(\boldsymbol{\chi}^*_t) - \mathcal{P}_t(\boldsymbol{\chi}^*_t) + \int_t^{t+h}\int_\Omega \boldsymbol{\sigma}_s \cdot \dot{\boldsymbol{\varepsilon}}^{\rm th}_s \,\mathrm{d}\mathbf{x}\,\mathrm{d}s \end{aligned} \tag{C.11}$$

   where $\boldsymbol{\sigma}_s = (1-\alpha_s)^2\mathsf{A}(\boldsymbol{\varepsilon}(\mathbf{u}_s) - \boldsymbol{\varepsilon}^{\rm th}_s)$, $\boldsymbol{\chi}_{t+h} = (\mathbf{u}_{t+h},\alpha_{t+h})$ and $\boldsymbol{\chi}^*_t = (\mathbf{u}^*_t,\alpha^*_t)$. A first expansion of (C.11) gives

$$\begin{aligned} 0 &= \mathcal{P}'_{t+h}(\boldsymbol{\chi}^*_t)(\boldsymbol{\chi}_{t+h} - \boldsymbol{\chi}^*_t) + \frac{1}{2}\mathcal{P}''_{t+h}(\boldsymbol{\chi}^*_t)(\boldsymbol{\chi}_{t+h} - \boldsymbol{\chi}^*_t) + \mathcal{P}_{t+h}(\boldsymbol{\chi}^*_t) - \mathcal{P}_t(\boldsymbol{\chi}^*_t) \\ &\quad + \int_t^{t+h}\int_\Omega \boldsymbol{\sigma}_s \cdot \dot{\boldsymbol{\varepsilon}}^{\rm th}_s \,\mathrm{d}\mathbf{x}\,\mathrm{d}s + o(\|\boldsymbol{\chi}_{t+h} - \boldsymbol{\chi}^*_t\|^2) \end{aligned} \tag{C.12}$$

   where $\mathcal{P}''_t(\boldsymbol{\chi}^*_t)$ is the quadratic form defined in (3.11), $\|\cdot\|$ denotes the natural norm on $\mathcal{C}\times\mathcal{D}$. A second expansion leads to

$$\begin{aligned} 0 &= \mathcal{P}'_t(\boldsymbol{\chi}^*_t)(\boldsymbol{\chi}_{t+h} - \boldsymbol{\chi}^*_t) + h^2\dot{\mathcal{P}}'_t(\boldsymbol{\chi}^*_t)(\dot{\boldsymbol{\chi}}) + \frac{h^2}{2}\mathcal{P}''_t(\boldsymbol{\chi}^*_t)(\dot{\boldsymbol{\chi}}) + h\dot{\mathcal{P}}_t(\boldsymbol{\chi}^*_t) + \frac{h^2}{2}\ddot{\mathcal{P}}_t(\boldsymbol{\chi}^*_t) \\ &\quad + h\int_\Omega \boldsymbol{\sigma}^*_t \cdot \dot{\boldsymbol{\varepsilon}}^{\rm th}_t \,\mathrm{d}\mathbf{x} + \frac{h^2}{2}\int_\Omega (\boldsymbol{\sigma}^*_t \cdot \ddot{\boldsymbol{\varepsilon}}^{\rm th}_t + \dot{\boldsymbol{\sigma}}^*_t \cdot \dot{\boldsymbol{\varepsilon}}^{\rm th}_t)\,\mathrm{d}\mathbf{x} + o(h^2) \end{aligned} \tag{C.13}$$

   where $\dot{\boldsymbol{\chi}} = (\dot{\mathbf{u}},\dot\alpha)$ and $\dot{\boldsymbol{\sigma}}$ is the right derivative of $t \mapsto \boldsymbol{\sigma}_t$ at t. Let us examine the different terms of (C.13):

(a) Using (1.1), (1.13), (1.16), (3.19)–(3.23), one gets

$$\mathcal{P}'_t(\boldsymbol{\chi}^*_t)(\boldsymbol{\chi}_{t+h} - \boldsymbol{\chi}^*_t) = \int_{\Omega^d_{t+h}\setminus\Omega^d_t} \left(\mathsf{w}_1 - \mathsf{Ea}^2\vartheta^2\,{\mathsf{f}_\mathsf{c}}^2\left(\frac{x_2}{2\sqrt{\mathsf{k}_\mathsf{c}t}}\right)\right)\alpha_{t+h}(\mathbf{x})\,\mathrm{d}\mathbf{x}.$$

By virtue of Hypotheses 7 and 9, α_{t+h} is continuously differentiable and vanishes outside Ω^d_t. Therefore $\max_{\Omega^d_{t+h}\setminus\Omega^d_t}|\alpha_{t+h}| = o(h)$ since $\Omega^d_{t+h}\setminus\Omega^d_t$ is included in a strip of width Ch. Hence $\mathcal{P}'_t(\boldsymbol{\chi}^*_t)(\boldsymbol{\chi}_{t+h} - \boldsymbol{\chi}^*_t) = o(h^2)$ (in the case of the fundamental branch, this term is of the order of h^3);

(b) By virtue of (3.8), $\dot{\mathcal{P}}_t(\boldsymbol{\chi}^*_t) = -\int_\Omega \boldsymbol{\sigma}^*_t \cdot \dot{\boldsymbol{\varepsilon}}^{\mathrm{th}}_t\,\mathrm{d}\mathbf{x}$;

(c) By virtue of (3.9), $\ddot{\mathcal{P}}_t(\boldsymbol{\chi}^*_t) = \int_\Omega((1-\alpha^*_t)^2\mathsf{A}\dot{\boldsymbol{\varepsilon}}^{\mathrm{th}}_t\cdot\dot{\boldsymbol{\varepsilon}}^{\mathrm{th}}_t - \boldsymbol{\sigma}^*_t\cdot\ddot{\boldsymbol{\varepsilon}}^{\mathrm{th}}_t)\,\mathrm{d}\mathbf{x}$.

Using all these calculations, dividing (C.13) by h^2 and passing to the limit when h goes to 0, one finally obtains

$$\mathcal{P}''_t(\boldsymbol{\chi}^*_t)(\dot{\boldsymbol{\chi}}) + \dot{\mathcal{P}}'_t(\boldsymbol{\chi}^*_t)(\dot{\boldsymbol{\chi}}) = 0. \tag{C.14}$$

where by virtue of (3.12), $\dot{\mathcal{P}}'_t(\boldsymbol{\chi}^*_t)(\dot{\boldsymbol{\chi}}) = -\int_\Omega(\dot{\boldsymbol{\sigma}}\cdot\dot{\boldsymbol{\varepsilon}}^{\mathrm{th}}_t + (1-\alpha^*_t)^2\mathsf{A}\dot{\boldsymbol{\varepsilon}}^{\mathrm{th}}_t\cdot\dot{\boldsymbol{\varepsilon}}^{\mathrm{th}}_t)\,\mathrm{d}\mathbf{x}$.

Equation (3.31) is a direct consequence of (C.10) and (C.14). □

C.4 Proof of Proposition 15

Proof. $\|\cdot\|$ denotes indiscriminately the natural norm on $H^1(\Omega)$ and $H^1(\Omega)^2$. Let $s \in (t, t+t')$, $(\mathbf{v},\beta) \in \mathcal{C}\times\dot{\mathcal{D}}^+_s$, $(\mathbf{v},\beta)\neq(0,0)$ and let h be a small positive real number. Expanding with respect to h up to the second order gives

$$\mathcal{P}_s(\mathbf{u}_s + h\mathbf{v}, \alpha_s + h\beta) = \mathcal{P}_s(\mathbf{u}_s,\alpha_s) + \mathcal{P}'_s(\mathbf{u}_s,\alpha_s)(\mathbf{v},\beta) + \frac{1}{2}\mathcal{P}''_s(\mathbf{u}_s,\alpha_s)(\mathbf{v},\beta) + \wr(h)$$

Since the evolution is stationary, $\mathcal{P}'_t(\mathbf{u}_s,\alpha_s)(\mathbf{v},\beta)\geq 0$. Thus it is sufficient to prove $\mathcal{P}''_t(\mathbf{u}_s,\alpha_s)(\mathbf{v},\beta) > 0$ for proving the stability of $(\mathbf{u}_s,\alpha_s)$ in the direction $(\mathbf{v},\beta)$. By continuity the quadratic form $\mathcal{P}''_t(\mathbf{u}_s,\alpha_s)$ converges to the quadratic form $\mathcal{P}''_t(\mathbf{u}_t,\alpha_t)$ when s tends to t and

$$\forall(\mathbf{v},\beta)\in\mathcal{C}\times H^1(\Omega) \qquad |\left(\mathcal{P}''_s(\mathbf{u}_s,\alpha_s) - \mathcal{P}''_t(\mathbf{u}^*_t,\alpha^*_t)\right)(\mathbf{v},\beta)| \leq \mathcal{O}(s-t)(\|\mathbf{v}\|^2 + \|\beta\|^2)$$

where $\mathcal{O}(\cdot)$ is bounded on $[0,t')$ and $\lim_{\varsigma\to 0}\mathcal{O}(\varsigma) = 0$. Therefore it is sufficient to prove that there exist C_t such that

$$\forall(\mathbf{v},\beta)\in\mathcal{C}\times\dot{\mathcal{D}}^+_t \qquad \mathcal{P}''_t(\mathbf{u}^*_t,\alpha^*_t)(\mathbf{v},\beta) \geq C_t(\|\mathbf{v}\|^2 + \|\beta\|^2) \tag{C.15}$$

Indeed, in such a case for t' sufficiently small one has for all $s\in(t,t+t')$

$$\mathcal{P}''_s(\mathbf{u}_s,\alpha_s)(\mathbf{v},\beta) \geq (C_t - \mathcal{O}(s-t))(\|\mathbf{v}\|^2 + \|\beta\|^2) > 0$$

Since $t < t_s$ the state $(\mathbf{u}_t^*, \alpha_t^*)$ is stable and $\mathsf{R}_t^s = \min_{\mathcal{C}\times\dot{\mathcal{D}}_t^+} \mathcal{R}_t^* > 1$. By definition of see (3.37),

$$\forall (v,\beta) \in \mathcal{C}\times\dot{\mathcal{D}}_t^+ \qquad \mathcal{P}_t''(\mathbf{u}_t^*, \alpha_t^*)(\mathbf{v},\beta) \geq \left(1 - \frac{1}{\mathsf{R}_t^s}\right) \mathcal{A}_t^*(\mathbf{v},\beta) \geq 0$$

with the equality to 0 if and only if $(\mathbf{v},\beta) = (0,0)$. Thus (C.15) is obtained. □

C.5 Proof of Proposition 17

Proof. Throughout the proof the notations of Section 3.4.3 are used.

1. By virtue of the positivity of the sum of the first two terms in the right hand side of (3.45) and since $\mathsf{f_c} \leq 1$ everywhere, one gets

$$\bar{\mathcal{R}}_\tau^\kappa(\mathbf{V},\beta) \geq \frac{1}{3\delta_\tau^2\tau^2} \frac{\int_0^1 \beta'^2 \,\mathrm{d}\zeta}{\int_0^1 \beta^2 \,\mathrm{d}\zeta}, \quad \forall\, \mathbf{V} \in \mathbf{H}, \quad \forall \beta \in \mathcal{H}_0 \setminus \{0\}$$

and hence

$$\min_{\mathbf{H}\times\mathcal{H}_0} \bar{\mathcal{R}}_\tau^\kappa \geq \frac{1}{3\delta_\tau^2\tau^2} \min_{\beta\in\mathcal{H}_0\setminus\{0\}} \frac{\int_0^1 \beta'^2 \,\mathrm{d}\zeta}{\int_0^1 \beta^2 \,\mathrm{d}\zeta} = \frac{\pi^2}{12\delta_\tau^2\tau^2}.$$

Since, by Proposition 12, δ_τ varies continuously from δ_0 to δ_∞, $\max_\tau \delta_\tau < \infty$ and the result follows.

2. It is a direct consequence of the previous estimate, of the definition (3.47) of τ and of the definition (3.44) of R_t^b.

3. Let us consider the following pair $(\mathbf{v},\beta)$ in $\mathcal{C}\times\dot{\mathcal{D}}_t^+$:

$$\beta(\mathbf{x}) = \check{\beta}(\zeta)\Big(1 + \cos(k\pi\frac{x_1}{\mathsf{L}})\Big), \qquad \mathbf{v}(\mathbf{x}) = 2\mathsf{a}\vartheta\delta_\tau\sqrt{\mathsf{k_c}t}\,\check{V}(\zeta)\sin(k\pi\frac{x_1}{\mathsf{L}})\mathbf{e}_1,$$

where $\check{\beta} \in \mathcal{H}_0 \cap \{\beta \geq 0\}$, $\check{V} \in H^1(0,\infty)$ and $k \in \mathbb{N}_*$. Inserting into (3.37) and using (3.45)–(3.46) give

$$\mathsf{R}_t^s \leq \mathcal{R}_t^*(\mathbf{v},\beta) = \frac{2\bar{\mathcal{A}}_\tau^0(\mathbf{0},\check{\beta}) + \bar{\mathcal{A}}_\tau^\kappa(\check{V}\mathbf{e}_1,\check{\beta})}{3\bar{\mathcal{B}}_\tau(\check{\beta})}.$$

After some calculations, one gets $3\bar{\mathcal{B}}_\tau(\check{\beta}) = 9\int_0^1 \mathsf{f_c}(\delta_\tau\zeta)^2\check{\beta}(\zeta)^2\,\mathrm{d}\zeta$ and

$$\begin{aligned} 2\bar{\mathcal{A}}_\tau^0(\mathbf{0},\check{\beta}) + \bar{\mathcal{A}}_\tau^\kappa(\check{V}\mathbf{e}_1,\check{\beta}) \;=\; & \int_0^\infty (1-\bar{\alpha}_\tau(\delta_\tau\zeta))^2 \left(\frac{\kappa^2\check{V}(\zeta)^2}{1-\nu^2} + \frac{\check{V}'(\zeta)^2}{2(1+\nu)}\right) \mathrm{d}\zeta \\ & + \int_0^1 \Big(-4(1-\bar{\alpha}_\tau(\delta_\tau\zeta))\mathsf{f_c}(\delta_\tau\zeta)\kappa\check{V}(\zeta)\check{\beta}(\zeta) + 12\mathsf{f_c}(\delta_\tau\zeta)^2\check{\beta}(\zeta)^2\Big)\,\mathrm{d}\zeta \\ & + \frac{1}{\delta_\tau^2\tau^2}\int_0^1 \Big(\kappa^2\check{\beta}(\zeta)^2 + 3\check{\beta}'(\zeta)^2\Big)\,\mathrm{d}\zeta. \end{aligned}$$

Taking

$$\check{V}(\zeta) = \frac{1-\nu^2}{\kappa}\frac{\mathsf{f_c}(\delta_\tau\zeta)}{1-\bar{\alpha}_\tau(\delta_\tau\zeta)}\check{\beta}(\zeta)$$

and passing to the limit when $t \to \infty$ yields

$$\lim_{t\to\infty} \mathsf{R}_t^s \leq \frac{8-4\nu^2}{9} + \frac{C(\check{\beta})}{\kappa^2},$$

where $C(\check{\beta})$ depends on $\check{\beta}$ but not on κ. Passing to the limit when κ goes to ∞ gives the desired inequality for R_t^s. Since $\mathsf{R}_t^b \leq \mathsf{R}_t^s$ (Remark 9) the result follows.

4. When $\kappa = 0$, the crossed term of β with $\mathbf{V}$ vanishes in $\bar{\mathcal{R}}_\tau^\kappa(\mathbf{V},\beta)$. Therefore, $\mathbf{V} = \mathbf{0}$ is the minimizer of $\mathcal{R}_\tau^0$ at every $\tau > 0$. Accordingly, one gets

$$\min_{\mathbf{H}\times\mathcal{H}_0} \mathcal{R}_\tau^0 = \frac{4}{3} + \frac{1}{3\delta_\tau^2\tau^2} \min_{\beta\in\mathcal{H}_0\setminus\{0\}} \frac{\int_0^1 \beta'(\zeta)^2\,\mathrm{d}\zeta}{\int_0^1 \mathsf{f_c}(\delta_\tau\zeta)^2\beta(\zeta)^2\,\mathrm{d}\zeta},$$

from which one easily deduces the announced property.

5. The behavior of $\min_{\mathbf{H}\times\mathcal{H}_0} \bar{\mathcal{R}}_\tau^\kappa$ when κ goes to infinity is a problem of singular perturbation in which the sequence of minimizers degenerates. So, this asymptotic behavior is obtained by a direct approach. First, one deduces from (3.45)-(3.46) the following estimate:

$$\bar{\mathcal{R}}_\tau^\kappa(\mathbf{V},\beta) \geq \frac{\kappa^2}{3\delta_\tau^2\tau^2}\frac{\int_0^1 \beta(\zeta)^2\,\mathrm{d}\zeta}{\int_0^1 \mathsf{f_c}(\delta_\tau\zeta)^2\beta(\zeta)^2\,\mathrm{d}\zeta} > \frac{\kappa^2}{3\delta_\tau^2\tau^2}, \qquad \forall\,(\mathbf{V},\beta)\in\mathbf{H}\times(\mathcal{H}_0\setminus\{0\}),$$

where the second inequality is due to $\mathsf{f_c} < 1$ in $(0,1)$. Therefore one obtains the following lower bound for the limit of the minimum when $\kappa \to \infty$:

$$\lim_{\kappa\to\infty} \frac{\min_{\mathbf{H}\times\mathcal{H}_0} \bar{\mathcal{R}}_\tau^\kappa}{\kappa^2} \geq \frac{1}{3\delta_\tau^2\tau^2}.$$

It remains to construct a minimizing sequence such that the equality holds at the limit. Let β^κ be the sequence defined by $\beta^\kappa(\zeta) = \max\{1-\kappa\zeta, 0\}$. Hence $\beta^\kappa \in \mathcal{H}_0$ and $\bar{\mathcal{R}}_\tau^\kappa(\mathbf{0},\beta^\kappa)/\kappa^2$ is given by

$$\frac{\bar{\mathcal{R}}_\tau^\kappa(\mathbf{0},\beta^\kappa)}{\kappa^2} = \frac{1}{3\delta_\tau^2\tau^2}\frac{\int_0^{1/\kappa}(1-\kappa\zeta)^2\,\mathrm{d}\zeta + 1/\kappa}{\int_0^{1/\kappa}\mathsf{f_c}(\delta_\tau\zeta)(1-\kappa\zeta)^2\,\mathrm{d}\zeta} + \frac{4}{3\kappa^2}$$

and passing to the limit yields

$$\lim_{\kappa\to\infty} \frac{\bar{\mathcal{R}}_\tau^\kappa(\mathbf{0},\beta^\kappa)}{\kappa^2} = \frac{1}{3\delta_\tau^2\tau^2}.$$

The proof is complete. □

Bibliography

[Abdelmoula *et al.* 2010] R. Abdelmoula, J.-J. Marigo and T. Weller. *Construction and justification of Paris-like fatigue laws from Dugdale-type cohesive models.* Annals of Solid and Structural Mechanics, vol. 1, pages 139–158, 2010. 10.1007/s12356-010-0011-3. (Cited on page 67.)

[Alessi *et al.* 2013] R. Alessi, J.-J. Marigo and S. Vidoli. Nucleation of cohesive cracks in gradient damage models with plasticity. 2013. (Cited on page 68.)

[Ambrosio & Tortorelli 1990] L. Ambrosio and V. M. Tortorelli. *Approximation of functional depending on jumps by elliptic functional via t-convergence.* Communications on Pure and Applied Mathematics, vol. 43, no. 8, pages 999–1036, 1990. (Cited on page 46.)

[Ambrosio 1990] L. Ambrosio. *Existence theory for a new class of variational problems.* Archive for Rational Mechanics and Analysis, vol. 111, no. 4, pages 291–322, 1990. (Cited on pages 12 and 29.)

[Amestoy & Leblond 1992] M. Amestoy and J. Leblond. *Crack paths in plane situations II. Detailed form of the expansion of the stress intensity factors.* International Journal of Solids and Structures, vol. 29, no. 4, pages 465 – 501, 1992. (Cited on page 68.)

[Amor *et al.* 2009] H. Amor, J.-J. Marigo and C. Maurini. *Regularized formulation of the variational brittle fracture with unilateral contact: Numerical experiments.* Journal of the Mechanics and Physics of Solids, vol. 57, no. 8, pages 1209 – 1229, 2009. (Cited on page 28.)

[Bahr *et al.* 1986] H. A. Bahr, G. Fischer and H. J. Weiss. *Thermal-shock crack patterns explained by single and multiple crack propagation.* Journal of Materials Science, vol. 21, pages 2716–2720, 1986. (Cited on page 121.)

[Bahr *et al.* 1988] H.-A. Bahr, H.-J. Weiss, H. Maschke and F. Meissner. *Multiple crack propagation in a strip caused by thermal shock.* Theoretical and Applied Fracture Mechanics, vol. 10, no. 3, pages 219 – 226, 1988. (Cited on page 72.)

[Bahr *et al.* 2010] H.-A. Bahr, H.-J. Weiss, U. Bahr, M. Hofmann, G. Fischer, S. Lampenscherf and H. Balke. *Scaling behavior of thermal shock crack patterns and tunneling cracks driven by cooling or drying.* Journal of the Mechanics and Physics of Solids, vol. 58, no. 9, pages 1411 – 1421, 2010. (Cited on pages 72, 73, 103, 119, 121, 124, 126, 133, 134 and 136.)

[Balay *et al.* 1997] S. Balay, W. D. Gropp, L. C. McInnes and B. F. Smith. *Efficient Management of Parallelism in Object Oriented Numerical Software Libraries.* In E. Arge, A. M. Bruaset and H. P. Langtangen, editeurs, Modern Software Tools in Scientific Computing, pages 163–202. Birkhäuser Press, 1997. (Cited on page 31.)

[Balay *et al.* 2012a] S. Balay, J. Brown, , K. Buschelman, V. Eijkhout, W. D. Gropp, D. Kaushik, M. G. Knepley, L. C. McInnes, B. F. Smith and H. Zhang. *PETSc Users Manual*. Rapport technique ANL-95/11 - Revision 3.3, Argonne National Laboratory, 2012. (Cited on page 31.)

[Balay *et al.* 2012b] S. Balay, J. Brown, K. Buschelman, W. D. Gropp, D. Kaushik, M. G. Knepley, L. C. McInnes, B. F. Smith and H. Zhang. *PETSc Web page*, 2012. http://www.mcs.anl.gov/petsc. (Cited on page 31.)

[Bazant *et al.* 1979] Z. Bazant, H. Ohtsubo and K. Aoh. *Stability and post-critical growth of a system of cooling or shrinkage cracks*. International Journal of Fracture, vol. 15, no. 5, pages 443–456, 1979. (Cited on page 72.)

[Benallal & Marigo 2007] A. Benallal and J.-J. Marigo. *Bifurcation and stability issues in gradient theories with softening*. Modelling and Simulation in Materials Science and Engineering, vol. 15, no. 1, page S283, 2007. (Cited on pages 8, 12, 24 and 82.)

[Benallal *et al.* 1993] A. Benallal, R. Billardon and G. Geymonat. *Bifurcation and localization in rate independent materials*. Bifurcation and Stability of Dissipative Systems, CISM Lecture Notes, Springer, 1993. (Cited on page 7.)

[Bérest *et al.* 2012] P. Bérest, H. Djakeun-Djizann, B. Brouard and G. Hévin. *Rapid Depressurizations: can they lead to irreversible damage?* In SMRI Spring 2012 Technical Conference, 2012. (Cited on page 72.)

[Bérest *et al.* 2013] P. Bérest, H. Djakeun-Djizanne, B. Brouard and A. Frangi. *A simplified solution for Gas Flow during a Blow-out in an H2 or air storage cavern*. In Technical Conference Book, Proceedings SMRI Spring Conference, Lafayette, Louisiana, pages 125–144, 2013. (Cited on pages 129, 130 and 131.)

[Bernard *et al.* 2012] P. Bernard, N. Moës and N. Chevaugeon. *Damage growth modeling using the Thick Level Set (TLS) approach: Efficient discretization for quasi-static loadings*. Computer Methods in Applied Mechanics and Engineering, vol. 233 - 236, pages 11 – 27, 2012. (Cited on page 32.)

[Bisschop & Van Mier 2002a] J. Bisschop and J. Van Mier. *Effect of aggregates on drying shrinkage microcracking in cement-based composites*. Materials and Structures, vol. 35, no. 8, pages 453–461, 2002. (Cited on page 135.)

[Bisschop & Van Mier 2002b] J. Bisschop and J. Van Mier. *How to study drying shrinkage microcracking in cement-based materials using optical and scanning electron microscopy?* Cement and Concrete Research, vol. 32, no. 2, pages 279 – 287, 2002. (Cited on page 135.)

[Bisschop & Wittel 2011] J. Bisschop and F. K. Wittel. *Contraction gradient induced microcracking in hardened cement paste*. Cement and Concrete Composites, vol. 33, no. 4, pages 466 – 473, 2011. (Cited on page 72.)

[Bisschop 2002] J. Bisschop. *Drying shrinkage microcracking in cement-based materials.* PhD thesis, 2002. (Cited on pages 135 and 136.)

[Bourdin *et al.* 2000] B. Bourdin, G. Francfort and J.-J. Marigo. *Numerical experiments in revisited brittle fracture.* Journal of the Mechanics and Physics of Solids, vol. 48, no. 4, pages 797 – 826, 2000. (Cited on pages 8, 12, 29, 58, 68 and 139.)

[Bourdin *et al.* 2008] B. Bourdin, G. Francfort and J.-J. Marigo. *The Variational Approach to Fracture.* Journal of Elasticity, vol. 91, no. 1-3, pages 5–148, 2008. (Cited on pages 29, 30, 31 and 46.)

[Bourdin *et al.* 2013] B. Bourdin, J.-J. Marigo, C. Maurini and P. Sicsic. Morphogenesis and propagation of complex cracks induced by thermal shocks. In Preparation, 2013. (Cited on pages 125 and 127.)

[Bourdin 2007] B. Bourdin. *Numerical implementation of the variational formulation for quasi-static brittle fracture.* Interfaces and Free Boundaries, vol. 9, pages 411—430, 2007. (Cited on pages 31, 46, 47 and 116.)

[Braides 1998] A. Braides. Approximation of free-discontinuity problems. Lecture notes in Mathematics, vol. **1694**. Springer, 1998. (Cited on page 29.)

[Braides 2002] A. Braides. γ-convergence for beginners. Oxford Lecture Series in Mathematics and its Applications **22**. Oxford University Press, Oxford, 2002. (Cited on pages 29 and 46.)

[Cazes *et al.* 2009] F. Cazes, M. Coret, A. Combescure and A. Gravouil. *A thermodynamic method for the construction of a cohesive law from a nonlocal damage model.* International Journal of Solids and Structures, vol. 46, no. 6, pages 1476 – 1490, 2009. (Cited on page 67.)

[Chambolle *et al.* 2009] A. Chambolle, G. Francfort and J.-J. Marigo. *When and how do cracks propagate?* Journal of the Mechanics and Physics of Solids, vol. 57, no. 9, pages 1614 – 1622, 2009. (Cited on page 29.)

[Charlotte *et al.* 2006] M. Charlotte, J. Laverne and J.-J. Marigo. *Initiation of cracks with cohesive force models: a variational approach.* European Journal of Mechanics - A/Solids, vol. 25, no. 4, pages 649 – 669, 2006. (Cited on page 30.)

[Chertkov 2002] V. Y. Chertkov. *Modelling cracking stages of saturated soils as they dry and shrink.* European Journal of Soil Science, vol. 53, no. 1, pages 105–118, 2002. (Cited on page 72.)

[Comi & Perego 2001] C. Comi and U. Perego. *Fracture energy based bi-dissipative damage model for concrete.* International Journal of Solids and Structures, vol. 38, no. 36â37, pages 6427 – 6454, 2001. (Cited on page 36.)

[Comi 1999] C. Comi. *Computational modelling of gradient-enhanced damage in quasi-brittle materials.* Mechanics of Cohesive-frictional Materials, vol. 4, no. 1, pages 17–36, 1999. (Cited on pages 8 and 12.)

[Cousteix & Mauss 2006] J. Cousteix and J. Mauss. Analyse asymptotique et couche limite, volume 56. Springer Verlag, 2006. (Cited on page 8.)

[Dacorogna 2008] B. Dacorogna. Direct methods in the calculus of variations, volume 78. Springer, 2008. (Cited on page 21.)

[Dauge 1988] M. Dauge. Elliptic boundary value problems on corner domains: Smoothness and asymptotics of solutions. Lecture notes in Mathematics. Springer-Verlag, 1988. (Cited on page 40.)

[Dormieux & Kondo 2004] L. Dormieux and D. Kondo. *Approche micromécanique du couplage perméabilité endommagement.* Comptes Rendus Mécanique, vol. 332, no. 2, pages 135 – 140, 2004. (Cited on page 75.)

[Dormieux *et al.* 2006] L. Dormieux, D. Kondo and F.-J. Ulm. *A micromechanical analysis of damage propagation in fluid-saturated cracked media.* Comptes Rendus Mécanique, vol. 334, no. 7, pages 440 – 446, 2006. (Cited on page 75.)

[Dunn *et al.* 1997] M. L. Dunn, W. Suwito and S. Cunningham. *Fracture initiation at sharp notches: Correlation using critical stress intensities.* International Journal of Solids and Structures, vol. 34, no. 29, pages 3873 – 3883, 1997. (Cited on page 36.)

[Francfort & Marigo 1998] G. Francfort and J.-J. Marigo. *Revisiting brittle fracture as an energy minimization problem.* Journal of the Mechanics and Physics of Solids, vol. 46, no. 8, pages 1319 – 1342, 1998. (Cited on pages 8, 11, 28, 30 and 33.)

[Gauthier *et al.* 2010] G. Gauthier, V. Lazarus and L. Pauchard. *Shrinkage star-shaped cracks: Explaining the transition from 90 degrees to 120 degrees.* European Physics Letters, vol. 89, no. 2, 2010. (Cited on page 72.)

[Geyer & Nemat-Nasser 1982] J. F. Geyer and S. Nemat-Nasser. *Experimental investigation of thermally induced interacting cracks in brittle solids.* International Journal of Solids and Structures, vol. 18, no. 4, pages 349 – 356, 1982. (Cited on page 72.)

[Giacomini 2005] A. Giacomini. *Ambrosio-Tortorelli approximation of quasi-static evolution of brittle fractures.* Calculus of Variations and Partial Differential Equations, vol. 22, pages 129–172, 2005. (Cited on page 29.)

[Goehring *et al.* 2009] L. Goehring, L. Mahadevan and S. W. Morris. *Nonequilibrium scale selection mechanism for columnar jointing.* Proceedings of the National Academy of Sciences, vol. 106, no. 2, pages 387–392, 2009. (Cited on page 72.)

[Grisvard 1992] P. Grisvard. Singularities in boundary value problems. RMA 22. Masson, 1992. (Cited on page 40.)

[Guosheng 1998] L. Guosheng. *Determination of Rock Salt Fracture Toughness with Hydraulic Fracturing Method.* Journal of Southwest China Institute of Technology, 1998. (Cited on page 129.)

[Hansen *et al.* 1984] F. D. Hansen, K. D. Mellegard and P. E. Senseny. *Elasticity and strength of ten natural rock salts.* In Proc First Conf. on the Mechanical Behavior of Salt, pages 71–83, 1984. (Cited on page 129.)

[Hasselman 1969] D. P. H. Hasselman. *Unified Theory of Thermal Shock Fracture Initiation and Crack Propagation in Brittle Ceramics.* Journal of the American Ceramic Society, vol. 52, no. 11, pages 600–604, 1969. (Cited on page 72.)

[Henry & Levine 2004] H. Henry and H. Levine. *Dynamic Instabilities of Fracture under Biaxial Strain Using a Phase Field Model.* Physical Review Letters, vol. 93, page 105504, Sep 2004. (Cited on page 32.)

[Henry 2010] H. Henry. *Study of three-dimensional crack fronts under plane stress using a phase field model.* EPL (Europhysics Letters), vol. 92, no. 4, page 46002, 2010. (Cited on page 32.)

[Hernandez *et al.* 2005] V. Hernandez, J. E. Roman and V. Vidal. *SLEPc: A Scalable and Flexible Toolkit for the Solution of Eigenvalue Problems.* ACM Transactions on Mathematical Software, vol. 31, no. 3, pages 351–362, 2005. (Cited on page 94.)

[Huon *et al.* 2009] V. Huon, B. Cousin, B. Wattrisse and O. Maisonneuve. *Investigating the thermo-mechanical behaviour of cementitious materials using image processing techniques.* Cement and Concrete Research, vol. 39, no. 6, pages 529 – 536, 2009. (Cited on page 16.)

[Jagla 2002] E. A. Jagla. *Stable propagation of an ordered array of cracks during directional drying.* Physical Review E, vol. 65, page 046147, 2002. (Cited on pages 72, 73 and 103.)

[Jenkins 2005] D. R. Jenkins. *Optimal spacing and penetration of cracks in a shrinking slab.* Physical Review E, vol. 71, page 056117, May 2005. (Cited on pages 72, 73, 103 and 116.)

[Jiang *et al.* 2012] C. Jiang, X. Wu, J. Li, F. Song, Y. Shao, X. Xu and P. Yan. *A study of the mechanism of formation and numerical simulations of crack patterns in ceramics subjected to thermal shock.* Acta Materialia, vol. 60, no. 11, pages 4540 – 4550, 2012. (Cited on pages 72, 73 and 121.)

[Jones *et al.* 01] E. Jones, T. Oliphant, P. Peterson*et al.* *SciPy: Open source scientific tools for Python*, 2001–. (Cited on page 95.)

[Karma & Lobkovsky 2004] A. Karma and A. E. Lobkovsky. *Unsteady Crack Motion and Branching in a Phase-Field Model of Brittle Fracture.* Phys. Rev. Lett., vol. 92, page 245510, Jun 2004. (Cited on page 32.)

[Karma *et al.* 2001] A. Karma, D. A. Kessler and H. Levine. *Phase-Field Model of Mode III Dynamic Fracture.* Physical Review Letters, vol. 87, page 045501, Jul 2001. (Cited on page 32.)

[Lagerstrom 1988] P. Lagerstrom. Matched asymptotic expansions: Ideas and techniques, volume 76 of *Applied Mathematical Sciences.* Springer-Verlag, 1988. (Cited on pages 8, 39 and 50.)

[Leblond 2000] J.-B. Leblond. Mécanique de la rupture fragile et ductile. Collection Études en mécanique des matériaux et des structures. Editions Lavoisier, Paris, 2000. (Cited on pages 52, 57 and 59.)

[Lemaitre & Chaboche 1978] J. Lemaitre and J.-L. Chaboche. *Aspect phénoménologique de la rupture par endommagement.* J Méc Appl, vol. 2, no. 3, 1978. (Cited on page 7.)

[Logg *et al.* 2012] A. Logg, K.-A. Mardal, G. N. Wells*et al.* Automated solution of differential equations by the finite element method. Springer, 2012. (Cited on page 94.)

[Lu & Fleck 1998] T. Lu and N. Fleck. *The thermal shock resistance of solids.* Acta Materialia, vol. 46, no. 13, pages 4755 – 4768, 1998. (Cited on page 72.)

[Marigo 1981] J.-J. Marigo. *Formulation d'une loi d'endommagement d'un matériau élastique.* CR Acad. Sci. Paris II, vol. 292, pages 1309–1312, 1981. (Cited on page 11.)

[Marigo 1985] J. Marigo. *Modelling of brittle and fatigue damage for elastic material by growth of microvoids.* Engineering Fracture Mechanics, vol. 21, no. 4, pages 861 – 874, 1985. (Cited on page 13.)

[Marigo 1989] J. Marigo. *Constitutive relations in plasticity, damage and fracture mechanics based on a work property.* Nuclear Engineering and Design, vol. 114, no. 3, pages 249 – 272, 1989. (Cited on pages 11 and 13.)

[Marigo 2000] J.-J. Marigo. *L'endommagement et la Rupture: hier, aujourd'hui et demain.* Technical Report 8, IPSI, 2000. (Cited on page 12.)

[Marigo 2010] J.-J. Marigo. *Initiation of Cracks in Griffith's Theory: An Argument of Continuity in Favor of Global Minimization.* Journal of Nonlinear Science, vol. 20, no. 6, pages 831–868, 2010. (Cited on pages 28, 29 and 30.)

[Miehe *et al.* 2010a] C. Miehe, F. Welschinger and M. Hofacker. *Thermodynamically consistent phase-field models of fracture: Variational principles and multi-field FE implementations.* International Journal for Numerical Methods in Engineering, vol. 83, no. 10, pages 1273–1311, 2010. (Cited on page 32.)

[Miehe *et al.* 2010b] C. Miehe, M. Hofacker and F. Welschinger. *A phase field model for rate-independent crack propagation: Robust algorithmic implementation based on operator splits.* Computer Methods in Applied Mechanics and Engineering, vol. 199, no. 45 - 48, pages 2765 – 2778, 2010. (Cited on page 32.)

[Mielke 2006] A. Mielke. *Chapter 6 Evolution Of Rate-Independent Systems.* volume 2 of *Handbook of Differential Equations: Evolutionary Equations*, pages 461 – 559. North-Holland, 2006. (Cited on pages 8 and 20.)

[Moës *et al.* 2011] N. Moës, C. Stolz, P.-E. Bernard and N. Chevaugeon. *A level set based model for damage growth: The thick level set approach.* International Journal for Numerical Methods in Engineering, vol. 86, no. 3, pages 358–380, 2011. (Cited on page 32.)

[Morris *et al.* 1992] P. H. Morris, J. Graham and D. J. Williams. *Cracking in drying soils.* Canadian Geotechnical Journal, vol. 29, no. 2, pages 263–277, 1992. (Cited on page 72.)

[Munson *et al.* 2012] T. Munson, J. Sarich, S. Wild, S. Benson and L. C. McInnes. *TAO 2.0 Users Manual.* Rapport technique ANL/MCS-TM-322, Mathematics and Computer Science Division, Argonne National Laboratory, 2012. http://www.mcs.anl.gov/tao. (Cited on page 31.)

[Negri 1999] M. Negri. *The anisotropy introduced by the mesh in the finite element approximation of the mumford-shah functional.* Numerical Functional Analysis and Optimization, vol. 20, no. 9-10, pages 957–982, 1999. (Cited on pages 29 and 131.)

[Negri 2010] M. Negri. *A comparative analysis on variational models for quasi-static brittle crack propagation.* Advances in Calculus of Variations, vol. 3, no. 2, pages 149–212, 2010. (Cited on page 29.)

[Nguyen *et al.* 2013] S. Nguyen, L. Jeannin, L. Dormieux and F. Renard. *Fracturing of viscoelastic geomaterials and application to sedimentary layered rocks.* Mechanics Research Communications, vol. 49, no. 0, pages 50 – 56, 2013. (Cited on page 129.)

[Nguyen 1984] Q.-S. Nguyen. *Bifurcation et stabilité des systèmes irréversibles obéissant au principe de dissipation maximale.* Journal de Mécanique théorique et appliquée, vol. 3, no. 1, pages 41–61, 1984. (Cited on page 71.)

[Nguyen 1987] Q. Nguyen. *Bifurcation and post-bifurcation analysis in plasticity and brittle fracture.* Journal of the Mechanics and Physics of Solids, vol. 35, no. 3, pages 303–324, 1987. (Cited on page 71.)

[Nguyen 1994] Q. S. Nguyen. *Bifurcation and Stability in Dissipative Media (Plasticity, Friction, Fracture).* Applied Mechanics Reviews, vol. 47, no. 1, pages 1–31, 1994. (Cited on page 82.)

[Nguyen 2000] Q. Nguyen. Stability and nonlinear solid mechanics. Wiley & Son, London, 2000. (Cited on page 82.)

[Ortner & Negri 2008] C. Ortner and M. Negri. *Quasi-static crack propagation by Griffith's criterion.* Mathematical Models and Methods in Applied Sciences, vol. 18, no. 11, pages 1895–1925, 2008. (Cited on page 29.)

[Pham & Marigo 2010a] K. Pham and J.-J. Marigo. *Approche variationnelle de l'endommagement : I. Les concepts fondamentaux.* Comptes Rendus Mécanique, vol. 338, no. 4, pages 191–198, 2010. (Cited on pages 8, 12, 17 and 19.)

[Pham & Marigo 2010b] K. Pham and J.-J. Marigo. *Approche variationnelle de l'endommagement : II. Les modèles à gradient.* Comptes Rendus Mécanique, vol. 338, no. 4, pages 199–206, 2010. (Cited on pages 8, 12, 19, 46 and 139.)

[Pham & Marigo 2013] K. Pham and J.-J. Marigo. *From the onset of damage to rupture: construction of responses with damage localization for a general class of gradient damage models.* Continuum Mechanics and Thermodynamics, vol. 25, no. 2-4, pages 147–171, 2013. (Cited on pages 8, 12, 17, 22, 26, 33, 35, 46, 58, 65, 100, 113 and 139.)

[Pham *et al.* 2011] K. Pham, J.-J. Marigo and C. Maurini. *The issues of the uniqueness and the stability of the homogeneous response in uniaxial tests with gradient damage models.* Journal of the Mechanics and Physics of Solids, vol. 59, no. 6, pages 1163 – 1190, 2011. (Cited on pages 24 and 58.)

[Pham 2010] K. Pham. *Construction et analyse de modèles d'endommagement à gradient.* Phd, Université Pierre et Marie Curie, france, 2010. (Cited on page 24.)

[Pijaudier-Cabot & Bazant 1987] G. Pijaudier-Cabot and Z. Bazant. *Non Local damage theory.* Journal of Engineering Mechanics ASCE, vol. 113, pages 1512–1533, 1987. (Cited on page 12.)

[Shao *et al.* 2010] Y. Shao, X. Xu, S. Meng, G. Bai, C. Jiang and F. Song. *Crack Patterns in Ceramic Plates after Quenching.* Journal of the American Ceramic Society, vol. 93, no. 10, pages 3006–3008, 2010. (Cited on pages 72 and 126.)

[Shao *et al.* 2011] Y. Shao, Y. Zhang, X. Xu, Z. Zhou, W. Li and B. Liu. *Effect of Crack Pattern on the Residual Strength of Ceramics After Quenching.* Journal of the American Ceramic Society, vol. 94, no. 9, pages 2804–2807, 2011. (Cited on pages iv, 72, 101, 121, 122, 123, 126 and 128.)

[Sicsic & Marigo 2013] P. Sicsic and J.-J. Marigo. *From Gradient Damage Laws to Griffith's Theory of Crack Propagation.* Journal of Elasticity, vol. 113, no. 1, pages 55–74, 2013. (Cited on page 47.)

[Sicsic *et al.* 2013] P. Sicsic, J.-J. Marigo and C. Maurini. *Initiation of a periodic array of cracks in the thermal shock problem: a gradient damage modeling.* Journal of the Mechanics and Physics of Solids, 2013. in press. (Cited on page 58.)

[Simone *et al.* 2004] A. Simone, H. Askes and L. J. Sluys. *Incorrect initiation and propagation of failure in non-local and gradient-enhanced media.* International Journal of Solids and Structures, vol. 41, no. 2, pages 351 – 363, 2004. (Cited on page 66.)

[Stolz & Moës 2012] C. Stolz and N. Moës. *A new model of damage: a moving thick layer approach.* International Journal of Fracture, vol. 174, no. 1, pages 49–60, 2012. (Cited on page 32.)

Abstract: This thesis explores the use of damage models to predict the onset and propagation of cracks in a coherent manner. The results are based on the definition of a bulk energy density and a stability principle. Firstly, we study the nucleation of cracks in a notched domain. The limit loading can be decomposed as the product of three stress intensity factors: a scale effect, a geometry induced factor, function of the angle of the notch, and one due to the damage model. The cracks that appear have a characteristic profile whose width is of the order of the internal length. When the latter is small in front of the dimensions of the structure, by separating scales, and using a local minimum principle, we prove that the length of these damage bands follow Griffith's law. This fundamental results extends those based on global minimization but with a sounder physical base. A thorough investigation of the thermal shock problem leads to a better understanding of the nucleation of cracks. Especially the global property of crack periodicity is exhibited. These results are based on the variational approach and the properties would probably be lost for models developed in an other framework. Finally, numerical results based on an alternate minimization algorithm are established. The nucleation phase is controlled by the critical stress whereas the propagation is governed by the toughness. Size effects in two and three dimensions are captured. These numerical simulations are then confronted to experimental results.

Keywords: fracture, non-local damage, variational approach, size effect, asymptotic analysis

---

Résumé : Cette thèse explore l'utilisation de modèles d'endommagement pour prédire la nucléation et la propagation de la rupture de manière cohérente. Les résultats sont basés sur la donnée d'une énergie, qui définit le matériau, et d'une loi d'évolution construite sur un principe de stabilité, de conservation d'énergie et d'irreversibilité. Dans un premier temps, on étudie l'initiation de fissures dans une structure contenant un coin. Le chargement limite se réduit à trois composantes : un facteur d'échelle, une composante géométrique fonction de l'angle, et une composante propre au modèle. Ces modèles donnent naissance à des fissures dont le profil est caractéristique et dont la largeur est de l'ordre de la longeur interne du modèle. Cette dernière étant petite devant les dimensions de la structure, dans le cadre d'une séparation d'échelles et en utilisant un principe de minimum local, on montre que le modèle d'endommagement considéré converge vers la loi de propagation de Griffith. Ce résultat fondamental étend ceux existants, basés sur la minimisation globale, mais avec une base physique plus forte. Une étude approfondie donne une meilleure compréhension de la phase d'initiation dans le cas d'un choc thermique et on établit la propriété globale qu'est l'émergence d'une solution périodique. Ces résultats s'appuient sur le cadre variationnel, les propriétés seraient probablement perdues pour un modèle d'endommagement développé dans un autre cadre. Dans un dernier temps, les résultats numériques basés sur un algorithme de minimisation alternée capturent une initiation contrôlée par la contrainte critique, ainsi que la propagation des fissures controlée par la densité d'énergie de fissuration. Des effets d'échelle en deux et trois dimensions sont mis en évidence. Les simulations sont alors confrontées à des résultats expérimentaux.

Mots-clés : rupture, endommagement à gradient, approche variationnelle, effets d'échelle, analyse asymptotique